An investigation into the role of ATM protein in mitochondrial defects associated with cardiovascular pathology resulting from insulin resistance

Marguerite Blignaut

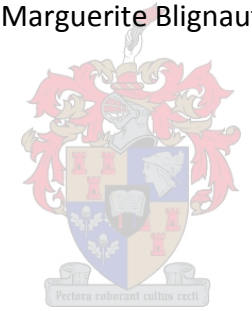

Dissertation presented for the degree of Doctor of Medical Physiology in the Faculty of Medicine and Health Sciences at Stellenbosch University

Supervisor: Prof B Huisamen

Co-supervisors: Prof A Lochner, Prof A-M Engelbrecht, Dr D Van Vuuren

April 2019

Declaration:

By submitting this dissertation electronically, I declare that the entirety of the work contained therein is my own, original work, that I am the sole author thereof (save to the extent explicitly otherwise stated), that reproduction and publication thereof by Stellenbosch University will not infringe any third party rights and that I have not previously in its entirety or in part submitted it for obtaining any qualification

Date: .....

This dissertation includes 1 original papers published in peerreviewed journals and 1 unpublished publication. The development and writing of the papers (published and unpublished) were the principal responsibility of myself and for each of the cases where this is not the case, a declaration is included in the dissertation indicating the nature and extent of the contributions of co-authors.

Abstract:

Background: Ataxia-telangiectasia (A-T) is a rare, recessive disorder that develops in the absence of Ataxia-Telangiectasia Mutated protein kinase (ATM). This complex disease is characterised by neurodegeneration, increased risk of cancer, a high incidence of insulin resistance and Type 2 diabetes (T2D) as well as cardiovascular disease. Mitochondrial dysfunction is associated with the development of cardiomyopathy and T2D. Obesity and insulin resistance contribute towards the development of cardiac dysfunction, and have been linked with mitochondrial disturbances. ATM has previously been associated with mitochondria, and the absence thereof results in decreased mitochondrial respiration and ATP synthesis as well as structural abnormalities.

This study aimed to investigate the role of ATM in mitochondrial oxidative phosphorylation and mitophagy as possible contributors towards cardiovascular dysfunction in obesity.

Methodology: The effects of high palmitic and oleic acid, either alone or in combination with insulin or high glucose on ATM expression levels were investigated in an H9c2 cardiomyoblast model. Insulin signal transduction intermediates were determined by western blotting and glucose uptake by [^{3}H]2-deoxyglucose accumulation. Mitoplasts were prepared from cardiac mitochondria of male Wistar rats with digitonin and the quality thereof confirmed with transmission electron microscopy (TEM). The location of ATM was determined with Super-resolution structured illumination microscopy (SR-SIM) and western blotting.

Oxidative phosphorylation (oxphos) analysis was performed polarographically (Clark-type electrode) on mitochondria obtained from 1) young male Wistar rat hearts perfused with the ATM specific inhibitor, KU60019 or vehicle (DMSO), and 2) chow fed age-matched controls and diet induced obese (DIO) rat hearts perfused *ex vivo* with either DMSO or ATM-specific activators and its inhibitor (KU60019 ± insulin or KU60019 ± chloroquine). Oxphos was determined in carbohydrate (glutamate+malate) or fatty acid (palmitoyl-L-carnitine+malate) substrates while protein expression levels of ATM as well as markers of mitophagy and mitochondrial fission were measured (western blotting). The redox status of

NAD(P)H was determined with 2-photon fluorescence lifetime imaging microscopy in H9c2 cells ± KU60019.

Results: This study showed that: (i) high levels of fatty acids and insulin affects the expression levels of ATM; (ii) ATM is located on the inner mitochondrial membrane of cardiac mitochondria. iii) Inhibition of ATM decreased carbohydrate-stimulated oxidative phosphorylation in cardiac mitochondria ($p=0.0024$), potentially through Complex I. This was supported by the observation that ATM inhibition decreased NADPH ($p=0.02$) and increased NADH accumulation in H9c2 cells. iv) The effect of ATM inhibition on oxidative phosphorylation was not influenced by diet; v) ATP synthesis as well as respiratory control index improved with the addition of insulin ($p<0.005$). vi) The inhibition of ATM was associated with decreased fission ($p=0.0038$). vii) The decrease in the autophagosomal membrane marker, LC3-II ($p<0.0001$) seems to be associated with the cytosolic role of ATM.

Conclusion: ATM is located on the inner mitochondrial membrane and inhibition thereof influences mitochondrial ATP synthesis, potentially through Complex I substrate oxidation. Inhibition of ATM did not affect oxidative phosphorylation in obesity, but resulted in mitochondrial autophagy disruption as well as decreased fission.

Opsomming:

Agtergrond: Ataxia-telangiectasia (A-T) is ‘n raar, resessiewe siekte wat in die afwesigheid van Ataxia-Telangiectasia gemuteerde proteïen kinase (ATM) ontwikkel. Hierdie komplekse siekte word gekarakteriseer deur neuronale afwykings, ‘n verhoogde risiko vir ontwikkeling van kanker, verhoogde insidensie van insulien weerstandigheid en Tipe 2 diabetes (T2D) sowel as kardiovaskulêre siektes. Mitokondriale afwykings kan lei tot die ontwikkeling van kardiomiopatie en T2D. Vetsug sowel as insulien weerstandigheid dra by tot mitokondriale afwykings. Vorige studies het aangedui dat ATM by die mitokondrion betrokke is, en dat die afwesigheid daarvan kan lei tot ‘n afname in mitokondriale respirasie, ATP sintese, en strukturele veranderinge.

Die doel van hiedie studie was om die die rol van ATM in die hart te bepaal met spesifieke fokus op mitokondriale oksidatiewe fosforilasie en mitofagie as moontlike bydraende faktore tot kardiovaskulêre disfunksie in vetsug.

Metodiek: ATM uitdrukking is ondersoek in ‘n H9c2 kardiomioblast sel model met die vetsure, palmitaat en oleaat, alleen of in kombinasie met hoë insulien en hoë glukose. Insulien seintransduksie proteïene is deur middel van Western-klad tegniek ondersoek en glukose opname met [^{3}H]2-deoksieglukose. Lokalisering van ATM in die mitokondriale binnemembraan is bepaal in mitoplaste berei uit hartweefsel van manlike Wistar rotte met behulp van digitonien. Kwaliteit van die mitoplaste is met behulp van transmissie elektron mikroskopie (TEM) gekontroleer, en die posisie van ATM is met super resolusie gestruktureerde beligte mikroskopie (SR-SBM) en Western-klad bepaal.

Oksidatiewe fosforilasie is polarografies (Clark-tipe elektrode) bepaal in mitokondriē geïsoleer uit (i) harte van jong, kontrole manlike Wistar rotte, geperfuseer met of die draer (DMSO) of die ATM inhibitor, KU60019; (ii) harte van ouderdoms-gepaarde kontrole rotte of rotte gevoer met ‘n hoë kalorie diëet wat vetsug bevorder (DIO), *ex vivo* geperfuseer met of DMSO, of KU60019 ± insulien of KU60019 ± klorokien. Oksidatiewe fosforilasie is bepaal met koolhidraat (glutamaat+malaat) of vetsuur (palmitoyl-L-karnitien+malaat) substrate en proteïen uitdrukkingsvlakke van ATM asook merkers van mitofagie en mitokondriale fissie is bepaal met Western-klad. Die redoks status van NAD(P)H is bepaal met 2-foton fluoresensie leeftyd visualiserings mikroskopie in H9c2 selle met of KU60019 óf DMSO.

Resultate: Hierdie studie het getoon dat (i) hoë vetsuur vlakke asook insulien die uitdrukking van ATM beïnvloed; ii) ATM op die mitokondriale binnemembraan gelokaliseer is; iii) Inhibisie van ATM onderdruk mitokondriale koolhidraat-geïnduseerde mitokondriale oksidatiewe fosforilasie ($p=0.0024$), moontlik deur Kompleks I. Hierdie waarneming is gesteun deur die bevinding dat ATM inhibisie NADPH vlakke ($p=0.02$) laat afneem en NADH vlakke laat toeneem in H9c2 selle. iv) Die effek van ATM onderdrukking op oksidatiewe fosforilasie is onafhanklik van diēet. v) ATP sintese asook die respiratoriese kontrole indeks het verbeter in die teenwoordigheid van insulien($p<0.005$). vi) Die onderdrukking van ATM met KU60019 het ook mitokondriale fissie verlaag ($p=0.0038$). vii) Die afname in autofagie membraan merker, LC3-II ($p<0.0001$), blyk weens die sitosoliese rol van ATM te wees.

Gevolgtrekking: ATM is gelokaliseer op die mitokondriale binnemembraan en die inhibisie daarvan beïnvloed mitokondriale ATP sintese, moontlik deur Kompleks I substraat verbruik. Die inhibsie van ATM het nie ‘n rol gespeel in mitokondriale oksidatiewe fosforilasie in vetsug nie, maar het wel mitofagie ontwrig as ook mitokondriale fissie verlaag.

Acknowledgements:

- I would like to thank my supervisor, Prof B Huisamen, for being a mentor to me. Thank you for all the guidance and advice. Also, thank you for allowing me to grow with the project and the project to grow with me.
- Thank you to Prof Lochner, for an open door, good discussions (and good questions!)
- Prof A-M Engelbrecht and Dr D van Vuuren for infinite patience, and very (and many) useful suggestions and comments during the preparation of this dissertation.
- Profs. Stan Botchway and Tony Parker-Thank you for the opportunity to visit you at RAL, many fruitful discussions and always listening to me when I mention that I have been thinking….
- Mignon, Sybrand, Festus, Sana, Yolandi, and everyone in office 572. Especially Mignon for all the help in the lab, moral support and chats, and Festus for long academic discussions and many philosophical questions.
- The Harry Crossley foundation for a personal bursary as well as project funding, the FHMS for travel grants to attend a conference in the US and my visit the UK (RAL); the Newton fund and GWRC for project and personal funding during my time at the UK.
- Last but not least, Pieter Neething, my anchor and compass, thank you for all the love and support. Without you none of this would be possible.

Peer-reviewed research outputs during study:

- Blignaut, M., Espach, Y., van Vuuren, M., Dhanabalan, K., Huisamen, B. (2019) Revisiting the cardiotoxic effect of chloroquine, *Cardiovascular Drugs and Therapy*. https://doi.org/10.1007/s10557-018-06847-9.
- Blignaut, M., Loos, B., Botchway, SW., Parker, AW., Huisamen, B. (2019) Ataxia-Telangiectasia Mutated is located in cardiac mitochondria and impacts oxidative phosphorylation, *Scientific Reports*. Reviewers comment addressed, resubmitted
- Huisamen, B., Blignaut, M., Lochner, A. (2017) ATM regulates cardiac mitochondrial oxidative phosphorylation potential, Frontiers in CardioVascular Biology 2018, Vienna, Fifth Congress of the ESC Council on Basic Cardiovascular Science, *Cardiovascular Research* (S22)
- Blignaut, M., Lochner, A., Huisamen, B. (2017) The role of mitochondrial ATM in cardiac oxidative phosphorylation and obesity, Keystone Symposium on Mitochondria, Metabolism and Heart, Santa Fe, New Mexico, USA
- Huisamen, B., van Vuuren, M., Blignaut, M., Lochner, A. (2017) A link between low ATM, myocardial insulin resistance and mitochondrial dysfunction in obesity. ATW2017: Ataxia-Telangiectasia Workshop, Milan
- Blignaut, M., Huisamen, B (2016). First report of ATM protein kinase location and potential function within cardiac mitochondria. 44th Conference of the Physiology Society of Southern Africa, Cape Town

Awards and achievements:

2017: First prize-Oral presentation; Department of Biomedical Sciences Annual Research day

2017: Keystone Symposia Scholarship; Keystone Symposium on Mitochondria, Metabolism and Heart, Santa Fé, New Mexico, USA

2017 and 2018: Faculty of Health and Medical Sciences, Stellenbosch University travel grant to attend Keystone Symposia; travel grant for long term visit to RAL, UK.

2017: Harry Crossly Foundation project funding (SU-PT-16/10-00012)

2016: Faculty of Health and Medical Sciences, Stellenbosch University travel grant to attend PSSA, Cape Town 2016

Table of Contents

Abstract: iii

Opsomming: v

Acknowledgements: vii

Peer-reviewed research outputs during study: viii

Awards and achievements: viii

Table of Contents 1

List of Figures: 4

List of abbreviations: 6

Chapter 1 : General introduction 10

Chapter 2 : Literature review 13

2.1 Ataxia-Telangiectasia (A-T) and Ataxia Telangiectasia Mutated Protein Kinase (ATM): 13

2.2 ATM and the DNA Damage Response Pathway: 17

2.3 Cytosolic ATM and oxidative stress 22

2.3.1 Reactive oxygen and nitrogen species: 24

2.3.2 ATM and oxygen sensing: 26

2.3.3 ATM, autophagy and the peroxisome: 27

2.3.4 ATM, glycolysis and the pentose phosphate pathway: 31

2.4. ATM, mitochondria and mitophagy: 32

2.4.1 Mitochondrial morphology and function: 33

2.4.2 Electron transfer chain (ETC) and mitochondrial metabolism: 35

2.4.3 Mitochondrial oxidative stress: 38

2.4.4 Mitophagy and mitochondrial dynamics: 40

2.5 ATM and insulin signalling 45

2.6 ATM and drug efficacy: 51

2.6 Purpose of research: 52

Chapter 3 : ATM is downregulated *in vitro* by high free fatty acid concentrations in the rat cardiomyoblast cell line, H9c2. 56

3.1 Brief introduction to H9c2 (2-1) rat cardiomyoblast cells and applications in literature 57

3.2 Materials and methods: 59

3.2.1 Reagents: 60

3.2.2 Cell culture: 60

3.2.3 Western blotting: 61

3.2.5 Western blot analysis and normalization: 63

3.2.4 Glucose uptake: 64
3.2.5 Statistical analysis: 65
3.3 Results and discussion: 65
Chapter 4 : Ataxia-Telangiectasia Mutated protein kinase is located on the inner mitochondrial membrane of rat cardiac mitochondria 79
4.1 Development of a mitoplast isolation protocol: 79
4.2 Materials and methods: 84
4.2.1 Reagents: 84
4.2.2 Animals: 85
4.2.3 Mitochondrial isolation: 85
4.2.4 Mitochondrial subfractionation with digitonin and Lubrol WX: 86
4.2.5 Proteinase K digestion: 88
4.2.6 Western blotting: 89
4.2.7 Transmission electron microscopy: 90
4.2.8 Super –resolution Structured Illumination Microscopy (SR-SIM): 90
4.3 Results and discussion: 90
Chapter 5 : ATM plays a role in mitochondrial oxidative phosphorylation and mitophagy 100
5.1 Materials and Methods: 102
5.1.2 Reagents: 103
5.1.3 Animals: 103
5.1.4 Langendorff perfusions (for mitochondrial analysis): 104
5.1.5 Oxygen consumption in isolated mitochondria: 105
5.1.6 Western blotting: 106
5.1.7 Statistical analysis: 109
5.2 Results and discussion: 109
5.2.1 Inhibition of ATM decreases Complex I-mediated oxidative phosphorylation 109
5.2.2 The role of ATM in obesity and cardiac oxidative phosphorylation in isolated mitochondria 113
5.2.3 Insulin improves oxidative phosphorylation and protects against anoxia 118
5.2.4 Chloroquine improves recovery after anoxia that is further improved with the inhibition of ATM: 123
5.2.5 Chemical inhibition of ATM with KU60019 influences mitophagy in cardiac mitochondria: 129
Chapter 6 : Mitochondrial NAD+/NADH redox state and the use of fluorescent life-time imaging microscopy (FLIM) 142

6.1 Two-photon FLIM microscopy: 143
6.1 Materials and Methods: 146
6.1.1 Reagents: 147
6.1.2 Cell culture: 147
6.1.3 Fluorescence lifetime imaging microscopy: 147
6.1.4 Statistical analysis: 148
6.2 Results and discussion: 148
Chapter 7 : Conclusion 154
7.2 Future work: 159
7.3 Limitations: 160
Chapter 8 : References 162
Addendum A: Chapter 4 additional information 197
Addendum B: Publications 201
Addendum C : Insulin resistance in diet induced obese rats (DIO): 206
Addendum D: Mitochondrial respiration of hearts perfused with a combination of KU60019 and chloroquine compared to KU60019 alone 208

List of Figures:

FIGURE 2.1: ATM PROTEIN KINASE STRUCTURE. 15
FIGURE 2.2: SIMPLIFIED SCHEMATIC DIAGRAM OF THE ROLE OF ATM IN THE DNA DAMAGE RESPONSE PATHWAY. 21
FIGURE 2.3: ROS CAN ACTIVATE CYTOSOLIC ATM. 28
FIGURE 2.4: ATM ACTS AS A CYTOSOLIC REDOX SENSOR IN RESPONSE TO OXIDATIVE STRESS. 31
FIGURE 2.5: ELECTRON MICROGRAPH OF CARDIAC MITOCHONDRIA ISOLATED FROM A MALE WISTAR RAT. 34
FIGURE 2.6: A SIMPLIFIED, SCHEMATIC REPRESENTATION OF THE ELECTRON TRANSFER CHAIN (ETC) AND OXIDATIVE PHOSPHORYLATION. 36
FIGURE 2.7: A SCHEMATIC OVERVIEW OF MITOPHAGY AND AUTOPHAGIC CLEARANCE OF DAMAGED MITOCHONDRIA. 42
FIGURE 2.8: A SCHEMATIC REPRESENTATION OF THE CYTOSOLIC ROLE OF ATM IN RESPONSE TO INSULIN. 49
FIGURE 3.1: SCHEMATIC REPRESENTATION OF THE GLUCOSE UPTAKE ASSAY. 65
FIGURE 3.2: H9C2 CELL STRUCTURE BETWEEN DIFFERENT PASSAGES. 66
FIGURE 3.3: WESTERN BLOT ANALYSIS OF TOTAL ATM, TOTAL AKT AND MTOR PROTEIN LEVELS IN H9C2 CELLS TREATED WITH 0.1 MM PALMITATE. 67
FIGURE 3.4: H9C2 CARDIOMYOBLAST PRIOR TO AND AFTER 24 HOURS OF FFA TREATMENT. 69
FIGURE 3.5: H9C2 CARDIOMYOBLAST PRIOR TO AND AFTER 24 HOURS OF INSULIN AND INSULIN PLUS FFA TREATMENT. 70
FIGURE 3.6: 2-[^{3}H]-DEOXY GLUCOSE UPTAKE IN UNDIFFERENTIATED H9C2 CARDIOMYOBLAST CELLS. 71
FIGURE 3.7: WESTERN BLOT ANALYSIS OF TOTAL ATM AND PHOSPHORYLATED ATM, AS WELL AS AMPK AND PHOSPHORYLATED AMPK PROTEIN LEVELS IN H9C2 CELLS TREATED WITH 0.2 MM PALMITATE AND OLEIC ACID. 72
FIGURE 3.8: PHOSPHO-ATM/TOTAL ATM, PHOSPHO-AMPK/TOTAL AMPK AND PHOSPHO-AKT/TOTAL AKT RATIOS. 73
FIGURE 3.9: WESTERN BLOT ANALYSIS OF TOTAL MTOR AND PHOSPHORYLATED MTOR (SER^{2448}) IN H9C2 CELLS TREATED WITH 0.2 MM PALMITATE AND OLEIC ACID. 74
FIGURE 3.10: WESTERN BLOT ANALYSIS OF TOTAL TAKT AND PHOSPHORYLATED AKT (SER^{473}) IN H9C2 CELLS TREATED WITH 0.2 MM PALMITATE AND OLEIC ACID. 76
FIGURE 4.1: SCHEMATIC DIAGRAM OF MITOCHONDRIAL FRACTIONATION TO OBTAIN MITOPLASTS. 88
FIGURE 4.2: TRANSMISSION ELECTRON MICROGRAPHS OF MITOCHONDRIA AND MITOPLASTS AFTER 20 AND 30 MINUTES OF 1.2% DIGITONIN PERMEABILISATION. 92
FIGURE 4.3: WESTERN BLOT ANALYSIS AFTER THE SUBCELLULAR FRACTIONATION OF THE MITOCHONDRIAL, OUTER MITOCHONDRIAL (OMM) AND MITOPLAST (INNER MITOCHONDRIAL MEMBRANE {IMMI} AND MATRIX) FRACTIONS. 95
FIGURE 4.4: SUBFRACTIONATION OF THE MITOPLAST FRACTION INTO THE IMM AND MATRIX AND PROTEINASE K DIGESTION OF THE MITOCHONDRIAL FRACTION. 96
FIGURE 4.5: SUPER RESOLUTION STRUCTURED ILLUMINATION MICROSCOPY (SR-SIM) MICROGRAPHS OF ISOLATED MITOCHONDRIA AND MITOPLAST PREPARATIONS PROBED WITH VDAC (OMM, RED) AND ATM (IMM, GREEN) 97
FIGURE 4.6: SUPER RESOLUTION STRUCTURED ILLUMINATION MICROSCOPY (SR-SIM) MICROGRAPHS OF ISOLATED MITOCHONDRIA AND MITOPLAST PREPARATIONS PROBED WITH TOM20 (OMM, RED) AND ATM (IMM, GREEN) 98
FIGURE 5.1: EXPERIMENTAL DESIGN LAYOUT FOR OXIDATIVE PHOSPHORYLATION ANALYSIS IN THE PRESENCE AND ABSENCE OF THE ATM ACTIVATORS, INSULIN AND CHLOROQUINE WITH OR WITHOUT THE ATM INHIBITOR, KU60019. 105
FIGURE 5.2: INHIBITION OF ATM DECREASES COMPLEX I MEDIATED OXIDATIVE PHOSPHORYLATION RATE. 110
FIGURE 5.3: WESTERN BLOT ANALYSIS OF TOTAL ATM IN HEARTS PERFUSED RETROGRADELY WITH EITHER 0.03% DMSO OR 3 µM KU60019. 111

FIGURE 5.4: OXPHOS COMPLEX ANALYSIS OF CARDIAC MITOCHONDRIA. 113
FIGURE 5.5 WEIGHT, ADIPOSITY INDEX AND NON-FASTING BLOOD GLUCOSE OF DIET-INDUCED OBESE (DIO) MALE WISTAR RATS AND THEIR AGE-MATCHED COUNTERPARTS (AMC). 114
FIGURE 5.6: INHIBITION OF ATM DECREASED BASAL LEVELS OF STATE 3 OXYGEN CONSUMPTION AND OXIDATIVE PHOSPHORYLATION RATE. 117
FIGURE 5.7: INSULIN SIGNIFICANTLY IMPROVES BASAL LEVELS OF STATE 3 OXYGEN CONSUMPTION, OXIDATIVE PHOSPHORYLATION RATE IN BOTH A CARBOHYDRATE AND FATTY ACID SUBSTRATE. 119
FIGURE 5.8: THE COMBINATION OF KU60019 AND INSULIN PERFUSION SIGNIFICANTLY INFLUENCED ADP/O, RCR, AND RECOVERY AFTER ANOXIA IN ISOLATED MITOCHONDRIA. 121
FIGURE 5.9: MITOCHONDRIA FROM CHLOROQUINE-PERFUSED RAT HEARTS SHOW IMPROVED RECOVERY AFTER ANOXIA BUT ALSO INCREASED STATE 4 RESPIRATION. 125
FIGURE 5.10: MITOCHONDRIA FROM HEARTS PERFUSED WITH A COMBINATION OF CHLOROQUINE AND KU60019 DID NOT SHOW SIGNIFICANT EFFECTS ON INFLUENCE OXIDATIVE PHOSPHORYLATION. BOTH CHOW-FED AMC AND DIO HEARTS PERFUSED WITH A COMBINATION OF CHLOROQUINE AND KU60019 DID NOT SHOW ANY SIGNIFICANT CHANGES WHEN COMPARED TO HEARTS PERFUSED WITH EITHER CHLOROQUINE OR KU60019 ALONE FOR PANEL A) ADP/O RATIOS, OR PANEL B, RESPIRATORY CONTROL INDEX. STATE 3 (PANEL C) AND STATE 4 (PANEL D) RESPIRATION, AS WELL AS ATP SYNTHESIS (PANEL E) AND RECOVERY AFTER ANOXIA. 126
FIGURE 5.11: TOTAL AND PHOSPHO-ATM LEVELS, AS DETERMINED WITH WESTERN BLOTTING, WERE DECREASED WHEN PERFUSED WITH KU60019, BUT ACCUMULATED IN COMBINATION WITH INSULIN IN OBESITY. 130
FIGURE 5.12: CHLOROQUINE PERFUSION REDUCED THE DETECTABLE LEVELS OF TOTAL ATM LEVELS WITH WESTERN BLOTTING, IN BOTH CHOW-FED AND DIO CARDIAC MITOCHONDRIA. 131
FIGURE 5.13: WESTERN BLOT ANALYSIS OF THE MITOPHAGY MARKERS, PINK AND PARKIN IN CHOW-FED AND DIO CARDIAC MITOCHONDRIA PREPARED FROM HEARTS PERFUSED WITH DMSO, KU60019, INSULIN AND A COMBINATION OF INSULIN AND KU60019. 133
FIGURE 5.14: WESTERN BLOT ANALYSIS OF THE MITOPHAGY MARKERS, PINK AND PARKIN IN MITOCHONDRIA FROM CHOW-FED AND DIO HEARTS PERFUSED WITH DMSO, KU60019, CHLOROQUINE AND A COMBINATION OF CHLOROQUINE AND KU60019. 135
FIGURE 5.15: WESTERN BLOT ANALYSIS OF THE AUTOPHAGY MARKERS, LC3 IN MITOCHONDRIA FROM CHOW-FED AND DIO HEARTS PERFUSED WITH DMSO, KU60019, INSULIN AND A COMBINATION OF INSULIN AND KU60019. 137
FIGURE 5.16: WESTERN BLOT ANALYSIS OF THE AUTOPHAGY MARKERS, LC3 IN MITOCHONDRIA FROM AMC AND DIO HEARTS PERFUSED WITH DMSO, KU60019, CHLOROQUINE AND A COMBINATION OF CHLOROQUINE AND KU60019. 138
FIGURE 5.17: WESTERN BLOT ANALYSIS OF P62, DRP1 AND UCP3 IN MITOCHONDRIA FROM CHOW-FED AND DIO HEARTS PERFUSED WITH DMSO, KU60019, INSULIN OR A COMBINATION OF INSULIN AND KU60019 139
FIGURE 6.1: SCHEMATIC REPRESENTATION OF NADH AND NADPH. 144
FIGURE 6.2: INHIBITION OF ATM DECREASE NAD(P)H FLUORESCENCE DECAY. 149
FIGURE 6.3 : THE RELATIVE FRACTIONS OF FREE AND BOUND NAD(P)H IN H9C2 CELLS (N=3). 150
FIGURE 6.4: NAD(P)H FLUORESCENCE DECAY RESPONSES TO KU60019 TREATMENT IN HEK293 CELLS. 152

List of abbreviations:

Å: ångström (0.1 nanometer)

AA: amino acid

A-T: Ataxia Telangiectasia

ATM: Ataxia Telangiectasia Mutated protein kinase

ATMIN: ATM Interactor

AMPK: 5' adenosine monophosphate-activated protein kinase

ATP: adenosine triphosphate

ATR: Ataxia Telangiectasia and RAD3 related protein kinase

ATX/SMG1: human suppressor of morphogenesis in genitalia 1

BER: base excision repair

BNIP3: BCL2/adenovirus E1B 19 kDa protein-interacting protein 3

BRCA1: breast cancer type 1 susceptibility protein

BSA: Bovine serum albumin

CACT: carnitine acylcarnitine translocase

CHK1: cell cycle check point kinase 1

CHK2: cell cycle check point kinase 2

CPT1: carnitine palmitoyltransferase I

Cryo-EM: cryo- electron microscope

DDR: DNA damage response

DNA: Deoxyribonucleic acid

DNA-PKcs: DNA-dependent protein kinase catalytic subunit

Dox: doxorubicin

DSB: double strand breaks

ETC: electron transfer chain

ERK1/2: extracellular signal-regulated kinases 1/2

FADH2: flavin adenine dinucleotide

FCCP: arbonilcyanide p-triflouromethoxyphenylhydrazone

FAT: conserved sequence in FRAP, ATM and TRRAP

FFA: free fatty acid

FOXO3: Forkhead Box O3

FRAP: FKBP12-rapamycin–associated protein

FUNDC1: FUN 14 domain containing 1

G6PD: glucose-6-phosphate dehydrogenase

GAPDH: Glyceraldehyde 3-phosphate dehydrogenase

GSH: glutathione

H2AX: histone H2A variant

H_2O_2: Hydrogen peroxide

HAT: histone acetylase transferase

HEAT: huntingtin, elongation factor 3, protein phosphatase 2A, TOR1

HDL: High density lipoproteins

HIF-1α: Hypoxia-inducible factor 1

HOCl: hypochlorous acid

IR: ionizing radiation

LBE: LST8-binding element

LC3: microtubule-associated proteins 1A/1B light chain 3 (LC3)/GABAA receptor-associated protein (GABARAP)

LDL: Low density lipoproteins

LKB1: Liver kinase B1

LIR: LC3 interacting region

MDC1: Mediator Of DNA Damage Checkpoint 1

MMS: Methyl methanesulfonate

mnSOD: mitochondrial Superoxide dismutase

MRN: Mre11, Rad50 and Nbs1 complex

mTOR: mammalian Target of Rapamycin

NAC: N-acetylcysteine

NAD: Nicotinamide adenine dinucleotide

NADPH: nicotinamide adenine dinucleotide phosphate

NBS1: Nuclear poly (A)-binding protein 1

NCD: Non-communicable disease

NIX: BCL2/Adenovirus E1B 19 KDa Protein-Interacting Protein 3A

NO: nitric oxide

Nox: NADPH oxidases

O_2•-: oxygen radicals

'O_2: single oxygen

O_3: ozone

•OH: hydroxyl

ONOOH: peroxynitrite

PCNA: Proliferating cell nuclear antigen

PDH: pyruvate dehydrogenase

PDK: pyruvate dehydrogenase kinase

PI3-K: phosphatidylinositol 3-kinase

PIKK: phosphatidylinositol (PI) 3-kinase-like kinases

PRD: PIKK regulatory domain

PPP: Pentose phosphate pathway

REDD1: Regulated in development and DNA-damage response 1

RICTOR: rapamycin-insensitive companion of mTOR

RO•: alkoxyl

RO_2•: peroxyl

RNS: Reactive Nitrogen Species

ROS: Reactive oxygen species

S6K: protein S6 kinase

SIRT1: Sirtuin 1

SSB: single strand break

T2D: Type 2 Diabetes

TIM: translocase of the inner membrane

TOM70: translocase of outer membrane 70

TRAPP: transformation/transcription domain associated protein

TRD: tetratricopeptide repeat domain

Trx: thioredoxin

TSC2: tumour suppressor 2

UBD: ubiquitin-binding domain

UCP: uncoupling protein

ULK1: Unc-51 like autophagy activating kinase

VEGF: vascular endothelial growth factor

4E-BP1: 4E-binding protein 1

Chapter 1 : General introduction

Ataxia-telangiectasia (A-T) is a rare, recessive disorder that develops in the absence of Ataxia-Telangiectasia Mutated protein kinase (ATM). This complex disease is characterised by neurodegeneration, ataxia, oculocutaneous telangiectasia, an increased risk of cancer, premature ageing, radiosensitivity, a high incidence of insulin resistance and Type 2 diabetes (T2D) as well as cardiovascular disease (Taylor et al. 2015; Ambrose & Gatti 2013; Espach et al. 2015). The degree of disease severity is dependent on the type of mutation in the *ATM* gene (single or bi-allelic), and heterozygous patients, which make up as much as 1.4-2% of the general population, also exhibit a high incidence of ischaemic heart disease and insulin resistance (Su & Swift 2000; Connelly et al. 2016).

The absence of ATM has been associated with increased visceral obesity, glucose homeostasis dysfunction (Takagi et al. 2015) and metabolic syndrome (Schneider et al. 2006). Obesity is one of the hallmarks of metabolic syndrome, which is collectively characterised by increased low-density lipoprotein (LDL) cholesterol and decreased high-density lipoprotein (HDL) cholesterol, as well as hypertension and insulin resistance. All of these are major risk factors for Type 2 Diabetes (T2D) and cardiovascular disease (Qatanani & Lazar 2007). In light of the rapid increase in the incidence of obesity and its associated non-communicable diseases (NCDs) such as cardiovascular disease, diabetes and cancer worldwide, and more so in developing countries, there is a need to understand the underlying molecular pathogenesis associated with obesity, insulin resistance and cardiovascular disease.

Cellular oxidative stress is a recurrent theme in obesity, insulin resistance and the pathogenesis of cardiac dysfunction. Moreover, oxidative stress underlies metabolic syndrome and has been associated with obesity due to low-grade inflammation (Hopps et al. 2010). It is also a contributing factor to both insulin resistance and coronary artery disease (Ceriello & Motz 2004). Diabetes-linked cardiac dysfunction is associated with mitochondrial dysfunction and increased oxidative stress due to impaired insulin signalling (Boudina et al. 2009), the latter of which can contribute directly to mitochondrial dysfunction in obesity (Westermeier et al. 2015).

ATM acts as an important sensor of oxidative stress in cells and regulates defences against redox stress (Guo et al. 2010). ATM also regulates mitochondrial biogenesis and DNA content (Eaton et al. 2007), and can lead to mitochondrial dysfunction when absent (Ambrose et al. 2007; Valentin-Vega et al. 2012). It was shown that anti-oxidative treatment that targets the mitochondria can decrease metabolic syndrome, which supports the notion that A-T might be a mitochondrial disease (Mercer et al. 2012; D'Souza et al. 2012). Importantly, ATM also contributes to glucose homeostasis (Takagi et al. 2015), and is required for the phosphorylation of the insulin-dependent protein kinase, Akt (Viniegra et al. 2005; Halaby et al. 2008). Interestingly, ATM also mediates the rerouting of glycolysis to the pentose phosphate pathway in response to oxidative stress (Cosentino et al. 2011).

Our laboratory recently demonstrated that a high caloric diet resulted in decreased ATM expression in rat cardiac mitochondria (Huisamen et al. 2014), which possibly identifies a potential link between obesity and ATM. Moreover, in a previous study conducted within our laboratory where the role of ATM in cardiovascular dysfunction was investigated; it was found that acute chemical inhibition of ATM did not contribute significantly towards cardiac dysfunction, but could potentially play a significant role in vasoconstriction (Espach 2017). Interestingly, activation of ATM by insulin increased phosphorylation, which was decreased when administered in combination with the ATM specific inhibitor, KU60019. However, ATM activity could not be manipulated with insulin in a high caloric diet (HCD) rat model. However, haplodeficiency of ATM is sufficient to accelerate heart failure after myocardial infarction (Jia et al. 2017) whilst ATM deficiency exacerbated left ventricular dysfunction and remodelling late after myocardial infarction in mice (Daniel et al. 2016). This suggests that a chronic rather than an acute absence or decrease in ATM expression results in myocardial dysfunction, and implies that ATM expression can be influenced by chronic conditions such as obesity and insulin resistance.

In light of the importance of mitochondrial dysfunction associated with the development of cardiovascular disease due to obesity, insulin resistance and T2D, this study investigated the role of ATM both *in vitro* in H9c2 cardiomyoblasts and *ex vivo* within a well-characterised high caloric diet-induced obese (DIO) rat model. The aims of this study were as follows:

1) Investigate the potential role of ATM in insulin resistance in rat cardiomyoblasts exposed to a high free fatty acid (FFA) environment, specifically in the insulin sensitive Akt and insulin insensitive AMPK pathways.
2) Determine whether ATM expression or regulation influences mitochondrial function by investigating: i) oxidative phosphorylation, ii) mitofusion and mitophagy as well as iii) redox status in the mitochondria.

Chapter 2 : Literature review

2.1 Ataxia-Telangiectasia (A-T) and Ataxia Telangiectasia Mutated Protein Kinase (ATM):

Ataxia-telangiectasia (A-T) was initially identified in 1926 (Syllaba & Henner 1926) and described as a clinical entity in 1958 (Boder & Sedgwick 1958). The disease is named for characteristic cerebral ataxia that is associated with dilated blood vessels present in the conjunctivae of the eyes, also known as telangiectasia (Pickup and Pugh, 1960; reviewed by Gatti *et al.*, 2001). Ataxia telangiectasia is one of several genomic instability syndromes, and most notably include cerebral neurodegeneration, metabolic disease including insulin resistance and Type 2 diabetes (T2D), cardiovascular disease, premature ageing, radiosensitivity and an increased risk of developing cancer (reviewed by Shiloh, 2003; Shiloh and Ziv, 2013).

Due to the pleiotropic nature of A-T, it was postulated that different genes could mediate the disease, but linkage analysis mapped the causal region to chromosome 11q22-23 (Gatti et al. 1988). This led to the identification and complete sequencing of a single gene, *ataxia-telangiectasia mutated* (*Atm*) as the causative agent (Uziel et al. 1996; Savitsky et al. 1995a). The identification of ATM at the core of such a complex disease drove rapid progress in the elucidation of the multi-faceted molecular basis that is responsible for A-T. Whilst the majority of the mutations responsible for A-T results in the truncation and consequent reduction or abolishment of protein transcription (Buzin et al. 2003), a significant number of patients carry one of several missense or splice site mutations which maintains some ATM activity (Taylor et al. 2015). It is estimated that more than 80% of over 300 distinct mutations in the *Atm* gene, are base substitutions or insertions and deletions that result in premature termination or splicing abnormalities in gene transcription (Ahmed & Rahman 2006).

The *Atm* gene encodes for a conserved 350 kDa protein kinase (Savitsky et al. 1995b; Chen & Lee 1996) that can regulate signal transduction through the phosphorylation (Hunter 1995) of either a serine or threonine residue followed by a glutamine (SQ/TQ motif; Kim et

al. 1999). Consequently, ATM protein kinase (henceforth referred to as ATM) can potentially phosphorylate more than 400 substrates implicated in over 700 biological functions (Matsuoka et al. 2007).

This remarkable feat of ATM is achieved by its structure and post-translational modifications (Fig 2.1). The protein belongs to the super family of phosphatidylinositol (PI) 3-kinase-like kinases (PIKK; Savitsky *et al.*, 1995a). The PIKKs are a family of six large signalling proteins that contain a catalytic domain with homology to phosphatidylinositol 3-kinase (PI3-K). This catalytic domain consists of what was traditionally referred to as the conserved FAT (FRAP [FKBP12-rapamycin–associated protein], ATM and TRRAP [transformation/transcription domain associated protein]), and FAT-C (FAT-C-terminal) domain in conjunction with a kinase domain, and is present as a single unit in all known PIKK proteins (Jiang et al. 2006). This region constitutes approximately half of the PIKK and is referred to as FATKIN (Baretić et al. 2017; Imseng et al. 2018).

The PIKK family consists of the following six members: i) ATM (Fig 2.1), ii) Ataxia Telangiectasia and RAD3 related protein kinase (ATR), and iii) deoxyribonucleic acid - dependent protein kinase catalytic subunit (DNA-PKcs) that are responsible for DNA repair and genome maintenance; iv) mammalian Target of Rapamycin (mTOR) that coordinates cell growth, proliferation and protein synthesis; v) ATX/SMG1 (human suppressor of morphogenesis in genitalia) which is responsible for nonsense mediated mRNA decay, and vi) TRAPP that forms part of several complexes with histone acetylase transferase (HAT) complexes (Rivera-Calzada et al. 2015). The last protein, TRAPP, is the exception to the rule, and contains an inactive kinase domain that does not contain the conserved amino acids that is required for adenosine triphosphate (ATP) binding and catalytic activity.

Although several attempts have been made to resolve the structure of ATM (Llorca et al. 2003; Lau et al. 2016), the most recent report is by far the most detailed. The use of cryo-electron microscopy (cryo-EM) resolved human ATM protein structure at a resolution of 4.4 Å (Baretić et al. 2017). The latter study showed that the protein is present as an enzymatically active dimer that can be divided into two types: a closed dimer with symmetric FATKIN domains, and an open dimer, with asymmetric FATKIN domains, the latter of which seem to be more active (Baretić et al. 2017). The FATKIN domain of ATM is

responsible for ATM dimerization, and is essential for ATM activation. Currently, it is accepted that ATM is present as an inactive dimer that is activated by DNA damage through autophosphorylation at Ser^{1981} that results in dimer dissociation (monomerisation) and consequent activation (Bakkenist & Kastan 2003).

However, Baretić et al. (2017) could not find any evidence of free monomers in solution, although these might have been present but were not detected. They identified open and closed dimer conformations, which differ from each other in the complexity of the intermolecular interface between the monomers. The open dimer has a different and less complex intermolecular interface when compared to the less active closed dimer, but the Baretić et al. (2017) reported both the open and closed states in solution. Interestingly, they found that the dimeric ATM was enzymatically active in the presence of the ATM substrate, p53.

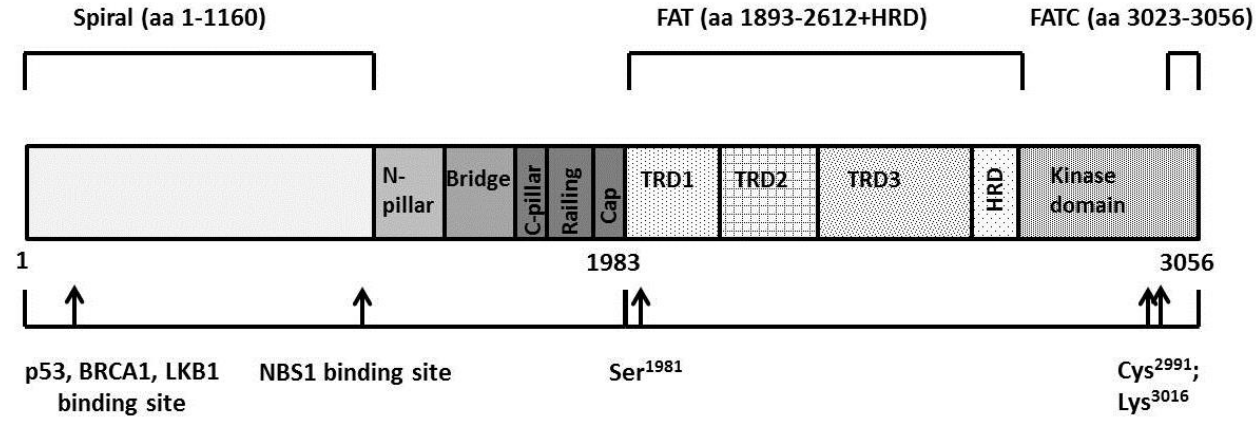

Figure 2.1: ATM protein kinase structure. The image (not drawn to scale) depicts an N-terminal (aa 1-1983) that contains binding sites for proteins such as p53, BRCA1 and LKB1 as well as NBS1 within the spiral (indicated with arrows at aa 90-97, and spiral/N-pillar interface). The C-terminal contains the FAT (aa 1893-2612), kinase and FATC domains (aa 3023-3056). Combined, these domains are referred to as FATKIN, and are essential for kinase activity. Activation of ATM is mediated by the autophosphorylation of Ser^{1981} due to DNA damage or through oxidative stress at Cys^{2991} through the formation of a disulphide bond. ATM can also be modified post-translationally through, for example, acetylation at Lys^{3016} (adapted from Bhatti et al. 2017; Baretić et al. 2017)

Both the closed and open dimer conformations of ATM have two interfaces: an upper interface where the tetratricopeptide repeat domain (TRD) 3 interacts with the kinase domain of its dimeric partner, and a lower interface where TRD2 interacts with TRD2 and TRD3 of the ATM partner.

The FATKIN domain is comprised of 1) three TRD domains and 2) a HEAT (huntingtin, elongation factor 3, protein phosphatase 2A, TOR1) repeat domain (HRD) that forms the FAT domain (amino acid[aa] 1893-2612), which is followed by the kinase domain (aa 2613-3056). The FAT-C domain is a unique, highly conserved sequence spanning approximately 33 aa sequence in the extreme C-terminus. Combined with the LST8-binding element (LBE), an activation loop (aa 2888-2910), and the PIKK regulatory domain (PRD; helices kα9b, kα9c and kα9d, aa 2966-2979), it forms a compact arrangement that is essential for the regulation of ATM. Baretić et al. (2017) suggest that the TRD3 helices (α21 and α22) interact with all of the components of this compact arrangement, and acts as a binding element in the closed conformation. The TRD3 binding element pushes on the PRD helices (kα9c and kα9d) of the dimeric partner, causing the helices to enter the active site. This prevents other peptide substrates from entering the active site that results in a closed and less active dimer.

When ATM is in an open dimer conformation, no intermolecular contacts can be observed in between the compact arrangement and TRD3 in the upper interface. The PRD helices become disordered and open up sufficiently to allow a substrate to bind. However, in the lower interface conformation of the open dimer, some of the contacts between TRD2 and TRD3 are partially retained.

The N-terminal, that consists of six domains (aa 1-1161), binds substrates, regulators and adaptors. It forms a spiral that wraps around a 30 Å cavity and is supported by several short helices that form part of the N-pillar. The N-terminal also offers several binding sites for proteins such as NBS1 (Nuclear poly (A)-binding protein 1) that maps approximately to the border region between the spiral and the N-pillar (Baretić et al. 2017) whilst amino acid residues, 90-97, form the binding site for several ATM substrates including p53, BRCA1 and LKB1 (Fernandes et al. 2005).

This suggests that the p53 site, for example, is exposed in both the open and closed dimer format. Baretić et al. (2017) propose that there may be another binding partner present that stabilises the closed dimer conformation, which is removed when activated. This could then allow for the binding of proteins such as p53. This notion supports evidence that found that although ATM phosphorylates p53 in response to DNA damage, binding of p53 to ATM could

only be detected after ATM activation. Moreover, the authors suggest that activating partners such as NBS1 and ATMIN (ATM Interactor), both of which are essential in the DNA damage response, might bind to this N-terminal region to lock ATM in an open confirmation.

This complex protein, whether in monomer or dimer form, is an apex protein kinase that is best known for its role in DNA damage.

2.2 ATM and the DNA Damage Response Pathway:

DNA is found in every cell and is, in essence, the keystone of life. Nonetheless, these molecules are in constant peril from exogenous and endogenous threats that include carcinogens, mutagens, reactive oxygen species (ROS) and spontaneous chemical changes during cellular replication.

Alterations that can range from a single basepair substitution in a DNA sequence to major chromosomal aberrations are sufficient to disrupt cellular homeostasis and pave the way for the development of cancer (Shiloh 2003). However, a cell has strict safeguards in place to protect itself against this constant barrage of existential threats. These safeguards, which include ATM as a key component, are cell cycle checkpoints that ensure timing, sequence and integrity of vital cell cycle events and mediate cellular responses to exogenous genotoxic stress (Sarkaria et al. 1999). If these fail, programmed cell death (apoptosis) follows.

Structurally intact and functional ATM is vital to this process: a single mutation in the kinase region of ATM is sufficient to disrupt the stability of ATM and drive the development of A-T (R2849P) or leukemia (R2186P) (Baretić et al. 2017).

ATM is consequently best known for its role in the prevention, signalling and repair of double strand breaks (DSB) in nuclear DNA and has been reviewed extensively (Shiloh 2001; Rotman & Shiloh 1998; Shiloh 2006; Paull 2015; Shiloh & Ziv 2012). DSB's can occur during eukaryotic mitosis and meiosis when forming replication forks, or in response to ionizing radiation (IR) and ultra violet (UV) light. There are two major pathways for DSB repair: homologous repair (HR) or non-homologous end-joining (NHEJ) (Hartlerode & Scully 2009),

and both are essential during the synthesis (S)-phase of mitotic cell replication. In a nutshell, nuclear ATM protein kinase prevents the formation of DSBs by restricting the replication of DNA containing single strand breaks (Khoronenkova & Dianov 2015). Should that fail, it can mobilize one of the most extensive cellular signalling networks, the so-called DDR (DNA damage response), in response to DSB's (Tomimatsu et al. 2007). The type of DNA damage determines the DDR response, and in cases where agents such as IR and free radicals inflict sufficient damage, the cell mounts a rapid, decisive response that activates ATM (Shiloh 2003). The absence of ATM, however, does not limit the rate of DSB repair: up to approximately 85% of all DSB's can be repaired through other cellular mechanisms, whilst only 15% of DSB's, such as radiation-induced breaks, necessitates ATM (Goodarzi et al. 2010).

DNA-PKcs play a role in NHEJ, which is also the predominant, albeit not the most accurate pathway for DSB repair in human cells, whilst ATM promotes the HR pathway that results in more accurate corrections of DSBs (Shiloh & Ziv 2012; Zhou et al. 2017). It is, however not clear how pathways are chosen in response to DSBs during the G1, S and G2 phase of cell replication. A recent study by Zhou et al. (2017) shows that crosstalk between DNA-PKcs and ATM might cooperatively initiate signalling and repair through the phosphorylation of ATM at multiple sites, which in turn negatively regulates the catalytic activity of ATM. Consequently, this might provide a mechanism for the DSB repair pathway choice as well as ATM inactivation upon repair.

Briefly, the DDR, which includes both the HR and NHEJ pathways, consists of four phases: 1) sensor proteins detect the DNA lesion or chromatin aberration immediately following a break; 2) the broken ends are processed in order to determine the type of response required based on the chemical nature of the breaks; 3) proteins, also known as transducers, that can quickly affect the operation of many pathways and often form part of the repair complexes at the site of damage, are recruited and activated; 4) once activated, transducers, can activate so-called effector proteins that determine cell-cycle checkpoints, activate the stress-response pathway or drive repair enzymes and complexes to repair DNA. The PIKK proteins, ATM, ATR and DNA-PKcs are initial and primary transducers in DSBs and phosphorylate many down-stream effectors, which, in the case of ATM, include proteins such as the cell cycle check point kinases, CHK1, CHK2, histone H2A variant (H2AX), breast

cancer type 1 susceptibility protein (BRCA1) and the tumour suppressor protein, p53 (Shiloh 2003; Bensimon et al. 2011).

Immediately following a DSB, nuclear ATM is catalytically activated, undergoes autophosphorylation at Ser^{1981} and is monomerised (Bakkenist & Kastan 2003). This is the initial step in ATM activation and requires the MRN (Mre11, Rad50 and Nbs1) protein complex to be fully completed (Paull 2015). The MRN complex is a large, multifunctional protein assembly; the Mre11 component contributes endo-and exonucleolytic activity whilst the Rad50 component provides ATP binding, hydrolysis, and adenylate kinase activity, which also determines its two different conformational states (Lee et al. 2013). The complex, that can bind to DNA through multiple interfaces such as DNA without sticky ends, only forms stable complexes with DNA ends in the presence of ATP, and is a requirement for ATM activation (Paull 2015). In addition to the interface between Nbs1 and ATM (mentioned in Section 2.1), Mre11-Rad50, that is bound through coiled-coil domains and a zinc-hook, allows for association with ATP and Nbs1, and binds to ATM through an interface located in the Rad50 protein (Lee et al. 2013; Paull 2015). Once bound, the complex can stimulate ATM activity by facilitating stable binding to its substrates (Lee & Paull 2004). Interestingly, the Nbs1 phosphorylation is critical for MRN mediated stimulation of ATM activity with regards to CHK2 but not to p53 (Lee & Paull 2004), whilst downstream p53 signalling is dependent on ATM activity and DSB repair efficiency that differs in different cell types and tissues (Stewart-Ornstein & Lahav 2017).

Although this sets the stage for the carefully orchestrated role of ATM in the DDR, the recruitment of the protein and maintenance of the ATM-MRN complex is still being elucidated. It is known that phosphorylation of Ser^{1981}, as well as the conserved sites, Ser^{367}, Ser^{1893} and Ser^{2996} are required for full activation of ATM in response to DSBs (Lavin 2008); nonetheless, mutations in mice analogues of these sites have no effect on the ATM dependent response (Daniel et al. 2008; Pellegrini et al. 2006). Autophosphorylation at Ser^{1981} is required for stabilisation of ATM at DSBs and allows for interaction with MDC1 (Mediator Of DNA Damage Checkpoint 1) resulting in prolonged association of ATM with DSBs (So et al. 2009). MDC1 tethers ATM to the DNA and binds directly to the phosphorylated tail of H2AX, which drives the recruitment of proteins to the DSB. Almost immediately following a DSB, ATM phosphorylates H2AX at Ser^{139}, which results in

chromatin decondensation and is essential for efficient DNA repair and protein recruitment such as BRCA1 and p53 (Burma et al. 2001).

Moreover, prior to autophosphorylation of ATM at Ser^{1981}, the protein undergoes acetylation at Lys^{3016} by Tip60 which is essential for the conversion of an inactive dimer to monomer (Sun et al. 2007). This process is mediated by Forkhead Box O3 (FOXO3a) and Tip60: the carboxy-terminal of domain of FOXO3a binds directly to the FATC-domain of ATM (Tsai et al. 2008) and forms a complex with ATM and Tip60 that in turn, binds to the MRN complex. This can be inhibited by NOTCH1 that competes with FOXO3 binding to ATM (Adamowicz et al. 2016). Concomitantly, Tip60 interacts directly with the chromodomain of histone H3 trimethylated on lysine 9 (H3k9me3) at DSBs, which in turn activates the acetyltransferase activity of Tip60 (Sun et al. 2009). Interestingly, Tip60 is recruited to H3k9me3 by the MRN complex, but is dependent on the initial displacement of heterochromatin protein 1β (HP1β) from H3k9me3. Tip60 can thus regulate the activation of both ATM and DNA-PKcs through the conserved FATC domain present in both proteins (Jiang et al. 2006). These observations can explain why chromatin alterations, rather than direct DNA contact, can act as a signal for ATM mediated DDR, as was noted originally by Bakkenist & Kastan (2003).

Baretić et al. (2017) suggests that Lys^{3016} is close enough to either Glu^{3021} or Tyr^{2864}, both of which have been implied in the closed dimer conformation of ATM, that their side-chains might interact prior to and break upon Lys^{3016} acetylation, resulting in a conformational change that could potentially favour an open dimer conformation. Interestingly, ATM can also be phosphorylated at Tyr^{370} by the nuclear epidermal growth factor receptor (EGFR) which translocates to and co-localizes with ATM at the site of a DSB (Lee et al. 2015). This implies that sites within the N-terminal spiral could also be required for ATM activation in response to DSBs, and not just the FATC kinase domain. This notion is supported by the recent study where it was found that DNA-PKcs can phosphorylate Thr^{86} and Thr^{373} within the ATM N-terminal HEAT repeat and is required, together with Thr^{370}, Ser^{794} and Ser^{1403}, for the regulation of ATM activity (Zhou et al. 2017). Phosphorylation of Thr^{86} by DNA-PKc peaks approximately 2-4 hours after DNA damage, which suggests that the phosphorylation of this site might offer a critical mechanism for ATM inactivation after DNA repair.

Moreover, phosphorylation of DNA-PKcs by ATM at Thr^{2609} is essential for effective DNA repair, suggesting a cooperative relationship between these two PIKKs (Chen et al. 2007)

ATM, which can also repair DSBs in heterochromatic regions (Goodarzi et al. 2010), initiates a cascade of phosphorylation events as well as protein recruitment of major cellular role-players (effectors) that can either arrest the cell cycle, repair DNA or initiate apoptosis (Bhatti et al. 2011).

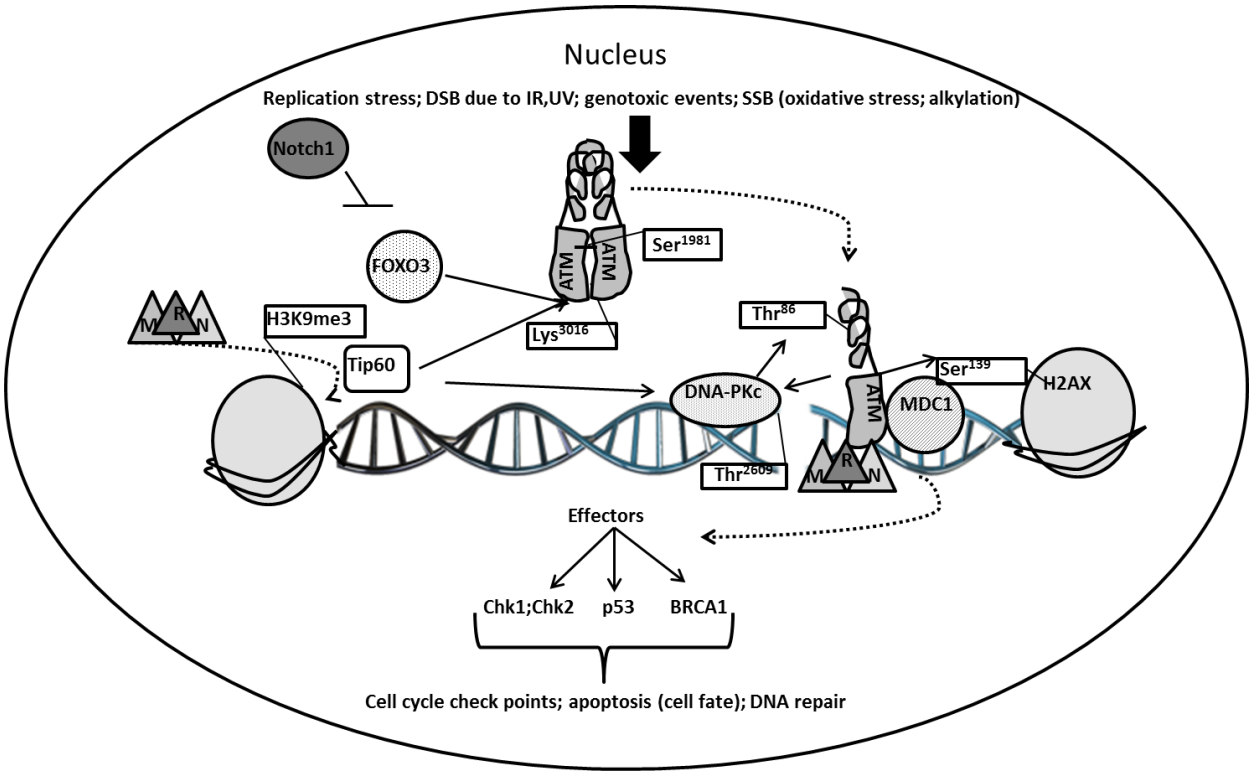

Figure 2.2: Simplified schematic diagram of the role of ATM in the DNA damage response pathway. Briefly, ATM is recruited to DSB mainly through the MRN complex where it binds to Rad50 and Nbs1 (Lee et al. 2013)**. Prior to this the ATM dimer is acetylated by FOXO3a and Tip60, which in turn interacts with H3K9me3**(Sun et al. 2007)**. Monomerised ATM phosphorylates H2AX at Ser^{139}, which in turn binds to Mdc1**(So et al. 2009)**. Mdc1 tethers ATM to DNA, and through the activation of H2AX, and can drive the recruitment of BRCA1 for DNA repair. ATM can phosphorylate, and in turn be phosphorylated by, DNA-PKcs which mediates a cooperative relationship of regulation**(Zhou et al. 2017)**. ATM also phosphorylates effectors such as (but not limited to) Chk1 and 2 to modulate cell cycle checkpoints or p53 to determine cell fate**(Shiloh & Ziv 2012)**.**

ATM can also be activated in response to DNA damaging agents that cause base oxidation such hydrogen peroxide (H_2O_2) (Guo et al. 2010) as well as alkylation (Adamson et al. 2002). Alkylated and oxidised DNA bases are mainly repaired by the base excision repair (BER) pathway. The pathway generates single strand breaks (SSBs) as intermediate products when a damaged base pair is excised, in order to create an abasic site (AP site) that can be

processed by a DNA polymerase and ligated (Dianov & Hübscher 2013). ATM is activated in response to SSBs generated during the repair of oxidative or alkylating DNA lesions, and result in a G1 cycle delay that allows for the ligation of SSBs (Khoronenkova & Dianov 2015). These base lesions do not activate ATM directly, but both oxidative stress and methyl methanesulfonate (MMS) can activate ATM through autophosphorylation (Khoronenkova & Dianov 2015).

This section briefly summarises (Figure 2.2) the fine-tuned role of ATM in the DDR. The number of substrates phosphorylated directly and indirectly by ATM spans across a network that counts into the hundreds. ATM is at the apex of cell cycle checkpoints, apoptosis, immune response, gene transcription and cell fate modulation pathways (Shiloh & Ziv 2012). Many of these responses stretch past the nucleus, and highlight the key question of ATM's role in cellular metabolism independently of the DDR.

Whilst the elucidation of ATM as a vital DDR transducer contribute towards a clearer picture of the severe radiosensitivity and increased cancer predisposition seen in A-T patients, it is the observation that ATM can be activated by oxidative stress (Guo et al. 2010) that might explain the plethora of metabolic and cardiovascular effects (reviewed by Espach et al. 2015) observed in the absence of ATM protein kinase.

2.3 Cytosolic ATM and oxidative stress

Shortly after the description of ATM as a single protein kinase, Barlow et al. (1996) noted oxidative stress markers in *Atm* deficient ($ATM^{-/-}$) mice organs that could not be explained on a histological level. The authors suggested an alternative pathway independent from p53 (DDR pathway) which was also reiterated by Shackelford et al. (2001), who found that phosphorylated ATM responds to certain aspects of oxidative stress. It was suggested that increased oxidative stress observed in the cerebella of these mice correspond with the degeneration of cerebellar neurons in A-T patients (Kamsler et al. 2001).

Constant oxidative stress is a common denominator in many of the A-T clinical and cellular phenotypes (Barzilai et al. 2002). This results in prolonged activation of stress response pathways in the cerebellum, but not in the cerebrum or liver (Watters 2003). More importantly, this suggests a cytoplasmic rather than nuclear role for ATM. Whereas ATM

resides predominantly in the nucleus of dividing cells (Shiloh 2003), ATM is found mainly in the cytoplasm of non-dividing neuronal cells where it maintains basal metabolic flux (Alexander & Walker 2011). In these types of cells, ATM maintains autophagy, a catabolic process in which cells deliver cytoplasmic components for degradation to the lysosome, as well as redox homeostasis rather than genomic stability and apoptosis. Moreover, Alexander & Walker (2011) suggested that these divergent pathways could be a result of ATM's subcellular localisation, as well as different mechanisms of activation and cell survival outcomes.

This observation was based on the seminal research of (Guo et al. 2010) who reported the direct activation of ATM by oxidative stress (H_2O_2). Previous research showed that ATM can be activated in response to oxidative stress and hypoxic conditions (Shackelford et al. 2001; Bencokova et al. 2009), but the question remained whether these events were initiated independently of the MRN pathway. (Guo et al. 2010) generated oxidative stress conditions with H_2O_2 and DSB with bleomycin, a well-known genotoxic agent, in human fibroblasts. Although p53 was phosphorylated at Ser^{15} and Thr^{68} in response to H_2O_2 and bleomycin, H2AX was only phosphorylated in response to the latter. Inhibition of ATM ablated p53, ATM and Chk2 phosphorylation in the presence of H_2O_2, whilst activation of ATM by H_2O_2 was inhibited in the presence of the strong hydroxyl scavenger, N-acetylcysteine (NAC). The authors found that oxidation resulted in a conformational change in ATM, but not the monomerisation observed in response to a DSB. Moreover, they found that ATM forms a reversible disulphide bond at the only cysteine site, Cys^{2991} within the FATKIN region. Mutation of this site from Cys^{2991} to Ala^{2991} resulted in a construct that could be activated in the presence of DSBs but not oxidative stress. Although ATM contains several disulphide bonds, it is the covalent disulphide bond at Cys^{2991} through which ROS modulates its effects. Low levels of ROS are sufficient to activate ATM at this residue, independently of DSBs and the MRN complex (Paull 2015), and these distinct activation mechanisms allow ATM to respond to different stresses and control different cytoplasmic pathways (Shiloh & Ziv 2013).

However, it should be noted that the interplay between oxidised ATM and DSB-activated ATM is complicated: (Guo et al. 2010) suggested that oxidative stress disrupts DNA binding at the MRN complex and can therefore inhibit consequent ATM activation by DSBs, resulting

in the oxidation of ATM under high ROS conditions. A more recent study showed that excess endogenous ROS represses ATM-dependent HR repair in cells obtained from patients with ataxia with oculomotor apraxia type 3 (AOA3 cells) which has implications for both neurodegeneration and tumorigenesis (Kobayashi et al. 2015). Irrespective of the lack of consensus regarding the oxidation of ATM under either high or low ROS conditions, many of the ATM substrates identified with proteomic analyses, implies ATM in metabolic signalling pathways (Ditch & Paull 2012).

2.3.1 Reactive oxygen and nitrogen species:

Under normal physiological conditions, ROS act as signalling intermediates in many cellular processes to induce redox homeostasis. On the other hand, elevated ROS levels, aptly described as oxidative stress, have been linked with over 150 diseases, most notably atherosclerosis, diabetes and cancer (Alexander et al. 2010). Moreover, it has been suggested that A-T might in essence be an oxidative stress disorder (Ambrose & Gatti 2013). In order to understand how ATM contributes towards the maintenance of basal metabolic flux and redox homeostasis, a short overview of oxidants and their cellular targets is required.

Briefly, ROS derive from the reduction of molecular oxygen which most notably includes oxygen radicals ($O_2^{\bullet-}$), hydroxyl ($^{\bullet}OH$), peroxyl ($RO_2\bullet$) and alkoxyl ($RO\bullet$), as well as certain non-radicals that are either oxidising agents or which can be converted into radicals such as hypochlorous acid (HOCl), ozone (O_3), single oxygen ($^1O_2$) and H_2O_2 (Bedard & Krause 2007). Metabolism of nitric oxide (NO) results in the formation of reactive nitrogen species (RNS) that can either contribute to oxidation, nitrosation or nitration (Patel et al. 1999). The enzymatic action of nitric oxide synthase (NOS) results in nitric oxide (NO), but can also produce $O_2^{\bullet-}$ under the right circumstances. A rapid reaction between NO and $O_2^{\bullet-}$ results in the formation of peroxynitrite (ONOOH) which is involved in oxidation, nitrosation and nitration. In the case of nitration, nitrotyrosine can be formed and can alter cell signalling pathways. For example, nitrite together with HOCl, has been detected in diseased human vascular tissue and drives the formation of artherogenic LDL which is implicated in artheroschlerosis (Podrez et al. 1999).

There are numerous sources of endogenous ROS, including the cytoplasm, cell membrane, endoplasmic reticulum (ER), peroxisome, mitochondria and the NOX-family (nicotinamide adenine dinucleotide phosphate [NADPH] oxidases) of which the latter two are the most important (Finkel 2011). NOX1, -2, -4 and -5 are expressed throughout the cardiovascular system and are one of the best known sources of cytoplasmic ROS, which in itself has been described as the cornerstone of cellular signalling and disease pathophysiology (Forrester et al. 2018). This is made possible by the large number of molecules that ROS can interact with, including small organic molecules, proteins, lipids, carbohydrates and nucleic acids. These interactions can either destroy or irreversibly change the function of the target molecule and can accordingly contribute towards pathogenesis (Bedard & Krause 2007).

Most redox reactions, however, occur through the reversible reduction and oxidation of crucial reactive cysteine residues that can form thiolate anions at a physiological pH (Holmström & Finkel 2014). Oxidation of this residue, as is the case for ATM at Cys^{2991}, results in a sulfenic residue (SOH), which is further modified to form an intramolecular disulphide bond. As mentioned previously, the addition of exogenous H_2O_2 *in vitro* forms an active ATM dimer of two covalently-linked monomers. Possible *in vivo* sources of oxidants, that are capable of reducing thiol and oxidizing disulphide bonds, are generated by the membrane bound NOX-family of NADPH oxidases. These enzymes produce extra-cellular super-oxide anions, that can be dismutated into H_2O_2 and selectively re-enter the cell through aquaporin channels (Finkel 2011).

NOX-4, which is located in close proximity of the nucleus in a wide range of human cells, produces ROS innately and is elevated in A-T cells (Weyemi et al. 2015). Specific inhibition of both NOX-4 and NOX-2 alleviates increased cancer risk in A-T null mice to that of control animals, whilst the inhibition of ATM increases NOX-4 expression in normal cells. NOX-4 is thus potentially a critical mediator of ROS and senescence in the development of A-T. On the other hand, mitochondrial oxidants that are produced as part of normal respiration, also participate in signalling events as well as the regulation of hypoxia-inducible factor 1 (HIF-1α) during low oxygen conditions.

2.3.2 ATM and oxygen sensing:

The transcription factor complex, HIF-1α, is a master regulator of oxygen sensing and mediates a genetic response to restore oxygen supply under low oxygen conditions (Fandrey et al. 2006). The complex can restore oxygen homeostasis by either increasing anaerobically stimulated glycolytic flux or by improving tissue oxygenation via stimulation of angiogenesis, vasodilation and erythropoiesis. However, the underlying mechanisms of oxygen sensing remain elusive. Guzy et al. (2005) found that cytosolic ROS is released by complex III of the mitochondrial electron transfer chain (ETC) and is required for hypoxic stabilization of HIF-1α in response to low oxygen conditions.

Interestingly, the absence of ATM leads to increased expression of HIF-1α which results in the transcription of genes involved in angiogenesis e.g., VEGF (vascular endothelial growth factor) as well as cellular metabolism e.g., GLUT-1 (Ousset et al. 2010). Additionally, it was suggested in this study that the absence of ATM increases HIF-1 protein biosynthesis, and that this effect is dependent on oxidative stress. ATM might thus act as an oxygen sensor - cells lacking ATM show a blunted response to mild hypoxia and cannot up- regulate HIF-1α due to impaired oxygen sensing (Mongiardi et al. 2011). Hypoxia also leads to the phosphorylation and activation of ATM in the absence of DNA damage and increase mitochondrial ROS production (Bencokova et al. 2009).

In line with this finding, Cam et al. (2010) showed that ATM phosphorylates HIF-1α on Ser^{696} and directly regulates the stabilisation of this protein under hypoxic conditions, consequently leading to the downregulation of mTORC1 (mammalian Target of Rapamycin Complex 1). Moreover, both Cam et al. (2010) and Bencokova et al. (2009) found that translocation of HIF-1α to the nucleus is attenuated in *Atm*-deficient cells, where it regulates the expression of hypoxia-inducible genes such as REDD1 (Regulated in development and DNA-damage response 1). REDD1 acts as a negative regulator of mTORC1 by binding to the inhibitory 14-3-3α proteins which enables dissociation from the tuberous sclerosis complex 2 (TSC2 complex) and results in the inhibition of mTORC1.

This mechanism implicates a cytosolic role for ATM in cancer where the down regulation of ATM drives elevated mTORC1 activity in hypoxic tumour tissue (Stagni et al. 2013). This also

holds for childhood sarcoma, where a negative feedback loop was identified between mTORC1 and ATM; mTORC1 negatively regulates ATM expression through upregulation of the small microRNAs 18a and 421 (Hu et al. 2010), both of which targets ATM for degradation (Shen & Houghton 2013).

This has important implications for cancer, since increased autophagy in hypoxic tumour tissue is associated with treatment resistance, for example in the case of glioblastoma (Jawhari et al. 2016). More importantly, autophagy is negatively regulated by mTORC1, and concomitantly increases in cells treated with H_2O_2.

2.3.3 ATM, autophagy and the peroxisome:

In light of the hypoxic and oxidative stress induced activation of ATM , as well as the pathophysiology associated with elevated ROS in *Atm*-deficient cells, Alexander et al. (2010) found that the activation of oxidised ATM increases autophagy through the activation of TSC2 via the Liver kinase B1 (LKB1)/ 5' adenosine monophosphate-activated protein kinase (AMPK) pathway, and results in the repression of mTORC1. Moreover, inhibition of mTORC1 with rapamycin results in the concomitant improvement of ROS levels in $ATM^{-/-}$ mice. The authors found that low concentrations of H_2O_2 rapidly induced mTORC1 repression that could, in turn, be rescued by the addition of NAC or pretreatment with catalase. Of relevance as well, is that chemical mitochondrial uncoupling which depletes glutathione, also repressed mTORC1 signalling, indicating that both exogenous and endogenous ROS activation of ATM can induce mTORC1 repression.

The same research group found that nitrosative stress (nitric oxide, NO) also activates ATM and results in the phosphorylation of AMPK through LKB1, activation of the TSC2 complex and consequent repression of mTORC1 (Tripathi et al. 2013). ATM-mediated repression of mTORC1 decreased phosphorylation of direct target proteins of mTORC1 such as 4E-BP1 (4E-binding protein 1), S6K (ribosomal S6 kinase) and ULK1 (Unc-51 like autophagy activating kinase). Consequently, nitrosative stress-mediated activation of ATM can increase autophagy by decreasing mTORC1-mediated phosphorylation of ULK1 at Ser^{757}, and increasing ULK1- phosphorylation at Ser^{317} by AMPK. However, the precise mechanism through which NO activates ATM is still unknown. Induction of autophagy by NO also

resulted in decreased cell viability, which suggests a cytotoxic response. This is summarised in Fig 2.3.

LKB1 can be phosphorylated directly at Thr^{366} by active ATM in response to ionising radiation (IR) (Sapkota et al. 2002) as well as through oxidative stress as discussed previously; consequently activating AMPK directly to modulate apoptosis (Shaw et al. 2004) or autophagy in the event of energetic stress.

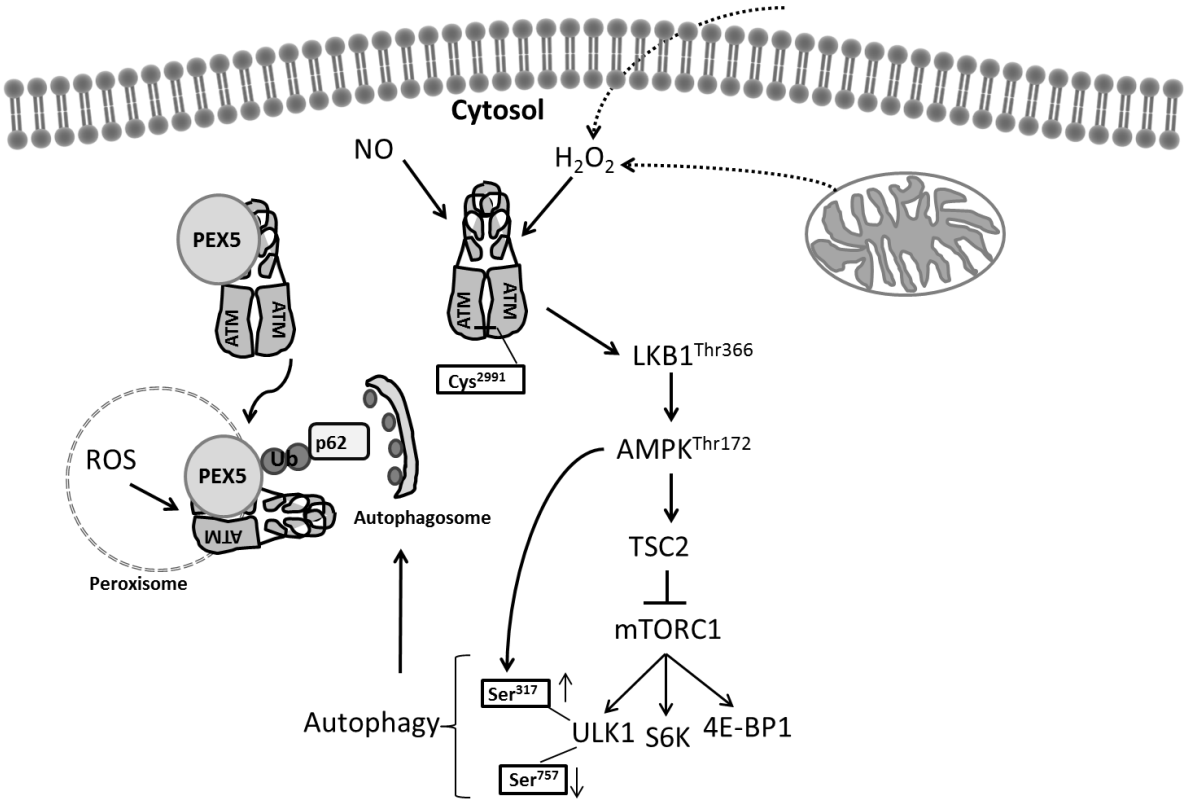

Figure 2.3: ROS can activate cytosolic ATM. ATM is activated in response to both endogenous and exogenous ROS, as well as NO. Once activated, it phosphorylates LKB1 at Thr366 which phosphorylates AMPK and drives the inhibition of mTORC1 through TSC2. The inhibition of mTORC1 down regulates S6K, 4E-BP1 and ULK1, which is also phosphorylated by AMPK. This initiates autophagy, and the formation of an autophagosome that targets peroxisomes specifically for degradation through the ATM-mediated ubiquitination of PEX5.

On the other hand, one of the key roles of AMPK in cardiac muscles is the response to hypoxia/ ischaemia, which is also under the direct control of LKB1; in the absence of LKB1, mice hearts show increased mTORC1 signalling which increases protein synthesis and can lead to hypertrophy (Ikeda et al. 2009). Interestingly, Emerling et al. (2009) showed that the hypoxic activation of AMPK in mouse fibroblasts is dependent on mitochondrial oxidative stress that is generated through the ETC and not the cytosolic adenosine monophosphate

(AMP)/ adenosine triphosphate (ATP) ratio. Although the authors did not evaluate the role of ATM in their study, it supports the notion that the oxidative activation of ATM, due to increased mitochondrial dysfunction, can potentially mediate the activation of AMPK in response to hypoxic stress. The total effect of AMPK activation results in the inhibition of lipid and glycogen synthesis, whilst concurrently activating free fatty acid oxidation and glycolysis (Kim et al. 2016).

Peroxisomes utilise β-oxidation to reduce long-chain fatty acids into medium length fatty acids that can be shuttled to the mitochondria. These highly metabolic organelles generate ROS during β-oxidation, and require homeostatic maintenance to prevent oxidative stress. ATM binds to the peroxisome importer receptor, PEX5, in response to excessive ROS and mediates peroxisome-specific autophagy (pexophagy) by phosphorylating PEX5 at Ser^{141} and promoting mono-ubiquitylation at Lys^{209}, whilst simultaneously inducing autophagy through the activation and phosphorylation of TSC2 and ULK1 (Zhang et al. 2015; Tripathi et al. 2016) and is shown in Fig 2.3. Ubiquitylated PEX5 is recognized by the autophagy adapter protein, p62, which directs the autophagosome to the peroxisomes for pexophagy. It is currently not known whether ATM binds PEX5 as a monomer or dimer.

Pexophagy is an example of selective autophagy that only targets peroxisomes, whereas macroautophagy is responsible for the general sequestering of organelles, proteins and portions of the cytoplasm for delivery to, and degradation by, the lysosome (He & Klionsky 2009). The importance of ATM in autophagy is highlighted by the accumulation of lysosomes, as well as increased oxidative stress in the cerebellum of ATM-null mice (Barlow et al. 2000). Loss-of function mutations in ATM, such as the ability to sense oxidative stress, can result in a reduction in mitochondrial antioxidant defences, lead to the accumulation of ROS and oxidative damage to mitochondria and other cellular components (Zhang et al. 2018), as well as protein aggregation (Lee et al. 2018). Selective autophagy seems to be mainly mediated by ubiquitination which is essential for conferring selectivity (Kraft et al. 2010), as is the case of ATM-mediated pexophagy. This also implies a potential role for ATM in aggrephagy (degradation of damaged or misfolded proteins) that is dependent on p62 ubiquitination (Evans et al. 2017). Proteasomal degradation is required for the maintenance of autophagy at physiological levels as is the case with ULK1; it is specifically ubiquitinated by the E3 ligase NEDD44 that marks it for proteasomal degradation, whilst still actively

translating and transcribing ULK1 mRNA that is inhibited by mTOR during prolonged autophagy (Nazio & Cecconi 2017). This maintains ULK1 protein at basal levels within the cell, and makes it available if needed.

It is possible that ATM can play a more active role in ULK1 phosphorylation through p32. Although p32 was first recognized as a novel substrate of ATM in cardiac DNA damage (Kato et al. 2008), it has recently been identified as a regulator of ULK1 stability (Jiao et al. 2015). Moreover, the phosphorylation of ULK1 by AMPK regulates the translocation of ULK1 to mitochondria in response to hypoxia (Tian et al. 2015) where it phosphorylates FUNDC1 and regulates mitophagy (Wu et al. 2014). Although ATM was not investigated in this context, it is tempting to hypothesize that ATM could influence ULK1 potentially through the phosphorylation of p32 in the heart.

Protein aggregation is classically associated with neurodegeneration but has been observed in nearly every cardiometabolic disease (Evans et al. 2017). It is, of course, well known that the accumulation of proteins and dysfunctional organelles contribute to the development of pathology in almost all tissues, and thus require a very fine balance between apoptosis and autophagy. There seems to be synergistic roles for ATM and p53 with regards to the regulation of autophagy, where ATM regulates mitochondrial homeostasis and oxidative stress in order to prevent cells from undergoing apoptosis in response to non-genotoxic p53 activation (Sullivan et al. 2015)

In a nutshell, autophagy is a catabolic process that is responsible for the degradation and recycling of damaged organelles, and is central to the maintenance of cellular homeostasis. The activation of ATM through ROS and NO places ATM directly upstream of AMPK, which in turn, drives the inhibition of mTORC1 and upregulation of autophagy through ULK1. This allows cells to eliminate damaged organelles that can drive increased oxidative stress and recycle these components to maintain nutrient and energy homeostasis.

Constitutive autophagy plays a protective role in mitochondrial rich cardiomyocytes, where accumulation of abnormal proteins and organelles, especially mitochondria, may directly cause cardiac dysfunction (Nishida et al. 2009).

2.3.4 ATM, glycolysis and the pentose phosphate pathway:

Overall, A-T patients' exhibit increased oxidative stress that can be improved by reducing mitochondrial ROS (D'Souza et al. 2012). Moreover, ATM promotes the overall antioxidant capacity in human cells by stimulating glucose-6-phosphate dehydrogenase (G6PD), a key enzyme in the pentose phosphate pathway (PPP), which leads to increased production of NADPH (nicotinamide adenine dinucleotide reduced; antioxidant co-factor) and nucleotide synthesis (Cosentino et al. 2011). This is mediated through ATM-mediated phosphorylation of p38 that can in turn phosphorylate Heat Shock Protein 27 (HSP27) in response to DNA damage (and is shown in Fig 2.4).

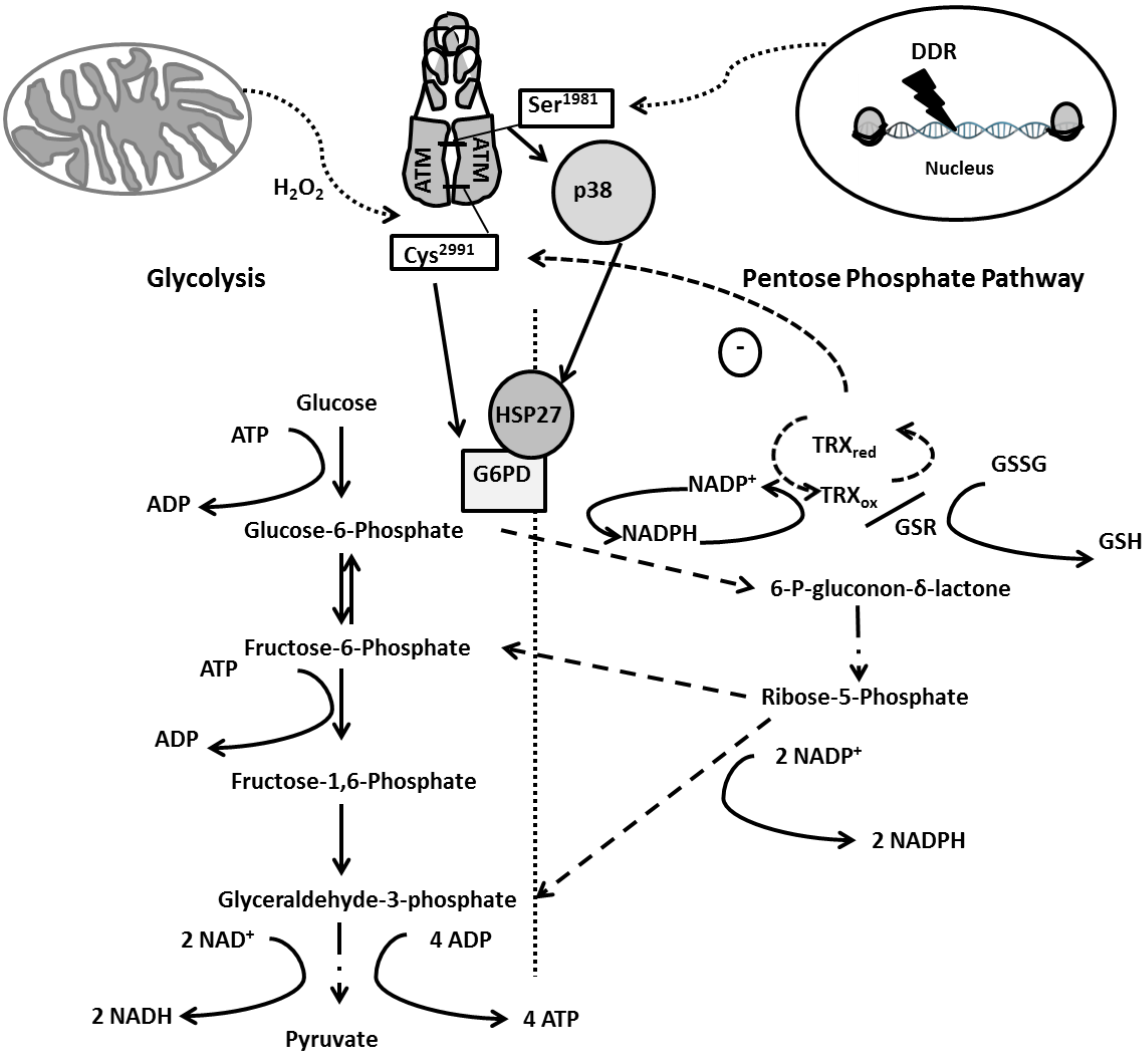

Figure 2.4: ATM acts as a cytosolic redox sensor in response to oxidative stress. ATM promotes glucose-6-phosphate dehydrogenase activity through the promotion of HSP27 phosphorylation by p38, and binding to G6PD in response to DNA damage to increase nucleotide production through ribose 5-phosphate (Cosentino et al. 2011)**. However, ATM can stimulate glucose flux through the**

PPP by increasing the abundance of G6PD in response to mitochondrial ROS and drive the regeneration of TRX1 which is potentially required for the reduction of ATM dimers, suggesting a negative feedback loop (Zhang et al. 2018)**.**

Interestingly, when investigating G6PD and NADPH levels in the context of obesity (Zucker rats), Serpillon et al. (2009) found significantly higher G6PD activity in obese Zucker rats (*fa/fa*) whereas superoxide dismutase (SOD) and glutathione peroxidase activity was significantly lower. Superoxide levels were elevated in the diabetic heart, and could be blocked by either a specific NOX inhibitor, through the inhibition of the mitochondrial ETC with either antimycin or rotenone, or through the inhibition of G6DP activity. It was found that in a model of severe hyperlipidaemia and hyperglycaemia, NOX-derived O_2^- generation was fuelled by elevated levels of PPP-derived NADPH production. Keeping in mind that NOX-4 is upregulated in A-T patient derived cells (Weyemi et al. 2015), it is might suggest a more specific role for ATM in the PPP when switching between oxidative to non-oxidative PPP, the latter of which drives NADPH production.

A progressive decrease in NADH, NAD^+ and $NADP^+$ have been observed in the cerebellum of ATM-null mice, whilst significantly higher levels of mitochondrial respiration was measured in the cerebrum of these mice compared to normal mice (Stern et al. 2002). Interestingly, NAD^+ replenishment improved DNA repair as well as mitochondrial homeostasis in ATM-null mice, and contributed towards the inhibition of thymic lymphoma development as well as increased lifespan (Fang et al. 2016).

Together with the pool of cytosolic NADH/NAD^+, glutathione (GSH) and thioredoxin (TRX) as well as NADPH/$NADP^+$ in the cytosol, there are also separate but interacting pools of these redox couples present in the mitochondrial intermembrane space and matrix. The GSH/TRX systems in the mitochondria are essential for the maintenance of H_2O_2 (Aon et al. 2012), and raise the question whether ATM can influence these redox couples in the mitochondria as well.

2.4. ATM, mitochondria and mitophagy:

Mitochondrial dysfunction that is linked to increased oxidative stress, defective energy metabolism or defective autophagy, seems to lie at the heart of ATM-deficiency. In light of the emerging role of ATM as a redox sensor and the role of oxidative stress in the

development of cardiovascular disease, a better understanding of ATM's role in mitochondria is required.

2.4.1 Mitochondrial morphology and function:

Mitochondria are essential, highly dynamic organelles which play an essential role in metabolism that goes beyond oxidative phosphorylation and includes fatty acid metabolism, amino acid catabolism, biosynthesis of heme and iron sulphur clusters as well as calcium storage to name but a few (Shadel & Horvath 2015; Roberts Stein & Shin-ichiro 2012). Cardiomyocytes are rich in mitochondria, and the normal heart can produce as much as 95% of the ATP required through oxidative phosphorylation (Lopaschuk et al. 2010). The vast amount of ATP produced in the heart is required for contractility, maintaining basal metabolic processes and ionic homeostasis. However, mitochondria are also the foremost source of ROS, and if dysfunctional, can contribute to cardiomyocyte death and heart failure (Tong & Sadoshima 2016).

These organelles are complex, both in form and function. Briefly, the outer mitochondrial membrane (OMM) surrounds the organelle and separates the inner mitochondrial membrane (IMM) and intermembrane space from the cytosol. The outer mitochondrial membrane acts as a permeability barrier for proteins larger than 1.5 kDa, whilst the inner mitochondrial membrane plays host to the electron transfer chain (ETC), phosphorylation apparatus, and membrane transporters. Parts of the inner membrane run parallel to the outer membrane, whilst the majority of the membrane forms invaginations into the matrix, known as cristae. The areas where the cristae connect to the inner mitochondrial membrane are known as pedicles or cristae junctions (Figure 2.5) (reviewed by Lesnefsky et al. 2001). The IMM and OMM also fuse to form contact sites, which are essential for protein import, energy coupling and the import of fatty acids.

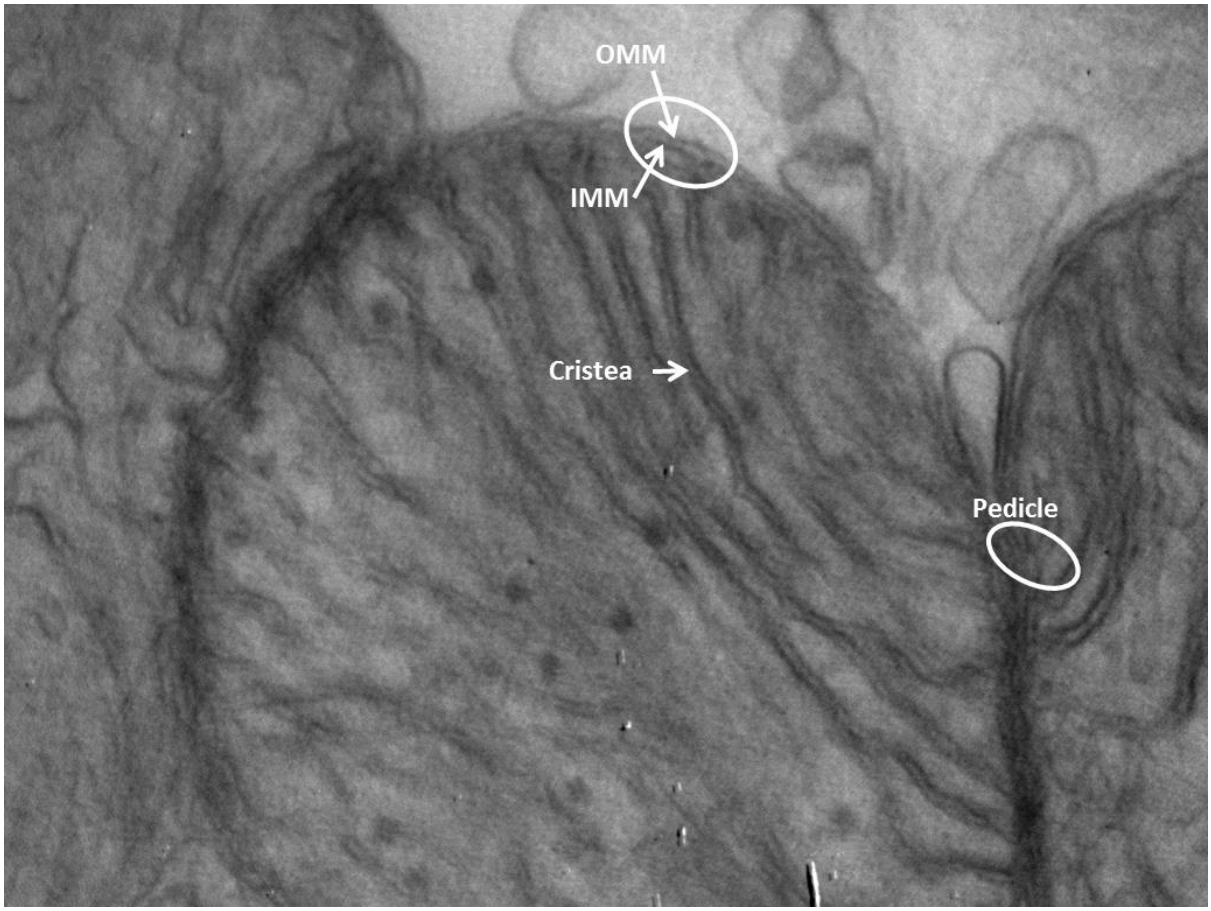

Figure 2.5: Electron micrograph of cardiac mitochondria isolated from a male Wistar rat. The arrows indicate the outer mitochondrial membrane (OMM) that encapsulates the mitochondrion and the inner mitochondrial membranes (IMM) that runs in parallel to the OMM, except where it forms invaginations into the matrix, known as cristae. The region where the cristae connect to the inner membrane is known as pedicles or cristae junctions (image generated at the National Health and Laboratory Services, Tygerberg Hospital, South Africa, courtesy of Mrs. N Muller).

The matrix contains metabolic enzymes, mitochondrial DNA and RNA, as well as the enzymes required for the tricarboxylic acid (TCA) cycle and fatty acid oxidation, all of which are critical for the maintenance of cellular energy metabolism (reviewed by Roberts Stein & Shin-ichiro 2012).

The mammalian mitochondrial genome is circular, double-stranded DNA that consists of approximately 16 600 base pairs which encodes for 13 coding genes that are transcribed into the protein subunits of the ETC, and a further 24 genes that specify ribosomal as well as transfer RNAs which are required for the synthesis of the 13 ETC proteins (Schon & Manfredi 2003). It has been suggested that the absence of ATM can lead to mtDNA copy number depletion, which suggests a role for ATM in either mtDNA replication or maintenance through dNTP synthesis (Eaton et al. 2007; Shadel 2008). Moreover, the

absence of ATM results in decreased mitochondrial DNA integrity and mitochondrial dysfunction that has been associated with defective mitochondrial DNA repair (Sharma et al. 2014). Interestingly, the latter study showed that whilst the mitochondrial DNA repair proteins were essentially normal, the absence of ATM specifically reduced DNA ligase III, which is involved in the mitochondrial base excision repair (BER) pathway. In light of the study by Khoronenkova & Dianov (2015) who showed that ATM is activated in response to single strand breaks in the BER pathway in nuclear DNA, the future study can address whether ATM can be activated in response to mtDNA breaks. Yhis has not yet been determined.

2.4.2 Electron transfer chain (ETC) and mitochondrial metabolism:

Mitochondria are best known for the ETC which consists of 5 complexes (shown in Fig 2.6): Complex I (NADH:ubiquinone-oxireductase), membrane bound Complex II (succinate ubiquinone oxidoreductase, also known as succinate dehydrogenase), Complex III (Coenzyme Q-cytochrome C oxireductase), Complex IV (cytochrome C oxidase, COX) and Complex V (ATP synthase also known as F_1F_0 complex). A proton gradient is generated across the inner mitochondrial membrane by the three large membrane complexes, Complex I, III and IV. Complex I feeds electrons (e^-) from NADH into the respiratory chain and transfers them to Coenzyme Q (ubiquinone) in the membrane. This releases energy that is used to pump four protons from the matrix to the inner membrane space where it maintains the proton gradient. Complex III receives the electrons from the reduced Coenzyme Q and transfer them to the electron carrier protein, Cytochrome *c*, which pumps one proton across the IMM in the process. Complex IV transfers the electrons from Cytochrome *c* to molecular oxygen and contributes to the proton gradient by using up to four protons per consumed O_2 molecule. Complex II transfers electrons directly to Coenzyme Q from succinate and does not contribute to the proton gradient (Figure 2.6, reviewed by Kühlbrandt 2015). The electrons are thus sequentially relayed through the complexes to reduce oxygen to water to generate the proton gradient required for ATP production.

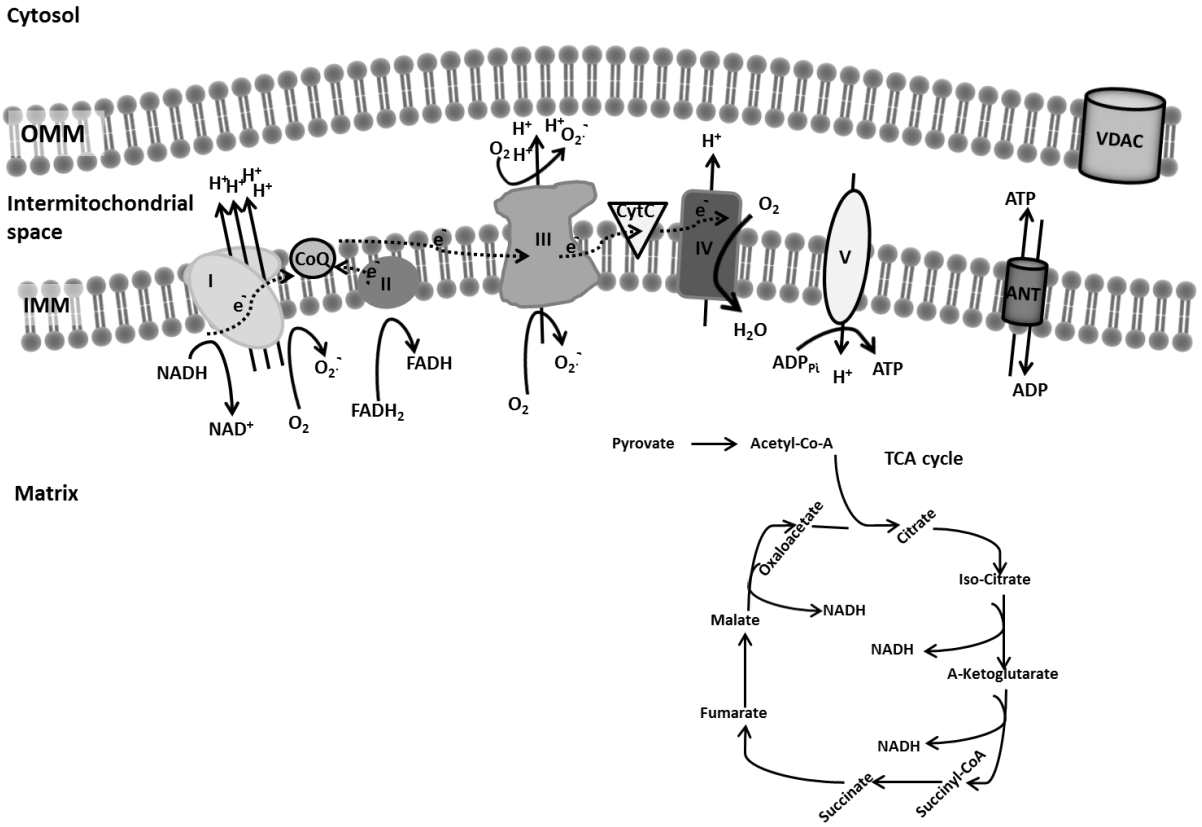

Figure 2.6: A simplified, schematic representation of the electron transfer chain (ETC) and oxidative phosphorylation. The figure (not drawn to scale) represents the ETC on the inner mitochondrial membrane, as well as the tricarboxylic acid cycle (TCA) that produces NADH which is oxidised by Complex I. Electrons are sequentially relayed from Complex I to Complex III and IV via Coenzyme Q (CoQ) and Cytochrome *c* (CytC), where molecular oxygen is converted to water. The proton gradient drives ATP production by ATP synthase (Complex V), which is exported out of the mitochondria in exchange for ADP by adenine nucleotide translocase (ANT). The voltage-dependent anion channel (VDAC) mediates the permeability of the outer membrane and can form contact sites with ANT to form a channel for Cytochrome *c* release which signals apoptosis (Williams et al. 2015).

The proton gradient, which changes the pH between the matrix and intermembrane space, together with the free energy released during the oxidation of NADH or flavin adenine dinucleotide ($FADH_2$) is stored as an electric potential, and is collectively responsible for the proton motive force (pmf) which drives proton leakage and ATP turnover (Brand & Nicholls 2011).

Complex I is the largest (1 MDa) and most complex of the three proton pumping complexes and consists of a matrix and a membrane arm. It also plays a central role in cellular bioenergetics and metabolism, and any defects in this complex result in a plethora of diseases, most notably neurodegenerative diseases (Sazanov 2015). The membrane arm of

Complex I contains eight Fe-S clusters that conduct the electrons from NADH to Coenzyme Q (Kühlbrandt 2015). It is however, still largely unknown how the transfer of electrons is coupled to proton translocation. Combined, the proton pumping complexes drive the translocation of ten protons for each NADH molecule that is oxidized. The coupling between the electron transfer and proton translocation can either be direct and involve chemical redox reaction intermediates that can be protonated or deprotonated and drives proton translocation, or indirectly through the mediation of long-range conformational changes (Sazanov 2015). Together, the three proton pumping complexes assemble into super complexes often referred to as respirasomes. Incorrect assembly of these respirasomes has been linked to decreased oxidative phosphorylation and the development of heart failure (Rosca et al. 2008).

The TCA cycle (also known as the Krebs cycle) generates NADH through NAD^+ which gains two electrons and a proton from several steps in the TCA cycle, and is reduced to NADH that is required for the ETC (Figure 2.6, adapted from Williams et al. 2015). In the healthy heart the TCA cycle utilizes acetyl-Coenzyme A (acetyl-CoA) that is generated mainly through the oxidation of fatty acids and glucose-pyruvate (Dorn et al. 2015). The rate of flux through the metabolic pathways is determined by the requirement for ATP to maintain the rate of ATP hydrolysis and the power generated by the myocardium, which is in turn is controlled by the expression of metabolic proteins and pathway regulation that is dependent on enzyme regulation and the substrate/product relationships (Stanley et al. 2005). Fatty acid oxidation is mediated by the carnitine-palmitoyl transferase shuttle (CPT) that imports fatty acids into the matrix where it can undergo β-oxidation that reduces FAD^+ and NAD^+ to $FADH_2$ and NADH, respectively, while producing acetyl-CoA (Cole et al. 2011).

Substrate-specific pathways are very important in the functioning of cardiac mitochondria, and have at least partially been associated with defects in cardiac oxidative capacity during pressure overload-induced heart failure (Bugger et al. 2010). Impaired metabolism also contributes to contractile dysfunction and left ventricular remodelling: a downregulation is observed in fatty acid oxidation, ETC activity and decreased mitochondrial flux whilst glycolysis and glucose oxidation increases in heart failure (Stanley et al. 2005). Furthermore, a high rate of β-oxidation serves as a cardiac metabolic hallmark of diabetes and obesity (Fukushima & Lopaschuk 2016). It is thus important to assess the ETC complexes in terms of

different substrates as this can give a good indication of potential mitochondrial dysfunction.

It is also possible to assess the function of isolated mitochondria with substrates specific to Complex I, II or III where the combination of glutamate and malate assesses the aspartate shuttle, and pyruvate and malate assesses the monocarboxylate and dicarboxylate transporters and pyruvate dehydrogenase (Rosca et al. 2008). Both substrate combinations produce NADH, which donates electrons to Complex I. The use of succinate in the presence of a Complex I inhibitor, such as rotenone, can be used to investigate Complex II, whereas palmitoyl-L-carnitine can be used to assess β-oxidation. Complex III, which is the major ROS producer and oxygen sensor during hypoxia (Guzy et al. 2005), can be inhibited with Antimycin C, which makes it possible to investigate to substrate utilization and individual complexes.

2.4.3 Mitochondrial oxidative stress:

Whereas most of the oxygen that is consumed is reduced to water, Complexes I and III can leak electrons, which leads to the generation of O_2^- due to the partial reduction of oxygen (Druzhyna et al. 2009). Superoxide can rapidly be dismutated into H_2O_2 by manganese superoxide dismutase (mnSOD), and is kept at minimal levels by the GSH/Trx ROS scavenging systems (Aon et al. 2012). Complex I and III are the major sites of ROS production in mitochondria (Finkel 2011). The inhibition of Complex I can reduce ROS production during ischaemia, whereas a blockade of electron flow to COX-IV can increase ROS production and oxidative damage (Chen et al. 2003).

The chronic oxidative stress observed in A-T has led to the suggestion that A-T might be a mitochondrial disease (Ambrose & Gatti 2013) and has also been linked with intrinsic mitochondrial dysfunction (Ambrose et al. 2007). The latter study found that lymphoblastoid cells from A-T patients contain an increased population of mitochondria with a decreased membrane potential, when compared to control cells. Proteins with specific roles in mitochondrial DNA damage and/or ROS scavenging, including mnSOD, peroxiredoxin 3 and mitochondrial topoisomerase, I are also elevated in these cells. Indeed, the decreased membrane potential translated into decreased respiratory activity in the A-T

cells compared to the wild type controls. This study was the first to show that ATM might be required for mitochondrial function. However, there are discrepancies between studies with regards to the role of ATM in mitochondrial content (Eaton et al. 2007; Ambrose et al. 2007). This was highlighted in the study by Valentin-Vega et al. (2012) who found increased mitochondrial content, contrary to the studies of Eaton et al. (2007) and Ambrose et al. (2007).

Concomitantly, the authors showed that the *in vivo* loss of *ATM* in mice resulted in mitochondrial dysfunction in thymocytes that was accompanied by increased mitochondrial content and mitochondrial ROS due to a decrease in mitophagy. Interestingly, they observed a significant decrease in Complex I activity as well as ATP production, and an increase in oxygen consumption. They also found that autophagy was not affected by the absence of ATM, and suggested that mitochondrial dynamics such as fission and fusion could contribute towards defective mitophagy. The authors concluded that the observed defects in the absence of ATM suggest that ATM might localise directly to mitochondria. Returning to a cellular model, fractionation studies revealed that the mitochondrial fraction of HepG2 cells was enriched with ATM and activated ATM in response to H_2O_2 treatment (Morita et al. 2014). In contrast to a previous study that found that ATM associates with the peroxisomal fraction (Watters et al. 1999), Morita et al. (2014) detected almost no ATM. However, we now know that ATM binds to and is imported into peroxisomes in response to oxidative stress (Zhang et al. 2015), and raises the question whether this is a cell-type specific phenomenon. This reverberates with the suggestion by Valentin-Vega et al. (2012) that both the cell type and culture conditions of immortalized A-T cells can affect mitochondrial homeostasis and autophagic responses which explain the differences in mitochondrial content reported in A-T deficient cell lines.

Mitochondrial respiration inhibition can also lead to increased mitochondrial ROS production. Treatment of HeLa cells with either rotenone or Antimycin C failed to increase mitochondrial hydrogen peroxide production although it did increase mitochondrial super oxide production (Zhang et al. 2018). Superoxide in itself failed to drive ATM dimerization, and suggests that mitochondrial super oxide must be converted to H_2O_2 in order to activate ATM in either the cytosol or nucleus of HeLa cells.

Taken together, these studies suggest very strongly that ATM could be localised to the mitochondria, but the effect of the absence of ATM seems to be context specific. Moreover, ATM might have an effect on the ETC: $ATM^{-/-}$ thymocytes exhibit decreased complex I activity (Valentin-Vega et al. 2012), whereas the chemical inhibition of ATM results in a post-translational decrease of COX-IV (Patel et al. 2011). This is interesting because the inhibition of COX-IV has been associated with increased ROS production at Complex I, albeit in the mitochondrial matrix (Chen et al. 2003).

Interestingly, Beclin-1 heterozygosity in $ATM^{-/-}$ mice reduces mtROS and complex I abnormalities in thymocytes (Valentin-Vega et al. 2012). Beclin-1 forms part of the complex required for the induction of autophagy (Kobayashi & Liang 2015), but is also required for the recruitment of Parkin to the mitochondrial membrane where it induces ubiquitination and proteasomal degradation of proteins on the outer mitochondrial membrane which leads to the inhibition of fusion and the trafficking of dysfunctional mitochondria (Choubey et al. 2014). It is still unclear why the allelic loss of Beclin-I would promote improvement of mitochondrial dysfunction in $ATM^{-/-}$ mice, but it has led to the suggestion that Beclin-1 might have additional functions together with its role in autophagy (Valentin-Vega et al. 2012).

2.4.4 Mitophagy and mitochondrial dynamics:

Similarly to Valentin-Vega et al. (2012), Fang et al. (2016) reported increased mitochondrial content in ATM-knockdown (ATM-KD) rat neurons and increased ROS production, but also noted a higher mitochondrial membrane potential in contrast to that reported by Ambrose et al. (2007). They did however suggest that this could reflect decreased ATP production, and either inadequate or inefficient mitophagy. Moreover, the study showed that mitophagy is suppressed in ATM-KD HeLA cells and rat neurons, but that the phenotype could be rescued by replenishing NAD^+ in the cells which significantly improve life-span in $ATM^{-/-}$ mice (Fang et al. 2016).

Spermidine is a natural polyamine that is involved in several biological processes including cell-proliferation and apoptosis, and tends to decline with age (Eisenberg et al. 2009). Spermidine also elicits mitochondrial depolarization that elicits the formation of

mitophagosomes and mitochondrial targeted lysosomes, which has been suggested to be through ATM- dependent activation of the PINK/Parkin mitophagy pathway (Qi et al. 2016). Spermidine-induced mitochondrial depolarization is abrogated in the presence of the chemical ATM inhibitor, KU55933. Moreover, spermidine promotes the co-localisation of phosphorylated ATM and PINK on the outer mitochondrial membrane, which together with the translocation of Parkin can be blocked by the ATM inhibitor. The authors suggest a model whereby the addition of spermidine results in ROS which activates ATM and drives PINK1 accumulation as well as Parkin translocation with consequent mitophagy (Figure 2.7).

Terminally differentiated cells such as cardiomyocytes are dependent on the efficient removal and replacement of dysfunctional mitochondria to ensure cell survival and to maintain cardiac homeostasis (Moyzis et al. 2015). A decrease in ATP production and increased ROS production as a measure of mitochondrial dysfunction can result in either the release of apoptotic proteins or the selective clearance of the damaged mitochondria. Mitophagy thus serves as an early cardioprotective response through the removal of damaged mitochondria, and if this fails, apoptosis can be induced in response to excessive oxidative stress (Kubli & Gustafsson 2012). Moreover, reduced autophagy together with the accumulation of dysfunctional mitochondria have been associated with heart failure and aging (Moyzis et al. 2015). Inefficient mitophagy can, at least partially, contribute to diabetic cardiomyopathy (Liang & Kobayashi 2016).

The best established model of mitophagy involves the accumulation of PINK (which is normally degraded in healthy mitochondria) on the outer mitochondrial membrane (Valente et al. 2004) that drives the recruitment and translocation of Parkin (Kitada et al. 1998) to damaged mitochondria. Parkin is an E3 ubiquitin ligase that is phosphorylated by PINK, which stimulates its translocation to the mitochondria where it ubiquinates several OMM proteins. This promotes further PINK phosphorylation and the formation of ubiquitin chains that simultaneously bind ubiquitin-binding domains (UBDs) and microtubule-associated proteins 1A/1B light chain 3 (LC3)/GABAA receptor-associated protein (GABARAP) attached to autophagosomal membranes that can then envelop the damaged mitochondria (reviewed by Nguyen et al. 2016). PINK also phosphorylates the fusion protein, mitofusin 2 (Mfn2), which then can serve as a mitochondrial receptor for Parkin, promoting its ubiquination (Chen & Dorn II 2013). The loss of Mfn2 prevents the translocation of Parkin in

depolarized mitochondria and supresses mitophagy, which drives the accumulation of dysfunctional mitochondria and respiration in mouse cardiomyocytes.

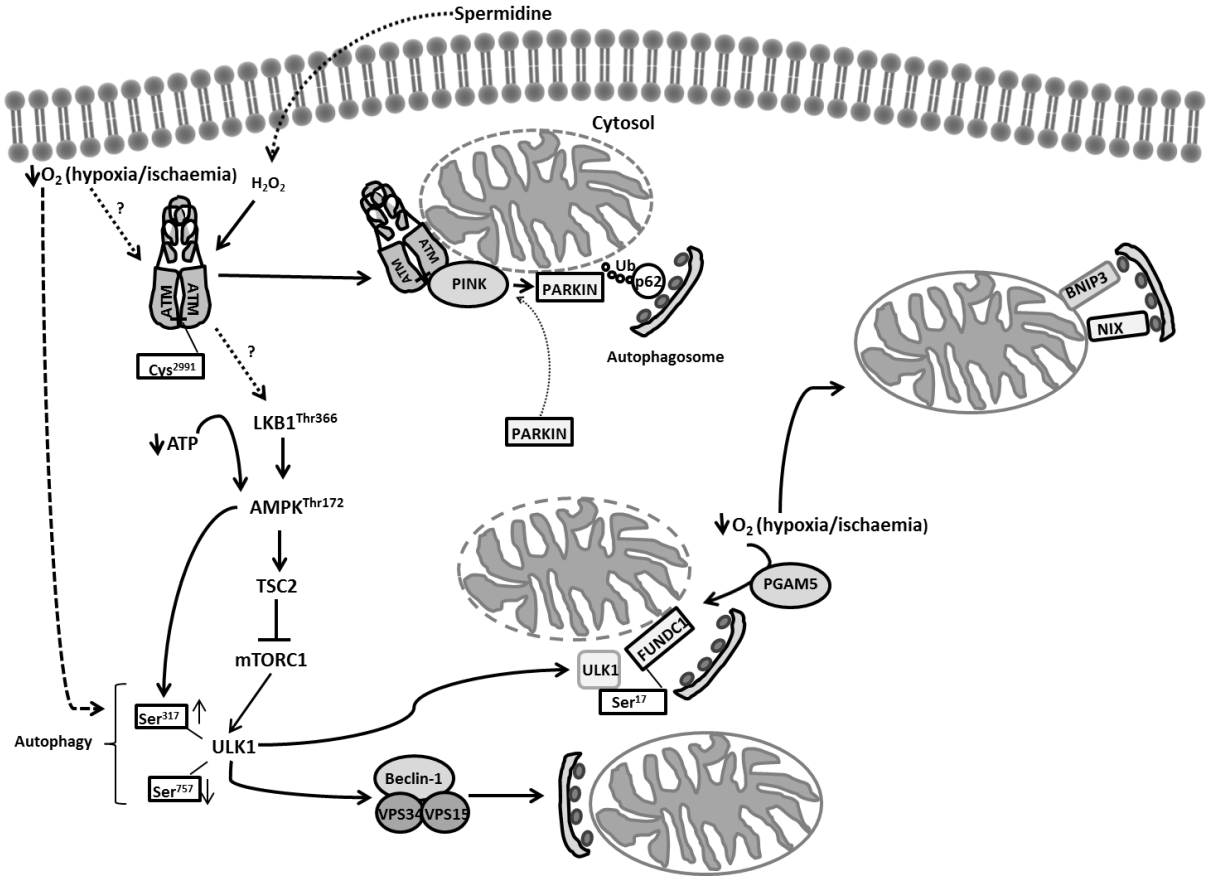

Figure 2.7: A schematic overview of mitophagy and autophagic clearance of damaged mitochondria. ATM have been implied in the PINK/Parkin mitophagy pathway in response to spermidine treatment, which induces ROS and consequently activate ATM, which is then recruited to the permeabilised mitochondrial membrane where it co-localise with PINK. This drives the recruitment of Parkin which is ubiquitinated. The ubiquitin chain binds to LC3 (shown as balls) on the autophagosome, which then engulfs damaged mitochondria for lysosomal degradation (not shown). Hypoxia or mitochondrial uncoupling can also activate ULK1, driving its translocation to the damaged mitochondrion membrane where it phosphorylates FUNDC1, which enhances its binding to LC3, whereas the dephosphorylation of FUNDC1 by PGAM5 also allows FUNDC1 to directly interact with LC3. BNIP and NIX can act as mitochondrial receptors in response to hypoxia when the mitochondrial membrane is not permeabilised and bind to LC3 on the autophagosome. Damaged mitochondria produce less ATP that activates AMPK, which in turn phosphorylates ULK1 and activates the Beclin1-VSP34-VSP15 complex and drives the formation of an autophagosome. Damaged mitochondria can also produce ROS which inhibits mTOR and leads to the activation of autophagy. Whether ATM is involved in either the activation of AMPK or suppression of mTOR in response to ROS to induce mitophagy is still unknown (indicated with a question mark).

The recent discovery that ULK1 and the autophagy protein (Atg), Atg9a are recruited directly to the damaged mitochondria during the early stages of Parkin-mediated autophagy, suggests that the autophagosomal membrane can also be formed *de novo* by the damaged

mitochondria opposed to a pre-formed isolation membrane that recognizes the damaged mitochondria (Itakura et al. 2012). In the event of hypoxia or FCCP-mediated mitochondrial uncoupling, ULK1 is upregulated and translocates to fragmented mitochondria upon mitophagy induction (Wu et al. 2014). In brief, once ULK1 translocates to the mitochondria, it interacts with FUNDC1 and phosphorylates it at Ser^{17}, which in turn enhances FUNDC1 binding to LC3. The authors conclude that FUNDC1 is crucial for ULK1 recruitment to damaged mitochondria, where its phosphorylation of FUNDC is essential for mitophagy in response to hypoxia and mitochondrial uncoupling. Moreover, the loss of either AMPK or ULK1 results in the accumulation of the autophagy adapter protein, p62 and defective mitophagy, whereas the loss of ULK1 phosphorylation by AMPK results in dysfunctional mitochondrial homeostasis during starvation, which collectively link nutrient status with autophagy and cell survival (Egan et al. 2011).

A very comprehensive review by Moyzis et al. (2015) is depicted in Figure 2.7, and summarises four pathways through which mitophagy can be mediated. Briefly, the first pathway is the PINK/Parkin ubiquitin-dependent pathway described previously. The second is mitochondrial receptor-mediated autophagy, where the pro-apoptotic proteins, BNIP3 and NIX localize to the outer mitochondrial membrane and act as receptors for targeting autophagosomes through direct interaction of conserved LC3-interacting regions (LIRs) with LC3 on the autophagsome, often in response to hypoxia (Zhang & Ney 2009), and in the absence of mitochondrial membrane permeabilization (Rikka et al. 2011). The third pathway is through FUNDCI, which has been mentioned previously in this document. FUNDCI is an outer mitochondrial membrane protein that has been implicated in hypoxia-mediated mitophagy in mammalian cells (Moyzis et al. 2015). Similar to BNIP3 and NIX, FUNDC1 acts as a receptor for the autophagosomal membrane and interacts directly with LC3 through LIR (Wei et al. 2015). The serine/threonine protein phosphatase, PGAM5 dephosphorylates FUNDC1 during hypoxia or mitochondrial membrane depolarization and promotes interaction with LC3 with consequent mitophagy. Lastly, cardiolipin, which is located on the inner mitochondrial membrane where it maintains the function of several proteins involved in mitochondrial metabolism, redistributes to the outer mitochondrial membrane during mitophagy where it binds to LC3. It has been suggested that the redistribution of cardiolipin can act as a signal for the elimination of damaged mitochondria, but this has only been

observed in neurons thus far and still needs to be evaluated in cardiomyocytes (Moyzis et al. 2015).

Mitophagy, together with mitochondrial biogenesis, fusion and fission, collectively classified as mitochondrial dynamics, balance the need for nutrients with energy demand (Vásquez-Trincado et al. 2016). Mitophagy is also dependent on the fission/fusion cycle, whilst many of the fission/fusion cycle proteins, including Drp1, Mfn1, Mfn2 and Opa1 have been linked with the transcriptional activation of PGC1α, which regulates mitochondrial biogenesis (Martin et al. 2014). Mitochondrial fission is accelerated prior to mitosis to ensure equal mitochondrial distribution, but can also participate in the removal of damaged mitochondria through mitophagy by packaging the damaged DNA and proteins into one daughter organelle whilst directing the undamaged components into the other daughter organelle, ensuring the destruction of the dysfunctional components (Dorn & Kitsis 2015). Mitophagy can also be triggered in response to mild oxidative stress in a Drp1-dependent manner, triggering selective mitophagy, whilst starvation and increased ROS induces both non-selective autophagy and to a lesser extent, mitophagy (Frank et al. 2012). Interestingly, inhibition of Drp1 results in hyperfusion which triggers cellular replication stress and results in delays in the G2/M cell cycle, consequently activating ATM and the G2 to M cell cycle checkpoint (Qian et al. 2012). Normal cardiac mitochondrial fusion on the other hand, seems to be a much slower process, albeit essential for both organelle function and homeostasis (Chen et al. 2011).

Currently, ATM has not yet been implicated in the regulation of either fission or fusion, but is known to play a role in mitophagy (Valentin-Vega et al. 2012; Qi et al. 2016), mitochondrial homeostasis (Ambrose et al. 2007) and mitochondrial biogenesis (Fu et al. 2008). It was shown in the latter study that ATM can be activated by etoposide, an apoptosis-inducing agent, which can lead to mitochondrial biogenesis through the activation of AMPK. The authors suggest that ATM-dependent mitochondrial biogenesis may play a role in the DDR and ROS regulation, and that combined, this can lead to the development of A-T.

In conclusion, studies have shown that ATM is activated directly by mitochondrial ROS, and more specifically mitochondrial-derived H_2O_2 (Zhang et al. 2018). ATM can also be recruited

to, and co-localize with PINK at the mitochondrial membrane in response to spermidine induced mitochondrial depolarization (Qi et al. 2016). Moreover, ATM activates ULK1 through AMPK phosphorylation (Zhang et al. 2015) in response to oxidative stress, and this could imply a possible link between ATM and ULK1/FUNDC1 mitophagy due to hypoxia (Wu et al. 2014), another activator of ATM (Cam et al. 2010). Collectively, this suggests a role for ATM in mitochondrial dynamics.

Of relevance though is that the absence of functional ATM can increase oxidative stress and drive mitochondrial dysfunction. Heterozygous ATM ($ATM^{+/-}$) in an apolipoprotein $ApoE^{-/-}$ mouse model can accelerate the development of atherosclerosis as well as multiple features of metabolic syndrome. This could respectively be alleviated with transplantation of $ATM^{+/+}$ bone marrow (Mercer et al. 2010), and treatment with the mitochondrial specific ROS scavenger, MitoQ (Mercer et al. 2012).

2.5 ATM and insulin signalling

Collectively, risk factors such as hypertension, insulin resistance, excess visceral fat and hyperlipidaemia are known as the metabolic syndrome (Roberts & Sindhu 2009) and the cumulative contribution can increase the risk of developing cardiovascular dysfunction (Kahn et al. 2005). Ren et al. (2010) have suggested that literature indicates that decreased myocardial mitochondrial fatty acid metabolism, biogenesis and antioxidant defence mechanisms can lead to reduced cardiac substrate flexibility, cardiac energy efficiency, and diastolic dysfunction. It is also becoming clear that mitochondrial dysfunction can play an important role in the development and pathogenesis associated with cardiac contractile dysfunction in obesity, insulin resistance and Type 2 diabetes (Bugger & Abel 2010). Altered insulin signalling in the heart can contribute directly to mitochondrial dysfunction and result in hyperglycaemia-induced oxidative stress, which can lead to the onset of diabetic cardiac myopathy (Boudina et al. 2009).

A-T patients have elevated glycaemia and decreased insulin sensitivity (Connelly et al. 2016) that can develop into severe insulin resistance (Bar et al. 1978). It is suggested that as many as 1.4-2% of the general US/Canadian population are heterozygous carriers of ATM mutations, significantly elevating their risk to develop ischaemic heart disease (Su & Swift

2000). Moreover, and as mentioned previously, targeting mitochondrial ROS specifically in heterozygous $ATM^{+/-}$ $ApoE^{-/-}$ mice, reduced oxidative damage to mitochondrial DNA and inhibited the development of various features of metabolic syndrome (Mercer et al. 2012). In knock-out mouse studies of ATM, it has been shown that the absence of ATM induces both structural and functional changes such as increased myocardial fibrosis and myocyte hypertrophy in the heart (Foster et al. 2012). Increased myocyte apoptosis and expression of fibrosis-related genes in the absence of ATM was also observed in the same study. Furthermore, it was demonstrated that ATM activates the tumour suppressor, p53, in response to β-adrenergic receptor stimulation, and plays a protective role against cardiac remodelling (Foster et al. 2011). Taken together, these studies suggest a potential role for ATM in both insulin signalling and ischaemic heart disease.

ATM was first implicated in the insulin-response pathway in the context of protein synthesis. Yang & Kastan (2000) found that ATM phosphorylates eukaryotic translation initiation factor 4E-binding protein 1 (4E-BP1) at Ser^{111} *in vitro* and *in vivo* in response to insulin treatment. The authors also demonstrated that insulin enhances the specific kinase activity of ATM and that the absence of ATM significantly decreases the dissociation of 4E binding protein 1 (4E-BP1) from eukaryotic translation initiation factor 4E, which is required for translation initiation and mRNA stability. This led Schneider et al. (2006) to hypothesise that ATM might be involved in insulin signalling, and the authors consequently demonstrated that the absence of ATM results in insulin resistance as well as vascular disease in high-fat diet fed mice. Activation of ATM with a low dose of chloroquine (7 mg/kg/week) decreased features of metabolic syndrome, such as increased visceral fat and decreased adiponectin, as well as atherosclerosis. Endogenous glucose production could not be suppressed by insulin in an $ATM^{+/-}$ $ApoE^{-/-}$ mouse model, and insulin-induced phosphorylation of Akt at Ser^{473} and Thr^{308} was decreased in this model. The absence of ATM also increased insulin receptor substrate 1 (IRS-1) as well as Jun-C-kinase (JNK) in aortas (Schneider et al. 2006). JNK has been implicated in obesity and the development of Type 2 diabetes (Solinas & Becattini 2017; Han et al. 2013). Lastly, Schneider et al. (2006) found that chloroquine improved both fasting and non-fasting glucose metabolism through ATM-mediated p53 Ser^{15} activation in fat, muscle and aortas of *ob/ob* (leptin deficiency) and *db/db* mice (leptin receptor mutation) (Schneider et al. 2006). Interestingly, the activation

of ATM with chloroquine in $p53^{+/+}$ $ApoE^{-/-}$ and $p53^{-/-}$ $ApoE^{-/-}$ mice improved atheroprotection in a p53-dependent manner, but improved glucose intolerance and insulin-sensitivity independent of the p53-pathway (Razani et al. 2010). The tumour-suppressor, p53, is also activated and phosphorylated by ATM in response to DNA damage caused by hypoxia and UV- or ionizing radiation, and can mediate cell survival, angiogenesis inhibition or apoptosis (Kastan & Lim 2000). In a mouse model with a germline p53 mutation (Ser^{18} changed to alanine; murine Ser^{15}), increased metabolic stress and glucose homeostasis defects were observed, and led to the development of insulin resistance (Armata et al. 2010). N-Acetyl cysteine (NAC) treatment restored insulin signalling in late-passage primary mouse fibroblasts, whereas an antioxidant in the diet of the p53 Ser^{18}-deficient mice made them glucose tolerant, which led the authors to conclude that p53 phosphorylation by ATM plays an important role in glucose homeostasis (Armata et al. 2010).

Insulin-like growth factor 1 (IGF-1) is a potent activator of the insulin sensitive Akt-pathway, and stimulates ATM phosphorylation, which is important for AMPK-α subunit phosphorylation during IGF-1 signalling, and most interestingly, does this in an LKB1-independent manner (Suzuki et al. 2004). Moreover, it has been reported that ATM phosphorylates Akt at Ser^{473} in response to insulin or ionizing radiation (Viniegra et al. 2005), which led to the suggestion that ATM might play a role in IGF-1 signalling through the Akt/mTOR pathway (Ching et al. 2014). In differentiated C2C12 cells as well as in isolated soleus muscle from $ATM^{-/-}$ mice results support the suggestion that ATM might be a modulator of IGF-1 signalling downstream of IRS-1 to stimulate phosphorylation of Akt at Ser^{473} and Thr^{308} as well as mTOR and S6K (Ching et al. 2014).

In an insulin resistant high-fat fed rat model, ATM expression was significantly decreased in isolated gastrocnemius muscle tissue, and Akt Ser^{473} phosphoprylation decreased correspondingly in response to intraperitoneal insulin treatment (Halaby et al. 2008). In contrast to Schneider et al. (2006), no differences in JNK expression in muscle from either control chow-fed rats or high-fat fed rats were observed. The authors also showed that phosphorylation at ATM-mediated Akt Ser^{473} are important for the subsequent phosphorylation of Thr^{308} in mouse fibroblast cells. The authors observed the same result in L6-myoblast cells, and showed that insulin-induced Akt phosphorylation by ATM, as well as glucose transporter 4 (GLUT4) translocation to the cellular membrane can be abrogated in

the presence of the ATM inhibitor, KU55933. However, the same result was not observed in L6-myotubes (C2C12 and RD cells), where the use of KU55933 abrogated GLUT4 transport and decreased AS160 (Akt substrate of 160 kDa) phosphorylation, but did not affect the insulin-stimulated phosphorylation of Akt at Ser^{473} (Jeong et al. 2010). The latter study suggested that this might have been due to the use of a lower concentration of KU55933 (1 µM compared to 10 µM) or the use of myotubes compared to a myoblast cell-line, suggesting that the cellular model could play an important role in the evaluation of specific protein activity. Similarly, ATM inhibition failed to interfere with insulin-stimulated phosphorylation of Akt at Ser^{473} or Thr^{308} in 3T3-L1 adipocyte cells, which was mediated by mTOR complexed to RICTOR (rapamycin-insensitive companion of mTOR) (Hresko & Mueckler 2005).

Irrespective, cytoplasmic ATM plays an important role in glucose homeostasis because of its role in i) protein translation through the phosphorylation of 4E-BP1 (cytoplasmic translation-regulatory protein) (Yang & Kastan 2000); ii) mediating full activation of Akt in certain cell types (Viniegra et al. 2004; Halaby et al. 2008; Jeong et al. 2010; Hresko & Mueckler 2005); and iii) regulating glucose transporter 4 (GLUT4) translocation, which is responsible for glucose uptake in response to insulin (Halaby et al. 2008). Glucose can be imported into cells by GLUT4 either in an insulin-dependent manner (mediated by the Akt-pathway; Ditch & Paull 2012), or insulin-independent manner through the AMPK-pathway (O'Neill 2013) in response to low glucose, hypoxia or ischaemic conditions. The translocation of the GLUT4 vesicle, which is also the main isoform present in fully differentiated cardiomyocytes, is severely limited both in the absence of ATM (Halaby et al. 2008) and in insulin resistance. However, the underlying mechanisms of GLUT4 translocation in response to ATM and insulin, are still unclear (Ditch & Paull 2012). The cytoplasmic role of ATM is presented schematically in Fig 2.8.

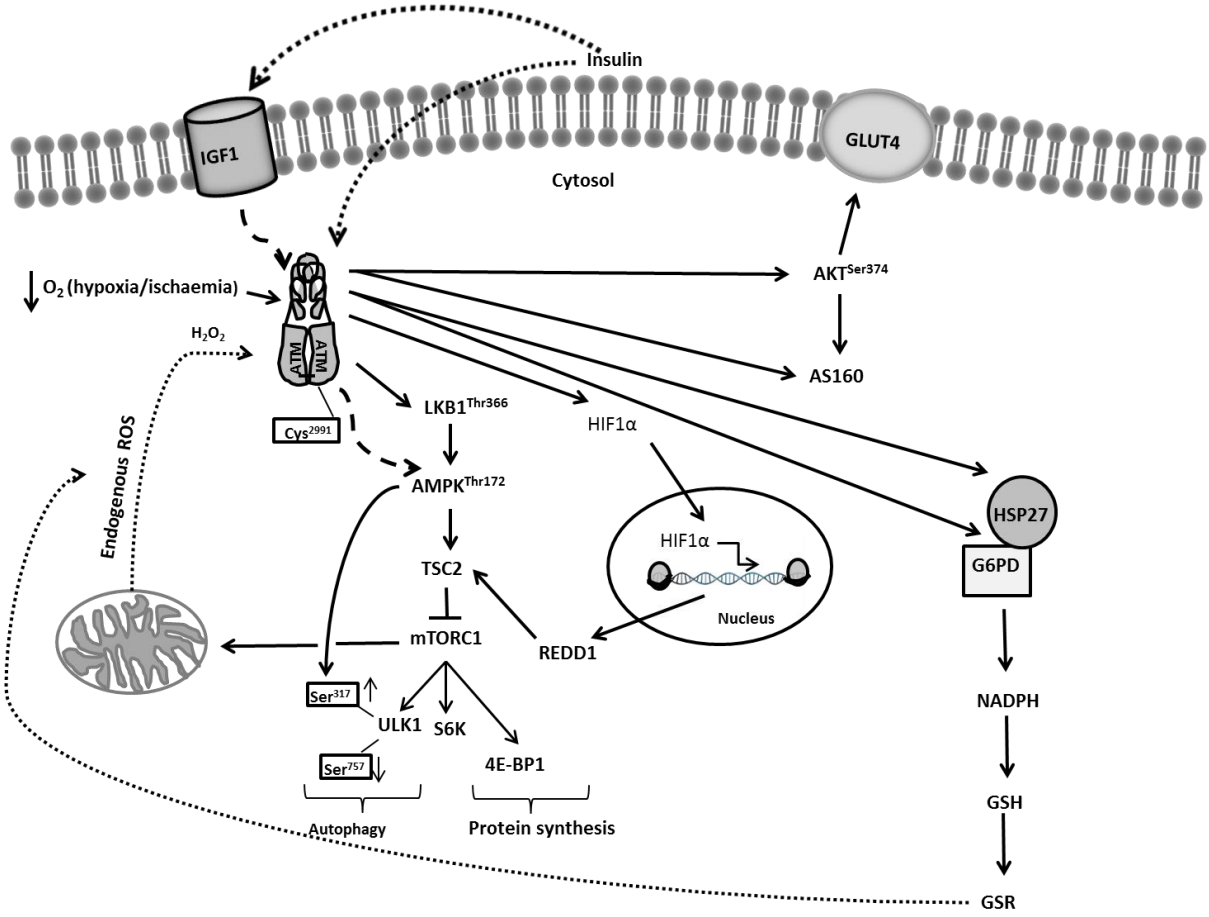

Figure 2.8: A schematic representation of the cytosolic role of ATM in response to insulin. Insulin-like growth factor 1 (IGF-1), which is a potent activator of the Akt-pathway, stimulates ATM phosphorylation which is required for AMPK-α phosphorylation during IGF-1 signalling, in an LKB1-independent manner. ATM also enhances protein synthesis through the phosphorylation of 4E-BP1 in response to insulin stimulation both *in vivo* and *in vitro*. ATM is required for the phosphorylation of Akt at Ser^{473} in response to insulin or ionizing radiation, and can phosphorylate AS160 independently of Akt in certain cell types. As described elsewhere, ATM is sensitive to endogenous ROS, as well as hypoxia, and can phosphorylate as well as mediate HIF1-α translocation. It also plays a role in the PPP either through HSP27 or direct interaction with G6PD.

Obesity and its associated ROS is an early marker of metabolic syndrome (Hopps et al. 2010). Insulin resistance is a frequent complication observed in obesity (Kahn et al. 2006), whereas A-T patients often exhibit with poor weight gain and a progressive decrease in body mass index and can still develop diabetes (Schubert et al. 2005). This paradox led Takagi et al. (2015) to investigate adipose tissue distribution in $ATM^{-/-}$ mice in order to determine whether defective adipose tissue development might be responsible for the lipoatrophic diabetes observed in A-T patients. Two major role players in adipocyte differentiation are CCAAT/enhancer binding protein 1 (C/EBP1) and peroxisome proliferator activated receptor γ (PPARγ). Furthermore, it is well-known that alterations in adiposity

differentiation can impact glucose homeostasis (Takagi et al. 2015). It was found in this study, similarly to Schneider et al. (2006), that $ATM^{+/-}$ mice did not exhibit glucose intolerance or insulin resistance, but quickly developed both pathologies when fed a high fat diet. Conversely, $ATM^{-/-}$ mice that were fed a high fat diet had increased visceral fat, decreased adiponectin and decreased leptin levels. This was suggested to be due to a redistribution of fat that led to decreased subcutaneous fat whilst increasing visceral fat, as well as an increased appetite due to decreased leptin levels. Mouse embryonic fibroblasts (MEFs) derived from $ATM^{-/-}$ mice were defective in adipocyte differentiation and had significantly reduced glucose uptake compared to MEFs from $ATM^{+/+}$ mice. Similarly, both caffeine and the ATM inhibitor, KU55933 could block adipocyte differentiation in 3T3-L1 cells. This was due to defective expression of the transcriptional factors, C/EBP1 and PPARγ. No differences in IGF-1 receptor levels were found. The authors conclude that ATM plays a role in the key adipocyte transcription factors, which contribute to glucose homeostasis *in vivo* (Takagi et al. 2015).

Moreover, the heterozygous $ATM^{+/-}$ $ApoE^{-/-}$ mouse model exhibits hyperlipidaemia on both normal chow-fed and high fat diets (Mercer et al. 2010) which can be reduced with the oral administration of MitoQ which prevents the increased adiposity, hypercholesterolaemia, and hypertriglyceridaemia associated with metabolic syndrome development in fat-fed heterozygous ATM mice (Mercer et al. 2012). Cells that are ATM deficient, exhibit decreased anti-oxidant capacity and increased sensitivity to ROS. The oxidation of low-density lipoprotein (oxLDL) and its uptake by macrophages, activates both ATM and p21 in fibroblasts and endothelial cell, and can act as a trigger in the development of atherosclerosis (Semlitsch et al. 2011). However, in the absence of ATM, oxLDL induces DNA double-strand breaks and chromosome breaks, as well as decreasing cell viability and colony formation of A-T fibroblasts, whilst significantly increasing oxLDL-induced reactive oxygen species which can be rescued with anti-oxidant pretreatment (Semlitsch et al. 2011). It was concluded in this study that ATM maintains antioxidant defence against oxLDL-mediated cytotoxicity (Semlitsch et al. 2011), which implies a potential role for ATM in lipid peroxidation as oxidized phospholipids have a high affinity for oxLDL which is increased in cardiovascular disease (Anderson et al. 2012).

Collectively, an important role for ATM in glucose homeostasis, adipocyte differentiation, as well as redox homeostasis is suggested, all of which can contribute towards the development of metabolic syndrome, Type 2 diabetes and cardiovascular disease when disrupted. This highlights the need to further elucidate the role of ATM within cellular metabolism and potentially within a more tissue specific manner.

2.6 ATM and drug efficacy:

Lastly, ATM also potentially plays a role in drug efficacy, which gives it clinical relevance. Metformin, the most commonly used first line treatment for T2D, is potentially associated with ATM. The drug increases cellular glucose uptake through activation of the AMPK pathway (Zhou et al. 2001) by increasing cellular AMP through the inhibition of the mitochondrial respiratory chain (Owen et al. 2000). The considerable variability in glycaemic response to metformin treatment among patients led to a genome wide association study (GWAS) that associated a single nucleotide polymorphism (SNP), located at the locus containing the ATM gene, with metformin treatment success (Zhou et al. 2011). It was found in the same study that inhibition of ATM with KU55933 decreased AMPK-activation by metformin, and concluded that ATM acts upstream of AMPK and is required for a full response. Although the presence and association of metformin treatment success with this SNP have both been confirmed and refuted independently (Van Leeuwen et al. 2012; Florez et al. 2012), it is also argued that AMPK-activation, in response to metformin, is independent of ATM, and rather acts through the organic cation transporter, OCT1, which is also inhibited by KU55933 (Yee et al. 2012). However, long-term metformin treatment stimulates cardiomyocyte glucose uptake through an AMPK-dependent decrease in GLUT-4 endocytosis (Yang & Holman 2006) and improved glucose intolerance in ATM knockout mice (Takagi et al. 2015), and highlights the need for further research in this regard. Although little research has been done with regards to the effect of metformin or KU55933 on the rat cardiomyoblast cell line, H9c2, it was shown that KU55933 effectively inhibits ATM phosphorylation in post-mitotic myotubes (Fortini et al. 2012). Furthermore, inhibition of ATM with KU60019, which is 10-fold more effective and has half the IC_{50} value of KU55399, blocked AMPK activation by metformin in small-cell lung cancer cells (Storozhuk et al. 2013). It is, however, also known that metformin is cardioprotective (Kobashigawa et al. 2014) and

has been found to delay the development of diabetes and cardiovascular dysfunction in Goto-Kakizaki rats (non-obese model of T2D) by inhibiting the generation of superoxide in mitochondria (Rösen & Wiernsperger 2006). It has been suggested that ATM could be activated by ROS prior to metformin treatment with consequent mitochondrial inhibition (Ditch & Paull 2012), which implicates a possible role for ATM in response to hyperglycaemia-induced oxidative stress within the AMPK-pathway.

ATM has also been implicated in doxorubicin-induced (Dox) cardiotoxicity (Zhan et al. 2016). Dox is a potent and widely used anti-cancer drug, but its usage is limited by cumulative dose dependent cardiotoxicity due to underlying mechanisms such as free radical formation, lipid peroxidation, p53 accumulation and activation of pro-apoptotic signalling cascades (Deavall et al. 2012). Dox, which is a topoisomerase II-stabilizing drug, results in ATM-dependent accumulation and phosphorylation of p53 and promotes the phosphorylation of ATM-dependent DDR proteins, which can be attenuated by NAC treatment (Kurz et al. 2004). This suggests that hydroxyl-radicals contribute to Dox-induced activation of ATM-dependent pathways. Interestingly, ATM-KO mice show attenuated Dox-induced cardiotoxic effects (Zhan et al. 2016). The study showed that ATM is primarily expressed and activated in cardiac fibroblasts, where it activated the Fas-ligand, which when activated, can mediate apoptosis in cardiomyocytes. Systemic inhibition of ATM with KU55933 prevented Dox-induced cardiotoxicity, and suggests that the antagonism of ATM may have potential therapeutic implications (Zhan et al. 2016).

2.6 Purpose of research:

Taken together, ATM seems to play a central role in cellular metabolism. Oxidative stress has been identified as a contributing factor in insulin resistance and coronary artery disease (Ceriello & Motz 2004). ATM can mediate autophagy via the AMPK-pathway in response to ROS (Shiloh & Ziv 2013) as well as hypoxia (Cam et al. 2010). Even though hypoxic conditions, such as ischaemia, can activate AMPK independently of the AMP/ATP ratio of the cell (as is the case with metformin), it still requires mitochondrial DNA and ROS generation to activate ATM (Emerling et al. 2009). This also holds true for ATM's role in the regulation of mitochondrial homeostasis and oxidative stress that allows the protein to be

activated in order to prevent apoptosis is response to non-genotoxic p53 activation (Sullivan et al. 2015). Nevertheless, further studies are required to elucidate the relationship between the metformin-glycaemic response and ATM-dependent glucose metabolism and its activation in response to oxidative stress (Takagi et al. 2015).

ATM is a key regulator of adipocyte transcription factors (CEBP1 and PPARγ) and adipocyte differentiation via the DDR pathway (Takagi et al. 2015). On the other hand, cardiomyocyte differentiation is directed by mitochondrial fusion which is mediated by the proteins, Mitofusin-1 and -2 (Kasahara et al. 2013). Mitofusin-2 is involved in the rearrangement of the outer mitochondrial membrane, and cardiac myocytes lacking this protein tend to be pleiomorphic and contain enlarged mitochondria (Papanicolaou et al. 2011). This observation corresponds to the increased mitochondrial numbers and structural abnormalities that were observed in lymphoblastoid cells obtained from A-T patients (Ambrose et al. 2007). In a study with thymocytes where a fraction of ATM was localised to the mitochondria, defects in mitophagy (mediated by the autophagy protein, Beclin-1) as well as a reduction in respiration rates in cell culture lacking ATM, was shown (Valentin-Vega et al. 2012). Furthermore, ATM can induce pexophagy (autophagy of peroxisomes) independently of genotoxic shock and in response to ROS (Zhang *et al.*, 2015), which implies a vital role for ATM in cellular and organelle cell fate.

More than 30% of cardiac cell volume is occupied by mitochondria and is essential for normal functioning of the cardiovascular system (Westermeier et al. 2015). In light of the decreased mitochondrial respiration and the intrinsic mitochondrial DNA repair defects associated with the absence of ATM protein kinase (Sharma et al. 2014), it is possible that A-T and its associated conditions might very well be a mitochondrial disease (Valentin-Vega et al. 2012).

In summary, mitochondrial dynamics such as fusion, fission and mitophagy are essential for sustained mitochondrial function in a healthy heart. In the milieu of obesity and Type 2 diabetes, altered insulin signalling could contribute directly towards mitochondrial dysfunction (Boudina et al. 2009). Moreover, mitochondrial dysfunction has been linked to the onset of diabetic cardiac myopathy due to hyperglycaemia induced oxidative stress (Westermeier et al. 2015). ATM protein kinase plays a definitive role in adipocyte

differentiation, mitochondrial function and integrity as well as in glucose, redox and peroxisome homeostasis, but many of the underlying molecular mechanisms with regards to ATM's function, especially in the mitochondria, still need to be elucidated.

In light of the importance of mitochondrial dysfunction associated with the development of cardiovascular disease and ATM protein kinase's potential underlying role, this study proposes to investigate the role of ATM within a well-characterised high fat diet (DIO) rat model with known myocardial dysfunction as well as H9c2 cardiomyoblasts *in vitro* by determining whether (1) ATM expression is influenced in cardiac mitochondria or high fat exposure and (2) ATM expression or regulation influences mitochondrial function by investigating: i) oxidative phosphorylation, ii) mitofusion and mitophagy as well as iii) redox status in the mitochondria.

Aims of investigation:

1. To determine the effects of lipid-induced insulin resistance on ATM expression using a H9c2 cardiomyoblast cell line.
2. To determine whether ATM expression or regulation influences mitochondrial function (oxidative phosphorylation): We will measure oxidative phosphorylation capacity of myocardial mitochondria from both control and HFD rats in response to either activation or inhibition of ATM respectively with insulin, chloroquine and a specific ATM inhibitor, KU60019.
3. To determine whether ATM expression or regulation correlates with mitochondrial dynamics: The association between ATM and the autophagy protein, Beclin-1, as well as the involvement of ATM protein kinase in the autophagic pathways such as AMPK- activation by oxidative stress or hypoxia, suggests a potential role for ATM in mitophagy (i.e PINK/Parkin) and mitofission/fusion (i.e Drp1). Mitochondrial dysfunction is often associated with a decrease in mitophagy and an increase in mitochondrial fusion, which in turn could lead to increased oxidative stress, and decreased respiration. This study will determine whether chemical inhibition of ATM will inhibit mitophagy by investigating PINK, Parkin, LC3 and p62 protein levels, as well as the fission protein, Drp1 in an aim to possibly elucidate a direct correlation

between the absence of ATM and cardiac dysfunction due to dysregulation of the mitophagy, fission and –fusion pathways.

Chapter 3 : ATM is downregulated *in vitro* by high free fatty acid concentrations in the rat cardiomyoblast cell line, H9c2.

Obesity, unhealthy diets and decreased physical activity contribute to non-communicable diseases (NCDs) such as cardiovascular disease, diabetes and cancer (Vorster 2002). The incidence of these diseases is increasing worldwide and more so in developing countries. In South Africa, the heaviest NCD burden is found in poor urban communities (Mayosi et al. 2009) and is a common phenomenon observed in low- and middle income countries (Alwan et al. 2010), suggesting a link with socio-economic conditions (Mayosi et al. 2009). This increase in NCD prevalence is, amongst others, driven by the rapid migration of ethnic black Africans to urban centres which has led to an increase in conventional cardiovascular risk factors (obesity, hypertension and increased cholesterol) and coronary heart disease (Yusuf et al. 2001). The obesity epidemic in South Africa mainly reflects a nutritional transition, which is defined as a shift away from traditional diets and decreased physical activity due to urbanisation (Kruger et al. 2005). A nutritional shift is also associated with increased dietary fat and energy intake as well as over-nutrition, and it has been suggested that SA is further along the nutrition transition than other Sub-Saharan countries (Micklesfield et al. 2013).

Obesity is one of the hallmarks of metabolic syndrome, which in turn, is characterised by increased LDL cholesterol and decreased HDL cholesterol, hypertension and insulin resistance. Cellular oxidative stress underlies metabolic syndrome and has been associated with obesity due to low-grade inflammation, insulin resistance and consequently, cardiac dysfunction (Hopps et al. 2010). Obesity-associated insulin resistance is also a major risk factor for T2D and cardiovascular disease, and an increase in abdominal obesity predisposes a person to systemic insulin resistance (Qatanani & Lazar 2007).

The absence of ATM has been associated with increased visceral fat accumulation in $ATM^{-/-}$ mice that are fed a high fat diet in an $ApoE^{-/-}$ background (Schneider et al. 2006). These animals also exhibited pathologies similar to that of metabolic syndrome observed in humans. The absence of ATM results in decreased subcutaneous fat, whilst increasing visceral fat, which contribute to the development of T2D, and suggests a role for ATM in

adipocyte differentiation as well as glucose homeostasis (Takagi et al. 2015). ATM is known to play a role in glucose metabolism (Armata et al. 2010) and is activated by insulin (Halaby et al. 2008). Likewise, mutations in the *Atm* gene have been associated with an increased risk of ischaemic heart disease (Su & Swift 2000), as well as elevated glycaemia (blood glucose) and low insulin sensitivity in patients without diagnosed diabetes (Connelly et al. 2016). Collectively, this results in a high incidence of insulin resistance in A-T patients (Bar et al. 1978).

The finding that a high caloric diet can decrease ATM expression in cardiac rat mitochondria and heart tissue which was shown in our laboratory, as well as the finding that ATM is significantly decreased in rat muscle tissue in a high fat diet (Halaby et al. 2008), suggests a potential link between obesity and ATM. This study aimed to establish a high fat cardiomyoblast cell-culture model using H9c2 rat cardiomyoblast cells. The model is a pilot study intended to develop a rat cardiomyoblast model that can easily be manipulated in order to determine which pathways are involved in ATM-signalling under high-fat and insulin resistant conditions.

3.1 Brief introduction to H9c2 (2-1) rat cardiomyoblast cells and applications in literature

The clonal cell-line, H9c2, was originally derived from ventricular BDIX rat heart tissue (Kimes & Brandt 1976) and exhibits skeletal muscle characteristics. The mononucleated myoblast cells retain some cardiac specific characteristics such as voltage dependent Ca^{2+} channels (Hescheler et al. 1991), and can be differentiated into multinucleated myotubes that are capable of producing and controlling action potentials in response to chemical or electropotential stimulation (Kimes & Brandt 1976). The cells originate from a 13 day old embryonic rat heart, and propagate as mononucleated myoblasts that present as flat, spindle shaped cells with two to four prominent nucleoli in their nuclei.

The cardiomyoblasts only form multinucleated tubular structures upon reaching confluency, and can be stimulated to maintain a cardio-phenotype with trans-retinoic acid treatment which stimulates Ca^{2+} channel expression (Menard et al. 1999). However, differentiation of H9c2 cells with trans-retinoic acid can also result in a heterogeneous cell population, since

some cells show resistance to differentiation (Patten et al. 2017). Interestingly, the authors noted increased oxidative phosphorylation upon differentiation. Even in the absence of differentiation, H9c2 cells exhibit a higher respiration rate, mitochondrial biogenesis and ATP production when compared to the mouse atrial heart cell line, HL-1 (Kuznetsov et al. 2015). These characteristics suggest that H9c2 cells are energetically more similar to primary cardiomyocytes and thus render them a valuable *in vitro* model for ischaemia-reperfusion experiments (Kuznetsov et al. 2015). It should be noted though, that undifferentiated H9c2 cells prefer glycolysis as a main energy source. However, the cell line is often used for the analysis of cardiotoxic effects of anti-cancer drugs such as doxorubicin, and mechanisms of myocyte damage (Witek et al. 2016). H9c2 cells proliferate well in *in vitro* conditions (Watkins et al. 2011), but can age with the number of passages which changes the cells' sensitivity to cardiotoxicity effects (Witek et al. 2016). This cell line also mimics cardiac hypertrophy and supports its use as a cardiac *in vitro* model (Watkins et al. 2011).

An *in vitro* model of differentiated H9c2 cells were used to investigate the role of metformin in cardioprotection (Hu et al. 2016), as well as the role of apoptosis in hyperglycaemia and its contribution to diabetic cardiomyopathy (Cai et al. 2002). Cardiomyocytes undergo apoptosis in the presence of high free fatty acids, such as palmitate, which has been implicated in lipotoxic cardiomyopathy. Palmitate was found to induce apoptosis in undifferentiated H9c2 cells by increasing ROS generation and activation of the ERK1/2 (extracellular signal-regulated kinases) pathway (Wei et al. 2013).

Free fatty acids are associated with several cardiovascular factors and mortality in patients with angiographic coronary artery disease (Pilz et al. 2006). The replacement of saturated fatty acids with polyunsaturated fats can prevent the development of coronary heart disease (Jakobsen et al. 2009). Saturated palmitic acid (palmitate) is the most abundant circulating saturated fatty acid (Ubhayasekera et al. 2013), and can induce myocardial inflammatory injury through the Toll-like receptor 4 (TLR4) accessory protein MD2 in both mouse and undifferentiated H9c2 cell-culture models (Wang et al. 2017). However, a recent study found that a high fat diet (HFD) in obese-prone Sprague-Dawly rats increases the proportion of circulating polyunsaturated fatty acids whilst decreasing the monounsaturated and saturated fatty acids in serum (Liu et al. 2015). This led to the suggestion that fatty acid mixtures should be enriched with poly- and monounsaturated

fatty acids in *in vitro* studies when attempting to model lipid exposures during *in vivo* HFD conditions (Liu et al. 2015).

The current high fat diet that is used in our laboratory contains 11.5 g/100g fat of which 7.6 g/100g consist of saturated fats and 2.9 g/100g consists of monounsaturated fats (Salie et al. 2014). Oleate (oleic acid) is a monounsaturated fat that protects neuronal cells against palmitate induced mitochondrial dysfunction, insulin resistance and inflammatory signalling (Kwon et al. 2014). In hyperlipidaemic conditions induced by high levels of archinodonic, stearic and oleic acids in differentiated H9c2 cells, the fatty acids suppressed GLUT4 and PPARγ transcription (Armoni et al. 2005). Oleate is accumulated in undifferentiated H9c2 cells by the TLR4, and silencing of this receptor can ameliorate lipid accumulation in these cells (Dong et al. 2012). Oleic acid alleviates palmitate-induced cardiotoxicity in neuronal cells, and does so in the presence and absence of bovine serum albumin (BSA) (Kwon et al. 2014). It has been suggested that the addition of BSA to FFAs such as oleate could partially mediate its protective effects in L6-muscle cells with regards to mitochondrial activity (Gao et al. 2009), although Kwon et al. (2014) found oleate-mediated cytoprotection irrespective of the presence of BSA. Lastly, undifferentiated H9c2 cells show palmitate uptake rate similar to that of cardiac myocytes (Van Nieuwenhoven et al. 1998).

Taken together, and in view of a study that established an *in vitro* insulin resistant myocyte model with differentiated H9c2 cells and palmitate (Nobuhara et al. 2013), this study aimed to establish an undifferentiated, insulin resistant *in vitro* H9c2 model induced with palmitate and oleic acid. This pilot study aimed to determine whether ATM can be downregulated in such a model, and investigate the effect of high FFAs on 1) Akt in the phosphatidylinositol 3-kinase/protein kinase B (Akt) pathway which is a crucial in the cellular insulin response (Bertrand et al. 2008) and 2) the insulin insensitive protein, AMPK.

3.2 Materials and methods:

The effect of insulin resistance mediated by saturated and monounsaturated free fatty acid was determined in undifferentiated H9c2 cardiomyoblast cells treated with five different conditions: 1) 0.1% of 100% ethanol stock vehicle control; 2) 0.1 mM palmitic and 0.1 mM oleic acid (henceforth referred to as 0.2 mM FFA), 3) 0.2 mM FFA and 5.5 mM glucose, 4)

100 nM insulin and 5) 100 nM insulin + 0.2 mM FFA. It should be noted that H9c2 cells are grown in DMEM that contains 25 mM glucose which is the basal glucose level present in all of the conditions listed. Protein expression levels were determined with western blotting. The cellular uptake of radiolabelled 2-deoxy-glucose was used to determine glucose uptake by the treated cells.

3.2.1 Reagents:

The H9c2 cardiomyoblast cells were a kind gift from Dr Danzil Joseph, Dept. of Physiology, SU (originally obtained from American Type Culture Collection (ATCC)) and were used at passages ranging from 10-16. Dulbecco's Modified medium (DMEM) with 4.5 g glucose/l (25 mM) and L-glutamine (Biowhitaker Lonza, BE12-604F, distributed by Whitehead Scientific), Fetal Bovine serum (FBS, Capricorn Scientific, FBS-12A, distributed by Biocom Biotec), penicillin-streptomycin (Pen-strep, P4333, Sigma-Aldrich Merck) and 10X trypsin (59427C , Sigma-Aldrich) were purchased from the distributors indicated. Radiolabelled 2-deoxy glucose (2-DG-[^{3}H] NET549005MC) was purchased from Perkin-Elmer, and HumulinR (100 U/ml, Eli Lilly and Company) was purchased on prescription, commercially. Palmitic acid (P0500) and oleic acid (O1008) were purchased from Sigma-Aldrich Merck. The FFAs were prepared in 100% ethanol and dissolved by heating to 37°C and intermittent mixing with a Vortex mixer. Western blot reagents were purchased from BioRad (Lasec, South Africa), except for SignalBoost™Immunoreaction Enhancer Kit (EMD Millipore-Merck), and the Immobilon®-P PVDF membrane (EMD Millipore-Merck). The stain used for total-protein membrane imaging was 2,2,2 Trichloroethanol and was purchased from Sigma-Aldrich (T54801-500g). The antibody details are listed under materials and methods (Table 3.1).

3.2.2 Cell culture:

H9c2 cells were maintained in DMEM with 10% FBS and 1% penicillin/streptomycin (growth medium. Cells were maintained at 37°C and 5% CO_2 in a humidified incubator, and media was changed every 2 to 3 days. Cells were grown to a confluency of 70-80% in 100 mm culture plates, where after cells were harvested with the addition of 0.25% trypsin, and after 2 gentle washes with warm sterile PBS (phosphate buffered saline, 137 mM NaCl, 10 mM Phosphate, 2.7 mM KCl). The cells were centrifuged at 92 x *g* and resuspended in growth

medium. Cells were replated in a ratio of 1:3, and treated with either (i) 0.1% ethanol, (ii) 0.1 mM palmitic acid and 0.1 mM oleic acid (0.2 mM FFA), (iii) 0.2 mM FFA + 5.5 mM D-glucose, (iv) 100 nM insulin and (v) 100 nM insulin + 0.2 mM FFA for 24 hours. The cells were not starved prior to treatment as insulin was added to the assay, and treatment was stopped with two 1 x PBS washes, where after the cells were scraped and collected in PBS, and harvested with centrifugation at 92 x *g* for 4 minutes. The PBS was removed with aspiration. Each of the treatments were performed in triplicate (n=3/condition), and each complete experiment was repeated three times. The treatment volume made up 0.3% of the total media volume per plate, and was assumed not to contribute towards dilution of the media (0.03 ml in a 10 ml volume.)

Cell growth and integrity were monitored during growth phase as well as before and after the addition of the treatments described above with an Oxion Inverso inverted microscope and CMEX USB camera (Euromex Microscopes Holland), and size markers were added to the images in Euromex ImageFocus 4.0 (Euromex).

3.2.3 Western blotting:

The collected cells were lysed in 500 µl cell lysis buffer (20 mM TRIS-HCl (pH 7.5), 1 mM EGTA, 1 mM EDTA, 150 mM NaCl, 1 mM β-glycerophospate, 2.5 mM tetra sodium pyrophosphate, 10 mM sodium orthovanadate, 1% Triton X-100, 10 µg / mL leupeptin, 10 µg / mL aprotinin and 50 µg / mL PMSF). Zirconium oxide beads (0.5 mm, Next Advance, Biocom Biotech) were added to the cell lysates, where after the cells were further lysed in a Bullet blender (Next Advance laboratory equipment) at 4 000 revolutions per minute (rpm) making use of three cycles at 4°C for 1 minute with a 5 minute resting period in between. The lysates were rested on ice for 20 minutes prior to centrifugation at 12074 x *g* for 10 min at 4°C. The supernatants were carefully removed and placed in a new set of 1.5 ml Eppendorf tubes. Protein concentration was determined with a Bradford protein assay (Bradford 1976).

Cell lysates were prepared to a total volume of 15 µl containing 20 µg protein in lysis buffer and one volume 3X Laemmli sample buffer (2.5 M glycerol, 0.189 M TRIS-HCl (pH 6.8), 10% SDS, 1.275 mM bromophenol blue, 15% β- mercaptoethanol). The samples were boiled for

four minutes and stored at -80° Celsius until use. Samples were boiled again for 4 minutes prior to being loaded on 7.5% resolving denaturing SDS-PAGE gels (7.5% acrylamide/bis-acrylamide (Sigma-Aldrich Merck), 0.375 M TRIS-HCl (pH 8.8), 1% SDS, 0.5% APS, 0.05% TEMED, 50 µl 2,2,2 Trichloroethanol (Stainfree), Sigma-Aldrich), and 4% stacking gels (0.126 M TRIS-HCl, 1% SDS, 0.5% APS and 0.05% TEMED) which were subjected to electrophoresis for 1 hour at 200 V and 200 mA. The proteins that were investigated in these experiments are summarised in Table 3.1.

A modified transfer buffer was used (25 mM TRIS, 190 mM glycine and 10% methanol v/v), and the gels were allowed to rest for 30 minutes in the buffer prior to activation in the ChemiDoc MP system (Bio-Rad Laboratories), where after it was transferred. An image of the gel was stored by the ChemiDoc MP system. Transfer was performed at 200 V and 200 mA for 1 hour 30 minutes at 4° Celsius onto an Immobilon®-P PVDF membrane (EMD Millipore). An image of the transferred proteins on the membrane was again stored for normalization purposes. The membranes were briefly placed in methanol, and allowed to dry before blocking in a 5% liquid fat-free milk solution. After blocking, the membranes were washed three times in TBS-T (20 mM TRIS-HCl (pH 7.6), 137 mM NaCl, 0.1% Tween-20), for 5 minutes at a time. The membranes were then cut above and below the protein of interest in order to investigate several proteins on the same membrane. The membrane was incubated in primary antibody (Table 3.1) overnight (maximum 16 hours) at 4°C and washed three times (as described previously) after incubation. The membrane was placed in secondary antibody (1:4000 dilution of HRP-linked secondary antibody #7074, CST in TBS-T) for one hour at room temperature.

The membrane was washed three times (as described previously) prior to being imaged with Clarity™Western ECL Blotting Substrate and visualised on the Chemidoc MP system on the Chemi Hi sensitivity setting, which was stopped prior to overexposure (which appears red on program settings). Membranes from the same experiment were analysed in parallel.

Table 3.1: Summary of antibodies used to investigate the insulin-resistant H9c2 cell culture model:

Protein antibody	Size	Dilution and dilutant	Species origin	Supplier	Product code
ATM	350 kDa	1:1000 TBS-T	Rabbit	Abcam	ab199726
Phospho-ATM (Ser1981)	350 kDa	1: 1000 Primary SignalBoost™Immuno-reaction Enhancer Kit	Rabbit	CST	(D25E5) #13050
Akt (PKB)	60 kDa	1: 1000 TBS-T	Rabbit	CST	(C67E7) #4691
Phospho-Akt (Ser473)	60 kDa	1: 1000 TBS-T	Rabbit	CST	(193H12) #4058
AMPK	62 kDa	1:1000 TBS-T	Rabbit	CST	(D63G4) #5832
Phospho-AMPK Thr172	62 kDa	1:1000 TBS-T	Rabbit	CST	(D4D6D) #50081
mTOR	289 kDa	1:1000 TBS-T	Rabbit	CST	(7C10) #2983
Phospho-mTOR Ser 2448	289 kDa	1:1000 TBS-T	Rabbit	CST	#2971

*CST: Cell Signaling Technology

3.2.5 Western blot analysis and normalization:

Protein levels were normalised to total protein loaded on the gel and transferred to the membrane, in ImageLab 5.0. The software calculates the total pixel intensity per lane across the surface area of the lane, and accordingly normalises the pixel intensity of the protein band in question to that of its total protein lane (Gilda & Gomes 2014; Rivero-gutiérrez et al. 2014). Consequently, each lane was adjusted manually to include as much of the visible lane surface area in ImageLab 5.0, and analysed using the software function for normalisation to total protein. The normalised pixel intensities for each protein band of interest were exported to Excel (Microsoft Office 2010) and the fold-change compared to the control-treated cells (0.1% EtOH) were determined by calculating the average pixel intensity of

normalised band values for the control group, and dividing the average normalised pixel intensities of each treatment by that of the control group. Once analysed, the data were exported to Graphpad Prism 6.0 for statistical analysis. This method negates the use of a loading control to normalize for equal loading.

3.2.4 Glucose uptake:

Radiolabelled 2-deoxy glucose (2-DG) uptake by H9c2 cells was performed as described previously (Fischer et al. 1991; Huisamen et al. 2001) with modifications. Similarly to cardiomyocytes the cells were washed twice with PBS, and serum starved for 3 hours in DMEM without FBS or Pen/Strep, followed by a period of 30 minutes where the cells were deprived of all substrates using Solution E (6 mM KCl, 1 mM Na_2HPO_4, 0.2 mM NaH_2PO_4, 1.4 mM $MgSO_4$, 128 mM NaCl, 10 mM HEPES, 1.25 mM $CaCl_2$ and 2% fatty acid free BSA fraction V, pH 7.4). The cells were pre-incubated for 5 min in a shaking benchtop incubator (37°C) with or without phloretin (400 µM) for measurement of non-carrier mediated glucose uptake. Phloretin was dissolved in DMSO and stored as 6.4 mM stock solution and diluted with medium immediately before use. Each experimental treatment (n=3/ condition, five conditions) was incubated with or without 10 nM insulin under the same conditions for 15 min, after which glucose uptake was initiated by addition of 2-deoxy-D-[3^H]glucose (1.5 µCi/ml; final concentration 1.8 µM) (2-DG). Glucose uptake was allowed to progress for a further 30 min before the reaction was stopped by adding 100 µl phloretin to give a final concentration of 400 µM. The cells were washed twice in HEPES buffer to remove extracellular 2-DG, and dissolved in 1M NaOH. The assay is represented graphically in Figure 3.1.

Afterwards, samples were diluted with dH_2O to 0.5 M NaOH. A small aliquot of this was used to assay the protein content of every aliquot in triplicate by the method of Lowry et al. (1951), whilst the rest was counted in duplicate for radioactivity in a Beckman LS 6500 multi-purpose scintillation counter. The specific activity of the radiolabelled solution was determined and the 2-DG uptake calculated as pmol 2-DG/mg prot/30 min.

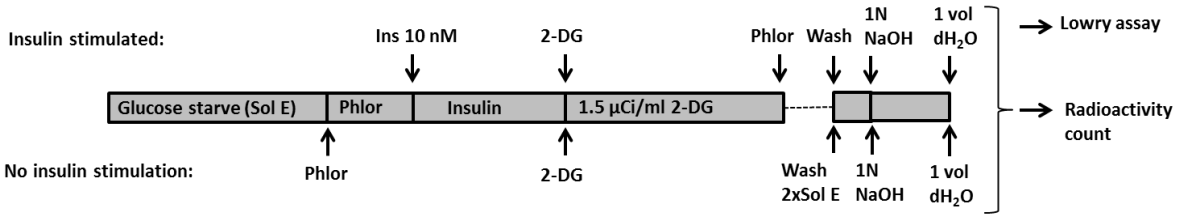

Figure 3.1: Schematic representation of the glucose uptake assay. Two sets of experiments (5 treatment conditions, n=3/condition) were prepared in parallel and were either stimulated with insulin (top protocol) or only treated with phloretin (bottom protocol), respectively. The cells were serum starved for three hours, prior to being substrate starved (start of protocol) for 30 min in Solution E. Phloretin was added to the cells that were not stimulated with insulin and incubated for 5 minutes (bottom), before insulin was added to the cell cultures that were stimulated with insulin (15 min). 2-DG was added to both sets of experiments and incubated for 30 minutes, and stopped with the addition of phloretin to the insulin-stimulated experiment. Both sets of experiments were aspirated, washed and aspirated twice with HEPES buffer, and incubated with 1N NaOH at 37°C for 1 hour. One volume of distilled H_2O was added for a final concentration of 0.5N NaOH. A volume of cell lysate was incubated overnight in scintillation fluid prior to being counted in duplicate, and the remaining cell lysate was used for a Lowry assay protein concentration determination (protocol adapted from (Fischer et al. 1991; Huisamen et al. 2001)**).**

3.2.5 Statistical analysis:

The data was analysed using GraphPad Prism 6.0 software (GraphPad Software, Inc., La Jolla, CA). Statistical comparisons were made using a two-tailed Student's t-test or 1-way analysis of variance (ANOVA) followed by a Bonferroni post-hoc test where applicable. All values and error bars are presented as mean ± s.d., and the level of significance was set at $p < 0.05$.

3.3 Results and discussion:

The H9c2 cells used during this experiment conformed to the description by Kimes & Brandt (1976), and showed 2-4 distinct nucleoli in the nuclei of the cells (Fig 3.2). No differences were noticed visually between the different passages, and the cells maintained their structural integrity. The cells were not differentiated in light of a previous report that showed that some cells within a H9c2 cell population can be resistant to differentiation (Patten et al. 2017), that can result in a heterogenous population.

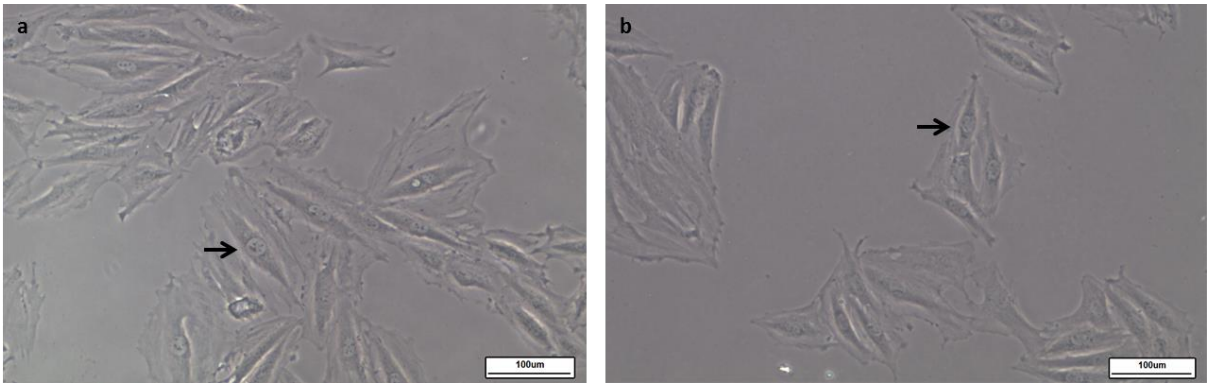

Figure 3.2: H9c2 cell structure between different passages. Images of cells were taken on a regular basis during proliferation to monitor confluency, integrity and general cell health. Panel a shows cells at passage 9 and panel b at passage 13. The arrows indicate a typical H9c2 cell with its nucleus and nucleoli. The scale bar is 100 µm, at 40x magnification.

The experimental design was initially optimised with a 0.1 mM palmitic acid, which is widely reported to induce inflammation (Wang et al. 2017), insulin resistance (Nobuhara et al. 2013) and mitochondrial dysfunction (Wei et al. 2013) in H9c2 cells. The protein expression levels of ATM, Akt and mTOR were investigated to gauge the sensitivity of the cells to 0.1 mM palmitic acid in line with studies that have shown that ATM can be activated by insulin (Halaby et al. 2008).

No differences were observed in total mTOR protein levels after 24 hours of 100 nM palmitic acid or 100 nM insulin incubation of H9c2 cells. The downregulation of ATM in HFD conditions and obesity in rats led to suggestion that ATM is required for the full activation of Akt in response to insulin stimulation in mouse fibroblasts (Halaby et al. 2008). Similarly, this study shows that ATM protein levels are decreased with 0.1 mM palmitic acid treatment, albeit not significantly (Figure 3.3). The addition of 0.1 mM palmitic acid together with insulin significantly decreased Akt protein levels ($p<0.005$, 1-way ANOVA, Bonferroni post-hoc test) compared to insulin treatment alone as well as compared to the control H9c2 cells. The same trend was observed for ATM, where the combination of 100 nM insulin together with 0.1 mM palmitic acid significantly decreased ($p<0.05$,1-way ANOVA, Bonferroni post-hoc test) total ATM protein levels. This corresponds well with the suggestion that ATM is required for the full activation of Akt in response to insulin stimulation (Halaby et al. 2008), and suggests that the combination of palmitic acid and high insulin concentrations influence the protein levels of both Akt and ATM in a similar manner.

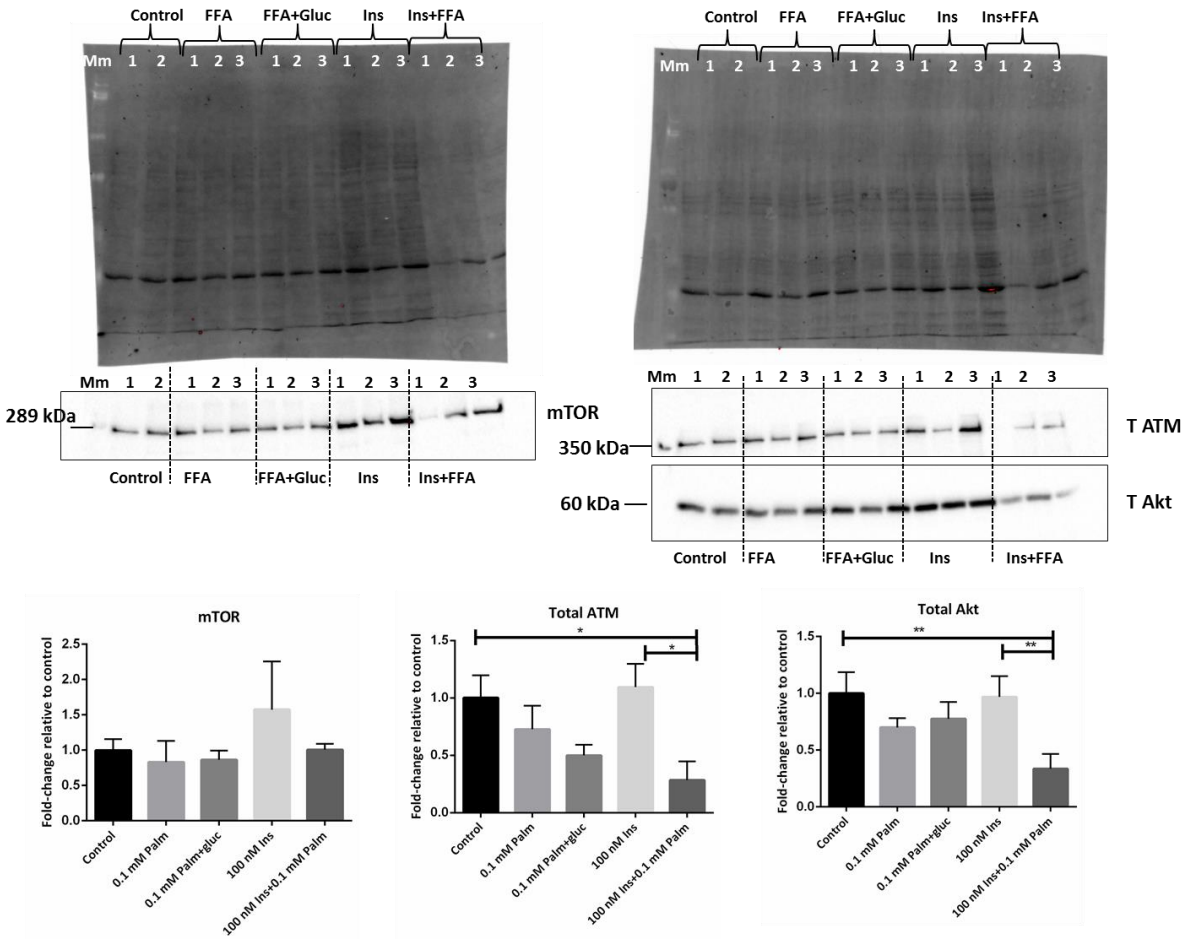

Figure 3.3: Western blot analysis of total ATM, total Akt and mTOR protein levels in H9c2 cells treated with 0.1 mM palmitate. Undifferentiated H9c2 cells were treated respectively with either 0.1% EtOH (vehicle control indicated as 'Control" on the graph), 0.1 mM palmitic acid (FFA), 0.1 mM FFA and 5.5 mM glucose, 100 nM insulin or 100 nM insulin + 0.1 mM FFA (n=3/condition). The cells were lysed and analysed with western blotting. Protein expression levels for mTOR was normalised to membrane 1 (left) and ATM and Akt was normalised to membrane 2 (right). The samples were loaded as shown on the membrane and a high molecular weight marker (mm) was loaded in the first lane. Lane 1 from the Ins+FFA was excluded from analysis due to less protein loaded initially. The fold-change in protein levels for each of the proteins are shown relative to the mean pixel intensity of the control group. A one-way ANOVA was performed for each protein of interest and all values and error bars are presented as mean ± s.d., and the level of significance was set at $p < 0.05$.* $p<0.05$, **$p<0.005$.

The aim of this experiment was to determine whether a similar model can be established in H9c2 cells with the addition of oleate and palmitate in order to establish a model closer to that of an in vivo HFD-induced obesity model, as was suggested by Liu et al. (2015). Consequently, this study investigated the effect of a saturated and monounsaturated free fatty acids on H9c2 cells. Oleic acid protects neuronal cells against palmitate induced insulin resistance and inflammatory signalling (Kwon et al. 2014) as well as mitochondrial dysfunction, which was also observed in L6-muscle cells (Gao et al. 2009). High

concentrations of palmitate in undifferentiated H9c2 cells have been associated with apoptosis and ROS generation (Wei et al. 2013) as well as insulin resistance and mitochondrial dysfunction (Nobuhara et al. 2013). A previous study within our laboratory stimulated neonatal cardiomyocytes a with 0.25 mM oleate and palmitate and found that this concentration of FFA had no effect on cell viability assessed with trypan blue or propidium iodide (Ms S Pêrel, MSc thesis, 2009). Cell viability was not assessed during this study, and is a major shortcoming.

H9c2 cardiomyoblasts were treated with final concentrations of either 0.1% EtOH (vehicle), 0.2 mM FFA (0.1 mM palmitic and 0.1 mM oleic acid dissolved in EtOH), 0.2 mM FFA+5.5 mM glucose, 100 nM HumulinR insulin and 100 nM insulin+0.2 mM FFA. The use of 0.2 mM palmitate has previously been shown to induce insulin resistance in differentiated H9c2 cells (Nobuhara et al. 2013), whilst apoptosis was observed in response to 0.1 mM palmitate treatment of undifferentiated H9c2 cells (Wei et al. 2013). Mitochondrial dysfunction has also been reported in C2C12 cells treated with 0.2 mM palmitate (Jheng et al. 2012). This study observed no difference in cellular morphology between untreated H9c2 cardiomyoblasts, or cells treated with 0.1% EtOH after 24 hours (Fig 3.4 a and b). However, treatment with 0.2 mM FFA resulted in shorter, rounder cells (insert, Fig 3.4 d) after 24 hours similar to that observed in palmitic acid treated H9c2 cells (Wang et al. 2017). Rounded cells was also observed in cells treated with 0.2 mM FFA and 5.5 mM glucose.

It should be noted that this is merely an observation and was not quantified. Quantification of hypertrophy should be interesting in this case, together with an assessment of lipid accumulation, based on previous observations that H9c2 cardiomyoblasts mimics hypertrophy in a manner similar to that of primary cardiomyocytes (Watkins et al. 2011).

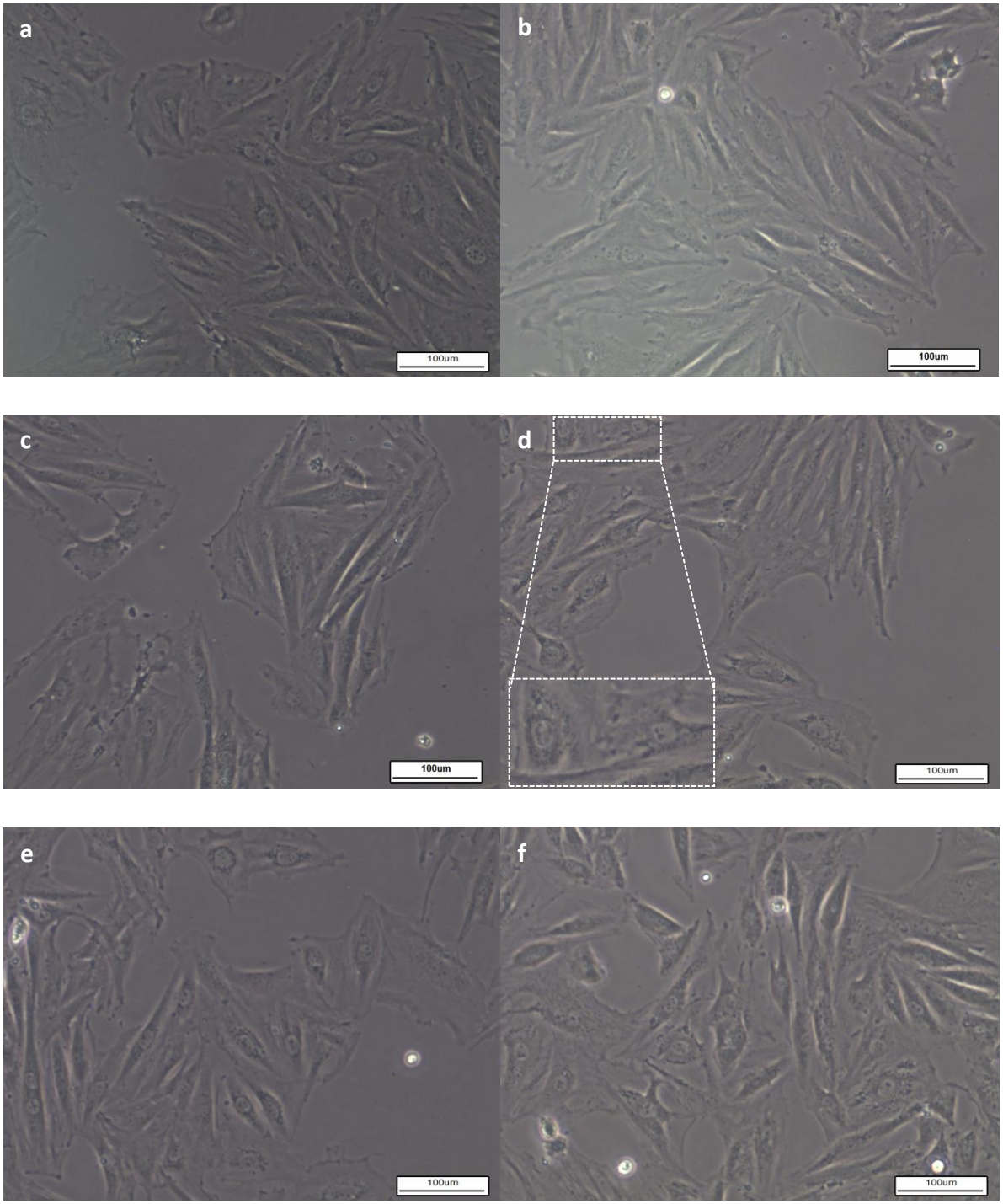

Figure 3.4: H9c2 cardiomyoblast prior to and after 24 hours of FFA treatment. H9c2 cardiomyoblasts were imaged directly prior to treatment (panels a, c and e) and after 24 hours of either 0.1% EtOH (panel b), 0.2 mM FFA (panel d) where cells started to exhibit a rounded compard to an elongated shape(insert), or 0.2 mM FFA + 5.5 mM glucose treatment (panel f). H9c2 cells are maintained in high glucose medium (25 mM) under normoxic conditions, and 5.5 mM glucose was added to increase the glucose concentration. The scale bar represents 100 µm.

Insulin also seemed to result in rounding of cells compared to elongated cells in the H9c2 cardiomyoblasts after 24 hours of treatment, whilst dark aggregates could be observed in

cells treated with insulin and FFA (Fig 3.5). Again, this was not quantified, but can be suggestive of increased cytoplasm vacuolization similar to that observed in H9c2 cardiomyoblasts treated with supra-therapeutic doses of doxorubicin (Sardão et al. 2009). Although lacking in this study, this suggests that further investigation into the formation of vacuoles and autophagy as well as the quantification of hypertrophy, could extend this model to provide a better understanding of lipotoxicity and hyperinsulinaemia in the heart.

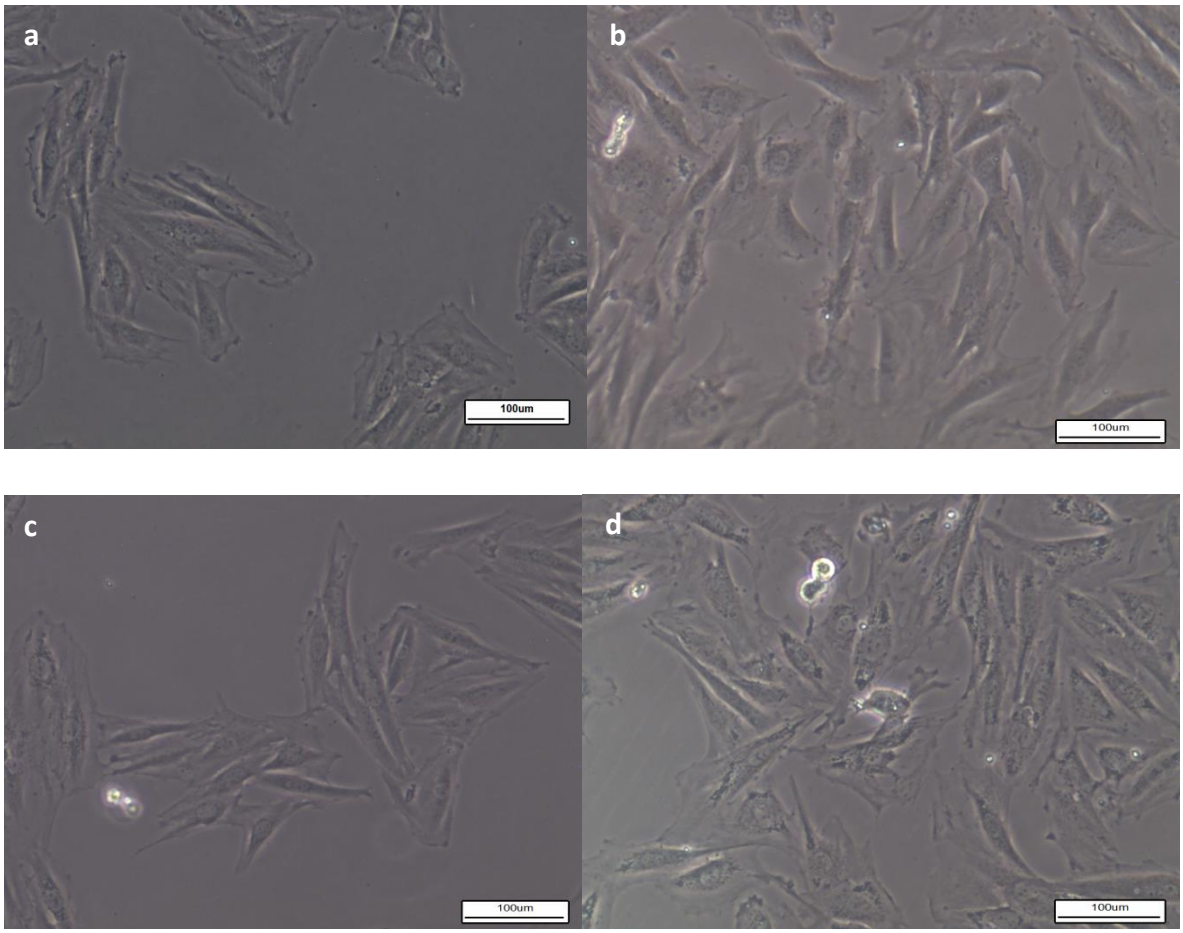

Figure 3.5: H9c2 cardiomyoblast prior to and after 24 hours of insulin and insulin plus FFA treatment. H9c2 cardiomyoblasts were imaged prior to (panel a and c) and directly after treatment with 100 nM insulin (panel b) and 100 nM insulin plus 0.2 mM FFA (panel d). The scale bar represents 100 µm.

Contrary to Nobuhara et al. (2013) who did not observe any glucose uptake in undifferentiated H9c2 cardiomyoblasts compared to differentiated myoblasts with 10 nM insulin stimulation, this study shows insulin-stimulated 2-DG uptake in the presence of 10 nM insulin alone, albeit not significantly because of the wide scatter in the small sample size. All the treatments used in this study suppressed glucose uptake when stimulated in the presence of 10 nM insulin. The 24 hour treatment of 0.2 mM FFA alone and the

combination of 0.2 mM FFA + 100 nM insulin treatment suppressed 2-DG-uptake glucose uptake in the presence of 10 nM insulin and the readings were well grouped. Although no significant difference was observed.

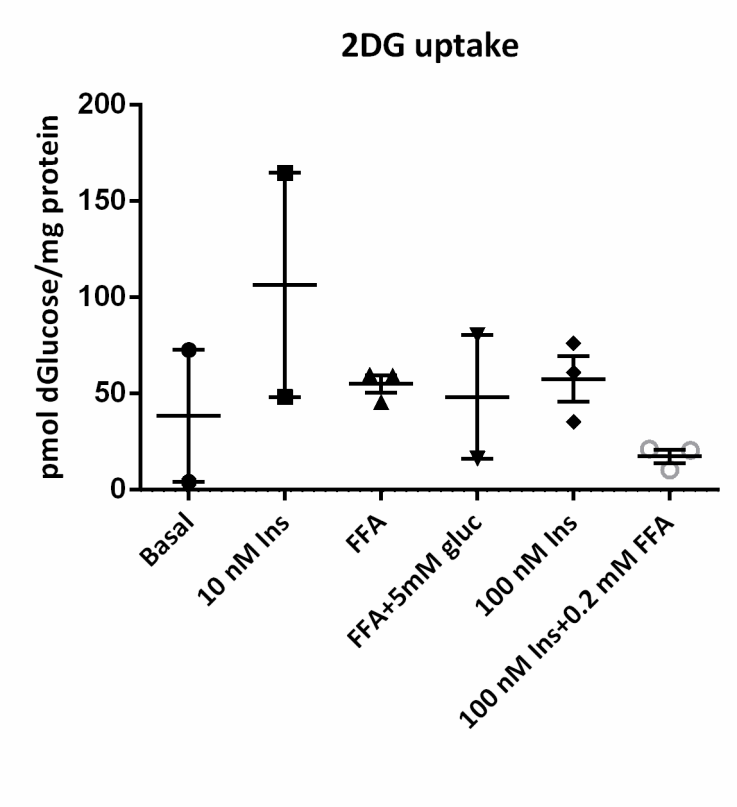

Figure 3.6: 2-[^{3}H]-deoxy glucose uptake in undifferentiated H9c2 cardiomyoblast cells. Glucose uptake was measured in undifferentiated H9c2 cells under either basal conditions, with the stimulation of 10 nM insulin in untreated cells, or with 10 nM insulin stimulation in cells treated with 1) 0.2 mM FFA, 2) 0.2 mM FFA + 5 mM glucose, 3) 100 nM HumulinR insulin or 4) 100 nM HumulinR insulin + 0. 2 mM FFA, respectively after 24 hours of treatment. No significant differences were observed (one way ANOVA with Bonferroni-post hoc analysis (n=2-3)).

In line with a previous study that showed that the addition of 100 nM insulin to H9c2 cells elicits an insulin resistant response (Ha & Pak 2005), the current study found a similar result when stimulating glucose uptake with 10 nM insulin in cells that have been treated with 100 nM of insulin over 24 hours. Insulin stimulated uptake in cells that were treated with a combination of 5 mM glucose and 0.2 mM FFA gave no significant results (n=2, Fig. 3.6). However, none of these results were significant compared with either basal uptake or 10 nM insulin stimulated uptake in control vehicle cells.

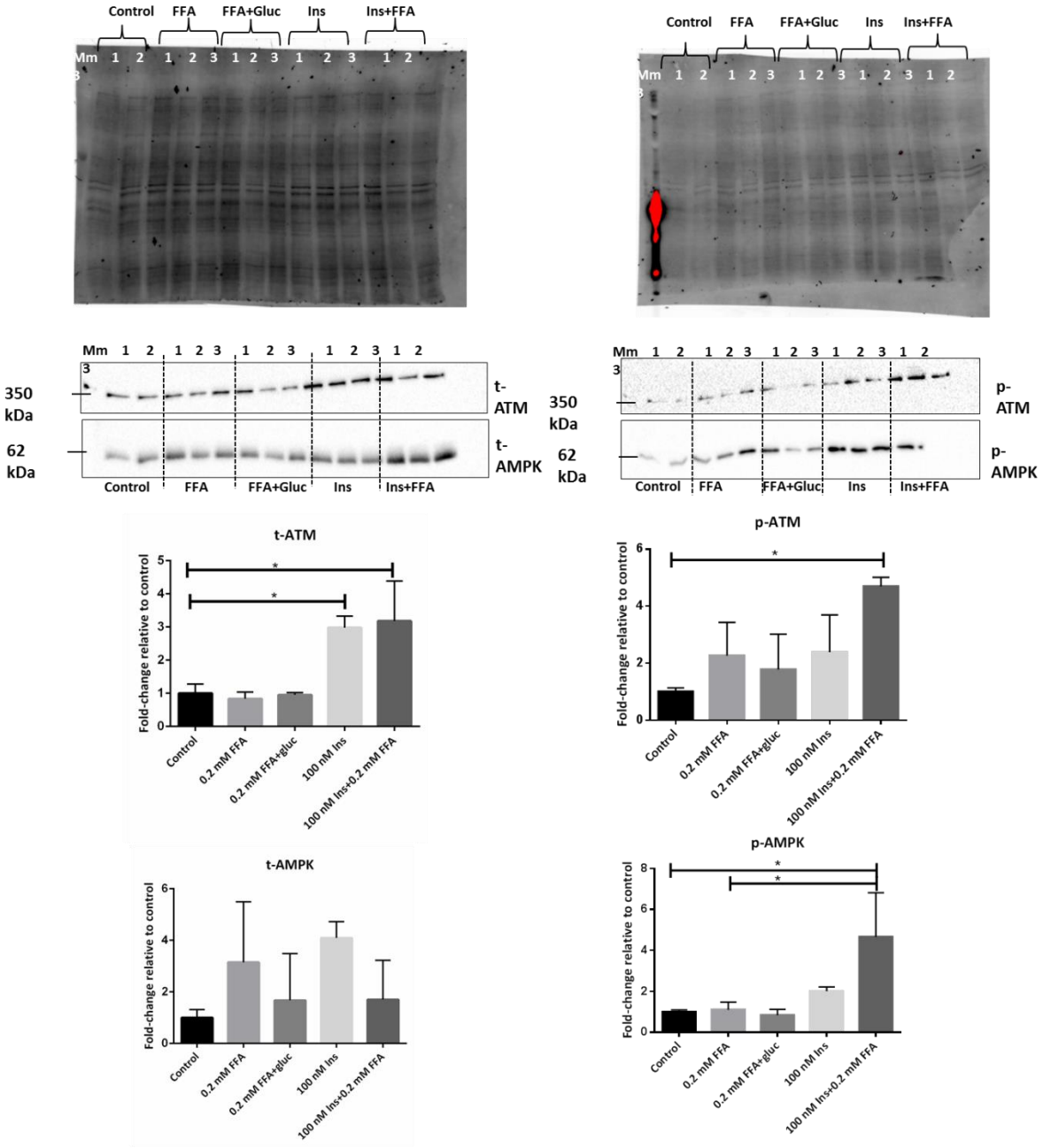

Figure 3.7: Western blot analysis of total ATM and phosphorylated ATM, as well as AMPK and phosphorylated AMPK protein levels in H9c2 cells treated with 0.2 mM palmitate and oleic acid. Undifferentiated H9c2 cells were treated respectively with either 0.1% EtOH (vehicle control), 0.2 mM palmitic and oleic acid (FFA), 0.2 mM FFA and 5.5 mM glucose, 100 nM insulin or 100 nM insulin + 0.2 mM FFA (n=3/condition). Protein expression levels for total ATM and total AMPK was normalised to membrane 1 (left) and phospho-ATM and phospho-AMPK was normalised to membrane 2 (right). The samples were loaded as shown on the membrane and a high molecular weight marker (mm) was loaded in the first lane. The fold-change in protein levels for each of the proteins are shown relative to the mean pixel intensity of the control group.

The insulin-sensitive protein, Akt and phospho-Akt, as well as the insulin-insensitive protein, AMPK and phosphorylated AMPK (at Thr172) were investigated. The latter were included

because of the increased autophagy that was previously reported in response to lipotoxicity in H9c2 cells (Cai et al. 2002).

Both total ATM as well as phosphorylated ATM increased significantly in the presence of 0.2 mM FFA and 100 nM insulin, whilst phosphorylated AMPK increased significantly, although total AMPK levels did not when compared to the control treated cells ($p<0.05$, one-way ANOVA) (Fig. 3.7). This however, did not translate to a significant increase in the phospho-ATM/total ATM ratio or phospho-AMPK/total AMPK ratio (Fig 3.8) in this model. It does suggest that the addition of the monounsaturated fatty acid, oleate, can be protective via an ATM-mediated mechanism in hyperinsulinaemia-induced insulin resistance in the presence of high free fatty acids (0.2 mM FFA+100 nM insulin), but not in the presence of free fatty acids alone (0.2 mM FFA).

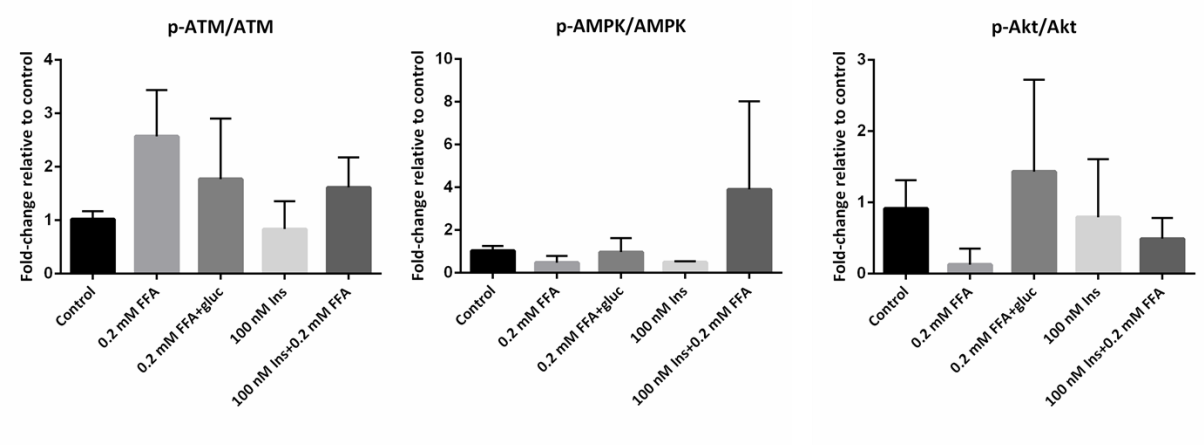

Figure 3.8: Phospho-ATM/total ATM, phospho-AMPK/total AMPK and phospho-Akt/total Akt ratios. The arbitrary units calculated after normalisation to the total protein for each lane was used to determine the ratio for each corresponding lane by division of the phospho-protein value by the total protein.

An increase in AMPK Thr^{172} phosphorylation in response to palmitate was reported previously, where it was shown that increased AMPK activity resulted in increased fatty acid oxidation, independently of changes in the AMP/ATP ratio in L6 cells (Watt et al. 2006). Oleate treatment inhibits palmitate-induced activation of AMPK, and this has been suggested to be one of the mechanisms through which oleate mediates its protective effects (Palomer et al. 2018).

Kwon & Querfurth (2015) also showed that the addition of oleate improved pAMPK, and found that palmitate alone inhibits the phosphorylation of AMPK, decreases phosphorylation of Raptor and 4E-BP1 and activates p70S6K, without changing the phosphorylation levels of mTOR or Rictor. This was completely prevented by the addition of oleate, in a similar fashion to that of metformin-mediated activation of AMPK (Kwon & Querfurth 2015).

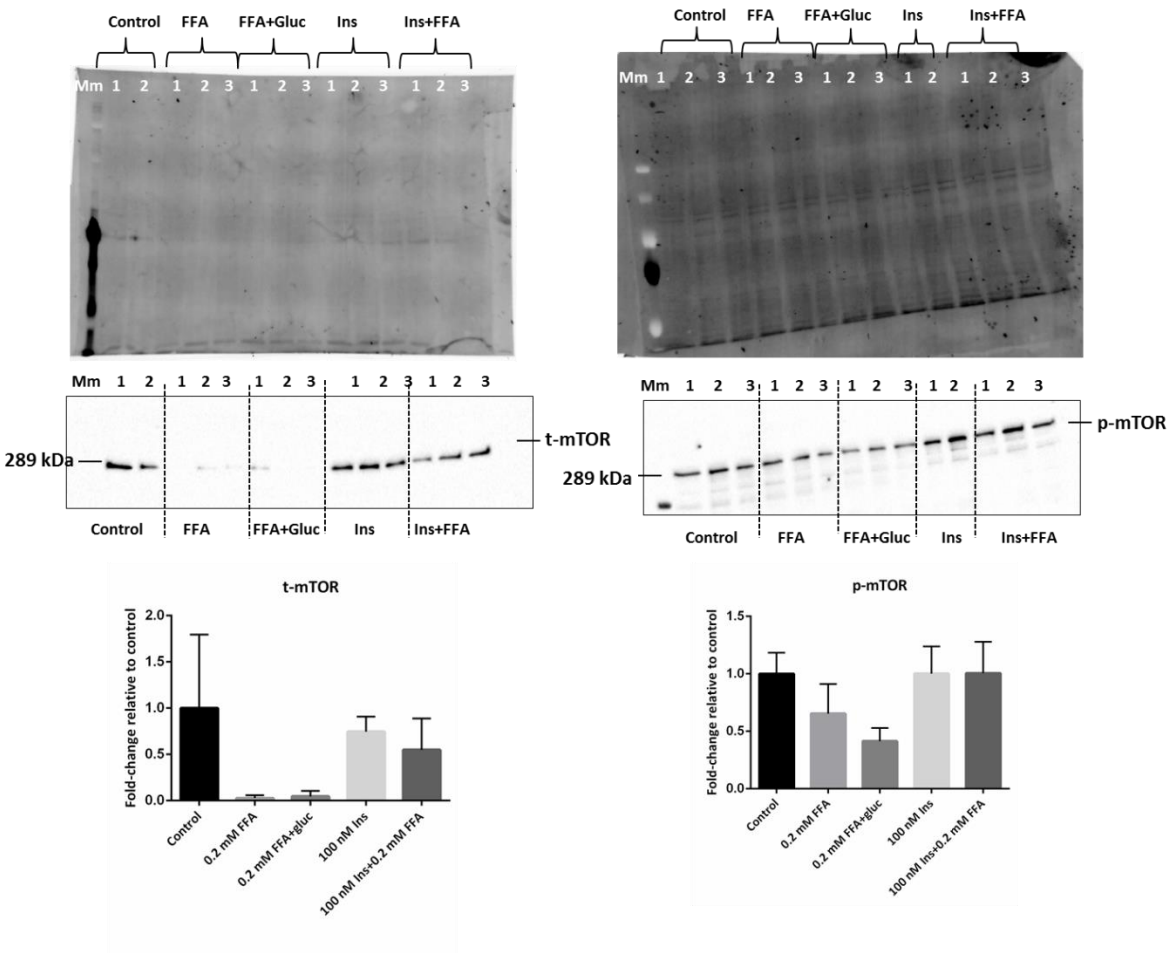

Figure 3.9: Western blot analysis of total mTOR and phosphorylated mTOR (Ser^{2448}) in H9c2 cells treated with 0.2 mM palmitate and oleic acid. Undifferentiated H9c2 cells were treated respectively with either 0.1% EtOH (vehicle control), 0.2 mM palmitic and oleic acid (FFA), 0.2 mM FFA and 5.5 mM glucose, 100 nM insulin or 100 nM insulin + 0.2 mM FFA. The cells were lysed and analysed with western blotting. Protein expression levels for mTOR was normalised to membrane 1 (left) while p-mTOR was normalised to membrane 2 (right).

AMPK is also located upstream of mTOR, and ATM activates AMPK either via LKB1 in response to oxidative stress (Alexander et al. 2010), or independently of LKB1 in response to growth factors in an IGF-1 mediated manner (Suzuki et al. 2004). Moreover, there might also exist a negative feedback loop between ATM and mTOR (Shen & Houghton 2013), and

mTOR was thus included in the study. The inhibition of AMPK phosphorylation by palmitate has also been implicated in the pathogenesis of obesity due to increased mTOR activity (Kwon & Querfurth 2015; Palomer et al. 2018).

Our study could not find any significant effects on mTOR protein levels or phospho-mTOR with the addition of 0.2 mM FFA, 0.2 mM FFA+5.5 mM glucose, or insulin to H9c2 cardiomyoblasts. Although decreased mTOR expression was observed in the presence of FFA and a combination of FFA and glucose, no significant differences were observed (Fig 3.9). A reduction was observed in mTOR phosphorylation at Ser^{2448} with the addition of 5 mM glucose to the FFA, which was restored to basal levels in the presence of 100 nM insulin and 100 nM insulin together with 0.2 mM FFA (Fig 3.9). These membranes represent lysates from two repeated experiments that were electrophoresed on different days, and consequently a ratio could not be determined between phospho-mTOR and total mTOR.

The decrease observed in mTOR Ser^{2448} phosphorylation, could potentially suggest an increase in autophagy as a manner to cope with hyperglycaemic and hyperlipidaemic conditions. A study found that H9c2 cells that are treated with angiotensin II show increased expression of hypertrophy marker genes as well as decreased TSC2 phosphorylation which concomitantly decreased AMPK activation, increased glucose uptake and mTOR activation (Stuck et al. 2008), which potentially implicates the activation of the insulin sensitive Akt-pathway. Moreover, both mTOR and Rictor (mTORC2) are required for the phosphorylation of Akt at Ser^{473}, and a reduction in either mTOR or Rictor can inhibit the activation of Akt (Sarbassov et al. 2005).

A recent study that characterised insulin resistance in vascular smooth muscle cells found that oleate and insulin induced phosphorylation of Akt at Thr^{308}, whilst oleate alone caused phosphorylation of AMPK (Perdomo et al. 2015). The study also found that palmitate treatment over a period of 18 hours induced insulin resistance that was characterised by a decrease in phosphorylated Akt as well as phosphorylated p70S6K. Similarly, the present study found that phosphorylated Akt was decreased compared to insulin alone in the presence of 100 nM insulin and 0.2 mM FFA, whilst being significantly increased in the presence of a 100 nM insulin when compared to 0.2 mM FFA treatment alone ($p<0.05$, one-way ANOVA) (Fig. 3.10). Phosphorylated mTOR levels remained at basal levels. These results

are summarized in Table 3.2, which shows the relative protein expression of each of the proteins investigated in response to the different treatments relative to the vehicle control cells.

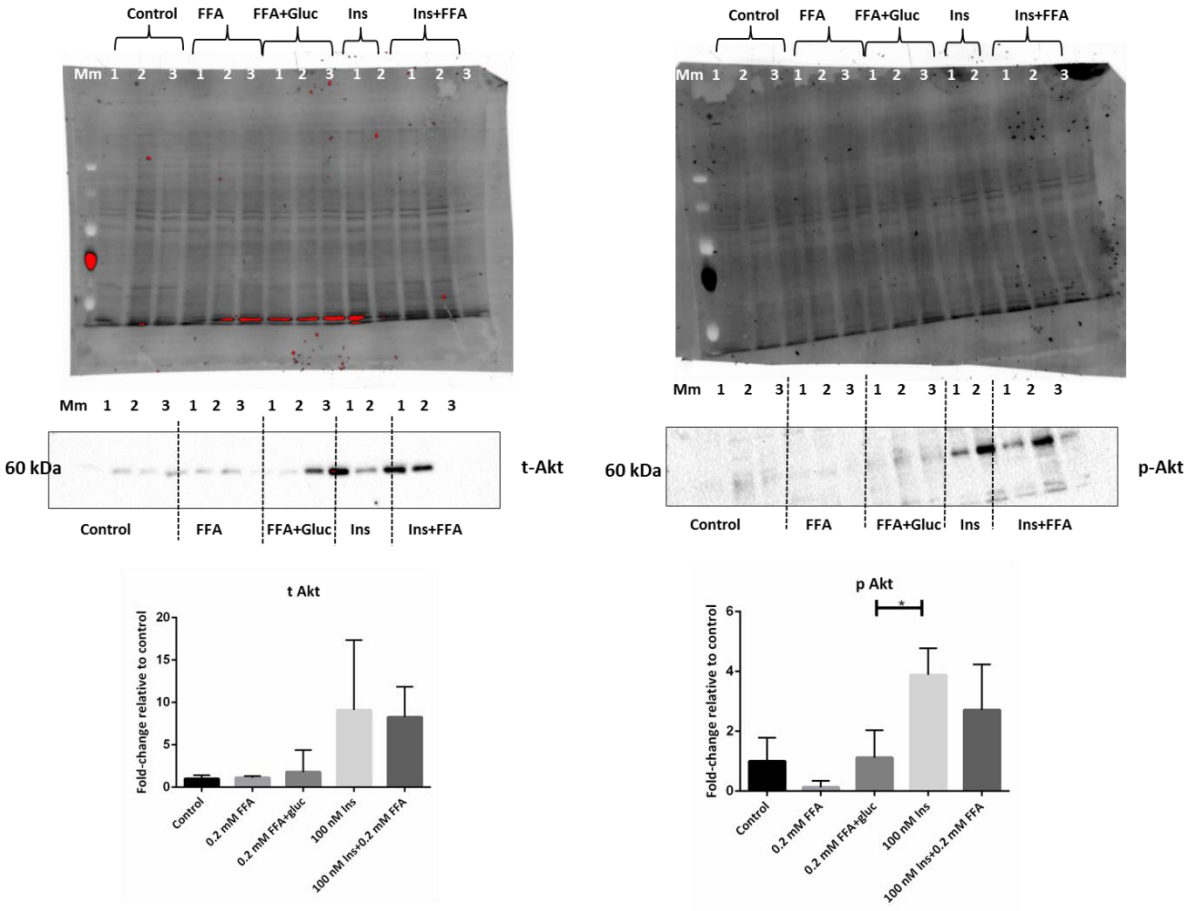

Figure 3.10: Western blot analysis of total tAkt and phosphorylated Akt (Ser^{473}) in H9c2 cells treated with 0.2 mM palmitate and oleic acid. Undifferentiated H9c2 cells were treated respectively with 0.1% EtOH (vehicle control), 0.2 mM palmitic and oleic acid (FFA), 0.2 mM FFA and 5.5 mM glucose, 100 nM insulin and 100 nM insulin + 0.2 mM FFA. The cells were lysed and analysed with western blotting. Protein expression levels for Akt was normalised to membrane 1 (left) and p-Akt was normalised to membrane 2 (right).

In summary, the use of 0.2 mM palmitate and oleic acid, both in the presence and absence of 100 nM insulin is sufficient to induce insulin resistance in undifferentiated H9c2 cells (Fig 3.6) although this was not significant and needs to be repeated.

Table 3.2: Protein expression levels compared to vehicle control cells after 24 hours of treatment where the FFA is listed in the first row and the combination of treatments in the next row. The first block represents 0.1 mM palmitic acid and the second block 0.2 mM FFA (0.1 mM palmitate + 0.1 mM oleate):

Condition	t-ATM	p-ATM	t-Akt	p-Akt	t-AMPK	pAMPK	mTOR	p-mTOR
0.1 mM palmitate	↓		↓				-	
+ 5.5 mM glucose	↓		↓				-	
+100 nM insulin	↓*		↓**				-	
100 nM insulin alone	-		-				↑	
0.2 mM FFA	-	↑	-	↓	↑	-	↓	↓
+ 5.5 mM glucose	-	↑	-	-	-	-	↓	↓
+100 nM insulin	↑*	↑*	↑	↑	-	↑*	-	-
100 nM insulin alone	↑*	↑	↑	↑	↑		-	-

*p<0.05; **p<0.005 fold change relative to control, 2-way ANOVA, Bonferroni post-hoc test↑

The phospho Akt/total Akt protein levels were also decreased by FFA compared to the vehicle control. It should be noted that these changes were not significant, but lays the ground work for a potential model that can be used to examine insulin resistance. The underlying mechanisms and role of ATM remains to be elucidated. The co-treatment with both oleic and palmitic acid in combination with insulin significantly increased both total

and phosphorylated ATM levels, which could suggest that oleate might act in a similar manner on ATM as AMPK (Kwon & Querfurth 2015; Palomer et al. 2018) . The decrease observed in the phospho-Akt/total Akt ratio is accompanied with a concomitant increase in the AMPK ratio when cells are treated with palmitic and oleic acid as well as insulin. No difference was noted in the phospho-ATM/ATM ratio. In agreement with Kwon et al. (2014) this study also only noted phosphorylation of Akt in the presence of insulin, and not with FFA alone. The study by Ussher & Jaswal (2009) also failed to induce AMPK phosphorylation with either 0.1 mM or 0.2 mM palmitate or oleate, respectively. This could potentially suggest different underlying mechanisms for insulin resistance induced with either hyperlipidaemia or a combination of hyperlipidaemia and hyperglycaemia as well as hyperlipidaemea and hyperinsulinaemia. Unlike Halaby et al. (2008) this study did not observe phosphorylation of ATM in response to insulin treatment alone, however ATM phosphorylation was significantly increased compared to control treated cells in response to the combination of insulin and FFA treatment. Moreover, total ATM levels increased significantly in the presence of palmitic and oleic acid together with insulin, compared to palmitate and insulin alone in Fig 3.7. However, this increase was not observed in Fig 3.3, and highlights the need for more experiments with 0.1 mM palmitate alone compared to a combination of 0.1 mM palmitate and 0.1 mM oleate. These results are summarised in Table 3.2.

Taken together, this pilot study provides an initial dissemination of a hyperlipidaemic insulin resistant H9c2 model that is sensitive to glucose and insulin addition. Moreover, similar models have been used to investigate the role of mitochondrial dysfunction in H9c2 cells (Kwon et al. 2014; Wang et al. 2017; Gao et al. 2009). The model described in the current study can thus potentially be used to study mitochondrial dysfunction in response to induced insulin resistance; moreover, the model can be easily manipulated which would suggest that the ATM specific inhibitor can be used to inhibit ATM.

Chapter 4 : Ataxia-Telangiectasia Mutated protein kinase is located on the inner mitochondrial membrane of rat cardiac mitochondria

ATM is activated by endogenous mitochondrial oxidative stress (Zhang et al. 2018) and acts as an important sensor of reactive oxygen species (ROS), independently of the DNA damage response pathways (Guo et al. 2010). Studies have shown that ATM is located in the mitochondrial fraction of fibroblasts (Valentin-Vega et al. 2012), and is activated more specifically within the mitochondria rather than the peroxisomes (Morita et al. 2014). Following on this finding and a study that showed that ATM co-localize with peroxisomes (Watters et al. 1999), it was demonstrated that ATM is recruited to peroxisomes in response to oxidative stress (Zhang et al. 2015). The question thus arises whether ATM is located within the mitochondria, or recruited as is the case with peroxisomes.

ATM has been implicated in the regulation of mitochondrial function, specifically with regards to mitochondrial respiration (Ambrose et al. 2007). In this regard, Complex I of the ETC was found to be down-regulated in the absence of ATM in $ATM^{-/-}$ fibroblasts (Valentin-Vega et al. 2012). Elucidation of the protein's location can thus contribute towards a better understanding of its role within mitochondria. This chapter describes the development of a digitonin-based mitoplast isolation technique in order to determine whether ATM is associated with the outer or inner mitochondrial membrane (OMM and IMM) or matrix of the mitochondria. The role of ATM as both an oxygen- and redox sensor suggests that the protein might be associated with the IMM or matrix of cardiac mitochondria, and could potentially play a role in oxidative phosphorylation.

4.1 Development of a mitoplast isolation protocol:

Mitochondria are often described as the powerhouses of cells, and supply the necessary energy for normal cell functioning and contraction of the heart. This and other essential functions, as well as the implication of mitochondrial dysfunction in many diseases such as Alzheimer's disease, Parkinson's disease and diabetes (Scheffler 2001), have led to the description of several applications and techniques for the isolation of mitochondria. The

IMM and matrix, when isolated together is known as a mitoplast, whilst the OMM can be removed without damaging the mitoplast. Each of these compartments is essential for the proper functioning of mitochondria as a whole.

Several protocols have been described for the isolation of mitoplasts from mitochondria. Many protocol optimizations led Bachmann et al. (1966) to suggest that the most effective procedure to obtain a well-resolved outer membranous fraction involves the disruption and consequent separation of the inner and outer membrane by sonication. In order to obtain the IMM, it was suggested that the best approach is to strip the outer membrane away from the IMM with phospholipase (Allmann et al. 1966). Today, the most commonly used techniques include digitonin and osmotic shock (Tzagoloff 1982). Although the French press is also sometimes used, its use is limited by the availability of the necessary equipment.

Digitonin, a mild non-ionic detergent, preferentially degrades the OMM, as measured by the release of monoamine oxidase, an enzyme only found on the outer membrane and accordingly, a suitable biochemical marker (Schnaitman et al. 1967). The seminal work of Greenawalt (1974) gives a detailed description of the isolation of mitoplasts from rat liver with a digitonin-based protocol. Even though Greenawalt (1974) reported that this method did not seem to be as effective for the isolation of mitoplasts from rat and bovine heart mitochondria, Javadov et al. (2011) successfully used this technique without any modification to isolate mitoplasts from Sprague-Dawley rat hearts. The latter study investigated the effect of NHE-I inhibition on mitochondrial fission and fusion proteins during post-infarction remodelling on mitoplasts isolated from the rat heart ventricles. Mitochondria were isolated from myocytes, and purified on a Percoll gradient, before being subjected to digitonin treatment. At a concentration of 1 % digitonin the mitoplasts tested positive for both adenine nucleotide translocase (ANT) and NHE-I, but not for the voltage-dependent anion channel (VDAC), which suggests that NHE-I is associated with the mitochondrial inner membrane. The VDAC proteins are found at contact sites between the inner and outer membrane (Doran & Halestrap 2000), and allows communication, together with ANT, between these membranes, although VDAC is typically associated with outer membrane whilst ANT is associated with the inner membrane.

A common issue associated with most mitoplast isolation techniques, is the release of the matrix components, which Burnette & Batra (1985) overcame by combining several techniques, including varying concentrations of Na-EDTA in the mitoplast isolation buffer. The intactness of the isolated mitochondria was based on NADH oxidation activity before and after sonication, and before being used for fractionation. This study's novel approach was to include EDTA in the sucrose buffer, suggesting that this would contribute towards the destabilization of the outer membrane by forming complexes with the polar head groups associated with membrane lipids. In conclusion, the authors suggest that gentle predigestion of the outer membrane with phospholipase will weaken the membrane without disruption, which can then be removed through hypotonic swelling and exposure to EDTA and digitonin, without rupturing the matrix.

Several studies since have also made use of sucrose gradient centrifugation. Sucrose gradient centrifugation was described for the isolation of mitochondria and mitochondrial fractions from rat liver (Ohlendieck et al. 1986). This study highlighted the fact that osmotically lysed mitochondria revealed a membrane fraction containing both outer and inner membranes, bound by membrane contacts. These membranes could not be separated through further centrifugation, and outer membrane contact with the inner membrane had to be removed through uncoupling with dinitrophenol, before the membranes could subsequently be separated on a density gradient (Ohlendieck et al. 1986).

The presence of outer membrane remnants, attached by contact sites to the inner membrane, has especially been noted in studies using microscopy to investigate mitoplasts prior to "patch-clamp" experiments. An example of such a study was reported by Ryu et al. (2011) that investigated and characterized a ryanodine-sensitive channel in heart mitoplasts that were isolated from Sprague-Dawley rat heart mitochondria. Mitoplasts were obtained through differential gradient centrifugation in a mannitol/sucrose buffer (M/S buffer), and were investigated visually using a phase contrast microscope. The mitoplasts appeared as transparent vesicles (2-5 µm in diameter) with "cap" regions that are remnants of the OMM, and were avoided in the patch-clamp experiments.

Osmotic shock was also used to obtain mitoplasts in a study that characterised a Ca^{2+} sensitive ion-channel on the IMM (Kirichok et al. 2004). In this study, mitochondria were

isolated from lysed Cos-7 cells. The mitochondria were subjected to osmotic shock in a hypotonic solution, whereafter the mitoplasts were sedimented from solution by centrifugation. The mitoplasts were resuspended in a hypertonic solution, and also investigated prior to patch-clamping. Several mitoplasts showed black spots on the inner membrane, which the authors suggested to be remnants of the outer membrane at several contact sites between the membranes.

A study by Beutner et al. (2001) used the protocol described by Ohlendieck et al. (1986) in order to identify a ryanodine receptor in rat heart mitochondria, and included a more rigorous centrifugation protocol to remove any OMM remnants from the isolated mitoplasts. Briefly, isolated mitochondria from two rat hearts was purified on a Percoll gradient and osmotically shocked. The membranes were disrupted by sonication, and intact mitochondria were removed through centrifugation. The supernatant was transferred as a final layer onto a continuous sucrose gradient and centrifuged for at least 8 hours to separate the membrane vesicles (Beutner et al. 2001). Similarly to Ohlendieck et al. (1986), Beutner et al. (2001) used succinate dehydrogenase (SDH) as a marker for the IMM, and tested for the presence of contact sites (CS) as well as the OMM with the VDAC antibody. The western blotting results showed clear bands for VDAC in all of the fractions that were probed including the cytosol, whole mitochondria, OMM and contact site fractions. However, no VDAC could be detected in the IMM fraction, which suggests that the IMM and thus the mitoplast, did not have any OMM remnants.

Unlike Beutner et al. (2001), a study that investigated cardiac mitochondrial thyroid receptor isoforms, used VDAC as a marker for both the IMM and OMM, COXIV for the inner membrane and mtHSP70 as a matrix marker (Morrish et al. 2006). The results showed that the VDAC marker was present in the whole, purified, mitochondrial, mitoplast, and mitochondrial membrane fractions. It was not present in the matrix fraction, which was also the only fraction to test positive for the HSP70 marker. Briefly, the mitochondria were isolated with a mitochondrial isolation kit, and used to produce mitoplasts with digitonin (Schnaitman & Greenawalt 1968), which were further sub-fractionated through swelling in a hypotonic solution. The inner membrane and matrix fractions were collected after several cycles of freeze-thawing and ultra-centrifugation (100 000 x *g* at 4°C for 1 hour). Morrish et al. (2006) also tested for Hexokinase-2 as a marker, which is associated with the OMM, but

not with the mitoplast, IMM or matrix, and showed no OMM contamination in the latter fractions. It is thus possible that the study detected VDAC in the mitoplast fraction due to contact sites between the inner and outer membranes which the hexokinase-marker could not detect.

However, in a different study, a time specific demonstration of the degradation of the outer membrane (and thus a decrease in VDAC) through digitonin fractionation (0.3 mg digitonin) of rat heart mitochondria, revealed no VDAC marker present after 30 minutes of fractionation, whilst the ANT marker stayed relatively consistent throughout (Srisakuldee et al. 2014). The latter study aimed to demonstrate that fibroblast growth factor 2 (FGF2) protects heart cells from ischeamic and reperfusion–induced death through a mechanism linked to PKC-mediated connexin43 phosphorylation. Connexin43 has previously been reported to be associated with the inner mitochondrial membrane (obtained with 0.6% digitonin fractionation; Rodriguez-Sinovas et al. 2006) through Western blotting that used VDAC and ANT respectively as the outer and inner membrane markers. Similar to the study of Morrish et al. (2006), the VDAC marker was present in both the outer membrane and mitoplast (inner membrane and matrix) fractions, but not in the matrix fraction alone. Both Srisakuldee et al. (2014) and Rodriguez-Sinovas et al. (2006) used Cyphilin D (CypD, a mitochondrial matrix protein), to investigate the purity of the matrix fraction. These studies also made use of Percoll gradient centrifugation in order to isolate clean, intact mitochondria prior to digitonin fractionation.

The studies discussed here represent but a few of the many studies that have investigated either the location or presence of certain proteins within mitochondria. A common theme throughout all of the above mentioned studies are the use of either sucrose or Percoll gradients to further purify mitochondria after isolation. Hypotonic disruption is sufficient when using the mitochondria for patchclamping experiments, but outer membrane contamination as well as disruption of the inner membrane seems to be problematic. Once intact, purified mitochondria are obtained, the lack of plasma membranes as well as nuclear contamination can be confirmed with the use of the plasma markers such as $Na^{+}K^{+}$ATPase and either PCNA (proliferating cell nuclear antigen) or GAPDH (glyceraldehyde 3-phosphate dehydrogenase) as a nuclear marker. The mitochondria can then be sub-fractionated with digitonin at varying concentrations.

The optimal concentration of digitonin used for fractionation is determined by the ratio of digitonin to mitochondrial protein, but can be influenced by other contaminating proteins (Greenawalt 1974). Once the mitochondria are sub-fractionated with digitonin, the different mitochondrial fractions can be identified with the markers previously mentioned (VDAC, outer membrane, but due to contact sites, potentially found on the inner membrane as well; ANT, inner membrane and either HSP70 or CypD as a matrix marker). The above mentioned studies commonly made use of western blotting, although several studies used either gold-labelling or fluorescent confocal microscopy for initial identification of the location of certain proteins prior to western blotting experiments.

Collectively, these studies were used to design a digitonin permeabilisation protocol for the isolation of OMM, IMM and matrix fractions from cardiac mitochondria obtained from male, Wistar rats. Isolation of intact mitoplasts was confirmed with transmission electron microscopy. The location of ATM was determined with western blotting and confirmed with super-resolution structured illumination microscopy (SR-SIM)

4.2 Materials and methods:

In order to identify the location of ATM within cardiac mitochondria, subsarcolemmal mitochondria were isolated from male Wistar rat hearts, subjected to digitonin- and Lubrol WX-based permeabilisation, and prepared for western blotting. Mitoplast isolation was confirmed with transmission electron microscopy (TEM), and ATM was detected with SR-SIM microscopy and western blotting.

4.2.1 Reagents:

All chemicals were purchased from Sigma-Aldrich-Merck, except where indicated otherwise. Sodium pentobarbitone (Eutha-naze) was obtained from Bayer. Proteinase K (recombinant, PCR grade) was purchased from Roche Diagnostics GmbH, Germany). Western blot reagents were purchased from BioRad (Lasec, South Africa), except for SignalBoost™Immunoreaction Enhancer Kit (EMD Millipore-Merck), and the Immobilon®-P PVDF membrane (EMD Millipore-Merck). The following antibodies were purchased from Cell Signaling Technologies (USA): ATM (D2E2) Rabbit mAb #2873 and VDAC rabbit polyclonal Ab #4866. The ANT

1/2/3/4 (#H-188), 34 kDa was purchased from Santa Cruz Biotechnology. For the SR-SIM experiments, rabbit mAB Anti-ATM antibody [EPR17059] (ab199726) was purchased from Abcam. TOM20 and VDAC anti-mouse antibodies were a kind gift from the Division of Molecular Biology and Human Genetics, Parkinson's Research group, Stellenbosch University. The goat Anti-Rabbit IgG H&L (Alexa Fluor® 488, ab150077) and goat Anti-Mouse IgG H&L (Alexa Fluor® 594, ab150116) secondary antibodies were a kind gift from the Dept of Physiology, SU (Prof Ben Loos).

4.2.2 Animals:

All the procedures involving animals were in compliance with the South African National Standard for the care and use of animals for scientific purposes (SANS 10386:2008); the Medical Research Council Guidelines on Ethics for Medical Research; Book 3: Use of Animals in Research and Training and the National Institutes of Health Office of Laboratory Welfare: The Guide for the Care and Use of Laboratory Animals, 8th Edition; USA, and was approved by the Research Ethics Committee: Animal care and Use, Stellenbosch University, South Africa (approval numbers SU-ACUM12-0040; SU-ACUD16-00179).

Male Wistar rats (weighing approximately 250 grams) were housed at the Central Research Facility (Stellenbosch University) in a temperature controlled (~23°C) environment with a 12-hour light/dark cycle and fed normal rat chow. The animals were injected with Euthanaze (Bayer, 200 mg/ml at an overdose of 200 mg/kg via intraperitoneal injection performed by a registered animal laboratory technologist, South African Veterinary Council, SAVC number: AL16/15486), and euthanised through exsanguination after rapid excision of the heart. Two animals were used per experiment, and the experiments were repeated five times for protocol optimisation and confirmation, once for TEM and once for SR-SIM experiments (total number of animals used: 14 animals)

4.2.3 Mitochondrial isolation:

The mitochondrial isolation protocol is based on the method described by Sordahl et al. (1972) and Venter et al. (1991). Briefly, after excision of the heart, the atria were removed and the ventricular tissue was placed in ice-cold KE isolation buffer (0.18 M KCl, 0.01 M

EDTA, pH 7.4) and finely diced with scissors. The tissue was washed in isolation buffer to remove all traces of blood, and briefly homogenised (2 X 5 seconds at speed 13 000 rpm) with a Heidolph SilentCrusher M. This was followed by a slow centrifugation step in a Sorvall RC6-PLUS centrifuge (755 x *g* for 10 minutes at 4° Celsius) in order to obtain a pellet containing the nuclei, cell membranes and any remaining tissue. The supernatant was transferred to a clean centrifuge tube and centrifuged at 18 800 x *g* for 10 minutes at 4°C to obtain a mitochondrial pellet. The pellet was re-suspended in ice-cold mitochondrial isolation buffer with a 2 cm^3 Potter-Elvehjem glass-teflon homogenizer, and stored on ice until use.

4.2.4 Mitochondrial subfractionation with digitonin and Lubrol WX:

For subfractionation, the atria were removed directly after excision of the heart, and the remaining ventricular tissue of two hearts were placed in ice-cold D-mannitol/sucrose buffer adapted from Greenawalt (1974) and Beutner et al. (2005) (M/S buffer; 70 mM sucrose, 220 mM D-mannitol, 10 mM HEPES, 0.5 M EGTA, pH to 7.2 with KOH). The tissue was finely diced as described previously, and subjected to homogenization (Heidolph SilentCrusher M). Mitochondria were isolated as described above and resuspended in ice cold M/S buffer. The mitochondrial fraction was washed with centrifugation at 5366 x *g* for 10 min at 4°C, and resuspended in ice-cold M/S buffer. Protein concentration was determined with a Bradford protein assay (Bradford 1976) prior to 1.2% digitonin treatment (Sigma, D141). A 1.2 % digitonin solution was prepared freshly before each fractionation experiment by boiling 12 mg digitonin (D141, Sigma-Aldrich) in 1 ml of M/S buffer for 1 minute, and allowed to cool to room temperature before use. Mitochondrial protein concentration was determined with a Bradford assay (Bradford 1976). A volume equal to 100 µg mitochondria was aliquoted into a clean Eppendorf tube, and an equal volume of 1.2% digitonin was added, to give a total amount of 50 µg mitochondria:1.2% digitonin. This reaction served as the master reaction from which aliquots were taken. An aliquot was taken at the moment of addition (0 minute time point), and the reaction was quenched and diluted 10 X with ice-cold M/S buffer containing bovine serum albumin (BSA, 25 µg/ml). The master digitonin-permeabilisation reaction was allowed to continue for 30 min whilst gently stirring at 0° Celsius, and aliquots were taken at 15 min, 20 min and 30 min time points, and quenched as

previously described. Aliquots were taken at different time points to determine the time point at which most of the OMM has been removed without rupturing the mitoplast. The quenched 10 X dilution time-point reactions were subsequently centrifuged at 5366 x *g* for 10 min at 4°C (Sigma 1-14K) to obtain the mitoplasts (sediment), and the supernatant was carefully aspirated. The supernatant was centrifuged at 100 000 x *g* for 1 hour at 4°C to obtain the outer mitochondrial membrane (OMM) fraction.

The mitoplast fraction was further subfractionated into a matrix and IMM fraction. The matrix fraction was obtained by resuspending the mitoplast fraction in ½ the original volume of M/S buffer, followed by centrifugation at 5 633 x *g* for 10 min at 4° C. The supernatant was carefully aspirated and added to OMM fraction, whilst the mitoplast fraction was resuspended in 0.16 mg/ml Lubrol WX (Sigma; Greenawalt 1974; Schnaitman & Greenawalt 1968), and rested in an ice bath for 15 min. The nonionic detergent, Lubrol WX is a solubilising agent for membrane bound proteins, and is capable of solubilising most of the matrix proteins whilst the IMM is impervious to solubilisation (Chan et al. 1970). The suspension was centrifuged at 100 000 x *g* for 1 hour. The supernatant contained the matrix proteins and the pellet contained the IMM fraction. A schematic diagram of the protocol is shown in Figure 4.1.

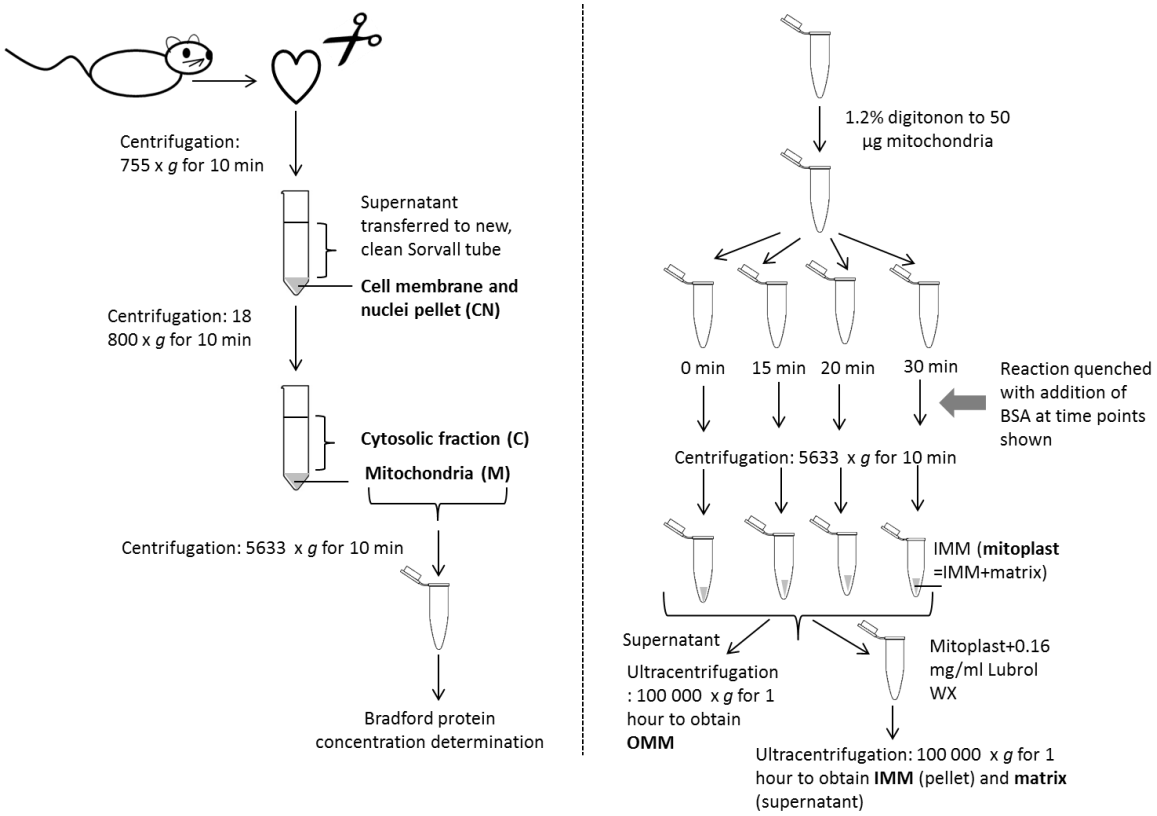

Figure 4.1: Schematic diagram of mitochondrial fractionation to obtain mitoplasts. Isotonically swollen mitochondria were prepared from the hearts of male Wistar rats in a modified M/S buffer with differential centrifugation (left panel). A ratio of 50 µg mitochondria: 1.2% digitonin was digested at 0°C and was either quenched immediately (0 min) with the addition of a 9 volumes of M/S buffer containing 25 mg/ml BSA or allowed to continue for 15, 20 or 30 minutes. The reactions were centrifuged to obtain mitolasts at each time point and the supernatant was further centrifuged to obtain the OMM fraction. The mitoplasts were subfractionated into the IMM and matrix with Lubrol WX and ultracentrifugation (right panel).

All fractions were resuspended in a small volume of M/S buffer and an equal volume of 1 X SDS buffer (10% glycerol, 50 mM TRIS-HCl pH 6.8, 30 mM β-glycerophosphate, 2.5 mM EGTA, 1 mM $NaVO_4$, 0.5 mM NaF, 10% SDS) was added for Western blotting purposes.

4.2.5 Proteinase K digestion:

Proteinase K is a stable serine protease that hydrolyzes a variety of peptide bonds and is commonly used to degrade nucleases in nucleic acid extractions preparations. However, the protease can also degrade many proteins in their native conformation and has been shown to degrade ATM in the presence and absence of Triton-X, as described by Zhang et al. (2015). Briefly, a total of 25 µg M/S-isolated mitochondria were subjected to Proteinase K digestion (0.1 µg/ml, Roche) in the presence of 0.1 % Triton-X (which disrupts membranes)

for 1 minute, 3 minutes, 5 minutes and 10 minutes at 37°C. The reactions were quenched with 5 mM phenylmethyl sulphonyl fluoride (PMSF) on ice, and centrifuged at 10 000 x *g* for 10 min at 4°C. The pellets were resuspended in M/S buffer and an equal volume of 1x SDS buffer for Western blotting purposes for western blotting purposes.

4.2.6 Western blotting:

Briefly, the cell membrane and nuclei (CN), cytosol(C), mitochondrial (M), OMM, IMM and matrix fraction lysates (indicated in Figure 4.1) were prepared for western blotting with the addition of one volume M/S buffer, one volume 1 X SDS buffer (10% Glycerol, 50 mM TRIS-HCl, pH 6.8, 30 mM β-glycerophosphate, 1 mM Na_3VO_4, 0.5 mM NaF, 2% SDS) and one volume 3 X Laemmli sample buffer (2.5 M glycerol, 0.189 M TRIS-HCl (pH 6.8), 10% SDS, 1.275 mM bromophenol blue, 15% β- mercaptoethanol). The samples were boiled for four minutes and stored at -80°C until use. Samples were boiled again for 4 minutes prior to being loaded on 4–15% Mini-PROTEAN® TGX™ Stain free Precast Protein Gels (Bio-Rad Laboratories), and subjected to electrophoresis for 1 hour at 200 Volt and 200 mAmp. Due to major size differences in the proteins investigated (ATM protein kinase, 350 kDa, #2873, Cell Signaling Technology (CST); VDAC #4866, 32 kDa, CST; and ANT 1/2/3/4 #H-188, 34 kDa Santa Cruz Biotechnology), a modified transfer buffer was used (25 mM TRIS, 190 mM glycine and 10% methanol v/v), and the gels were allowed to rest for 30 minutes in the buffer prior to activation in the ChemiDoc MP system (Bio-Rad Laboratories), and transfer. Transfer was performed at 200 V and 200 mA for 1 hour 30 minutes at 4°C onto an Immobilon®-P PVDF membrane (EMD Millipore). The membranes were briefly placed in methanol, and allowed to dry before blocking in a 5% liquid fat-free milk solution. The antibodies were diluted 1:1000 as follows: SignalBoost™Immunoreaction Enhancer Kit (EMD Millipore) for ATM protein kinase antibody (CST) and secondary antibody; TBS-T for VDAC antibody and secondary antibody, and TBS-T with 2.5% fat free milk solution for ANT 1/2/3/4 (SCBT) and its secondary antibody. After primary (overnight at 4° Celsius) and secondary antibody (1h at room temperature [~ 23° Celsius]) incubation the membranes were treated with Clarity™Western ECL Blotting Substrate and visualised on the Chemidoc MP system.

4.2.7 Transmission electron microscopy:

In brief, samples were processed with a Leica EM tissue processer, fixed in glutaraldehyde and scoped with a JEOL 10-11 transmission microscope (JEOL, Japan) and a SIS imaging according to standard protocol (National Health Laboratories Services, Tygerberg Hospital, Cape Town, South Africa). The microscopy was done by Mrs. N Muller at the NHLS.

4.2.8 Super –resolution Structured Illumination Microscopy (SR-SIM):

Super-Resolution Structured Illumination Microscopy (SR-SIM) was performed at the Stellenbosch University Central Analytical facility (CAF) Fluorescence Microscopy unit. Mitochondria and mitoplasts were prepared as described previously and fixed with 2.5% glutaraldehyde. The samples were incubated overnight at 4° Celsuis with either ATM (Abcam, anti-rabbit, mAb, ab199726) and VDAC (CST, anti-mouse), or ATM and Tom20 (Abcam, anti-mouse), washed and probed with the appropriate fluorescent Goat Anti-Rabbit IgG H&L (Alexa Fluor® 488, ab150077) and Goat Anti-Mouse IgG H&L (Alexa Fluor® 594, ab150116) secondary antibody. TOM 20 is an OMM import protein, whilst VDAC is associated with the contact points between the inner and outer mitochondrial membrane.

Samples were acquired with a Zeiss LSM 780 ELYRA PS.1 microscope. Thin (0.1 mm) z- stacks of high-resolution image frames were collected with 5 rotations by using an alpha Plan-Apochromat 1006/1.46 oil DIC M27 ELYRA objective and an ELYRA PS.1 (Carl Zeiss Microimaging) microscope equipped with a 488 nm laser (100 mW), 561 nm laser (100 mW) and Andor EM-CCD camera (iXon DU 885). Micrographs were reconstructed with ZEN software (black edition, 2011, version 7.04.287) using a structured illumination algorithm (Heintzmann & Cremer 1999). The sample fixation, as well as the majority of imaging, was performed by Prof B Loos at the Central Analytical facility (CAF), Department of Physiology, Stellenbosch University.

4.3 Results and discussion:

In order to evaluate whether mitochondria can be successfully isolated with the modified M/S buffer, and if the protocol enabled mitochondrial swelling in order to aid the removal of

the OMM with digitonin, samples of 1) mitochondria isolated with KE buffer (Fig 4.2 a and b), 2) freshly isolated M/S mitochondria prior to digitonin permeabilisation (0 min time point) (Fig 4.2 c and d) 3) 20 minutes after digitonin permeabilisation (Fig 4.2 e and f) and 4) 30 minutes after digitonin permeabilisation (Fig 4.2 g and h) were submitted for transmission electron microscopy at the NHLS, Tygerberg hospital, South Africa, for imaging (Figure 4.2).

Mitochondria that were isolated in M/S buffer were swollen (Fig 4.2, panel c , 2 µm, panel d, 0.5 µm) compared to mitochondria isolated in isotonic mitochondrial isolation buffer (KE buffer, Fig 4.2, panel a, 2 µm and panel b, 0.5 µm) exhibiting loosened outer membranes, which are shown in the enlargement in Fig 4.2, panel b and d. Hypotonically swollen mitochondria with M/S buffer (Fig 4.2, Panel d) also exhibited cristae rearrangement which appeared more rounded compared to well-structured cristae of mitochondria isolated in KE buffer (Figure 4.2, panel c and d compared to panel a and b). This suggests that the M/S buffer was sufficient to promote mitochondrial swelling and to loosen the OMMs to aid digitonin treatment. After 20 minutes of 1.2% digitonin treatment, dark, rounded structures could be observed that ranged in size, as well as OMM remnants in Figure 4.2, panel e (2 µm) and f (1 µm).

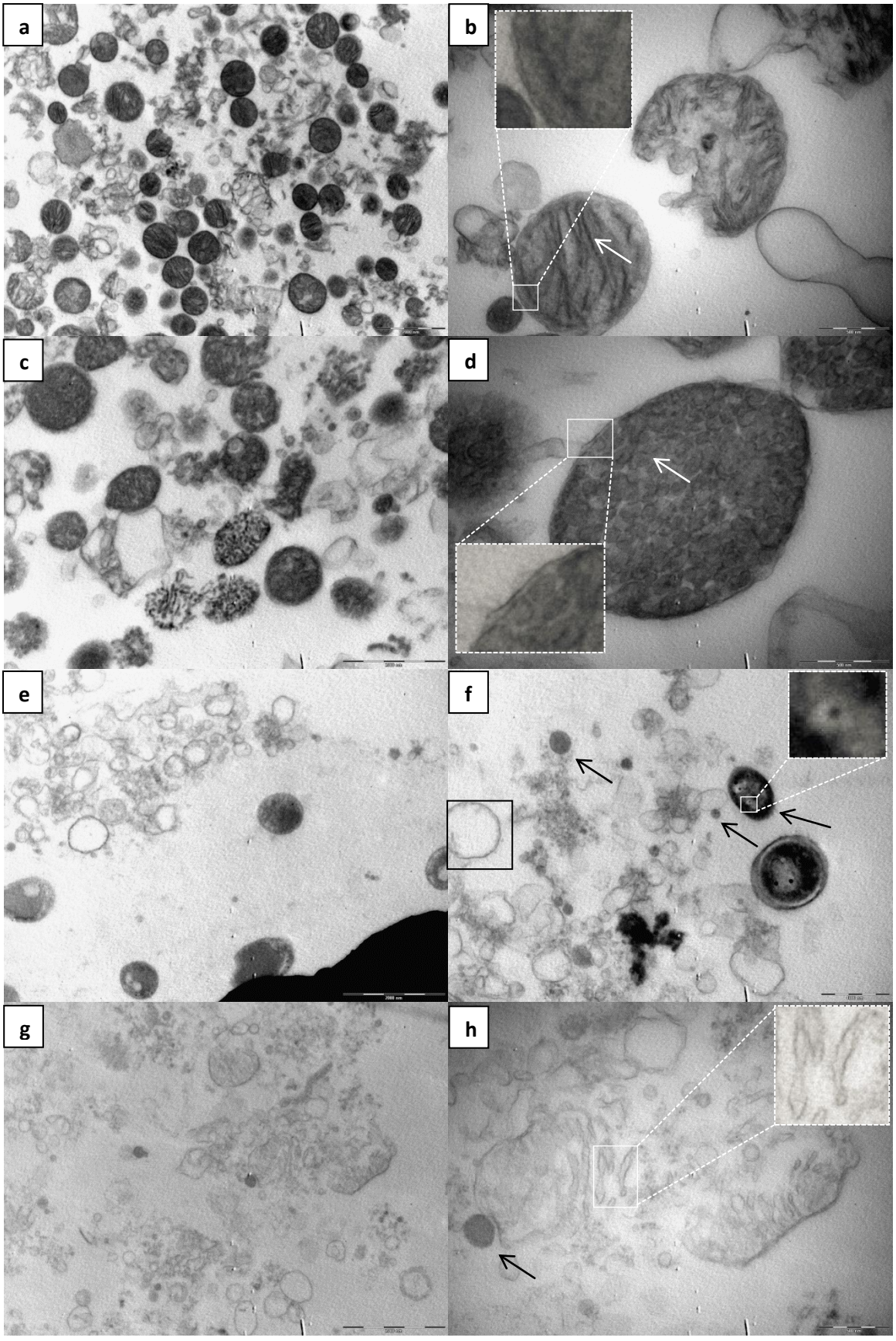

Figure 4.2: Transmission electron micrographs of mitochondria and mitoplasts after 20 and 30 minutes of 1.2% digitonin permeabilisation. Panel a represents functional mitochondria isolated with KE buffer (2 µm), where panel b is an enlargement of two mitochondria with well-coupled

IMM and OMM (insert), as well as structured cristae (white arrow; 0.5 µm). Panel c and d show M/S buffer isolated mitochondria that present as swollen, with disrupted cristae structure and exhibit loose OMM. Panel e and f respectively show mitoplasts (Panel e, 2 µm) that are highlighted in Panel f (1 µm, black arrows) as well as remnants of OMM (highlighted by the black box). Mitoplasts are identifiable through electron-opaque granules found in the mitochondrial matrix (insert) and can be observed in mitoplasts of all sizes. Panel g (2 µm) and panel h (0.5 µm) represents a mitoplast preparation after 30 min of digitonin treatment, where as the insert shows pinched cristea.

The mitoplast structures observed in Fig 4.2 panel f (black arrows) were also seen by Sileikyte et al. (2011) after 20 minutes of 1.2% digitonin treatment. The outer membrane (Fig 4.3, panel f, black block) resembles the same structures observed by Hoppel et al. (1998) and confirmed the successful removal of the outer membrane from the mitoplasts. Electron-opaque particles, which are associated with the matrix (Hackenbrock 1972), were also observed (enlargement, Fig 4.2, panel f) and used as an identifying marker of mitoplasts. Interestingly, fewer and smaller mitoplast structures were observed, whilst some of the OMM were retained after 30 minutes of digitonin permeabilisation (Figure 4.2, panel g, 2 µm). However, in Figure 4.2, panel h (0.5 µm) and the insert a broken mitochondrial structure can be observed with rod-like structures that resemble pinched cristea. Whether this is the case is unclear, however, it confirmed that 20 min digitonin treatment is sufficient to obtain rounded, swollen mitoplasts that resembles mitoplast structures reported in literature obtained with digitonin and sonication (Hovius et al. 1990) or digitonin alone (Sileikyte et al. 2011). This suggests that 20 minutes of 1.2% digitonin treatment is optimal to obtain intact mitoplasts from M/S isolated mitochondria, whilst removing the majority of OMM.

Taken together, the modified MS buffer aided mitochondrial swelling that loosened the OMM and contributed to the formation of mitoplasts after the addition of 1.2% digitonin. The optimal time point for permeabilisation is 20 minutes as fewer and smaller mitoplast structures are observed after 30 minutes.

The fractions obtained from the different time points were centrifuged (Fig 4.1) to obtain separated OMM and mitoplast fractions (indicated as IMM for western blot purposes) and probed for ATM, VDAC and ANT1/2/3/4 with western blotting (Fig 4.3). The fractions probed with western blotting were taken from each of the isolation steps, where CN represents the

cell membrane and nuclei obtained in the initial pellet and C, the cytosolic fraction after pelleting the mitochondrial fraction (M).

ATM was observed in the CN and mitochondrial fractions as well as at the 0 min time point in the OMM and IMM fractions. This time point served as a control prior to the removal the OMM from the mitoplast with digitonin, where it is expected that the OMM is still largely attached to the mitochondria, and was confirmed with TEM (Fig 4.2, panel d). ATM could not be observed at any other time point within the isolated OMM fractions after digitonin-based removal from the mitoplasts, but was present in the IMM fraction (mitoplast plus IMM) at each time point. This correlated well with the presence of the IMM marker, ANT 1/2/3/4 in each of the mitoplast time point fractions, which was absent in the OMM time-point fractions. The OMM marker, VDAC was predominantly present in the CN, M and OMM time-point fractions, although VDAC protein could be detected in the cytosolic, and IMM time-point fractions. This might be due to contact point contamination (also observed by Ryu et al. 2011; Kirichok et al. 2004; Srisakuldee et al. 2014), but did not result in any association between ATM and the OMM.

These observations suggest that ATM is associated with the mitoplast fraction (IMM and matrix), whilst the presence of ATM within the CN and M fractions served as a positive control, because of its well-known association with the nucleus as well as prior association with the mitochondria (Morita et al. 2014).

ATM has previously been associated with mitochondria (Valentin-Vega et al. 2012), and was further investigated with a differential centrifugation isolation (Morita et al. 2014), similar to the protocol used in our study. The resultant fractions were referred to as the heavy and light membrane fractions, and the heavy fraction, which consisted mainly out of mitochondria, was found to contain ATM and phosphorylated ATM (Morita et al. 2014). The current study expands on these results, and shows that ATM is associated with the mitoplast fraction of isolated cardiac mitochondria. It should also be noted that the work presented by Valentin-Vega et al. (2012) and Morita et al. (2014) was performed respectively in immortalized human fibroblast and Hep2G cells, which makes this the *first* report to show that ATM is located in cardiac mitoplasts under normoxic conditions.

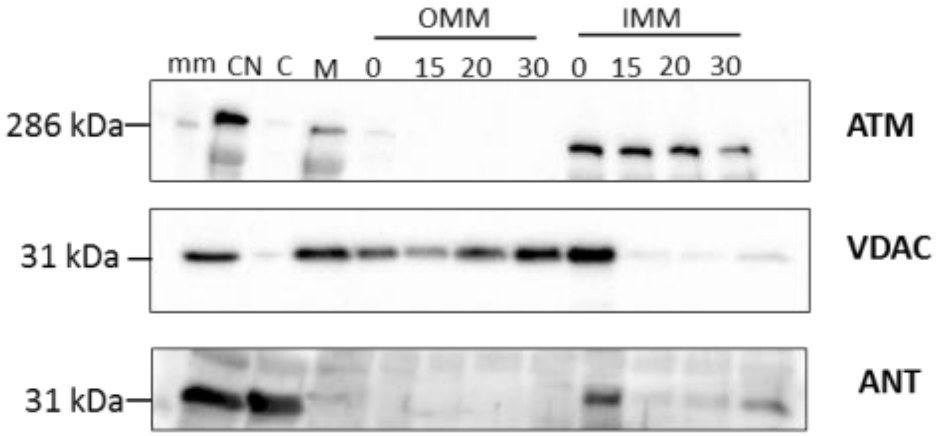

Figure 4.3: Western blot analysis after the subcellular fractionation of the mitochondrial, outer mitochondrial (OMM) and mitoplast (inner mitochondrial membrane {IMMI} and matrix) fractions. The first lane (mm) indicates the HiMark pre-stained protein standard (ThermoFischer Scientific), the second lane was loaded with the cellular membrane and nuclear (CN) fraction and served as a positive control for ATM, whilst C indicates the cytosolic fraction. The mitochondrial fraction (M) was digested over time (0 min, 15 min, 20 min and 30 min) and separated into OMM and IMM fractions with differential centrifugation prior to Western blotting with antibodies for ATM (350 kDa), Voltage Dependant Anion Channel (VDAC, 32 kDa) and Adenine Nucleotide Transproter 1/2/3/4 (ANT1/2/3/4, 34 kDa). The images were cropped and full-length blots as well as total protein membrane images are presented in Addendum A (Fig A1).

Mitoplasts can be separated into the IMM and matrix, the latter containing the mitochondrial DNA, enzymes and ribosomes. In light of the observed association between ATM and the mitoplast fraction, the mitoplast fractions at 0 min and 20 min were further separated into the IMM and matrix fractions with Lubrol-WX permeabilisation (Figure 4.4). ATM was again found to be mainly associated with the IMM at 0 and 20 min, whilst a light band can be observed in the OMM fraction at 20 min. This could suggest incomplete digitonin disruption and separation, because ANT1/2/3/4 was also seen in these fractions. ATM was observed in the nuclear (CN) and mitochondrial (M) fractions which served as a positive control, whilst VDAC was observed in all the fractions except at IMM 20 min and in the matrix. Neither ANT1/2/3/4 nor ATM were observed in the matrix fraction, and although it is tempting to suggest that ATM is not found in the matrix, a robust matrix marker should have been included to confirm the purity of the fraction.

The association of ATM with the outer membrane of the peroxisome was confirmed with Proteinase K digestion in the presence and absence of Triton-X (Zhang et al. 2015). In the study by (Zhang et al. 2015), the authors used proteinase K digestion in the presence and absence of Triton-X to show that ATM is present in the peroxisome, together with the

peroxisome membrane protein, PMP70 at 0 min, but is rapidly digested both in the presence and absence of Triton-X, and is not present after 5 minutes of proteinase K digestion. Conversely, ATM was not present after M/S -isolated mitochondria were digested for 1 minute with Proteinase K and Triton-X membrane disruption, but were observed after 3 and 5 minutes of digestion, and not after 10 minutes. Both the IMM marker, ANT1/2/3/4 as well as the OMM marker, VDAC are resistant to proteinase K digestion (Diokmetzidou et al. 2016) and was present at all time points (Fig 4.4). This confirms that ATM is located on the inner and not outer mitochondrial membrane, and supports the notion that it is not associated with the matrix.

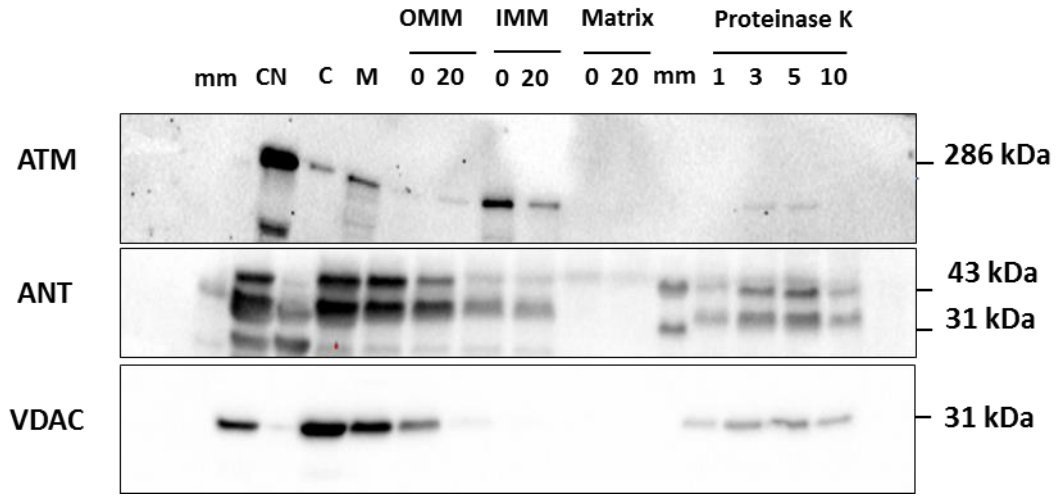

Figure 4.4: Subfractionation of the mitoplast fraction into the IMM and matrix and proteinase K digestion of the mitochondrial fraction. Mitoplasts were prepared from M/S isolated mitochondrial fractions and further digested with Lubrol WX to obtain the IMM and matrix fractions. Proteinase K digestion in the presence of Triton-X was performed on M/S isolated mitochondria to confirm the presence of ATM on the inner mitochondrial membrane. ATM was observed after 3 and 5 minutes whilst VDAC and ANT1/2/3/4 could be observed at all time points. The images were cropped and full-length blots as well as total protein membrane images are presented in Appendix 1 (Fig 2). The first lane (left, mm) indicates the HiMark pre-stained protein standard (ThermoFischer Scientific), and the 5th last lane (mm) represents the PageRuler Prestained Protein Ruler (ThermoFischer Scientific).

The association of ATM with the IMM (ANT), and not OMM (VDAC), which was observed in the IMM western blot fraction, was further investigated with SR-SIM. The different fractions of KE-isolated mitochondria, and M/S isolated mitochondria at 0 min and 20 min of digitonin treatment were imaged with either ATM (anti-rabbit) and VDAC (anti-mouse, Fig 4.5) or ATM (anti-rabbit) and TOM20 (anti-mouse, Fig 4.6) fluorescently labelled antibodies.

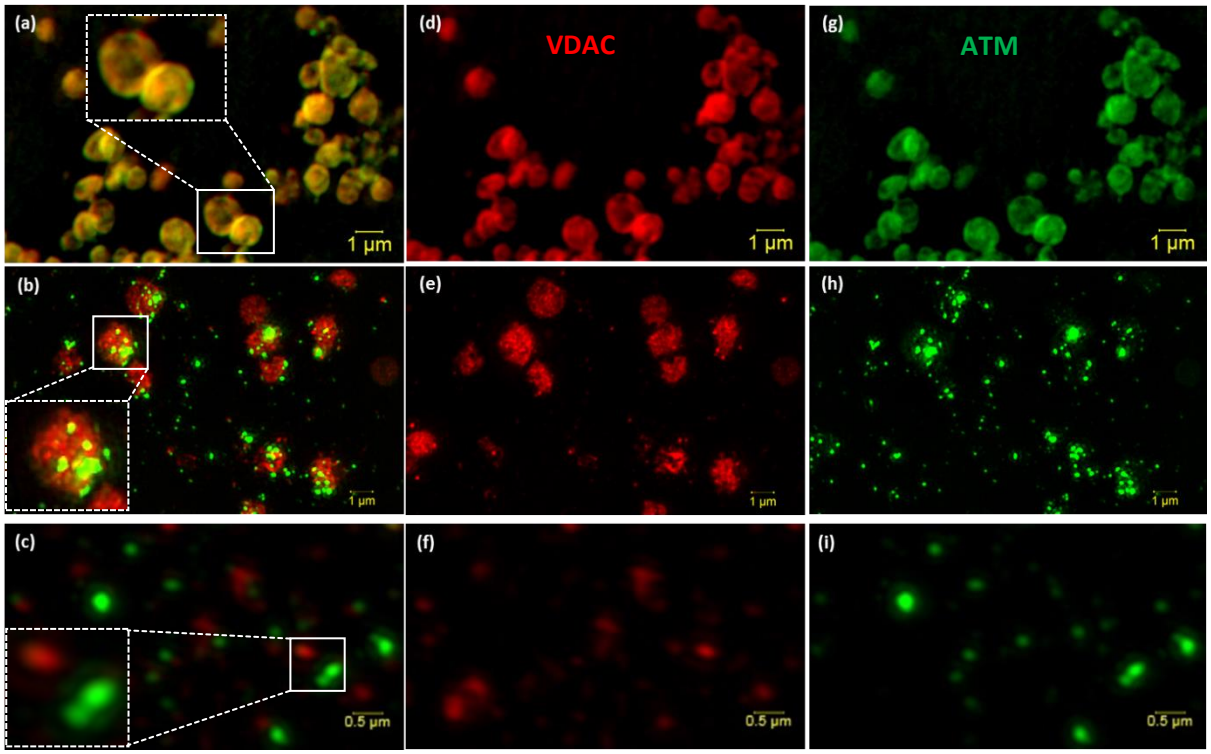

Figure 4.5: Super resolution structured illumination microscopy (SR-SIM) micrographs of isolated mitochondria and mitoplast preparations probed with VDAC (OMM, red) and ATM (IMM, green). Mitochondria were isolated with either KE buffer (panel a, overlay), or M/S buffer (panel b, overlay, 1 µm) at 0 min digitonin treatment and after 20 min digitonin treatment (panel c, overlay, 0.5 µm). Panels d-f show VDAC (red) respectively in KE-isolated mitochondria, M/S buffer isolated mitochondria at 0 min and after 20 min digitonin permeabilisation. Panels g-i show ATM (green) in KE isolated mitochondria and M/S-isolated mitochondria after 0 and 20 min of digitonin treatment, respectively.

As expected from the Western blot results, ATM (green) could be clearly observed in the fixed KE-buffer isolated mitochondria, and overlayed very well with VDAC, which suggests tightly coupled and intact mitochondria (Fig 4.5 a). The two fluorescently labelled proteins were sufficient to visualise the isolated mitochondria, and compared well to TOM20 in Fig 4.6 (panel d, 1 µm). Although ATM appeared more clustered (Fig 4.6, panel g, 1µm), the protein is still seen across the mitochondrial structure. The addition of digitonin (0 min) to M/S buffer isolated mitochondria, resulted in the clustering, or punctate formation of ATM, whilst both the OMM proteins (Fig 4.5, panel b, and fig 4.6 panel b, 1 µm) still indicate rounded mitochondrial structures. The structure corresponds with the swollen mitochondrial structure observed with TEM (Fig 4.2 panel d), whilst the punctate formation of ATM, might correspond with the structural rearrangement of the cristae or it might be facing towards the intermitochondrial space, which would make it vulnerable to surface disruption by digitonin.

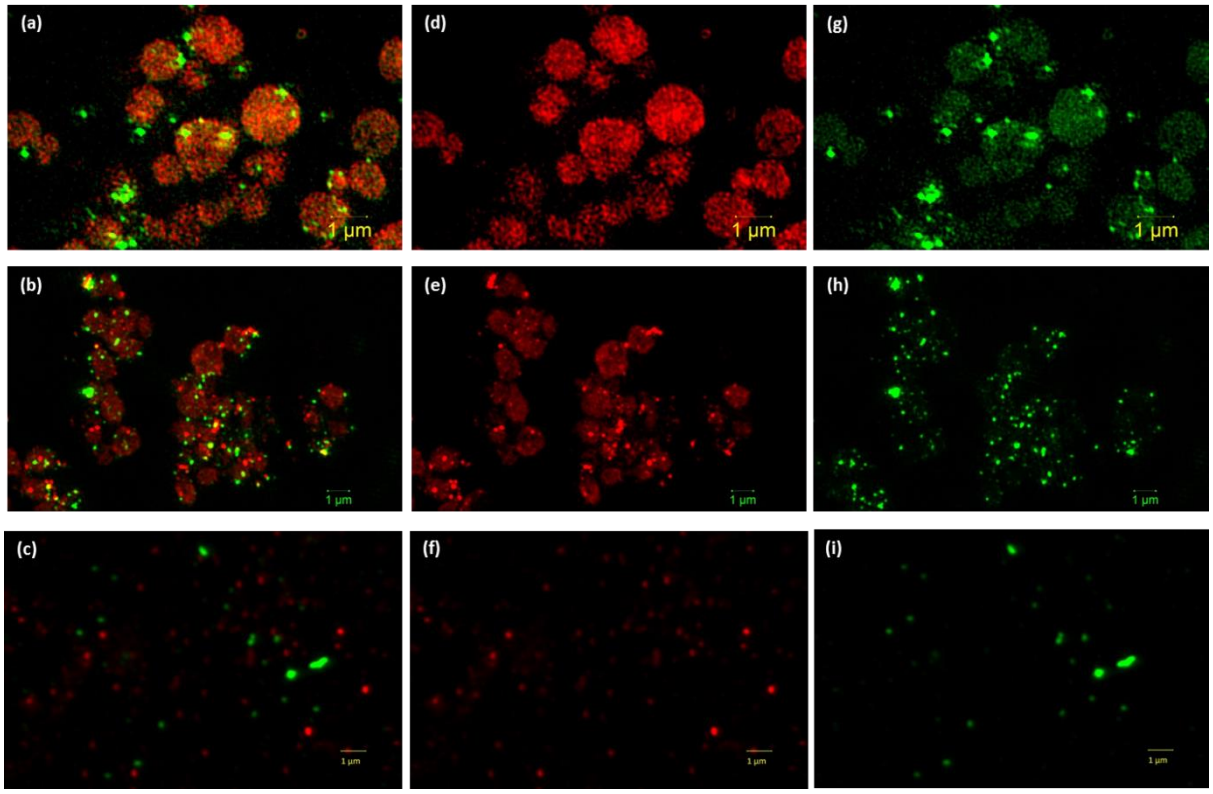

Figure 4.6: Super resolution structured illumination microscopy (SR-SIM) micrographs of isolated mitochondria and mitoplast preparations probed with TOM20 (OMM, red) and ATM (IMM, green). Mitochondria were isolated with either KE buffer (panel a, overlay), or M/S buffer (panel b, overlay, 1 µm) at 0 min digitonin treatment and after 20 min digitonin treatment (panel c, overlay, 0.5 µm). Panels d-f show TOM20 (red) respectively in KE-isolated mitochondria, M/S buffer isolated mitochondria at 0 min and after 20 min digitonin treatment. Panels g-i show ATM (green) in KE isolated mitochondria and M/S-isolated mitochondria after 0 and 20 min of digitonin treatment, respectively.

After 20 minutes of digitonin treatment, no association could be observed between ATM and VDAC (Fig 4.5, panel c, 0.5 µm), nor TOM20 (Fig 4.6, panel c, 0.5 µm), which supports the notion that ATM is associated with the IMM and not the OMM of cardiac mitochondria. It also suggests that ATM is not associated with contact points between the OMM and IMM; if this was the case, the expectation would be that ATM would be associated with VDAC after 20 min of digitonin permeabilisation, but not with TOM20, which was not the case. Whereas VDAC was previously observed in the mitoplast fraction, TOM20 is an import protein located on the OMM. Thus, in order to determine whether there is any association between ATM and the contact points, or between ATM and the OMM, a marker was chosen that is not associated with the IMM at all.

In conclusion, these results show that ATM is associated with the IMM of rat cardiac mitochondria. The protein was not be associated with VDAC, and was predominantly

present within the cellular and nuclear fractions, mitochondrial fraction, and the mitoplast fraction. Further subfractionation confirmed that ATM was associated with the IMM and not the matrix. The formation of punctates by ATM suggest that the protein could be facing towards the intermitochondrial space between the inner and outer membrane which would expose it to partial digitonin treatment. It is clear that greater resolution and more sensitive microscopy techniques, such as super resolution correlative light and electron microscopy (CLEM) are required to resolve the inversion of the mitoplast with sonication.

The association of ATM with the IMM suggests a potential role for ATM in oxidative phosphorylation, and is discussed in the next chapter.

Chapter 5 : ATM plays a role in mitochondrial oxidative phosphorylation and mitophagy

Mitochondria are essential for energy production in the heart, and dysfunction thereof has been linked with heart failure (Rosca et al. 2008; Rosca & Hoppel 2010), diabetic cardiomyopathy (Boudina et al. 2007; Boudina et al. 2009; Boudina & Abel 2010), as well as metabolic and inflammatory pathophysiology (reviewed by Forrester et al. 2018).

Under physiological conditions the heart produces approximately 95% of its required ATP through oxidative phosphorylation of free fatty acids (Opie 2004). Mitochondrial function is impaired in obesity, insulin resistance and T2D (reviewed by Bugger & Abel 2008), and can result in mitochondrial substrate oxidation and decreased ATP production. Inefficient nutrient oxidation decreases ATP production and oxygen consumption, and in turn, increase ROS production and stimulate inflammation as well as contributing to mitochondrial dysfunction and insulin resistance (Kim et al. 2008). Collectively, this can lead to the development of heart failure and cardiac hypertrophy (reviewed by Doenst et al. 2013). Moreover, increasing evidence suggests that changes in glucose homeostasis in cardiac hypertrophy includes altered glucose transport and increased glycolysis which is associated with the loss of metabolic flexibility as well as an increased dependence on glucose utilization (Shao & Tian 2016).

In the presence of increased glucose and insulin, the heart favours glucose as its preferred substrate, whereas metabolism of the diabetic heart is characterised by a decrease in glucose uptake and oxidation (Bertrand et al. 2008). Long chain fatty acid uptake and oxidation is enhanced, albeit not sufficiently, to prevent the accumulation of lipids and consequent lipotoxicity. It has been suggested that this can lead to the development of myocardial insulin resistance, although the underlying mechanisms are still poorly understood (Bertrand et al. 2008). Concomitant with the above, insulin resistance is characterised by alterations of the insulin-induced activation of PI-3K/Akt signalling pathway (Ouwens et al. 2007; Huisamen 2003) whereas the translocation of insulin-activated Akt to mitochondria in cardiac muscle may have important implications on myocardial bioenergetics (Yang et al. 2009). Biguanides, such as metformin, activate AMPK that can

stimulate glucose uptake in insulin-resistant cardiomyocytes through the stimulation of Akt phosphorylation in a PI-3K dependent manner (Bertrand et al. 2006). Furthermore, metformin is known to delay the development of diabetes and cardiovascular dysfunction in Goto-Kakizaki rats by inhibiting the generation of superoxide in the mitochondria (Rösen & Wiernsperger 2006). The combined effect of decreased myocardial insulin signalling, which promotes oxidative stress and mitochondrial uncoupling, as well as reduced flux through the TCA cycle and decreased fatty acid oxidation, all impairs mitochondrial energetics (Boudina et al. 2009).

Under physiological conditions, mitochondrial oxygen consumption is tightly coupled with ATP synthesis (Bugger & Abel 2008). Briefly, substrate oxidation produces the reducing equivalents, NADH and $FADH_2$ that donate electrons to the ETC. The electron transfer to oxygen atoms results in energy that generates an electrochemical gradient by pumping protons across the IMM into the intermitochondrial membrane space. These protons re-enter the matrix through Complex V (F_1F_0 ATPase) which uses energy to regenerate ATP from ADP, and is known as coupling of oxidative phosphorylation. A small proportion of the protons can bypass the F_1F_0 ATPase, which results in increased oxygen usage without concomitant ATP production and is known as mitochondrial uncoupling. In mice hearts lacking the uncoupling protein, UCP3, mitochondria are more coupled, although ROS production is increased which suggests that mitochondrial uncoupling can facilitate a reduction in oxidative stress (Vidal-Puig et al. 2000). UCP3 does not seem to be required for fatty acid oxidation (Vidal-Puig et al. 2000), but rather stimulates glucose transport and GLUT4 translocation to the cell surface in cardiac cells by activating the PI-3K/Akt dependent pathway (Huppertz et al. 2001). The protective role of UCP3 with regards to oxidative stress is especially relevant in a high fat diet, and seems to protect mitochondria against lipid induced mitochondrial dysfunction, although only after long-term exposure to high fat conditions (Nabben et al. 2011).

Insulin can also affect mitochondrial dynamics in cardiomyocytes, and was shown to increase Opa1 (mitochondrial dynamin like GTPase) protein levels which increased mitochondrial fusion as well as membrane potential whilst elevating both oxygen consumption and ATP production (Parra et al. 2014). Mitochondrial fusion is also crucial for the maintenance of mitochondrial morphology as well as for cardiac respiration (Chen et al.

2011). Interestingly, a recent study showed that mice lacking the mitophagy mediating protein, FUNDC1, were protected against high fat diet induced obesity, had improved insulin sensitivity and glucose tolerance, but presented with decreased mitochondrial energetics (Fu et al. 2018). The authors suggest that FUNDC1 plays a crucial role in maintaining mitochondrial quality control that is required for the regulation of cellular metabolism. Moreover, the autophagic protein BNIP3 reduces oxidative phosphorylation and ATP synthesis, possibly through the promotion of ETC protein degradation in the mitochondria, without triggering apoptosis (Thomas et al. 2011). In a study in humans and mice, it was found that a HFD alone is sufficient to downregulate the genes required for the oxidative phosphorylation ETC proteins as well as mitochondrial biogenesis (Sparks et al. 2005). Collectively, this suggests that insulin and mitochondrial dynamics are important for myocardial energy metabolism (Westermeier et al. 2015).

ATM has been implicated in mitophagy (Qi et al. 2016), is required for insulin-mediated activation of Akt (Halaby et al. 2008), and has been implicated in the pathogenesis of metabolic syndrome that can be alleviated through chloroquine-mediated activation of ATM (Halaby et al. 2013; Razani et al. 2010; Schneider et al. 2006). The silencing or absence of ATM also results in decreased mitochondrial respiration (Ambrose et al. 2007; Zakikhani et al. 2012), decreased mitochondrial membrane potential and ATP synthesis (Ambrose et al. 2007; Valentin-Vega et al. 2012) as well as in a down regulation of Complex I (Valentin-Vega et al. 2012). This suggests a potential role for ATM in oxidative phosphorylation and mitochondrial energetics in obesity and insulin resistance.

In view of this study's finding that ATM is located on the inner mitochondrial membrane of cardiac mitochondria (Chapter 4), this study further aimed to determine whether acute *ex vivo* inhibition of ATM with the ATM specific inhibitor, KU60019, influences mitochondrial oxidative phosphorylation in a high fat diet induced obese model of male Wistar rats in either the presence or absence of the ATM activators, insulin and chloroquine.

5.1 Materials and Methods:

Hearts were isolated from young, control male Wistar rats and perfused *ex vivo* with either 0.03% DMSO (vehicle, n=5) or 3 µM KU60019 (n=5). Isolated subsarcolemmal mitochondria

from the perfused hearts were used to determine mitochondrial oxygen consumption with a Clarke-type oxygraph in either a glutamate-malate buffer that assesses the malate-aspartate shuttle and NADH oxidation by Complex I, or a palmitoyl-L-carnitine-malate buffer that assesses β-oxidation. This study was extended to include 45 high fat fed diet induced obese (DIO) male Wistar rats and their chow fed age matched counterparts (AMC, n=42). Hearts from these animals were perfused with 0.3 IU/l insulin or 30 µM chloroquine in the presence of absence of 3µM KU60019. Each perfused heart was divided in two; one half was used for the isolation of mitochondria, and the other heart half was prepared for western blotting purposes (Fig 5.1).

5.1.2 Reagents:

Chloroquine diphosphate salt (C6628) and KU60019 (SML1416) was purchased from Sigma-Aldrich Merck. HumulinR (100 U/ml, Eli Lilly and Company) was purchased commercially on prescription. Sodium pentobarbitone (Eutha-naze) was obtained from Bayer. Western blot reagents were purchased from BioRad (Lasec, South Africa), except for SignalBoost™Immunoreaction Enhancer Kit (EMD Millipore-Merck), and the Immobilon®-P PVDF membrane (EMD Millipore-Merck). The antibodies were purchased from Cell Signaling Technologies (USA) and Abcam as indicated in Table 5.2. All other reagents were purchased as indicated previously.

5.1.3 Animals:

All the procedures involving animals were in compliance with the South African National Standard for the care and use of animals for scientific purposes (SANS 10386:2008); the Medical Research Council Guidelines on Ethics for Medical Research; Book 3: Use of Animals in Research and Training and the National Institutes of Health Office of Laboratory Welfare: The Guide for the Care and Use of Laboratory Animals, 8th Edition; USA, and was approved by the Research Ethics Committee: Animal care and Use, Stellenbosch University, South Africa (approval numbers SU-ACUM12-0040; SU-ACUD16-00179).

Male Wistar rats (weighing approximately 250 grams and 12 weeks of age) were housed at the Central Research Facility (Stellenbosch University) in a temperature controlled (~23°C)

environment with a 12-hour light/dark cycle and fed normal rat chow (n=10). For the DIO rats, the animals at 8 weeks of age were either continued on normal rat chow (n=50), or placed on a hyperphagic diet (Salie et al. 2014) (n=50) for a period of 16 weeks (Table 5.1). The animals were injected with Eutha-naze (200 mg/kg via intraperitoneal injection) performed by a registered animal laboratory technologist, South African Veterinary Council, SAVC number: AL16/15486), and euthanised through exsanguination after rapid excision of the heart. The hearts were arrested in Krebs-Henseleit buffer (KHB; 119 NaCl mM, 24.9 mM $NaHCO_3$, 4.7mM KCl, 1.2 mM KH_2PO_4, 0.6 mM $MgSO_4 \cdot 7H2O$, 0.59 mM Na_2SO_4, 1.25 mM $CaCl_2 \cdot 12H2O$ and 10 mM glucose; pH 7.4).

After anaesthetizing the animals, they were weighed and non-fasting blood glucose was measured by means of a tail prick and glucometer. Visceral (perirenal and perigonadal) fat deposits were removed and weighed post-exsanguination. The adiposity index was calculated as the ratio of visceral fat mass to total body mass (visceral fat/total bodymass) and expressed as percentage (Leopoldo et al. 2016; Jeyakumar et al. 2009; Pawlak et al. 2004).

Table 5.1: Compositions of the control chow diet compared to the diet induced obesity (DIO) diet:

	Fat (g/100 g)	Protein (%)	CHO (%)	Sugar (g/100 g)	Energy (kJ/100g)
Rat chow	4.8	17.1	34.6	6.6	1272
DIO	11.5	8.3	42.0	24.4	1354

CHO: carbohydrates; DIO: diet induced obesity

5.1.4 Langendorff perfusions (for mitochondrial analysis):

Excised hearts (n=10 young controls {12 weeks old}, n=50 for chow fed AMC DIO, n=50 DIO) were cannulated via the aorta and perfused with retrogradely in Langendorff mode with Krebs-Henseleit buffer at a constant pressure of 100 cm H_2O. Hearts were stabilized for 20 minutes, after which they were perfused in a recirculating manner with KHB containing 3 µM KU60019 (n=5) or an equal volume DMSO (0.03 %; n=5) for the 12-week old control rats. The chow fed age matched controls and DIO rat hearts were perfused in the same manner,

and the experimental protocols are shown schematically in Fig. 5.1. Protein determination for the mitochondrial data was performed with a Lowry assay (Lowry et al. 1951).

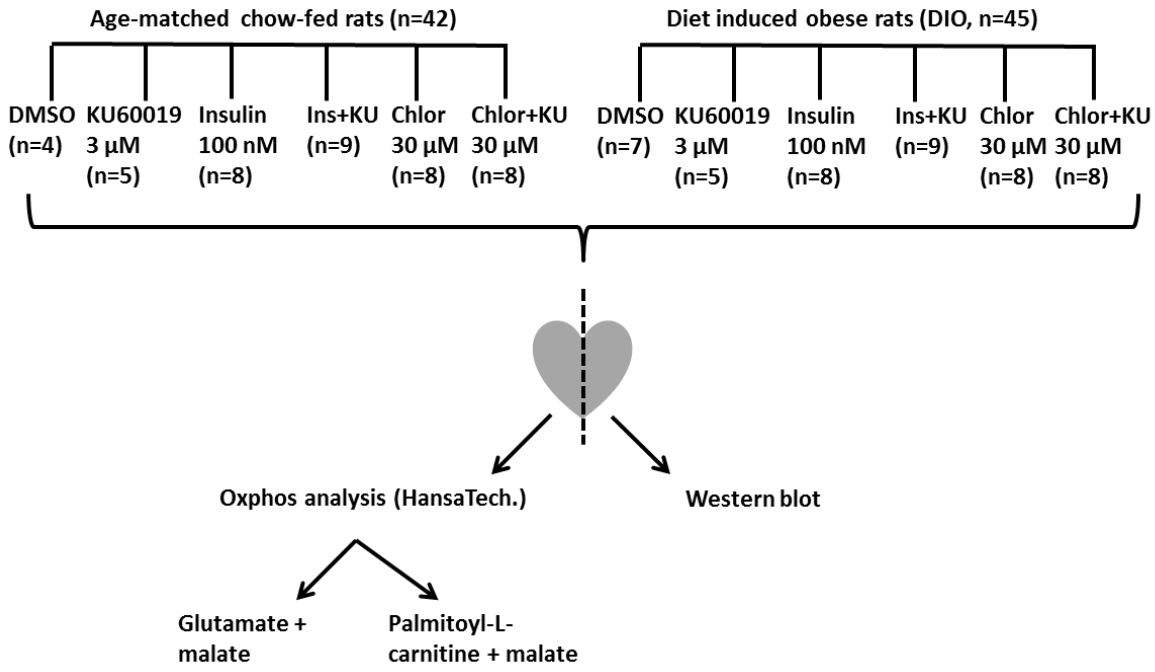

Figure 5.1: Experimental design layout for oxidative phosphorylation analysis in the presence and absence of the ATM activators, insulin and chloroquine with or without the ATM inhibitor, KU60019. Male Wistar rat hearts were perfused with the treatments indicated for both the chow-fed and DIO diets. After perfusion, the hearts were cut in half, of which one half was used for mitochondrial preparation in an isotonic solution for oxidative phosphorylation analysis with glutamate+malate or palmitoyl-L-carnitine+malate substrate. Mitochondria were prepared form the other half in precisely the same manner with the exception that the final mitochondrial pellet was lysed in a lysis buffer for western blotting purposes.

5.1.5 Oxygen consumption in isolated mitochondria:

Mitochondrial oxygen consumption was analysed with a Clarke-type oxygraph (Oxytherm system, Hansatech Instruments) immediately following isolation. Briefly, two chambers containing a glutamate or palmitoyl-L-carnitine assay buffer (250 mM sucrose, 10 mM TRIS-HCl (pH 7.4), 8.5 mM K_2HPO_4-$3H_2O$, 2 mM malate and 5 mM glutamate or 0.45 mM palmitoyl-L-carnitine; pH 7.4), equilibrated to ambient oxygen levels at 25°C, were analysed in parallel. Data were captured with HansaTechPlus software. Oxygen consumption prior to the addition of ADP (State 2), oxygen consumption in the presence of ADP (State 3), oxygen consumption after complete utilization of ADP (State 4) and State 3 oxygen consumption after 20 minutes anoxia followed by reoxygenation were noted. These values were used to

calculate the oxygen consumption (nano atoms O/min/mg mitochondrial protein), oxidative phosphorylation rate (nmol ATP/min/mg mitochondrial protein), respiratory control index (RCR, State 3/state 4), and the ADP/O ratio (number of ADP molecules for each oxygen atom consumed and is an index of the efficiency of oxidative phosphorylation) .

The rate of oxygen consumption over time as a function of substrate oxidation in the presence of saturating ADP concentrations was interpreted as the oxidative phosphorylation capacity of mitochondria and is widely used as a measure of mitochondrial function. It should be noted that many studies are performed in isolated mitochondria which in itself has the advantage of well-established protocols and easy-to interpret results that can be normalised to protein content or Cytochrome c, but has the disadvantage of lacking cellular context, is prone to damage and often requires large amounts of tissues (Brand & Nicholls 2011). Intact cells offer cell-specific context but cannot easily be manipulated chemically and are often not quantitative (Brand & Nicholls 2011). That being said, isolated mitochondria are widely used to assess mitochondrial dysfunction in heart failure, ischaemia and reperfusion (Chen et al. 2008; Lesnefsky et al. 2001), as well as in obesity and diabetes, which also give insight into oxidative stress

5.1.6 Western blotting:

Briefly, the mitochondrial lysates were prepared for western blotting with the addition of one volume 1 X lysis buffer (20 mM TRIS-HCl (pH 7.5), 1 mM EGTA, 1 mM EDTA, 150 mM NaCl, 1 mM β-glycerophospate, 2.5 mM tetra sodium pyrophosphate, 10 mM sodium orthovanadate, 1% Triton X-100, 10 µg / mL leupeptin, 10 µg / mL aprotinin and 50 µg / mL PMSF). Zirconium oxide beads (0.5 mm, Next Advance, Biocom Biotech) were added to the mitochondrial lysates, where after the mitochondria were further lysed in a Bullet blender (Next Advance laboratory equipment) at 4 000 revolutions per minute (rpm) making use of three cycles at 4°C for 1 minute with a 5 minute resting period in between. The lysates were rested on ice for 20 minutes prior to centrifugation at 12074 x *g* for 10 min at 4°C. The supernatants were carefully removed and placed in a new set of 1.5 ml Eppendorf tubes. Protein concentration was determined with a Bradford protein assay (Bradford 1976).

Mitochondrial lysates were prepared to a total volume of 15 µl containing up to 50 µg protein in lysis buffer (2 volumes) to one volume 3 X Laemmli sample buffer (2.5 M glycerol, 0.189 M TRIS-HCl (pH 6.8), 10% SDS, 1.275 mM bromophenol blue, 15% β-mercaptoethanol).The samples were boiled for four minutes and stored at -80° Celsius until use, with the exception of the samples used for the mitochondrial oxphos antibody kit (Abcam) that were not boiled at all. Samples were boiled again for 4 minutes prior to being loaded on 4–20% Criterion® TGX™ Stain free Precast Protein Gels (Bio-Rad Laboratories), and subjected to electrophoresis for 1 hour at 200 V and 200 mA. Due to major size differences in the proteins investigated, a modified transfer buffer was used (25 mM TRIS, 190 mM glycine and 10% methanol v/v), and the gels were allowed to rest for 30 minutes in the buffer prior to activation in the ChemiDoc MP system (Bio-Rad Laboratories), whereafter proteins were transferred. Transfer was performed at 200 V and 200 mA for 1 hour 30 minutes at 4° C onto an Immobilon®-P PVDF membrane (EMD Millipore). The membranes were briefly placed in methanol, and allowed to dry before blocking in a 5% liquid fat-free milk solution. Membranes were washed in TBS-T (20 mM TRIS-HCl (pH 7.6), 137 mM NaCl, 0.1% Tween-20) for 3 x 5 minutes. The antibodies used during this experiment are listed in Table 5.1. After primary and secondary antibody (donkey anti-rabbit secondary antibody; HRP-linked secondary antibody #7074, CST) incubation, the membranes were treated with Clarity™Western ECL Blotting Substrate and visualised on the Chemidoc MP system on the Chemi Hi sensitivity setting, which was stopped prior to overexposure (which appears red on program settings). The secondary antibody that was used against the Total oxphos rodent antibody cocktail was Anti-mouse IgG, HRP-linked Antibody #7076 (1:4000 dilution).

Table 5.2: : Summary of antibodies used to investigate ATM protein levels, oxidative phosphorylation, mitophagy and autophagy:

Protein antibody	Size	Dilution and dilutant	Species origin	Supplier	Product code
Total OXPHOS Rodent WB Antibody Cocktail	CI subunit NDUFB8-20 kDa CII-30kDa CIII-Core protein 2-48 kDA CIV subunit I-40 kDa CV alpha subunit-55 kDa	1:1000 TBS-T	Mouse	Abcam	(ab110413)
ATM	350 kDa	1:1000 in Primary SignalBoost™Immu no-reaction Enhancer Kit	Rabbit	CST	(D2E2) #2873
Phospho-ATM (Ser1981)	350 kDa	1: 1000 Primary SignalBoost™Immu no-reaction Enhancer Kit	Rabbit	CST	(D25E5) #13050
PINK	50, 60 kDa	1: 1000 in TBS:T	Rabbit	CST	(D8G3) #6946
Parkin	52 kDa	1:1000 in TBS-T+2.5% milk	Rabbit	Abcam	(ab233434)
Drp1	78-82 kDa	1:1000 in TBS-T	Rabbit	CST	(D6C7) #8570
LC3	14, 16 kDa	1:1000 TBS-T	Rabbit	CST	#4108
UCP3	30 kDa	1:1000 in TBS-T	Rabbit	CST	(D6J8K) #97000
TOM70	70 kDa	1:1000 in TBS-T	Rabbit	Abcam	(ab83841)

5.1.7 Statistical analysis:

The data was analysed using GraphPad Prism 6.0 software (GraphPad Software, Inc., La Jolla, CA). Statistical comparisons were made using a two-tailed Student's t-test or 2-way analysis of variance (ANOVA) followed by a Bonferroni post-hoc test where applicable. All values and error bars are presented as mean ± s.d., and the level of significance was set at $p < 0.05$.

5.2 Results and discussion:

5.2.1 Inhibition of ATM decreases Complex I-mediated oxidative phosphorylation

A small but significant reduction in mitochondrial respiration rates has previously been reported in ATM-deficient lymphoblastoid cells with a rezasurin assay (Ambrose et al. 2007). In view of the observed consistent association between ATM and the IMM of cardiac mitochondria (Chapter 4), this study investigated the effect of acute ATM inhibition on oxidative phosphorylation in isolated hearts obtained from 12-week old male Wistar rats (n=10; 295.7 ± 17.45 g). The hearts were stabilised and subjected to retrograde Langendorff perfusion with either DMSO (0.03%, dimethyl sulphoxide, n=5) or 3 µM KU60019 (ATM-specific inhibitor dissolved in DMSO, n=5) for 20 minutes prior to mitochondrial isolation in KE buffer.

The RCR did not differ significantly between mitochondria from DMSO and KU60019 perfused hearts (Figure 5.2). The substrates glutamate and malate, are utilised to investigate the mitochondrial aspartate shuttle that produces NADH which is oxidized by complex I (NADH dehydrogenase) of the electron transfer chain (ETC) to NAD^+ (Rosca et al. 2008). Oxidation of NADH donates an electron to complex I, which is used for ATP production.

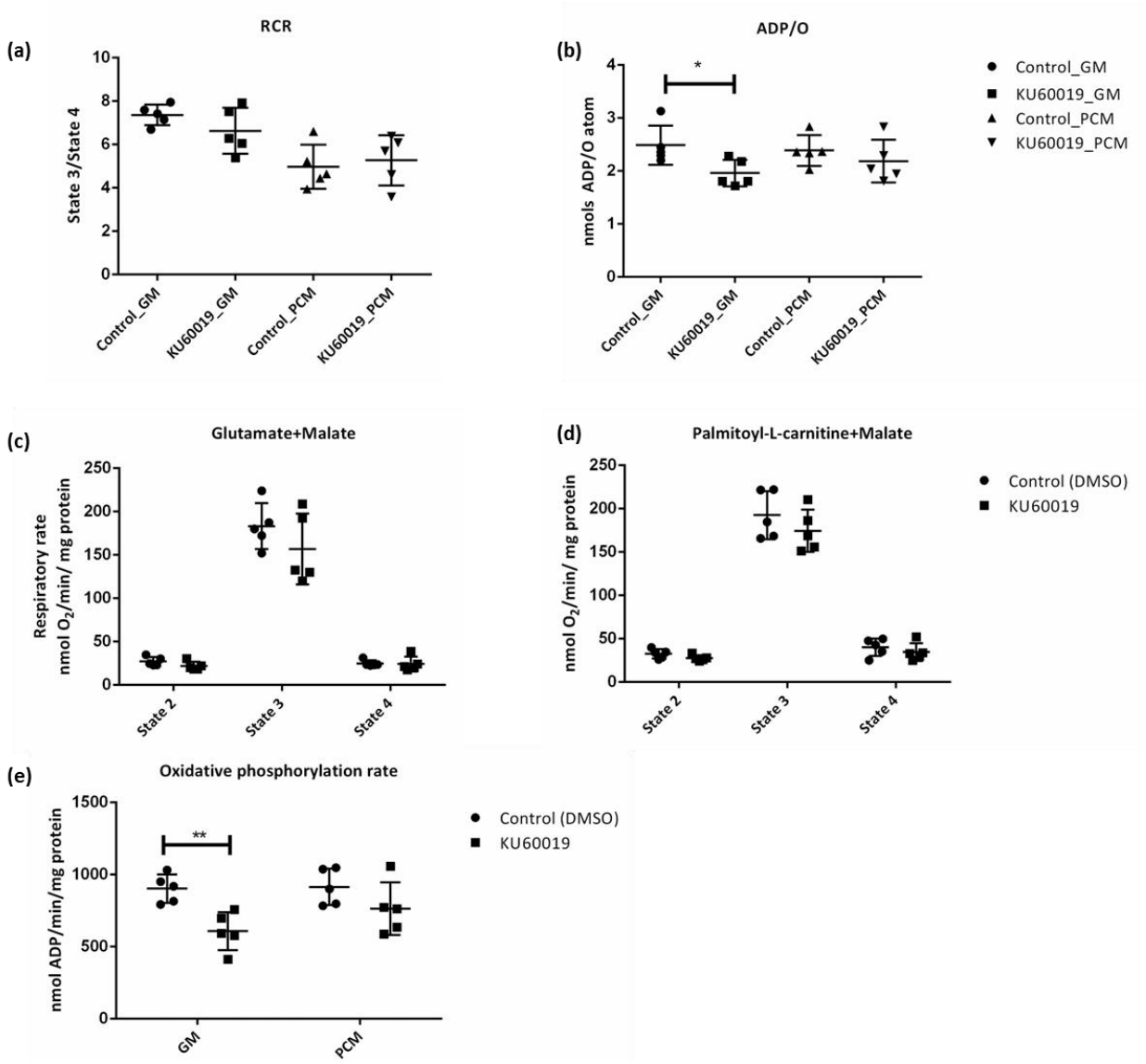

Figure 5.2: Inhibition of ATM decreases Complex I mediated oxidative phosphorylation rate. Male Wistar rat hearts were perfused with either DMSO (n=5) or KU60019 (n=5) and oxidative phosphorylation was determined polarographically. Panel a) shows the RCR values and panel b) ADP/O values. Both the active respiratory rate (State 3, panel c) and resting respiratory rate (State 2 and 4, panel c and d) were measured, and used to determine the oxidative phosphorylation rate (normalised to total protein) as shown in panel e. Values correspond to 10 individual experiments (0.03% DMSO control, n=5; KU60019, n=5), and error bars are presented as mean ± standard deviation.* p<0.05, **p<0.005.

The ADP/O ratio indicates the number of ADP molecules for each oxygen atom consumed and is an index of the efficiency of oxidative phosphorylation (Fig 5.2, panel b). This ratio differed significantly (p= 0.0298, Bonferroni post-hoc test) for the complex I-mediated reduction of the NADH-linked substrates, GM, in KU60019-perfused hearts compared to controls. This resulted in a significant reduction (p=0.0024, Bonferroni post-hoc test) in the

oxidative phosphorylation rate (ATP/min/mg mitochondrial protein) in GM, but not in the PCM respiratory buffer (Fig 5.2, panel e).

Interestingly, the changes observed with GM as substrate were not seen in PCM as substrate. Interestingly, western blot showed that ATM protein levels were decreased in the mitochondria isolated from hearts perfused with 3 µM KU60019 compared to hearts perfused with DMSO alone, albeit not significantly (p=0.2859, two-tailed Student's t-test, Fig 5.3), which agrees with the suggestion by (Patel et al. 2011) that acute incubation results in post-transcriptional changes induced by inhibition rather than transcriptional changes. The ATM inhibitor, KU60019 will decrease the kinase activity of the protein without necessarily changing its expression levels.

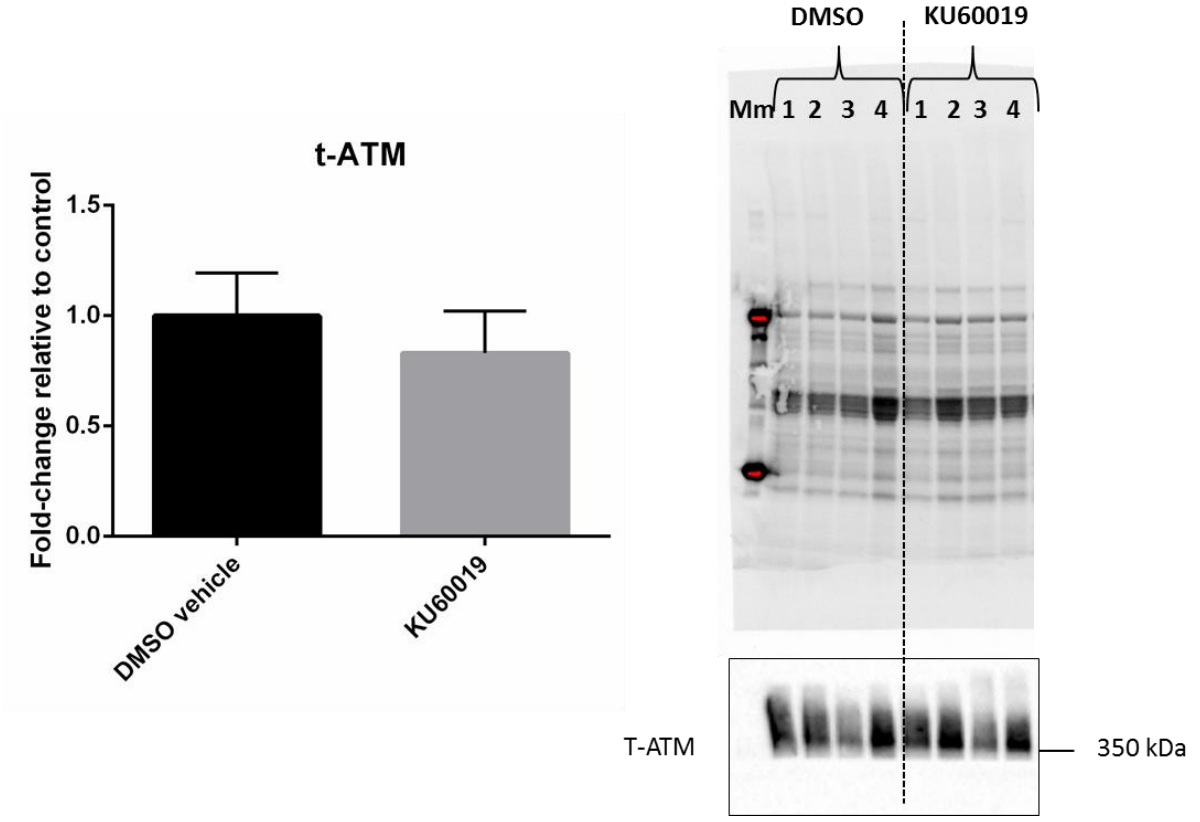

Figure 5.3: Western blot analysis of total ATM in hearts perfused retrogradely with either 0.03% DMSO or 3 µM KU60019. The total ATM protein level in mitochondrial lysates obtained from hearts perfused with either DMSO or KU60019 is shown and was normalised to the total protein membrane shown.

Palmitoyl-L-carnitine is imported into the mitochondrial matrix where it undergoes β-oxidation and produces Co-enzyme A (CoA), NADH and $FADH_2$ (flavin adenine dinucleotide). NADH transfers electrons to the ETC at complex I, whilst $FADH_2$ transfers electrons to the

ETC at complex II, which are the main source of ATP production in a healthy heart (Rosca & Hoppel 2010). As the glutamate-malate substrate assesses the aspartate-malate shuttle that produces NADH that provides electrons to complex I, our results suggest that the inhibition of ATM has a larger effect on complex I mediated NADH oxidation than $FADH_2$ oxidation at Complex II. Concomitantly, *Atm*-deficient murine thymocytes also exhibited a decrease in complex I enzyme activity and reduced ATP synthesis, but an increase in oxygen respiration was detected, which has been suggested to be context specific with regards to the cell-type (Valentin-Vega et al. 2012). For example, heterozygous $ATM^{+/-}$ mice hearts do not show any reduction in Complex I activity (Mercer et al. 2010). However, when investigating the effect of KU60019 on the subunits of the mitochondrial oxidative phosphorylation complex listed in Table 5.2, the present study found that all of the complexes were reduced after 20 minutes of acute *ex vivo* perfusion with significant effect of the inhibitor between mitochondria prepared from DMSO-perfused and KU60019 perfused hearts ($p=0.0136$, 2-Way ANOVA) but no significant differences were found between the individual complexes with a Bonferroni post-hoc test (Fig 5.4). Of the five subunits investigated all but one, are nuclear encoded, which supports the notion of a post-transcriptional rather than transcriptional response.

The underlying mechanism for ATM in this context, still remains unknown. Patel et al. (2011) showed that Complex IV is significantly decreased in the *extensor digitorum* longus muscles of mice after 1 hour of incubation with KU55933, and suggests a post-transcriptional role for ATM in oxidative phosphorylation. Moreover, the inhibition of Complex IV is known to increase ROS production and electron leak at Complex I or III by reducing the redox centres of these complexes (Chen et al. 2003).

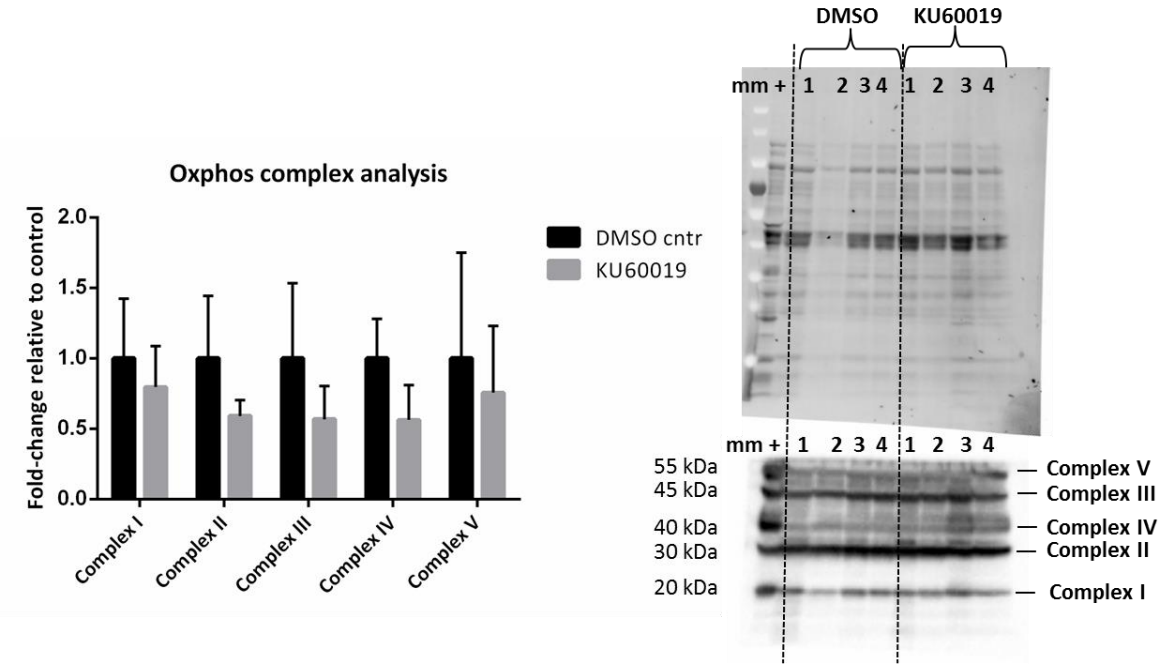

Figure 5.4: OXPHOS complex analysis of cardiac mitochondria. Mitochondria, obtained from male, Wistar rat hearts that were perfused *ex vivo* with either 0.03% DMSO (n=4) or 3 µM KU60019 (n=4), exhibited decreased electron transfer chain complexes. The positive control (+) was supplied with the Abcam Total OXPHOS Rodent WB Antibody Cocktail. The KU60019 complexes were normalised to their controls.

Whether KU60019 inhibits complex IV, which then decreases the redox centre of Complex I of the ETC, or whether the loss of ATM reduces all of the complexes, thereby exacerbating oxidative stress, is still unknown. It should be noted that the differences in complex reduction was small, and the role of ATM in this regard requires further investigation.

5.2.2 The role of ATM in obesity and cardiac oxidative phosphorylation in isolated mitochondria

Previous studies have shown that oxygen usage increases in high fat fed mice whilst decreasing cardiac efficiency, and was associated with increased mitochondrial uncoupling due to elevated UCP3 expression (Cole et al. 2011). Moreover, the Complex I-linked substrates, glutamate and malate, but not Complex II-linked substrates (succinate/rotenone) reduced respiration significantly in the muscle fibres of mice fed a high fat high sugar diet compared to mice fed standard chow (Bonnard et al. 2008). On the other hand, mitochondrial uncoupling was mediated by the activation UCPs in *db/db* mice, which was suggested to be due to increased delivery of reducing equivalents from β-oxidation to the ETC, and coupled with decreased oxidative phosphorylation capacity, increases ROS

production and lipid peroxidation and consequently drives uncoupling (Boudina et al. 2007). In view of the association between obesity and mitochondrial dysfunction (reviewed by Bhatti et al. 2017), as well as the potential role of ATM in obesity and insulin signalling, the current study evaluated the role of ATM in cardiac oxidative phosphorylation in DIO and their age-matched control chow fed male Wistar rats.

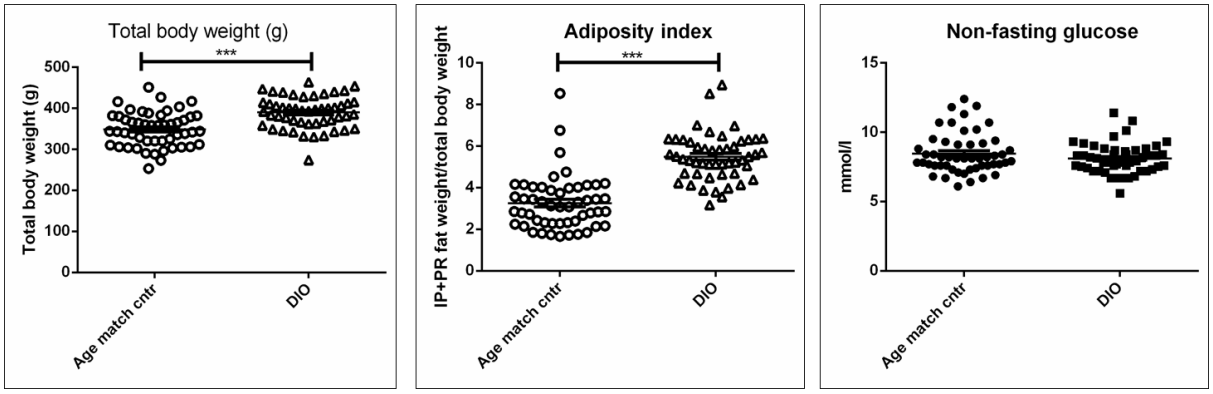

Figure 5.5 Weight, adiposity index and non-fasting blood glucose of diet-induced obese (DIO) male Wistar rats and their age-matched counterparts (AMC). Total body weight (left panel), adiposity index (middle panel) and non-fasting blood glucose (right panel) was determined for each of the AMC (n=50) and DIO rats (n=50) Significance was determined with a Student's t-test, mean ± s.d.).

This study investigated the role of ATM in oxidative phosphorylation of cardiac mitochondria obtained from a diet induced obese Wistar rat model. After 6 weeks of being fed a hyperphagic obesity inducing diet, the DIO-fed rats gained significantly more weight than their chow fed AMC (389.6 ± 38.75 g compared to 348.2 ± 42.33 g, $p<0.0001$, two-tailed Student's t-test). The adiposity index was significantly higher ($p<0.0001$) in DIO (5.479 ± 1.128%) than the chow-fed AMC group (3.255 ± 1.296%), whereas no difference ($p=0.1534$) was observed for non-fasting glucose values (nmol/l) between the DIO (8.088 ± 1.083) and chow fed AMC (8.461 ± 1.472) groups (Figure 5.5). These rats represent a much larger cohort of male, Wistar rats that were fed with normal rat chow or a DIO diet for 66 weeks from the age of 8 weeks, and were tested for insulin resistance with an oral glucose tolerance test, as well as homeostatic model assessment (HOMA) for insulin resistance (IR). These results were not generated within this study, and are thus not reported here but it is accepted that the rats used during this study were insulin resistant (Addendum C).

Unlike Boudina et al. (2007), the present study showed that ADP-stimulated oxygen consumption (State 3) as well as in the oxidative phosphorylation rate of mitochondria in

DIO hearts did not reduce significantly when compared with mitochondria from chow-fed AMC hearts regardless of the substrate present (Table 5.3). The model used by Boudina et al. (2007) is a well characterised mouse model of obesity and severe T2D (*db/db* mice), whereas the present study used a diet-induced, pre-diabetic obese rat model. Moreover, a study that investigated mitochondrial dysfunction in T2D patients compared to non-diabetic obese controls showed a significant reduction in subsarcolemmal mitochondrial ETC activity of T2D patients compared to obese controls (Ritov et al. 2005). They did however also notice a significant reduction in ETC activity in obese patients compared to lean controls. It is possible that the diet-induced obesity model used in the present study was not sufficient to mediate mitochondrial dysfunction, or it might merely be that the n-values used were too small to detect significant differences.

Table 5.3: Comparison of State 3 and State 4 (nano atoms O/min/mg protein) and oxidative phosphorylation rate (nmols ATP/mg mitochondrial protein/min) between chow-fed age-matched control and DIO animals:

	Glutamate + malate		Palmitoyl-L-carnitine + malate	
	Control (n=4)	**DIO (n=7)**	**Control (n=4)**	**DIO (n=7)**
State 3	219.70 ± 88.21	168.05 ± 50.41	246.05 ± 112.89	176.20 ± 33.35
State 4	33.54 ± 15.24	35.56 ± 16.92	36.74 ± 18.58	29.70 ± 3.94
Oxphos rate	525.68 ± 154.55	416.83 ± 143.45	634.39 ± 156.54	430.63 ± 130.76

Irrespective of diet, when evaluating the effects of inhibition of ATM in these hearts, a significant effect (p=0.0351) was detected with a 2-way ANOVA in State 3 respiration between KU60019-treated hearts and DMSO-perfused hearts (Fig 5.6). Likewise, KU60019 had a significant effect on the oxidative phosphorylation rate (p=0.0014) using a 2-way ANOVA analysis, but no specific differences were observed with a Bonferroni post-hoc test (Fig 5.6). This implies that the inhibition of ATM has a direct effect on oxygen consumption and ATP synthesis in rat heart mitochondria from both diet groups, and agrees with the observation in the young control cardiac mitochondria (Fig 5.2), although no differences were noted in the ADP/O ratio in GM substrate as was seen previously in mitochondria obtained from young, control rats with the chemical inhibition of ATM.

This could imply that the decrease in ATP synthesis (oxidative phosphorylation rate) were not due to uncoupling which is typically associated with increased oxygen consumption (reviewed by Bugger & Abel 2008), but rather decreased ETC efficiency. Interestingly, coupling efficiency (ADP/O) ratio is suggested to be a poor reporter of mitochondrial dysfunction (Brand & Nicholls 2011). It should be noted that ADP/O values (Fig 5.6a) were decreased in isolated mitochondria from KU60019-perfused hearts in AMC (2.03 ± 0.13, n=5, compared to 2.46 ± 0.23 DMSO-perfused, n=5) and DIO (2.03 ± 0.26 compared to 2.26 ± 0.47 DMSO perfused) in the GM substrate. Using PCM as substrate, the ADP/O ratio was decreased in mitochondria from AMC rat hearts perfused with KU60019 (1.93 ± 0.35) compared to DMSO-perfused mitochondria (2.12 ± 0.22), but was increased in DIO perfused with KU60019 (2.34 ± 0.35) compared to DMSO-perfused mitochondria. None of these differences were significant, and could again reflect the low n-values, or possibly reflect a change in substrate oxidation rather than a change to the ETC machinery, although the latter is probably unlikely in light of the finding that the ETC complexes were reduced overall (Fig. 5.4).

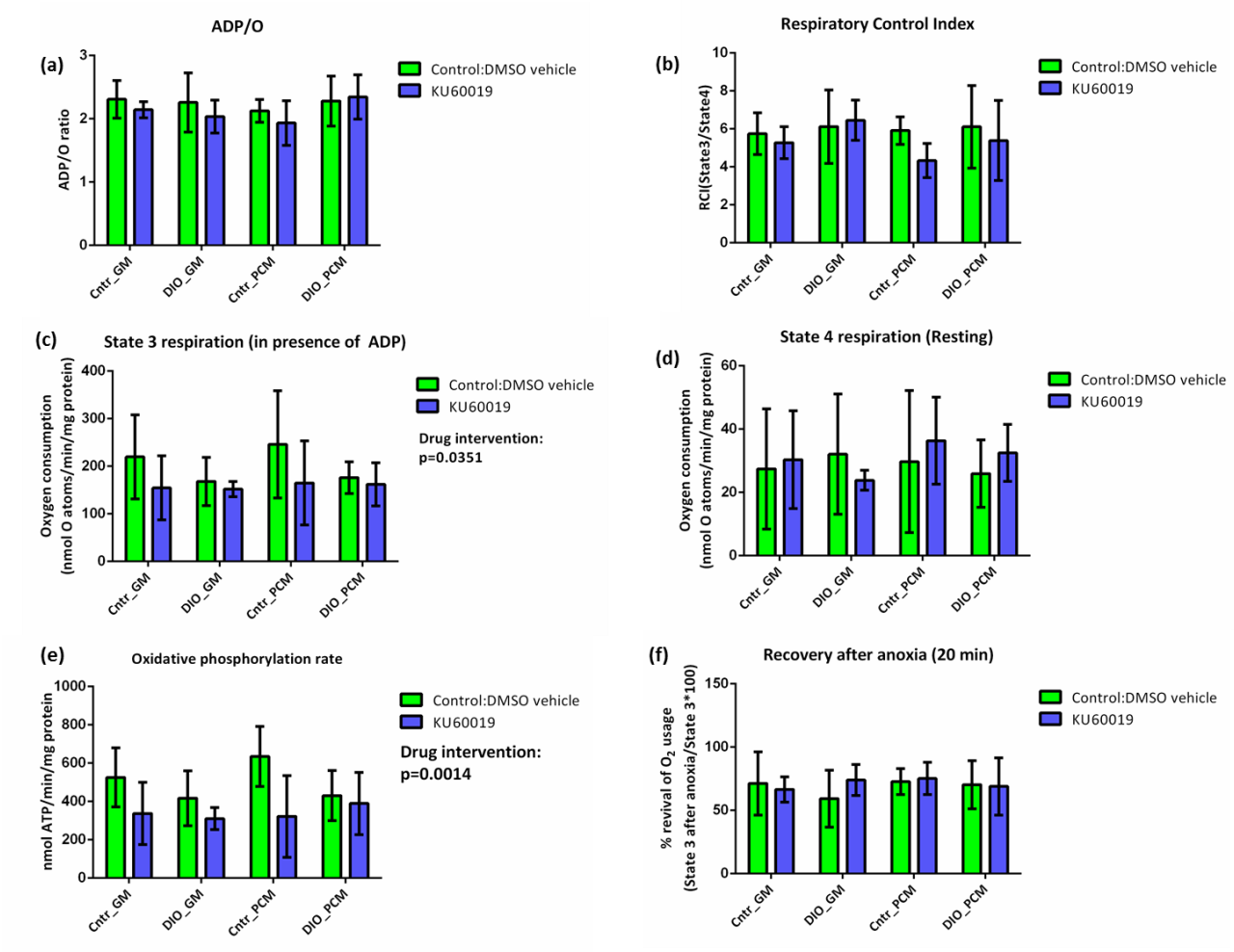

Figure 5.6: Inhibition of ATM decreased basal levels of State 3 oxygen consumption and oxidative phosphorylation rate. Male Wistar rat hearts from the AMC and DIO rats were perfused with either DMSO (n=4/group; green) or KU60019 (n=5/group; blue) and oxidative phosphorylation was determined polarographically in GM and PCM substrates. Panel a shows the RCR values and panel b) ADP/O values. Both the active respiratory rate (State 3, panel c) and resting respiratory rate (State 4, panel d) were measured, and used to determine the oxidative phosphorylation rate (normalised to total protein) as shown in panel e. Recovery of State 3 respiration after 20 minutes of anoxia is shown in panel f.

The respiratory control index (Fig 5.6b) was similar for both KU60019 and DMSO-perfused AMC and DIO hearts, which suggests that KU60019 did not influence mitochondrial capacity for oxidative efficiency, nor exhibit excessive proton leak. No difference was observed after 20 minutes of anoxia in either substrate or diet, and was not influenced by KU60019 perfusion (Fig 5.6f).

In summary, the inhibition of ATM in hearts from young control rats resulted in a significant decrease in ADP/O and oxidative phosphorylation rate in GM, but not PCM substrates. The

inhibition of ATM did not alter the total ATM levels (and activity of ATM was not determined), and had a small effect on the mitochondrial ETC complexes. Significant increases were observed in both weight and adiposity index in the DIO-fed rats compared to the chow-fed AMC rats, but no differences were observed with regards to State 3, State 4 respiration or the oxidative phosphorylation between these two groups. Inhibition of ATM decreased State 3 respiration overall, as well as oxidative phosphorylation, but no differences were observed between the chow-fed AMC group or DIO group, irrespective of the substrate used.

5.2.3 Insulin improves oxidative phosphorylation and protects against anoxia

Insulin is an important regulator of mitochondrial oxidative phosphorylation; it increases mitochondrial protein transcription in *vastus lateralis* muscle biopsies from healthy controls, whilst T2D patients have a reduced capacity to improve ATP production in response to high insulin levels (Stump et al. 2003). As early as 1960, Hall et al. (1960) showed that insulin improves oxygen consumption and ATP production in isolated liver mitochondria obtained from diabetic rats similar to levels found in normal control animals, and suggested that a small amount of endogenous insulin is sufficient to maintain mitochondria. It has been suggested that insulin specifically affects the succinate carbons that are metabolised in the mitochondrial TCA cycle (Bessman et al. 1986). Moreover, ATM is activated by insulin and is required for the activation of Akt in response to insulin treatment (Halaby et al. 2008). Thus, we aimed to determine whether (i) insulin improves oxidative phosphorylation in the DIO model used in this study and (ii) inhibition of ATM interferes with the action of insulin, by evaluating mitochondrial oxidative phosphorylation after *ex vivo* perfusion with 100 nM insulin (HumulinR) or 100 nM insulin + 3 µM KU60019 with both GM and PCM substrates.

Mitochondria from the insulin perfused chow-fed AMC and DIO hearts were first compared to mitochondria from DMSO-perfused chow-fed and DIO hearts. Insulin perfusion improved State 3 respiration ($p=0.0028$) and ATP synthesis ($p=0.01$) overall, irrespective of chow-fed ($n=9$) or DIO ($n=9$) diet, or substrate used (2-way ANOVA, Bonferroni post-hoc test, bars presented as mean ± s.d.) when compared to mitochondria from DMSO-perfused hearts, as shown in Fig. 5.7. Interestingly, the RCR was improved significantly in cardiac mitochondria from both control and DIO insulin-perfused hearts ($p<0.001$) in a GM, but not so in the PCM

substrate, when compared to mitochondria from DMSO perfused AMC and DIO hearts. This was reflected by the significant increase in State 4 respiration ($p<0.0036$) in Fig 5.7, which indicates a proton leak in the PCM substrate in cardiac mitochondria from both AMC and DIO animals.

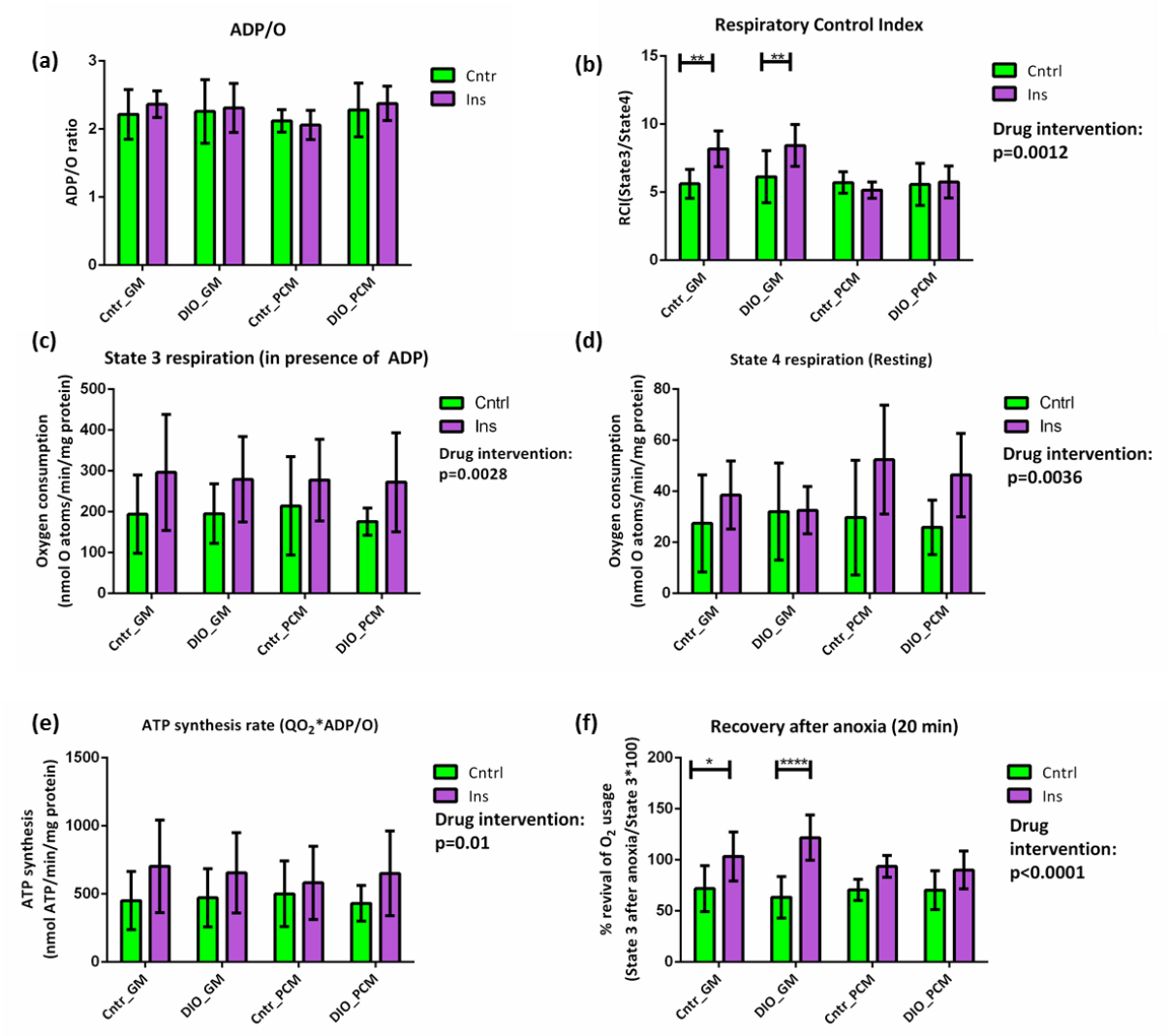

Figure 5.7: Insulin significantly improves basal levels of State 3 oxygen consumption, oxidative phosphorylation rate in both a carbohydrate and fatty acid substrate. Hearts from both the chow-fed AMC and DIO group were perfused with either DMSO or 100 nM insulin, and ADP/O (panel a), RCR (panel b), State 3 (panel c) and State 4 (panel d) respiration, as well as the ATP synthesis rate (panel e) and percentage recovery of State 3 respiration after 20 minutes of anoxia determined (panel f). * $p<0.05$; ** $p<0.005$, **** $p<0.0001$.

These observations suggest that the positive effects of insulin on oxidative phosphorylation are mediated via the malate-aspartate shuttle and TCA cycle, and agree with the finding that insulin mediates its effects via succinate in the TCA cycle (Bessman et al. 1986). The positive

effect with regards to RCR and recovery after anoxia is decreased when investigated in a PCM substrate.

Palmitoyl-L-carnitine enters the mitochondria independently of CPT1 (carnitine palmitoyltransferase I) via CACT (carnitine acylcarnitine translocase) where it undergoes sequential β-oxidation to produce reducing equivalents (Rosca et al. 2012). Fatty acids are known to cause mitochondrial uncoupling but the mechanism is still controversial. It has been suggested that there might be two potential mechanisms, the first being either in response to a high mitochondrial membrane potential that drives the negatively charged FFAs outwards (reviewed by Kadenbach 2003), and the second via the ADP/ATP antiporter (Goglia & Skulachev 2003).

Kadenbach (2003) suggested that ROS can activate the uncoupling proteins, UCP1-3, in the presence of excess FFA, consequently increasing proton leak and decreasing mitochondrial membrane potential in order to prevent further ROS production. On the other hand, Boudina et al. (2007) suggested that increased reducing equivalents often present in obesity, and coupled with a reduced ability to oxidise these equivalents, can drive mitochondrial ROS production, which will lead to uncoupling. Furthermore, mild uncoupling can be protective in the heart by lowering the oxidative phosphorylation and consequently reducing ROS production (Cadenas 2018). Mild uncoupling with the mitochondrial uncoupler arbonilcyanide p-triflouromethoxyphenylhydrazone (FCCP) improves post-ischaemic recovery via a ROS-dependent pathway that does not result in a decrease of cellular ATP or potassium channel activation (Brennan et al. 2006).

In view of the results that indicate that KU60019 decreases oxidative phosphorylation whilst insulin improves it when compared to controls, the present study compared mitochondria from chow-fed AMC and DIO hearts that were perfused with a combination of insulin and KU60019, to the groups previously discussed.

When comparing isolated mitochondria from chow-fed AMC (n=8) and DIO hearts perfused with a combination of KU60019 and insulin (n=9), (Fig. 5.8) to the KU60019 and insulin perfused groups discussed previously, all the measured parameters were influenced. The combination of KU60019 and insulin significantly decreased the ADP/O ratio in mitochondria from perfused DIO hearts in the GM-substrate ($p<0.05$,) and the PCM substrate when

compared to KU60019 alone ($p<0.05$) as well as compared to insulin alone ($p<0.005$). The treatments contributed to an overall effect of $p<0.0001$ (all statistical analysis performed by 2-way ANOVA, Bonferroni post-hoc test).

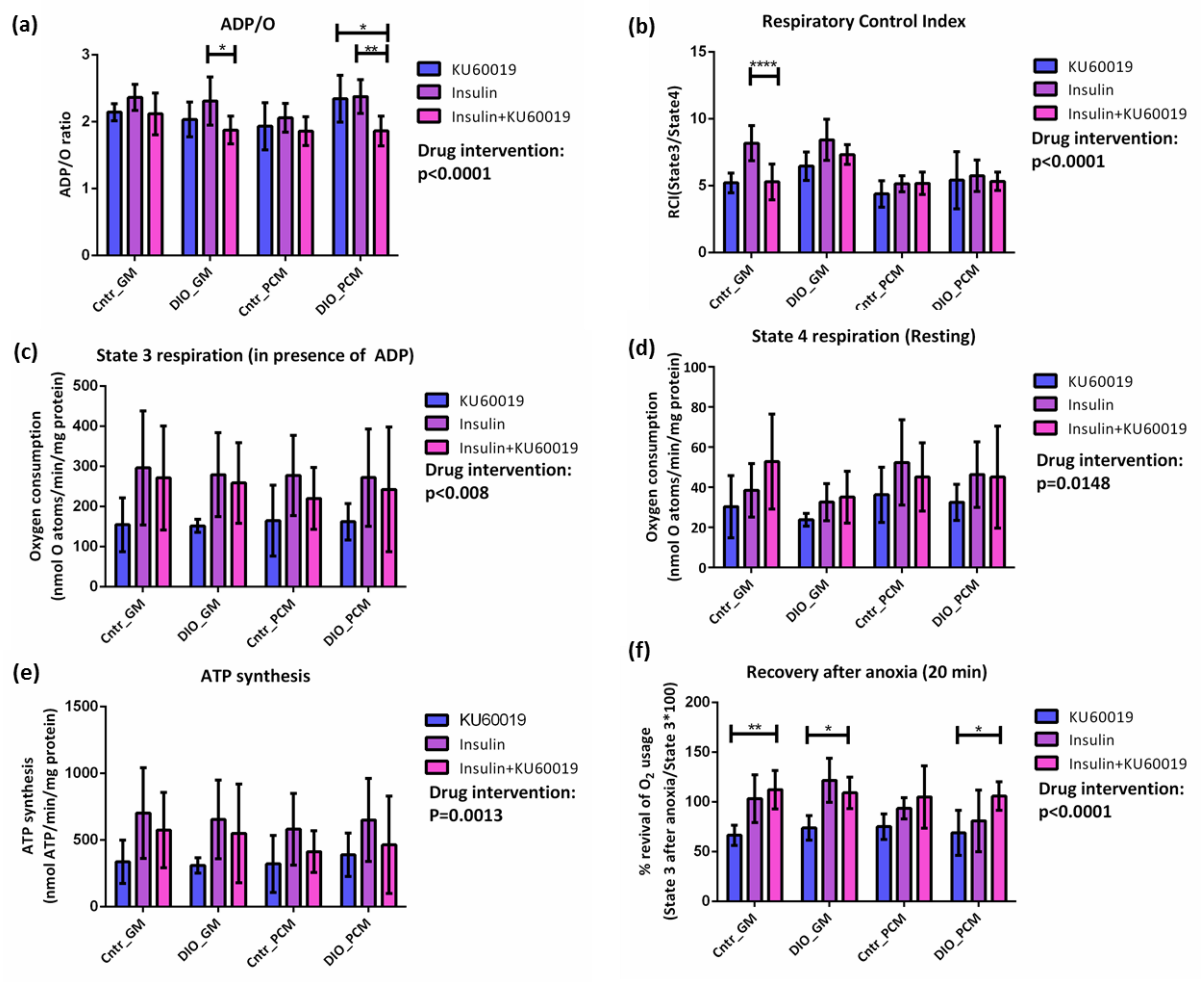

Figure 5.8: The combination of KU60019 and insulin perfusion significantly influenced ADP/O, RCR, and recovery after anoxia in isolated mitochondria. Isolated mitochondria from chow-fed AMC and DIO hearts were compared with the groups perfused with either KU60019 or insulin alone. ADP/O values (panel a), RCR values (panel b), and State 3 respiration recovery after 20 minutes of anoxia (panel f) was significantly influenced. The combination of insulin and KU60019 did not influence State 3 (panel c) or State 4 (panel d) respiration or ATP synthesis. $p<0.05$. * $p<0.05$; ** $p<0.005$, **** $p<0.0001$.

Interestingly, the combination treatment also resulted in a significant decrease ($p<0.0001$) in the RCI of mitochondria from chow-fed AMC hearts perfused with insulin alone in GM substrate. This suggests that any positive effects exerted by insulin through the malate–aspartate shuttle is decreased by the addition of KU60019, and supports the hypothesis that ATM might mediate an effect on substrate utilisation through Complex I. No effect was seen with the combination treatment in either chow-fed or DIO cardiac mitochondria in the PCM

substrate, and again supports the hypothesis that the effect of ATM is mediated through carbohydrate metabolism rather than β-oxidation. Drug intervention had an overall effect ($p<0.0001$, 2-way ANOVA) however the only significance detected with the Bonferroni post-hoc test was within the chow-fed controls in the GM-substrate, as mentioned already.

Both State 3 ($p=0.008$) and State 4 ($p=0.0148$) respiration was increased with insulin and the combination of insulin and KU60019 (2-way ANOVA) when compared hearts perfused with KU60019 alone, but no specific differences could be detected with a Bonferroni post-hoc test. A slight decrease was observed in State 3 oxygen consumption and ATP synthesis with the combination treatment compared to insulin alone for mitochondria from chow-fed animals in the GM-substrate, and can potentially be due to the observed decrease in RCR, which seems to be mainly driven by the increase in state 4 respiration.

Interestingly, the combination of insulin and KU60019 significantly improved recovery after anoxia for mitochondria from perfused hearts of chow-fed rats in GM substrate ($p<0.005$), as well as for DIO in a GM substrate ($p<0.05$) and PCM-substrate ($p<0.05$), whereas treatment contributed significantly to the effect observed ($p<0.0001$, 2-way ANOVA, Bonferroni post-hoc test). This would suggest that the positive effect observed in recovery after anoxia is mediated by insulin and not by inhibition of ATM. Furthermore, the inhibition of ATM improved recovery after anoxia in the PCM substrate both for mitochondria from chow-fed and DIO rats, which was not observed in mitochondria from hearts treated with insulin alone. However, the underlying mechanism for this is still unknown.

A possible hypothesis for the significant increase in recovery observed after 20 minutes of anoxia in a PCM buffer could potentially be the partial inhibition of Complex I by KU60019 that is improved by insulin. The inhibition of mitochondrial respiration is cardioprotective during ischaemia and reperfusion, and more specifically the inhibition of Complex I by either rotenone (Lesnefsky et al. 2004) or amobarbital (Chen et al. 2006). A previous study in our laboratory found that ATM inhibition improved cardiac function in control and high caloric fed rat hearts during early reperfusion but had no effect on cardiac function during later reperfusion (Espach 2017).

However, the mechanism of the observed improvement by perfusion with insulin followed by mitochondria incubation in a PCM substrate is unknown. The inhibition of ATM alone is

insufficient to obtain increased recovery after anoxia. It might be that insulin provides protection against oxidative stress which is improved by the inhibition of ATM potentially through a Complex I mediated effect. Alternatively, activation of the PI-3K/Akt pathway might inhibit the translocation of Bax (a pro-apoptotic protein which is mainly localised in the cytosol), to the mitochondria, and can promote cell survival (Tsuruta et al. 2002). However, this will have to be investigated further in the context of ATM.

Taken together, the mitochondrial ADP/O values of DIO rat hearts decreased significantly when perfused with a combination of insulin and KU60019 when compared to insulin-perfused hearts, irrespective of the substrate used. Moreover, perfusion with this combination significantly decreased the RCI when compared with hearts perfused with insulin alone in a GM but not PCM substrate. However, this did not influence the improved State 3 recovery after anoxia that was previously observed with insulin perfusion; as a matter of fact the combination of insulin and KU60019 significantly improved recovery after anoxia in both diets and substrates used.

5.2.4 Chloroquine improves recovery after anoxia that is further improved with the inhibition of ATM:

Chloroquine modulates chromatin conformation changes without causing DNA damage (Bakkenist & Kastan 2003), and can thus act as a non-canonical activator of ATM (Cremona & Behrens 2014). ATM is consequently phosphorylated at Ser^{1981}, allowing it to dissociate into monomers that bind with ATMIN (ATM interactor protein) and can phosphorylate, for example, p53. In the context of metabolic syndrome, low-dose chloroquine treatment improves glucose tolerance in an ATM dependent manner in an $ATM^{+/+}$ $ApoE^{-/-}$, *db/db* and *ob/ob* mouse models (Schneider et al. 2006). Chloroquine treatment also reduces the development of atherosclerosis in western diet fed (high fat) mice in a p53-mediated manner, but can improve glucose tolerance, insulin sensitivity and hepatic Akt signalling irrespective of p53 (Razani et al. 2010). Similarly, in a L6-muscle cell model, chloroquine improved insulin-stimulated Akt-phosphorylation and glucose uptake, as well as Akt activity in insulin resistant rats (Halaby et al. 2013).

The metabolic effects of chloroquine also have clinical relevance as it increases insulin secretion, decreases insulin clearance, improves peripheral glucose uptake and decreases

dyslipidaemia in patients (Asamoah et al. 1990; Powrie et al. 1991; Powrie et al. 1993). Chloroquine is an acidotrophic, lysosomotropic agent that prevents endosomal acidification and consequently inhibits lysosome-autophagosome fusion and degradation (Shintani & Klionsky 2004), effectively protecting insulin against endosomal degradation (Bevan et al. 1997). The drug increases cellular glucose uptake through the promotion of GLUT4 trafficking to, and fusion with, the cellular plasma membrane by increasing cellular Ca^{2+} uptake (Zhou et al. 2016). However, on a cellular level, chloroquine treatment increase mitochondrial fragmentation and cristae destruction which is associated with increased oxidative stress and mitochondrial dysfunction (Chaanine et al. 2015). Similar results were noted in cortical neurons where chloroquine treatment significantly increased mitochondrial DNA damage, inhibited key mitochondrial functions and consequently, resulted in significant alterations in cellular metabolism (Redmann et al. 2017).

Chloroquine is commonly used as an autophagy inhibitor *in vivo* and *in vitro* (Klionsky et al. 2016). Chloroquine treatment worsened cardiac performance in Type 1 Diabetes, whilst hearts from *db/db* mice exhibited poorer diastolic function when compared to hearts obtained from either control or heterozygous db/$^{+}$ mice (Kanamori et al. 2015). The latter study concluded that chloroquine decreased diastolic function in Type 2 Diabetes (T2D), and noted that this could be due to suppressed autophagy in the diabetic heart.

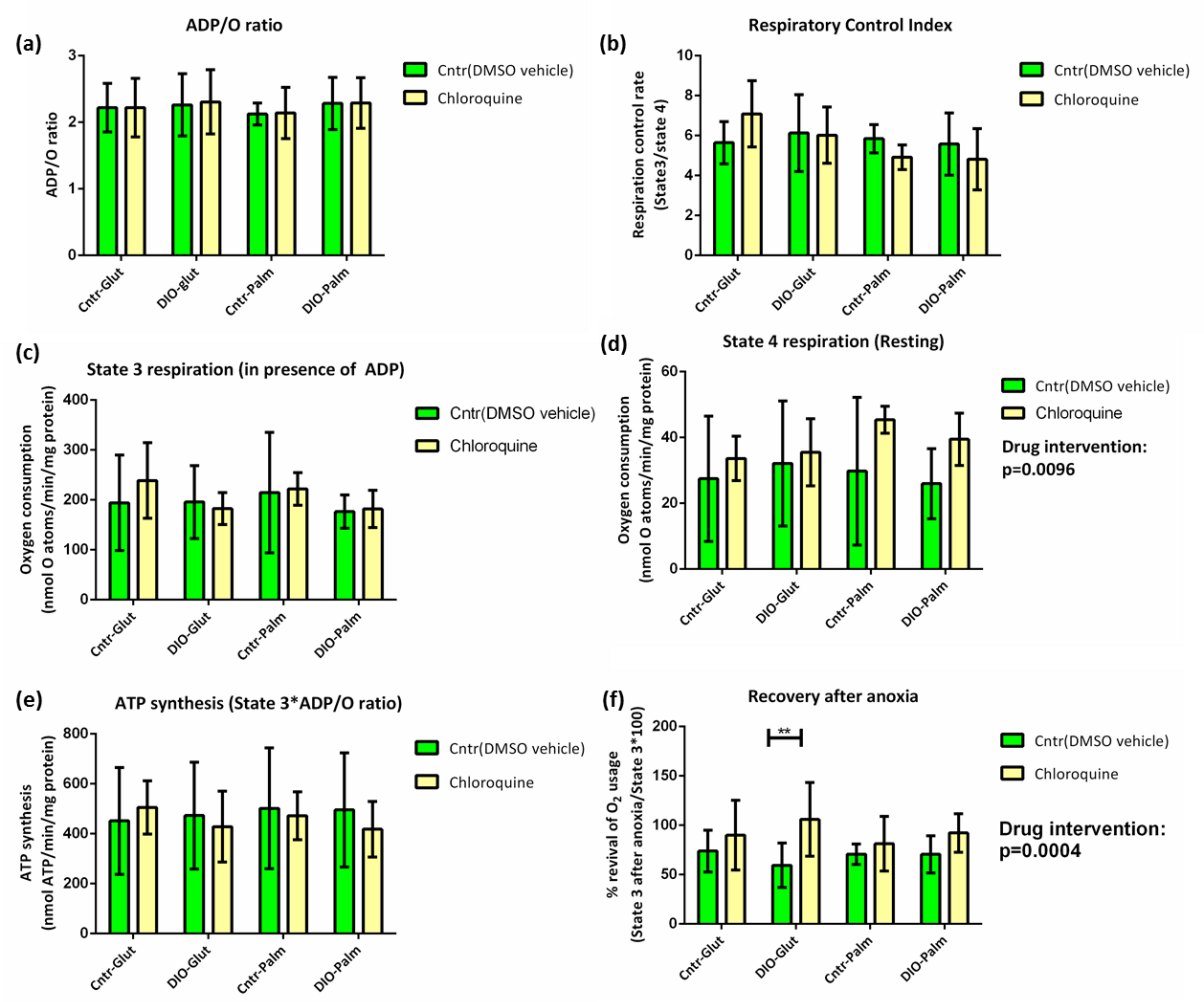

Figure 5.9: Mitochondria from chloroquine-perfused rat hearts show improved recovery after anoxia but also increased State 4 respiration. Mitochondria from chloroquine perfused chow-fed AMC and DIO hearts were compared to DMSO-perfused chow-fed and DIO hearts with regards to a) ADP/O ratio, b) RCR, c) Sate 3 respiration, d) State 4 respiration, e) ATP synthesis and f) Recovery after anoxia. p<0.05. ** p<0.005.

The present study observed significantly improved recovery after anoxia (p=0.0004) in response to chloroquine treatment, and specifically in mitochondria from DIO chloroquine perfused hearts (n=8) in a GM substrate (Fig 5.9; p<0.005, 2-way ANOVA, Bonferroni post-hoc test). However, State 4 respiration increased significantly overall upon treatment compared to control DMSO perfused cardiac mitochondria (p=0.0096, 2-way ANOVA, Bonferroni post-hoc test), and although not reflected in the ADP/O values, would suggest uncoupling (Fig 5.9).

In primary neurons, chloroquine has been shown to decrease mitochondrial enzymes both within the ETC and TCA cycle as a secondary effect of autophagy, which consequently resulted in decreased mitochondrial quality (Redmann et al. 2017). In this study,

chloroquine did not affect either the ADP/O ratios or RCR as a measure of mitochondrial quality (Fig 5.9). The combination of KU60019 and chloroquine likewise did not affect either ADP/O ratios or RCR, but notably increased state 3 respiration in DIO-perfused mitochondria in both GM and PCM substrates (Fig 5.10).

The current study also compared mitochondria from hearts perfused with a combination of chloroquine and KU60019, to the groups perfused with chloroquine alone (Fig 5.9) as well as the groups perfused with KU60019 alone (which is also shown in Fig. 5.6 compared to DMSO perfused hearts).

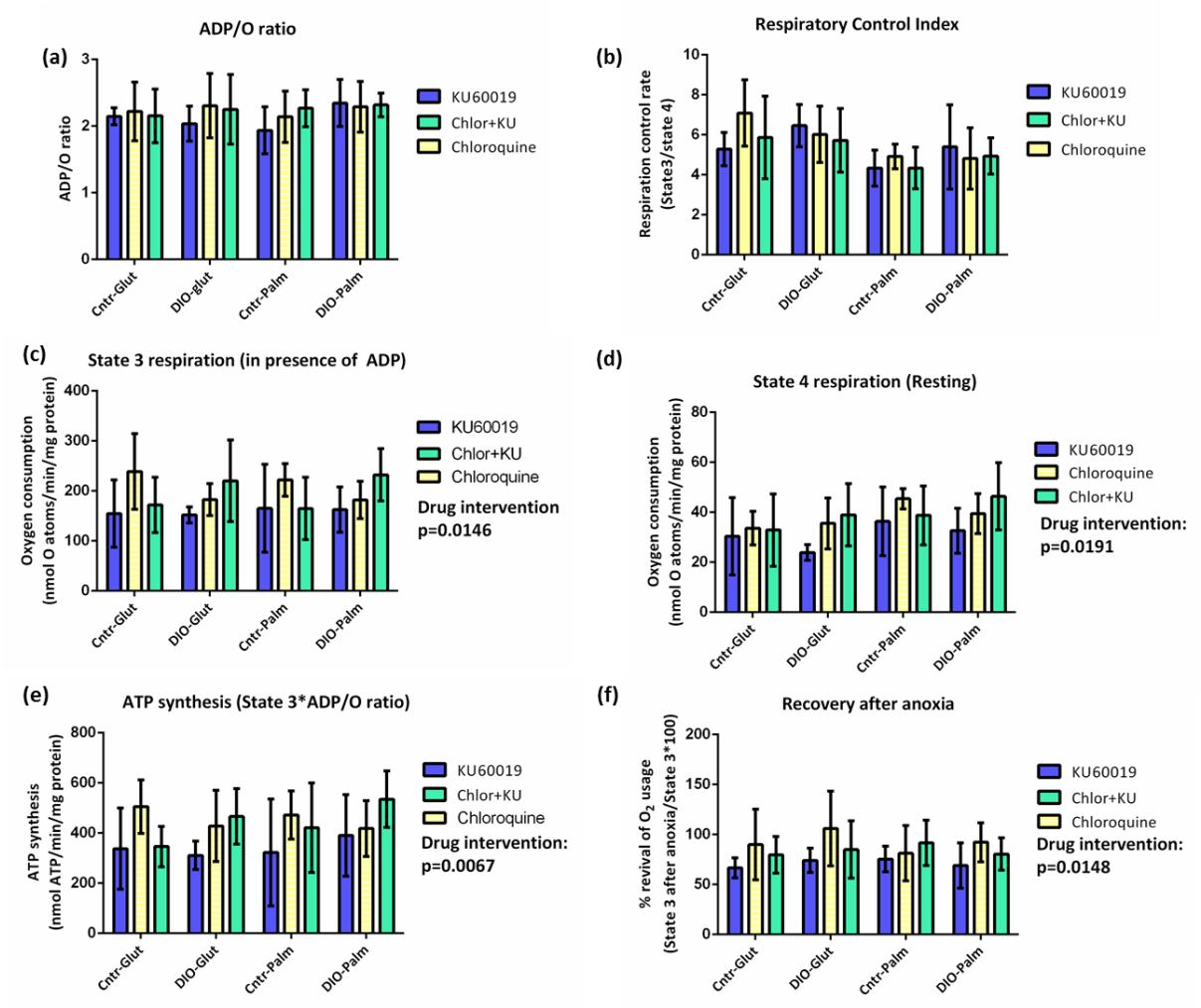

Figure 5.10: Mitochondria from hearts perfused with a combination of chloroquine and KU60019 did not show significant effects on influence oxidative phosphorylation. Both chow-fed AMC and DIO hearts perfused with a combination of chloroquine and KU60019 did not show any significant changes when compared to hearts perfused with either chloroquine or KU60019 alone for panel a) ADP/O ratios, or panel b, respiratory control index. State 3 (panel c) and State 4 (panel d) respiration, as well as ATP synthesis (panel e) and recovery after anoxia.

Overall, the combination treatment with both chloroquine and KU60019 (Fig 5.10) contributed significantly to the effect on State 3 respiration (p=0.0146, 2-way ANOVA), although no significant differences could be identified with Bonferroni post-hoc test. The notable but not significant decrease in chloroquine + KU60019 State 3 respiration compared to basal KU60019 levels in mitochondria from perfused chow-fed rat hearts in both GM and PCM substrates, suggests that the effect observed might be diet based. State 4 respiration increased in a similar fashion, with an overall significant contribution to the effect of drug treatment (p=0.0191, 2-way ANOVA) with the most marked increase in mitochondria from the DIO rats, irrespective of the substrate used (not significant, Bonferroni post-hoc test). The comparison of mitochondria from hearts perfused with KU60019 alone to hearts perfused with a combination of chloroquine and KU60019 is shown in Addendum D and shows that most of the changes observed are due to the addition of chloroquine.

Interestingly, the inhibition of ATM in the presence of chloroquine improved ATP synthesis compared to the inhibition of ATM alone in mitochondria from both control and DIO rats in PCM substrate, and DIO in a GM substrate (overall effect was p=0.0067, 2-Way ANOVA).

This would suggest that mitochondria that derive from a high free fatty acid environment (DIO fed rats) or mitochondria primarily utilising free fatty acids through β-oxidation (PCM substrate), might be protected against any detrimental effects of acute *ex vivo* chloroquine treatment. Chloroquine reversibly inhibits transmembrane electron transport (Crane et al. 1994), and was previously shown to be toxic to pig aortic cells (Crane et al. 1994). The addition of LDL protected the cells against chloroquine induced toxicity, although it did result in the accumulation of both lipid droplets and autophagic vacuoles (Crane et al. 1994). Likewise, isolated mitochondria in PCM substrate performed better, which indicates that the addition of palmitoyl-L-carnitine might protect the mitochondria against chloroquine toxicity.

The effect of chloroquine is most notable on the key components of glutaminolysis in the TCA cycle, which includes α-ketoglutarate, glutamate and glutamine, whilst succinate levels remain at basal levels in primary rat neurons treated with chloroquine (Redmann et al. 2017). This would potentially suggest that the inhibition of ATM together with chloroquine,

could exacerbate this effect on glutaminolysis, and supports the notion that ATM might play a role in Complex I mediated substrate oxidation.

Alternatively, the absence of ATM can result in a decrease in autophagy. ATM initiates autophagy via LKB1-mediated AMPK phosphorylation and mTOR suppression in response to ROS and RNS in the cytoplasm (Zhang et al. 2013; Tripathi et al. 2013). It can also promote autophagy by signalling AMPK in response to DNA damage (Li et al. 2017). Thus, the inhibition of ATM would result in an increase in mTOR, and decreased autophagy due to the inability to initiate the formation of autophagosomes. This would lead to the accumulation of damaged mitochondria. The main effect of chloroquine would thus become secondary if there are fewer autophagosomes formed, and would mean that the effect observed in mitochondria treated with both chloroquine and KU60019 would mainly be due to a decrease in mitochondrial oxidative phosphorylation and TCA cycle enzymes mediated by chloroquine, as was observed previously in neurons (Redmann et al. 2017). However, the last alternative is unlikely because chloroquine itself did not affect cardiac mitochondria in a similar fashion. It is very difficult to dissociate these two alternatives from each other and would require microscopy where the formation of autophagosomes are monitored, or a stepwise metabolomic analysis of liquid chromatography mass spectroscopy (LC-MS) similar to that performed by Redmann et al. (2017).

Taken together, chloroquine perfusion of chow-fed AMC and DIO hearts had little effect on oxidative phosphorylation compared to DMSO-perfused chow-fed AMC and DIO hearts, with the exception of mitochondria from chloroquine-perfused DIO hearts in GM substrate that exhibited significantly improved recovery after anoxia. The overall effect of drug treatment changed significantly in State 3 and 4 respiration, as well as ATP synthesis when hearts were perfused with a combination of chloroquine and KU60019 compared to either chloroquine or KU60019 alone. This was mainly driven by increased State 3 and 4 respiration rate in DIO-hearts perfused with a combination of chloroquine and KU60019 compared to KU60019 alone. Combined, it improved ATP synthesis in DIO hearts in both GM and PCM substrates, as well as recovery after anoxia.

5.2.5 Chemical inhibition of ATM with KU60019 influences mitophagy in cardiac mitochondria:

Cytosolic ATM is responsible for macroautophagy of peroxisomes (pexophagy, (Zhang et al. 2015) in response to ROS, and has been implicated in mitochondrial maintenance through mitophagy (Valentin-Vega et al. 2012). Recently, ATM was also shown to co-localise with PINK on the mitochondrial membrane in spermidine-induced mitophagy (Qi et al. 2016).

A high oxidative rate is linked to increased mitophagy and mitochondrial renewal, although the link between mitophagy and energy metabolism is still poorly understood (Melser et al. 2015). High oxidative rates have been linked with increased mitophagy through the recruitment of Rheb to the OMM which interacts with Nix and LC-3II to improve autophagy, and maintain oxidative phosphorylation efficiency (Melser et al. 2015). Conversely, BNIP3-mediated impairment of mitochondrial oxidative phosphorylation drives mitochondrial turnover through autophagy (Thomas et al. 2011). ATM deficiency in $ATM^{-/-}$ fibroblasts has been associated with a decrease in oxidative phosphorylation as well as decreased mitophagy (Valentin-Vega et al. 2012). Moreover, it has been shown that spermidine mediates mitophagy through the PINK-Parkin pathway in an ATM dependent manner (Qi et al. 2016). Whilst it is known that ATM is a positive regulator of autophagy and that its inhibitor, KU55933 markedly decreases autophagy, no studies in this regard have yet been done with the ATM inhibitor, KU60019. In light of the decreased oxidative phosphorylation observed in this study with KU60019, it raises the question whether this might be due to a reduction in either mitophagy or autophagy.

The inhibitor, KU60019, decreased both total ATM levels in chow-fed KU60019 perfused hearts, albeit not significantly (Fig 5.11). This was expected, as the inhibitor should not affect its expression levels, after 20 minutes of *ex vivo* perfusion (post-translational rather than a transcrptional response, Patel et al. 2011), but rather its activity. Several attempts to detect phospho-ATM(Ser^{1981}) was unsuccessful, and might suggest that if ATM, if it is phosphorylated in the mitochondria, it is not through the phosphorylation of Ser^{1981}, but rather possibly via the phosphorylation of Cys^{2991}, which is sensitive to oxidative stress (Zhang et al. 2018). This marker was not investigated in this study, but suggests that any changes that are observed, and potentially mediated through ATM in this study, might

rather be post-transcriptional and not in response to DNA damage induced during these experiments. It would thus be of great value to investigate the phosphorylation of ATM at Cys[2991] in the future, as it may corroborate the role of ATM in mitochondrial oxidative stress.

Unlike previous studies in our laboratory, the present study did not observe a difference in total-ATM levels in cardiac mitochondria between chow-fed and DIO animals. However, total ATM levels increased significantly in mitochondria from DIO hearts after perfusion with a combination of insulin and KU60019 compared to insulin alone ($p<0.005$, 2-way ANOVA, Bonferroni post-hoc test). Interestingly this was not observed in the cardiac mitochondria from control chow fed rats.

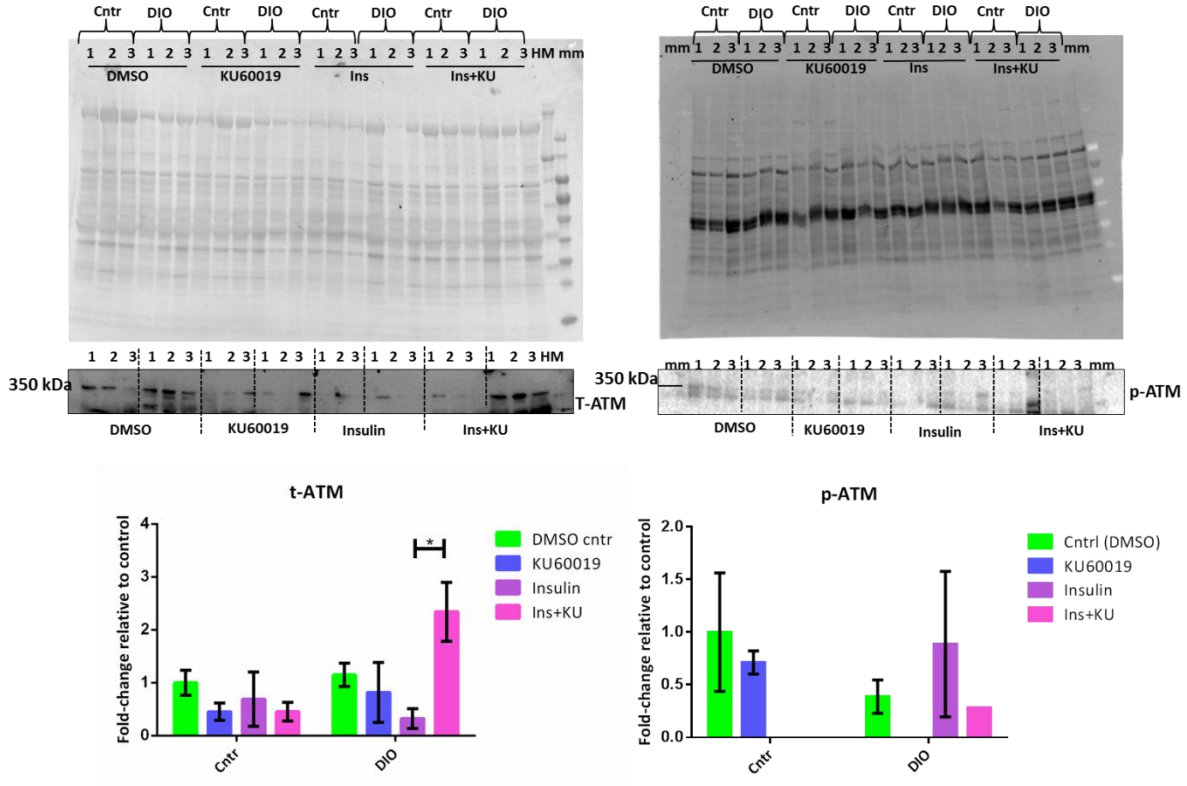

Figure 5.11: Total and phospho-ATM levels, as determined with western blotting, were decreased when perfused with KU60019, but accumulated in combination with insulin in obesity. Western blot analysis of total-ATM levels are shown in the left hand panel whilst phospho-ATM levels (Ser[1981]) are shown in the right hand panel for mitochondria from chow-fed AMC and DIO hearts perfused with DMSO, KU60019, insulin, and a combination of insulin and KU60019.

This indicates that insulin in combination with the inhibition of ATM, might lead to the accumulation of ATM in cardiac mitochondria in DIO hearts, but the underlying mechanism is unclear. This corresponds with a significant decrease in the ADP/O ratio, and interestingly, a significant increase in recovery after anoxia.

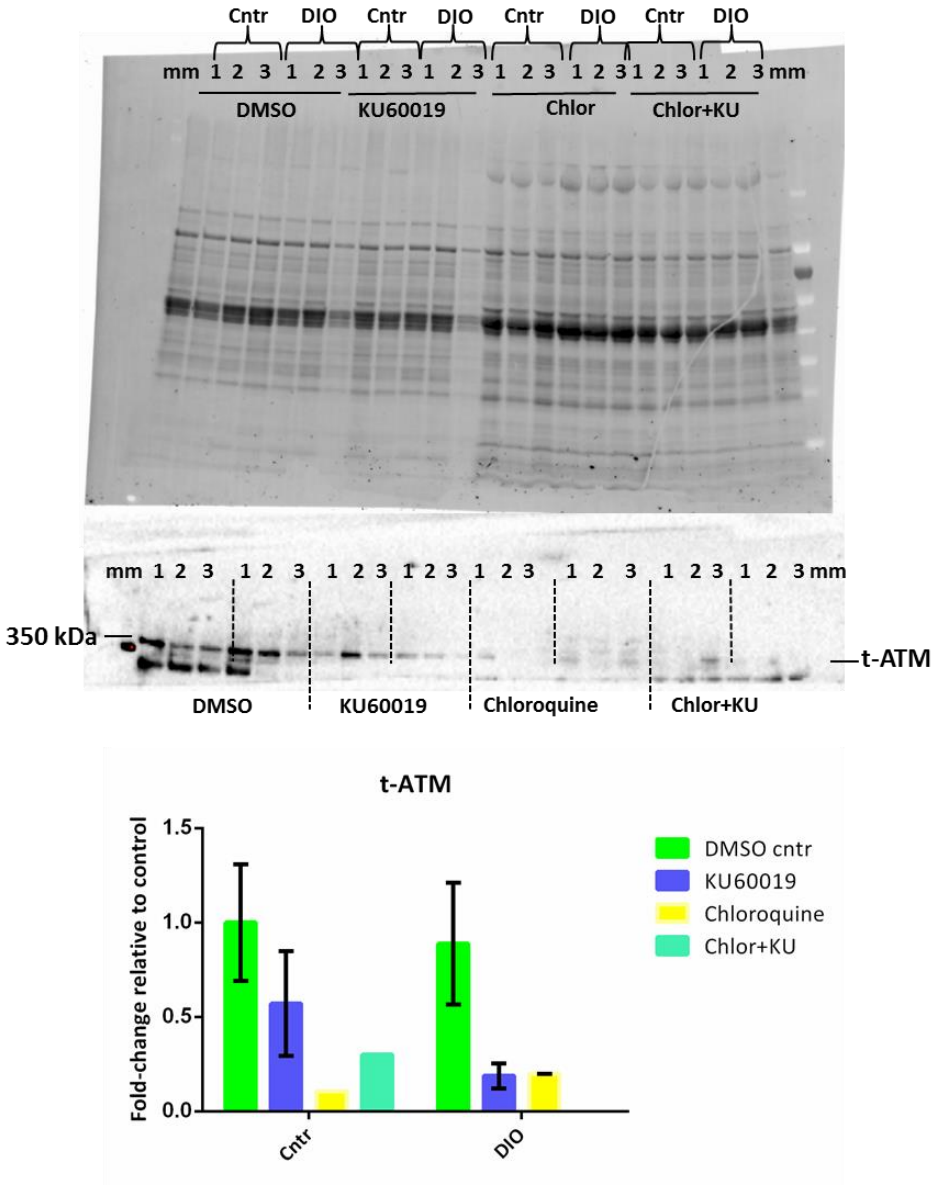

Figure 5.12: Chloroquine perfusion reduced the detectable levels of total ATM levels with western blotting, in both chow-fed and DIO cardiac mitochondria.

Total ATM was also detected in hearts perfused with chloroquine, and decreased when both chow-fed and DIO hearts were perfused with KU60019, although not significantly (Fig. 5.12). Again, no decrease was observed in the ATM levels of DIO heart mitochondria compared to that of chow-fed heart mitochondria. No phosphorylated ATM could be detected. This could again be indicative that ATM might not be phosphorylated at Ser^{1981} as it would be in response to DNA damage, but potentially rather activated in another manner such as phosphorylation at Cys^{2991} as discussed above.

It is however notable that the inhibition of ATM with KU60019 decreased its total levels in mitochondria from both chow-fed and DIO perfused hearts. Moreover, the inhibition of ATM influenced PINK, Parkin and TOM70 (Fig 5.13) and LC3-I/II levels (Fig 5.15), which indicates a role for ATM in mitophagy (Fig 5.13). Under normoxic circumstances PINK is imported into the mitochondria via TOM70 (translocase of outer membrane), and the TIM (translocase of the inner membrane) complex on the inner membrane. The N-terminal of PINK's mitochondrial targeting signal is removed, and the rest of the protein is then exposed to the cytosol, where it is rapidly degraded by the ubiquitin proteasome system (reviewed by Nguyen et al. (2016). Damaged mitochondria accumulate PINK on the OMM, where it is autophosphorylated when bound to the TOM-complex. This last step is required both for the activity of PINK as well as the recruitment of Parkin to the damaged mitochondria. Although no significant changes were observed for TOM70 (Fig 5.13) in mitochondria from DIO animals, treatment with KU60019 resulted in decreased TOM70 that can indicate that less PINK can be imported into the mitochondria and are consequently accumulate, thus driving Parkin-mediated autophagy. However, this is not the case for the combined insulin and KU60019 treatment, which could suggest that alternative pathways might be involved.

The present study demonstrated that PINK decreased in mitochondria from control chow-fed rat hearts perfused with insulin compared to DMSO-perfused mitochondria alone (Fig. 5.13; $p<0.0054$, 2-way ANOVA, Bonferroni post hoc test). This insulin-induced effect was not observed in cardiac mitochondria from DIO rats, which might be indicative that the rats were indeed insulin resistant and therefore had a reduced ability to respond to insulin. However, Parkin increased significantly in mitochondria from DMSO-perfused DIO hearts ($p<0.0005$, 2-way ANOVA) compared to the DMSO perfused chow-fed AMC hearts, and suggests a role for Parkin-mediated mitophagy in obesity A recent study found that a 100 nM insulin alone do not stimulate either the accumulation of PINK or the recruitment of Parkin in SHSY5Y cells, however when mitochondria become depolarised (with for example FCCP treatment), both PINK and Parkin are accumulated in response to insulin-stimulated Akt signalling (Soutar et al. 2018). Conversely, Kubli et al. (2015) found that Parkin can be recruited to depolarized mitochondria and activate mitophagy in the absence of PINK. It is also possible that insulin treatment resulted in increased ROS production, which would correlate with an increased oxidative phosphorylation rate, as was observed previously in

this study. Moreover, *in vitro* treatment with 100 nM insulin, as was used in this study, has previously been shown to significantly increase ROS production in 3T3-L1 adipocytes (Hoehn et al. 2009). A recent study also found that Parkin recruitment in response to ROS-mediated mitophagy is not dependent on increased PINK protein levels (Xiao et al. 2017).

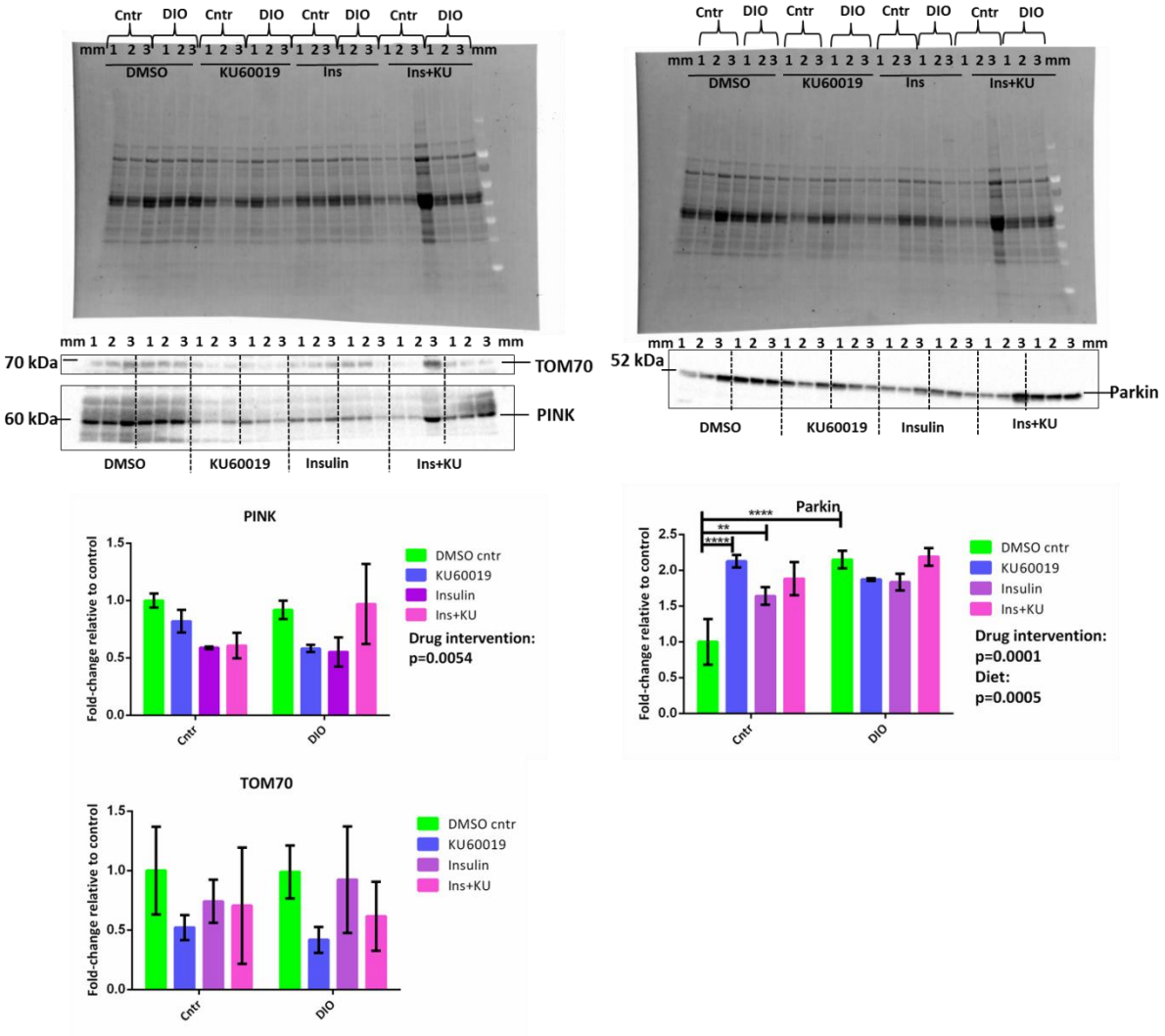

Figure 5.13: Western blot analysis of the mitophagy markers, PINK and Parkin in chow-fed and DIO cardiac mitochondria prepared from hearts perfused with DMSO, KU60019, insulin and a combination of insulin and KU60019. PINK and TOM 70 was probed on the same membrane (shown above, left) and normalised to total protein. Parkin was probed on and normalised to the membrane shown on the right. An n=3 was used per group, and bars represent the mean value ± s.d. * p<0.05, ** p<0.005, ****p<0.0005.

Briefly, insulin stimulates the accumulation of PINK and translocation of Parkin to depolarized mitochondria. Parkin can also be recruited to depolarized mitochondria in the absence of PINK. Moreover, Parkin can be recruited to mitochondria in response to ROS, independently of PINK.

KU60019 also significantly increased Parkin accumulation in mitochondria from chow-fed, perfused hearts ($p<0.0005$), which might again be associated with increased oxidative stress. Moreover, the effect of Parkin was significantly increased over all in response to the diet ($p=0.0005$) and with drug intervention ($p=0.0001$; 2-way ANOVA). In mitochondria from chow-fed AMC hearts, Parkin increased significantly ($p<0.0005$) when perfused with KU60019, compared to DMSO alone, as well as in insulin-perfused hearts ($p<0.005$) when compared to mitochondria from DMSO-perfused hearts.

The effects observed with regards to diet would be consistent with a model where obesity increases oxidative stress, which can, in turn result in increased mitophagy. It has indeed been shown that adiponectin, which is mainly produced by adipose tissue, can modulate mitophagy and suppress apoptosis in response to oxidative stress (Ren et al. 2017). Taken together, the inhibition of ATM seems to modulate mitophagy in a Parkin-dependent manner that is independent of PINK accumulation in chow-fed AMC and DIO hearts.

However, when autophagy is inhibited by chloroquine, which specifically targets the lysosomal degradation of autophagosomes, Parkin is significantly reduced in both the chow-fed and DIO heart perfused with KU60019 (Fig 5.14, $p<0.05$, 2-way ANOVA, Bonferroni post-hoc test). Previously a significant increase was observed in Parkin levels of KU60019-perfused chow-fed AMC hearts compared to DMSO perfused chow-fed AMC hearts as well as DMSO DIO perfused hearts. It would validate repeating the experiment to confirm whether Parkin is increased (Fig. 5.13) or decreased in response to KU60019 in *ex vivo* perfusions of chow-fed AMC hearts and DIO hearts (Fig 5.14). PINK protein levels changed significantly with KU60019, chloroquine and the combination of chloroquine and KU60019 treatment ($p<0.0005$, 2-way ANOVA, Bonferroni post-hoc test) in both mitochondria from chow-fed rats and DIO-rats.

Parkin was reduced in a similar fashion to PINK ($p<0.0001$, 2-way ANOVA, Bonferroni post-hoc test) in chow-fed AMC hearts perfused with chloroquine ($p<0.0005$, Bonferroni post-hoc test). Chow-fed AMC hearts perfused with a combination of chloroquine and KU60019 also presented with significantly decreased Parkin ($p<0.0005$, Bonferroni post-hoc test) when compared to chow-fed AMC hearts perfused with either DMSO or KU60019 alone. Parkin

levels were also significantly decreased in mitochondria from DIO hearts perfused with a combination of chloroquine and KU60019 ($p<0.005$) compared to KU60019 alone (Fig 5.14).

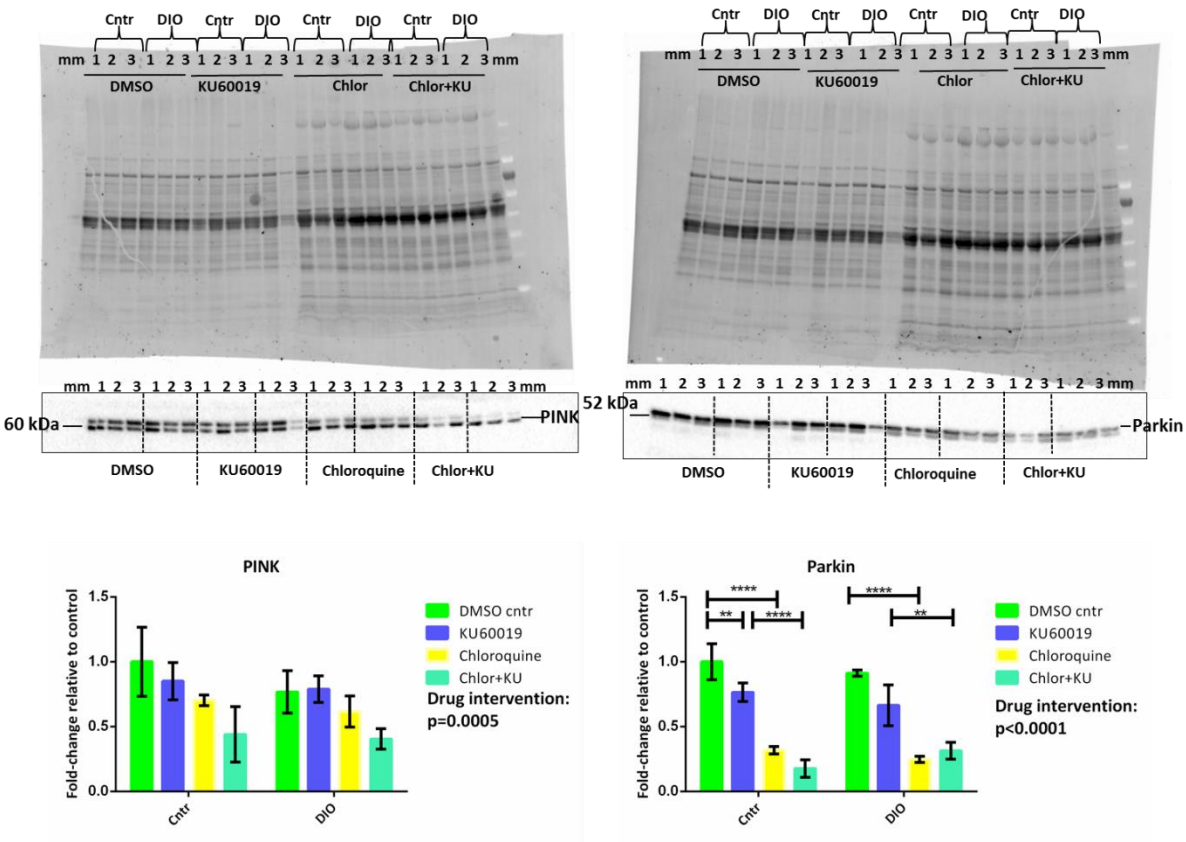

Figure 5.14: Western blot analysis of the mitophagy markers, PINK and Parkin in mitochondria from chow-fed and DIO hearts perfused with DMSO, KU60019, chloroquine and a combination of chloroquine and KU60019. Pink protein expression levels were normalised to the membrane shown on the left whilst Parkin protein expression levels were normalised to the membrane shown on the right. * $p<0.05$, ** $p<0.005$, ****$p<0.0005$.

This would suggest that chloroquine inhibits PINK/Parkin mitophagy, which could contribute towards mitochondrial dysfunction and the accumulation of damaged mitochondria. This is in line with the observation that chloroquine treatment in pressure overload hypertrophy impairs mitochondrial antioxidant capacity and increases oxidative stress (Chaanine et al. 2015). The question however remains what the underlying mechanisms for this would be. The combination of chloroquine and KU60019 significantly exacerbates the decrease in both PINK ($p<0.05$) in mitochondria from chow-fed animals and Parkin in both chow-fed ($p<0.0005$) and DIO animals ($p<0.005$, 2-way ANOVA, Bonferroni post-hoc test), and suggests that PINK/Parkin mitophagy is inhibited in this scenario.

A recent observation by Bartolomé et al. (2017) might shed light on this observation: the study observed that mTORCI regulation plays a synergistic role in mitophagy, where it is first required to initiate general autophagy but is also required for the selective targeting of PINK/Parkin mediated mitophagy in uncoupled mitochondria which is exacerbated in the presence of chloroquine. This was observed in $TSC2^{-/-}$ cells, which is a known target of ATM (Alexander et al. 2010). It is thus possible that the inhibition of ATM plays a similar role in cardiac mitophagy, leading to the upregulation of mTORC1 and consequent decreased PINK/Parkin localisation to damaged mitochondria that is further aggravated by the inhibition of lysosomal degradation.

It is possible that macroautophagy can also play a role in the selective clearance of mitochondria, with regards to ATM's cytosolic role as a positive regulator of autophagy (Stagni et al. 2018). The present study therefore evaluated LC3-I and II as well as p62 mitochondrial associated levels as markers of autophagy. Parkin recruitment to the OMM results in the ubiquitination of mitochondrial proteins that can recruit p62 to the mitochondria marked for mitophagy (Kroemer et al. 2010), and allows for interaction with the autophagosomal membrane (Yamano et al. 2016).

In line with the role of ATM in autophagy, a significant decrease ($p<0.0001$) was observed in LC3-II (autophagosome-bound) when mitochondria from chow-fed AMC hearts were perfused with a combination of insulin and KU60019 compared to mitochondria from hearts perfused with insulin alone (Fig 5.15; $p< 0.05$ 2-way ANOVA, Bonferroni post-hoc test). Interestingly, LC3-II was also significantly decreased in mitochondria from DIO hearts perfused with KU60019 ($p<0.005$, Bonferroni post-hoc test) compared to mitochondria from DIO hearts perfused with DMSO. LC3-I protein levels were difficult to detect, and this could potentially be ascribed to the fact the LC3-I is cytosolic until it is converted to its lipidated form on the autophagosomal membrane to LC3-II. The fractions analysed here were mitochondrial, and would thus concur with the expectation that LC3-I detection would be limited. Consequently, no significant differences were detected in either LC3-I or the LC3-II/I ratio. However, the decrease noted in the LC3-II levels indicate that there are decreased LC3-II bound autophagosomal membranes, and suggests a decrease in autophagy, which would concur with increased mTORC1 levels in the absence of ATM (Alexander et al. 2010). The effect observed here is thus potentially a consequence of the cytosolic role of ATM.

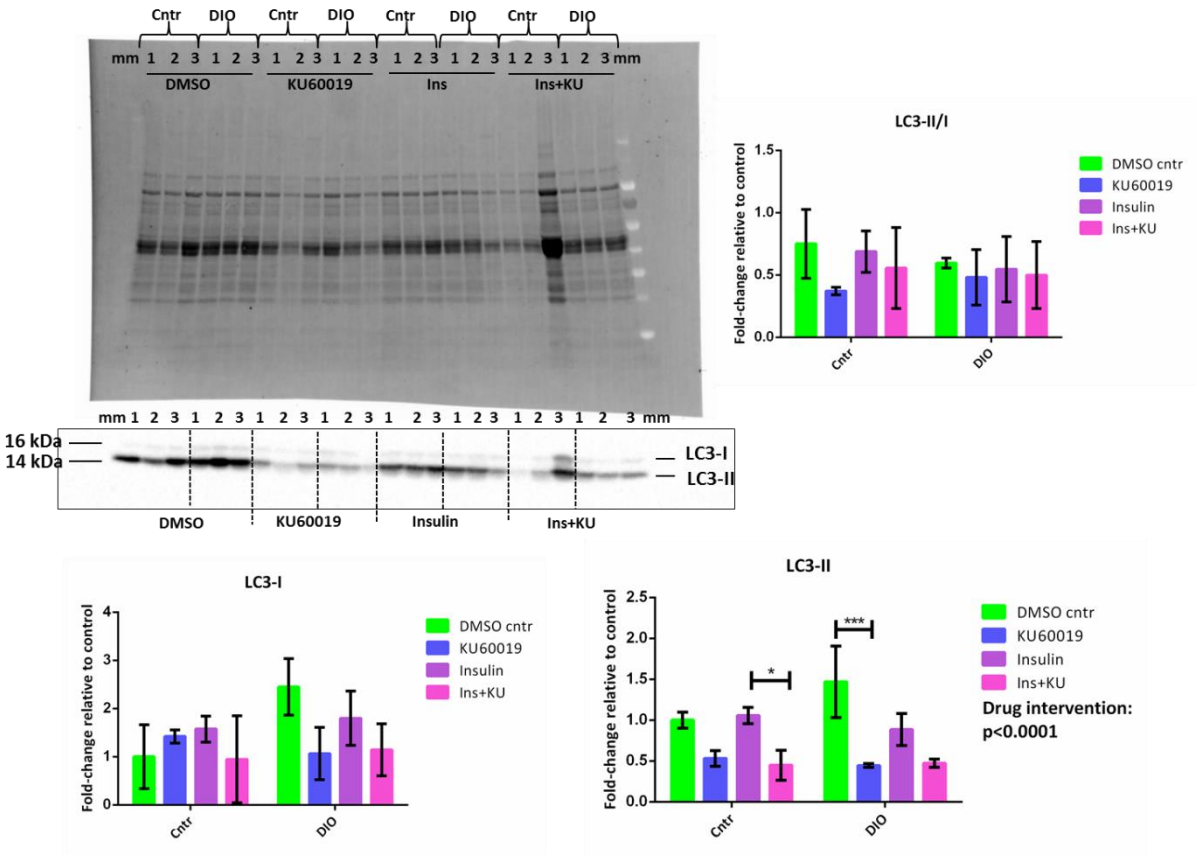

Figure 5.15: Western blot analysis of the autophagy markers, LC3 in mitochondria from chow-fed and DIO hearts perfused with DMSO, KU60019, insulin and a combination of insulin and KU60019. LC3-1 and LC3-II are both detected with the same probe and was normalised to the membrane shown. The normalised fold-change to control values was used to determine the ratio of LCII to LC3I. * p<0.05, ** p<0.005.

Likewise, the same effect was noted on LC3-II expression in mitochondria from both chow-fed AMC and DIO hearts perfused with KU60019, chloroquine and a combination of chloroquine and KU60019 when compared to mitochondria from DMSO perfused chow-fed AMC and DIO hearts. A significant increase in LC3-II levels were noted in mitochondria from chloroquine perfused chow-fed AMC hearts compared to mitochondria from DMSO perfused chow-fed AMC hearts ($p<0.005$, Bonferroni post-hoc test). However, LC3-II protein levels in mitochondria from KU60019 perfused chow-fed AMC hearts decreased significantly ($p<0.05$) compared to mitochondria from DMSO perfused chow-fed AMC hearts. Moreover, when chow-fed AMC hearts were perfused with a combination of chloroquine and KU60019, LC3-II levels decreased significantly to those seen in chow-fed AMC hearts perfused with chloroquine alone ($p<0.0005$, Bonferroni post-hoc test). This would suggest that the reduction in LC3-II levels in chow-fed AMC cardiac mitochondria is due to the inhibition of ATM. A similar reduction in LC3-II protein levels were seen in mitochondria

from DIO rat hearts perfused with KU60019 compared to mitochondria from DIO hearts perfused with DMSO ($p<0.05$). This reduction was again observed in mitochondria from DIO hearts perfused with a combination of chloroquine and KU60019, compared to LC3-II levels in mitochondria perfused with chloroquine alone ($p<0.0005$, Bonferroni post-hoc test). This supports the notion that the inhibition of ATM had the largest effect on LC3-II protein levels in both chow-fed AMC and DIO hearts.

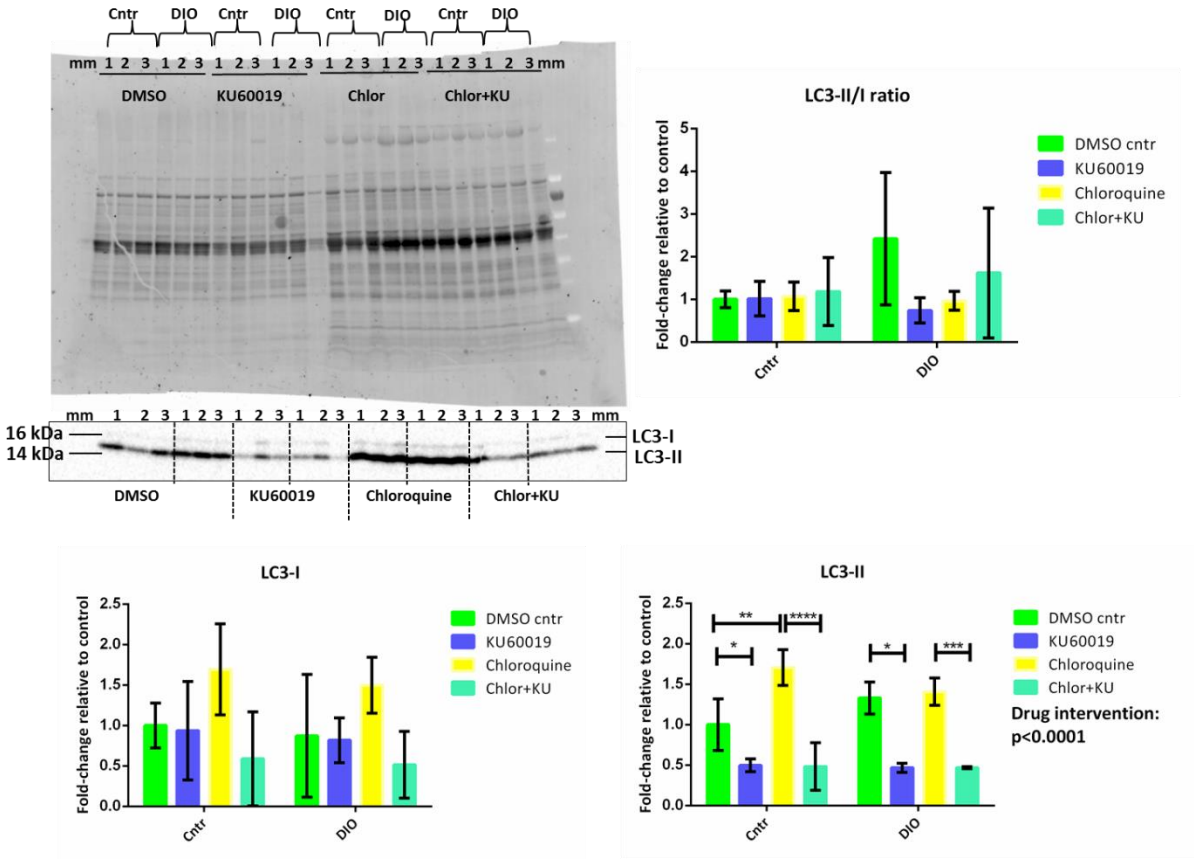

Figure 5.16: Western blot analysis of the autophagy markers, LC3 in mitochondria from AMC and DIO hearts perfused with DMSO, KU60019, chloroquine and a combination of chloroquine and KU60019. The probe for LC3 detects both LC3-I and LC3-II and was normalised to the membrane shown. The normalised fold-change to control values was used to determine the ration of LC3-II to LC3-I. * p<0.05, ** p<0.005, ****p<0.0005.

Taken together, these results suggest that the inhibition of cytosolic ATM rather than mitochondrial ATM interferes with the formation of an autophagosome, most probably through increased mTOR expression/activation (Alexander et al. 2010). The accumulation of LC3-II, which is well associated with chloroquine treatment, was significantly reduced in both chow fed AMC and DIO hearts treated with either a combination of insulin and

KU60019 or a combination of chloroquine and KU60019. This supports the hypothesis the inhibition of ATM contributes to a significant reduction of LC3-II levels.

Lastly, this study investigated the selective autophagy marker p62, the mitochondrial fission protein, DrpI and the mitochondrial uncoupling protein, UCP3.

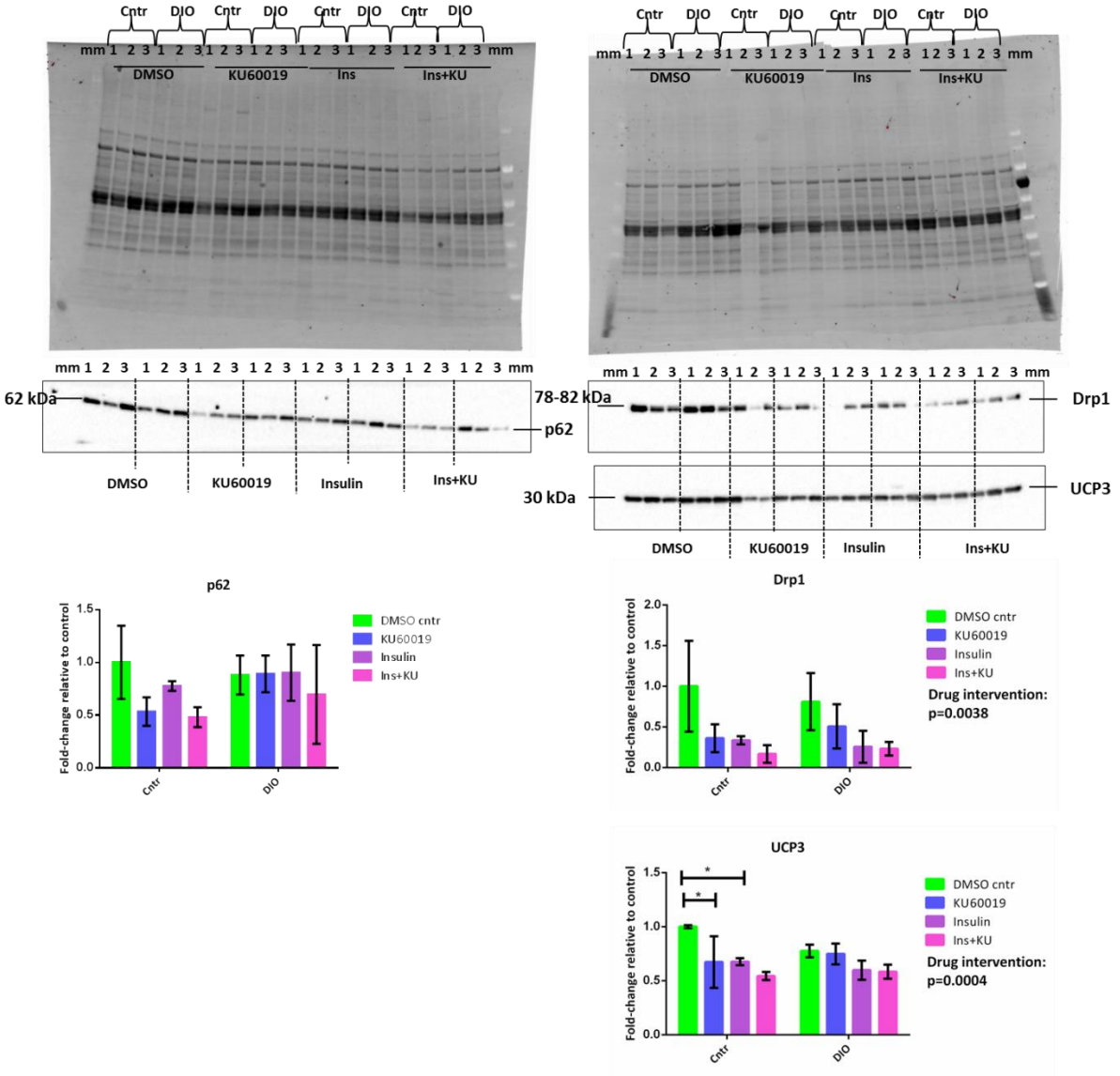

Figure 5.17: Western blot analysis of p62, Drp1 and UCP3 in mitochondria from chow-fed and DIO hearts perfused with DMSO, KU60019, insulin or a combination of insulin and KU60019. The autophagy marker, p62 was probed on and normalised to the membrane on the left, and Drp1 as well as UCP3 were probed on and normalised to the same membrane shown on the right hand side. An n=3 was used per group, and bars represent the mean value ± s.d. * p<0.05.

The selective autophagy marker, p62, is recruited to damaged mitochondria in response to ubiquitination of OMM proteins by Parkin, where it binds to the ubiquitin chain and interacts with LC3-II on the autophagosomal membrane. It is thus not surprising that a

similar decrease was noted in p62 protein levels to that seen in LC3-II (Fig 5.15), where chow-fed AMC hearts were perfused with either KU60019 or a combination of insulin and KU60019. No change were observed for p62 in obesity which corresponds to the lack of differences observed in Parkin levels overall in obesity. The role of p62 in the context of obesity will require further investigation, but these results indicate that KU60019 had a similar effect on p62 levels in mitochondria from chow-fed AMC hearts but not DIO hearts. This would suggest that it is not influenced by the negative feedback of ATM on mTORC1, or that an alternative mitophagy pathway is at play. Interestingly, it has been observed that p62 is required for the clustering of damaged mitochondria, but is dispensable in Parkin mediated mitophagy (Narendra et al. 2010).

BNIP3 mediated mitophagy, for example, entails Drp1 facilitated fission and Parkin recruitment in cardiac myocytes, where BNIP3 promotes the translocation of Parkin and Drp1 fission is correlated with increased autophagy (Lee et al. 2011). The current study showed both KU60019 and insulin as well as a combination of insulin and KU60010 had a significant effect (decrease) overall in Drp1 protien levels ($p<0.0038$) irrespective of diet. Interestingly, this correlated with a decrease in PINK levels with the exception of an increase in PINK levels when hearts were perfused with a combination of insulin and KU60019. In PINK deficient cells, increased oxidative stress as well as mitochondrial turnover is observed, which is mediated by an increase in fission (Dagda et al. 2009). What is of note though is that hyperglycaemia facilitates mitochondrial fission through Drp1, which was not observed in our DIO model, and concurs with the lack of difference observed in the non-fasting blood glucose levels of the chow-fed and DIO animals used in this study. Furthermore, insulin is known to stimulate mitochondrial fusion via Akt-mTOR-NFκB-Opa1 signalling pathway in cardiomyocytes (Parra et al. 2014). The decrease that is observed in fission (Drp1) in chow-fed and DIO hearts perfused with insulin or a combination of insulin and KU60019 thus agrees with the study by Parra et al. (2014). In the study by Valentin-Vega et al. (2012), enlarged mitochondria with a swollen appearance was noted in $ATM^{-/-}$ thymocytes, and agrees with the present study's observation that Drp1 is down-regulated in response to KU60019 perfusion in both chow-fed and DIO hearts.

Lastly, both KU60019 and insulin perfusion decreased UCP3 expression, in chow-fed but not DIO perfused hearts. Overall, drug treatement significantly decreased UCP3 expression

($p<0.0004$), whereas KU60019 perfusion significantly decreased UCP3 levels compared to chow-fed hearts ($p<0.05$) similar to the effect of insulin ($p<0.05$). No differences were noted in obesity. Likewise, Boudina et al. (2007), did not observe increased levels of UCP 3 in *db/db* mice, although they did observe increased uncoupled respiration and proton leak. This study did not observe any increase in UCP3 that can explain the increase observed in State 4 respiration in insulin perfused hearts in PCM substrate (Fig 5.7), but does not preclude the possibility of fatty acid induced uncoupling.

In conclusion, the perfusion of chow-fed and DIO hearts with KU60019 resulted in a reduction in State 3 respiration, which translated into decreased ATP synthesis, and was overall, associated with decreased total ATM levels, as well as a decrease in the autophagy markers, LC3-II and p62, decreased fission and interestingly, decreased uncoupling in chow-fed hearts. This corroborates with previous literature reporting decreased mitochondrial respiration (Ambrose et al. 2007) and ATP synthesis in the absence of ATM (Valentin-Vega et al. 2012). Although the underlying mechanisms regarding mitophagy could not be fully elucidated in this study, the results indicate that this might be due to inefficient PINK/Parkin mitophagy, although there are indications of PINK independent Parkin mitophagy. This phenotype could not be rescued with the addition of insulin to KU60019 in either chow-fed or obese hearts, although it did improve many of the parameters such as ATP synthesis.

Chapter 6 : Mitochondrial NAD+/NADH redox state and the use of fluorescent life-time imaging microscopy (FLIM)

The redox state is the key regulator of energy production and intermediary cellular metabolism, and is crucial in health and metabolic disease (Forrester et al. 2018). The redox pairs NAD^+/NADH reflects the balance of the TCA cycle to ETC activity and can result in the production of ROS in the event of TCA dysfunction, whilst the $NADP^+$/NADPH pool mediates the antioxidant defence (Blacker et al. 2014). NAD^+ is an essential co-factor that is central to ATP production via the oxidation of its reduced form, NADH, in mitochondria, whilst the cellular $NADP^+$/NADPH ratio governs lipid, amino acid and nucleotide synthesis in various metabolic pathways (Srivastava 2016). Under highly aerobic conditions, electrons are shuttled from cytosolic NADH to the mitochondria via glycerol-3-phosphate and the malate-aspartate shuttle, where it is oxidized by Complex I to NAD^+, and leads to the majority of ATP production via oxidative phosphorylation (Yu & Heikal 2009)(Fig 2.6).

On the other hand, $NADP^+$ is reduced to NADPH mainly through the oxidative branch of the PPP in the cytosol, and maintains the intracellular redox state through the synergistic action (Fig 2.4) of the antioxidant enzymes and thiol-containing antioxidants, such as glutathione (GSH) and thioredoxin (TRX) that require both ATP and NADPH for their regeneration (Cardaci et al. 2012). The role of ATM in the PPP and glycolysis have already been discussed (Chapter 2, Section 2.3.4; Zhang et al. 2018; Cosentino et al. 2011), as well as the observed reduction of NAD^+, NADH and $NADP^+$ in the cerebellum of $ATM^{-/-}$ mice (Stern et al. 2002). Replenishment of NAD^+ improved the lifespan of $ATM^{-/-}$ mice and worms (*C. elegans*), and ameliorated A-T phenotypes in mice through the upregulation of mitophagy and DNA repair (Fang et al. 2016). An increase in the NAD^+/NADH ratio, possibly through fasting, exercise or redox stress have also been linked with increased mitochondrial biogenesis through the deacetylation of PGC1α by activated Sirtuin 1 (SIRT1, Andres et al. 2015). An extensive review by Cheng et al. (2017) suggests that insulin signalling maintains the NAD^+/NADH ratio; it acts as a mediator for the PGC1α/SIRT1 pathway by maintaining the ETC and suppressing of FOXO1/HMOX1. This supports the hypothesis set forth by Valentin-Vega et al. (2012) which suggests that the accumulation of mitochondria in the absence of ATM could be due to ineffective mitophagy rather than increased biogenesis. A disruption in

insulin signalling as well as a decrease in the NAD^+/NADH redox pairs in $ATM^{-/-}$ (Stern et al. 2002; Fang et al. 2016) will decrease biogenesis rather than increase it. There is thus value in being able to quantify the ratio of NAD^+/NADH and $NADP^+$/NADPH. The redox pair ratios can give insight into the metabolic state of a cell as well as its oxidative and redox state. Understanding the metabolic and redox state of cells under pathological conditions can offer potential therapeutic value when replenished as demonstrated by Fang et al. (2016).

Lastly, the inhibition of ATM also decrease Cytochrome C oxidase (COX, or complex IV) activity in permeabilised muscle tissue in a post-transcriptional manner (within an hour of KU55933 treatment), and is correlated with a decrease in G6PD, which suggests a shift towards glycolysis (Patel et al. 2011). ATM promotes glucose flux through the PPP by increasing both the abundance as well as activity of G6PD, consequently increasing NADPH production which is required for the anti-oxidant response in cells (Zhang et al. 2018). Moreover, the inhibition of COX increases ROS production and electron leak at Complex I or III by reducing the redox centres of these complexes (Chen et al. 2003). A reduction in the redox centre of Complex I should thus lead to decreased NADH oxidation if ATM inhibition impacts complex I.

6.1 Two-photon FLIM microscopy:

In 1979, Chance et al. (1979) showed that NADH, primarily of mitochondrial origin, can be illuminated with ultraviolet light. The nicotinamide moiety of NADH absorbs light at 340 ± 30 nm and emits fluorescence at 460 ± 50 nm (Blacker & Duchen 2016), and because NADP is phosphorylated at a distant site within the molecule, the fluorescence properties of the nicotinamide ring of NADPH are identical to those of NADH (Figure 6.1; Blacker et al. 2014). Changes in autofluorescence intensity can thus reflect changes in either NADH or NADPH, and are collectively referred to as NAD(P)H due to the uncertain origin of the fluorescence (Duchen et al. 2003). The intrinsic fluorescence of these molecules have been used for label-free monitoring of *in vitro* and *in vivo* metabolic states (Mayevsky & Barbiro-Michaely 2009), and have improved significantly with the advent of time-resolved fluorescence measurements that allows the determination of autofluorescence lifetime in response to changes in the redox state (Blacker & Duchen 2016).

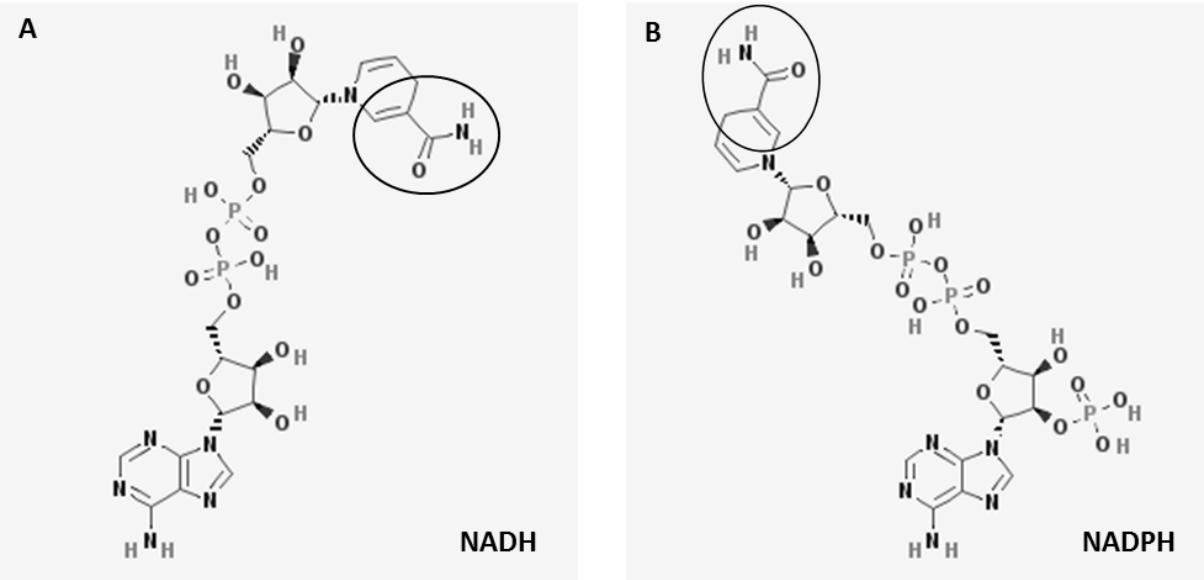

Figure 6.1: Schematic representation of NADH and NADPH. Panel A represents the molecular structure of NADH {(National Center for Biotechnology Information. PubChem Compound Database; CID=439153, https://pubchem.ncbi.nlm.nih.gov/compound/439153 (accessed Sept. 13, 2018)} and the circle surrounds the nicotinamide moiety of NADH that absorbs light at 340 ± 30 nm whereas panel B represents NADPH that also absorbs light at the nicotamide moiety (in circle) that is identical to that of NADH.

Fluorescence lifetime imaging microscopy (FLIM) can measure the rates of fluorescence decay of NAD(P)H. This means that when the NAD(P)H moiety absorbs light at 340 ± 30 nm, the fluorophores are excited from their ground state into an excited state. On average, the time for the decay from this excited state to the ground state occurs on a nanosecond timescale, with the accompanying emission of a fluorescence photon. The timespan between the emission of these fluorescence photons and their excitation can be measured accurately with time-correlated single photon counting (TCSPC). This provides a measurement of the excited state lifetime of an ensemble of fluorophores, and is highly sensitive to the immediate environment of the fluorophore (Blacker et al. 2014). The use of multiphoton FLIM (such as two-photon FLIM; 2P-FLIM) rather than single-photon FLIM at near-infrared excitation, allows for greater penetration depths and resolution as well as improved tissue viability compared to single-photon excitation (Skala et al. 2007a). Multiphoton FLIM has been widely used to monitor energy metabolism in human breast cancer cells (Bird et al. 2005; Yu & Heikal 2009), precancerous epithelial cells (Skala et al. 2007b), isolated mitochondria, hepatocytes and rat liver *in situ* (Wakita et al. 1995) as well as in cardiomyocytes (Huang et al. 2002) to name but a few.

The fluorescence decay lifetime of NADPH and NADH is identical in solution, and thus the fluorescence from free unbound pyridine nucleotides cannot be discriminated on the basis of their fluorescence lifetime (Blacker et al. 2013). However, the fluorescence decay lifetime can increase from 0.3 ns – 0.8 ns and from 1 - 6.5 ns when bound to an enzyme, dependent on the target to which the cofactor binds (Vishwasrao et al. 2005) as well as the simultaneous presence of a substrate molecule (Gafni & Brand 1976). Consequently, FLIM imaging can resolve two fluorescence lifetimes at each pixel, respectively at approximately 0.4 ns and more variably at 2 ns (Skala et al. 2007a), which represent the freely diffusing (τ_{free}) and enzyme-bound NAD(P)H (τ_{bound}) pools (Blacker et al. 2014) respectively. On average, the lifetime decay of free (τ_1) NAD(P)H is considerably shorter than that of bound (τ_2), and it is thus possible to quantify the relative fractions of free (α_1) and bound (α_2) NAD(P)H in a cell (Lakowicz et al. 1992). The enzyme-bound NAD(P)H pool is the parameter that varies most with changes in metabolism (Skala et al. 2007) and glucose homeostasis (Sharick et al. 2018). Moreover, it has been suggested that the enzyme-bound pool of NADH mainly localises in the mitochondria, whilst the free NAD(P)H pool is localised to the cytosol (Bird et al. 2005; Wakita et al. 1995)

The varying effects of the [NADPH]/[NADH] ratio on τ_{bound} have been quantified in a HEK293 cell model in the absence and overexpression of NAD^+ kinase (NADK), which is the key determinant of NADPH concentration in the cell (Blacker et al. 2014). Briefly, the authors found that the measured τ_{bound} lifetime reflects the proportion of the two co-factors present, and that an increase in NADPH will reflect an increase in τ_{bound} values. Inhibition of NADPH specifically, which does not interfere with NADH, significantly reduced τ_{bound} values but did not influence τ_{bound} values in either the absence of NADK or τ_{free} values. This is consistent with a model where, when combining the enzyme-bound τ_{bound} NAD(P)H values in both the $NADK^+$ and $NADK^-$ HEK293 cells, as well as the biochemically quantified [NADH] and [NADPH] concentration values in HEK293 cells (Pollak et al. 2007), the relative contribution of NADPH and NADH fluorescence decay to NAD(P)H enzyme-bound ratio can be defined as (Blacker et al. 2014; Supplementary material) :

$$\frac{[\mathrm{NADPH}]}{[\mathrm{NADH}]} = \frac{(\tau\mathrm{bound(ns)} - 1.5)}{4.4 - \tau\mathrm{bound(ns)}}$$

Changes in the τ_{bound} lifetime values have been used to describe the shift from oxidative phosphorylation to glycolysis in cancer cells (Skala et al. 2007b), and chemical manipulation of HEK293 cells yielded similar results (Blacker et al. 2014). Inhibition of the ETC with rotenone (Complex I inhibitor) significantly decrease τ_{bound} lifetime values (ns) in both the cytosol and mitochondria, which suggests a relative increase in NADH, whereas uncoupling with FCCP did not change the τ_{bound} lifetime values and suggests equal oxidation of NAD^+ and NADH by the mitochondrial nicotinamide nucleotide transhydrogenase (Nnt). It is believed that the reversal of the Nnt, which is responsible for the production of NADPH in mitochondria, is responsible for ROS production in heart failure through the production of NADH for ATP production at the cost of NADPH-linked anti-oxidative function (Nickel et al. 2015). Taken together, variation in τ_{bound} lifetime values seems to be specific to the type of metabolic disruption, such as mitochondrial dysfunction at Complex I (Blacker et al. 2014), or the utilization of different substrates following inhibition of glycolysis. Fluorescence lifetime of protein-bound NAD(P)H is also the most sensitive parameter to detect the diversion of carbon away from the TCA cycle to the PPP via G6PD, lactate production via LDH, as well as inhibition of carbon entry into the TCA cycle via pyruvate dehydrogenase kinase (PDK) by pyruvate dehydrogenase (PDH; Sharick et al. 2018).

This study utilised 2P-FLIM to determine whether the inhibition of ATM with KU60019 can influence the fluorescence life-time decay of NAD(P)H or any of its associated parameters in the rat cardiomyoblast cell line, H9c2 and confirmed this as well as the relative contribution of [NADPH]/[NADH] to NAD(P)H τ_{bound} in HEK293 cells.

6.1 Materials and Methods:

These experiments were performed personally at the Rutherford Appleton Laboratory, Science and Technology Facility Council, Oxfordshire, UK under the supervision of Prof SW Botchway and Prof AW Parker. The purpose of this study was to determine the NAD(P)H lifetime decay in the presence and absence of the ATM inhibitor, KU60019 in an undifferentiated H9c2 model, and confirm this in HEK293 cells, as well as calculate the relative contribution of [NADPH]/[NADH] to the τ_{bound} value of NAD(P)H.

6.1.1 Reagents:

The H9c2 cardiomyoblast cells were purchased from American Type Culture Collection (ATCC) at passage 14 and were maintained between passage 16 and 18 for experiments. Dulbecco's Modified medium (DMEM, Gibco) was supplemented with 4.5g glucose/l and 4 mM L-glutamine, fetal bovine serum (FBS) and penicillin-streptomycin. The SPCImage software was kindly made available by Becker and Hickel on a trail licence.

6.1.2 Cell culture:

H9c2 (2-1) cells were obtained from ATCC® (CRL-1446™, passage 14) and maintained in DMEM (GIbco) with 4 mM L-Glutamine, 4.5 g/L glucose, 10% FBS and 1% penicillin/streptomycin at 37°C and 5% CO_2. Cells were seeded at a concentration of $2.4x10^4$ cells/ml on 35 mm MaTIK plates 48 hours prior to treatment, and treated with either DMSO (0.05%, n=3) or 3 µM KU60019 (n=3), 3-6 hours prior to imaging. HEK293 were obtained from ATCC, and cells were maintained in MEM (Gibco) and supplemented with 10% FBS, 1 % pen/strep and 2 mM L-Glutamine. Cells were seeded at a concentration of 1.5 X 10^5 cells/ml on 35 mm MaTIK plates 48 hours prior to treatment, and treated with either DMSO (0.05%, n=1) or 3 µM KU60019 (n=1), 3-6 hours prior to imaging.

6.1.3 Fluorescence lifetime imaging microscopy:

Fluorescence intensity and lifetime images were acquired using a custom-built multiphoton fluorescence lifetime system around a modified inverted microscope (TiE, Nikon). Samples were imaged using a 60× , NA 1.2 water-immersion objective (Stubbs et al. 2005; Botchway et al. 2015). Multiphoton excitation was generated from a titanium: sapphire laser, tuned to 760 nm, operating at 76 MHz with 200 fs pulse width (Coherent, USA). A BG39 filter was used to block the near infra-red light before non-descan detection using a hybrid detector, HPM-100 (Becker and Hickl, GmbH). A pixel dwell time of 5.04 µs was used for 256 × 256 pixel images over a 212 µm × 212 µm field of view. TCSPC electronics (SPC 830, Becker & Hickl, Berlin, Germany) were used to acquire fluorescence decay curves with 256 time bins. Following a 3X3 binning of photons and a threshold of 25, two-component fluorescence decay curves were used to fit the decay curves for FLIM images using iterative reconvolution

in SPCImage (Version 7.1, Becker and Hickl) (Blacker et al. 2014). NAD(P)H fluorescence lifetime parameters were obtained from the FLIM data and reported as an average of 10 pixels over at least three to five regions of three separate cultures imaged on different days.

6.1.4 Statistical analysis:

The data were analysed using GraphPad Prism 6.0 software (GraphPad Software, Inc., La Jolla, CA). Statistical comparisons were made using a two-tailed Student's t-test or 2-way analysis of variance (ANOVA) followed by a Bonferroni post-hoc test where applicable. All values and error bars are presented as mean ± s.d, and the level of significance was set at $p < 0.05$.

6.2 Results and discussion:

In light of the finding that ATM is located on the inner mitochondrial membrane of cardiac mitochondria (Chapter 4), and that the inhibition thereof significantly decreases the Complex I mediated oxidative phosphorylation rate in a glutamate/malate buffer (Chapter 5), this study hypothesised that a reduction in the redox centre of Complex I should lead to decreased NADH oxidation if ATM inhibition impacts complex I. This suggestion is based on previous studies that showed that the inhibition of ATM decrease ETC COX-IV (Patel et al. 2011) and that the absence of ATM decreases Complex I in $ATM^{-/-}$ thymocytes (Valentin-Vega et al. 2012). Moreover, the inhibition of COX increases ROS production and electron leak at Complex I or III by reducing the redox centres of these complexes (Chen et al. 2003).

To test this hypothesis, this study utilised two-photon fluorescence lifetime imaging microscopy (2P-FLIM) which is sensitive to microenvironment changes at the molecular level and can distinguish between free ($\tau1$) and enzyme-bound NAD(P)H ($\tau2$) based on fluorescence lifetime (where $\tau1 > \tau2$), making it a useful tool for probing metabolism in living cells (Sharick et al. 2018). Reduced NADH, and its phosphorylated form, NADPH are autofluorescent electron donors with an identical fluorescent spectra, and is referred to as NAD(P)H due to the uncertain origin of the signal (Blacker et al. 2014). Changes in the lifetime of NAD(P)H are determined by fitting an exponential function to the observed time-resolved fluorescence decay, and have been used to distinguish between mitochondrial

protein localisation (Söhnel et al. 2016; Yadav et al. 2013), redox ratio (Bird et al. 2005; Chakraborty et al. 2016), and glucose carbon diversion (Sharick et al. 2018). It has been suggested that the protein-bound form of NADH localizes mainly within the mitochondria whilst free NADH is primarily located within the cytosol (Bird et al. 2005; Wakita et al. 1995). We observed a bound lifetime (τ-$_{bound}$) of 2.76 ± 0.26 ns (Fig 6.2) in H9c2 myoblasts, in agreement with previously reported mean values (± s.d.) of 2.8 ± 0.2 ns in isolated liver mitochondria (Wakita et al. 1995), 2.7 ± 0.2 ns in HEK293 cells (Blacker et al. 2014), and 2.5 ns in isolated mice cardiomyocytes (Blacker & Duchen 2016), whilst inhibition with KU60019 resulted in a significant reduction of NAD(P)H fluorescence lifetime decay to 2.57 ± 0.14 ns (Fig 6.2).

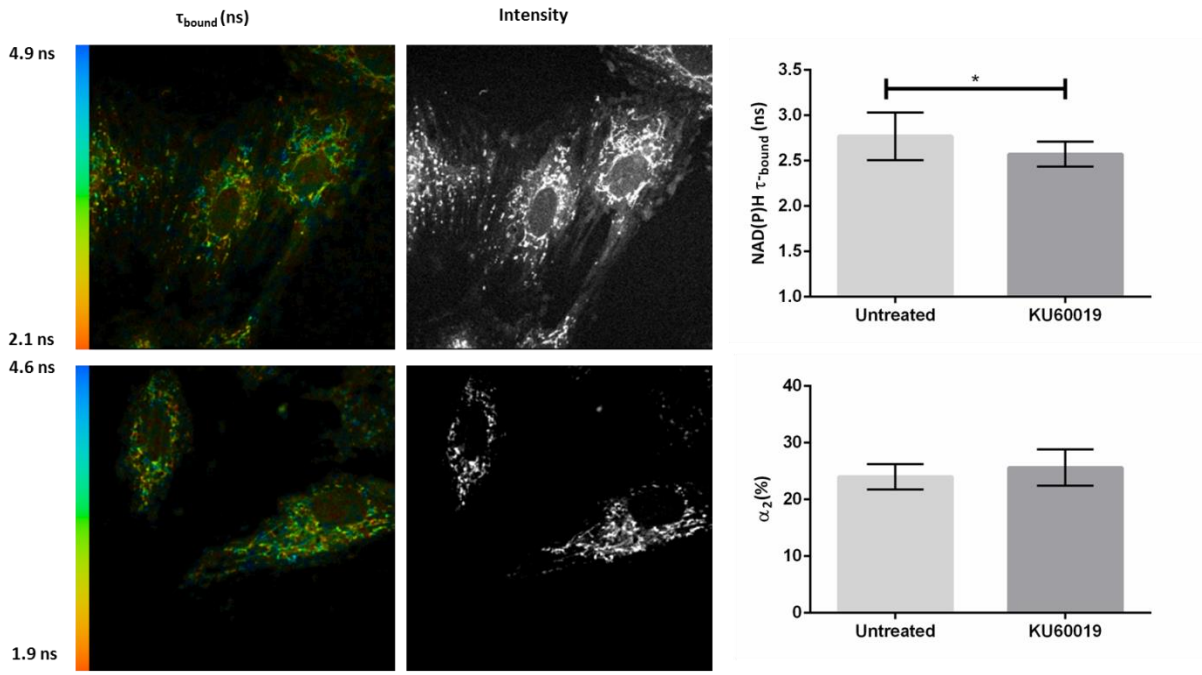

Figure 6.2: Inhibition of ATM decrease NAD(P)H fluorescence decay. Representative fluorescence decay images of H9c2 cells treated with DMSO (vehicle control; top; n=3) or KU60019 (3 µM; n=3), which decreased NAD(P)H τ-bound lifetime (ns) significantly (p=0.02, Student's t-test, mean ± s.d.), but did not influence α-bound values (fraction of bound NAD(P)H). Error bars are presented as mean ± standard deviation.

Inhibition of ETC respiration in cardiomyocytes with cyanide resulted in a similar significant decrease in NAD(P)H lifetime and caused an accumulation of NADH, which suggests that the NADPH/NADH balance defines the enzyme bound NAD(P)H lifetime(Blacker & Duchen 2016). Inhibition of Complex I with rotenone in HEK293 cells resulted in a significant decrease of τ-$_{bound}$ from 2.7 ± 0.2 ns to 2.52 ± 0.05 ns in both the cytosol and mitochondria

of the cells, and suggests that the inhibition of Complex I, and thus inhibition of NADH oxidation, can increase the concentration of NADH present in the cell relative to the NADPH concentration (Blacker et al. 2014).

The relative fraction of free (α1) NAD(P)H decreased in H9c2 cells when treated with KU60019 (74.38±3.202) compared to control cells (76.00±2.259, Fig 6.3), whereas the relative fraction of bound (α_2) NAD(P)H increased (control: 24.00±2.26; KU60019: 25.62±3.202; Fig 6.3), but these changes were negligible. The ratio of free and protein bound NAD(P)H (α_1/α_2) decreased, albeit not significantly (p=0.2, Fig. 6.3). No differences were observed in the autofluorescence lifetime decay of freely diffusing NAD(P)H (τ_{free}; ns) between untreated and KU60019 treated H9c2 cells. This is consistent with the suggestion that enzyme-bound NAD(P)H variation in τ_{bound} lifetime values seem to be specific to the type of metabolic disruption, such as mitochondrial dysfunction at Complex I (Blacker et al. 2014), or the utilization of different substrates following inhibition of glycolysis (Sharick et al. 2018).

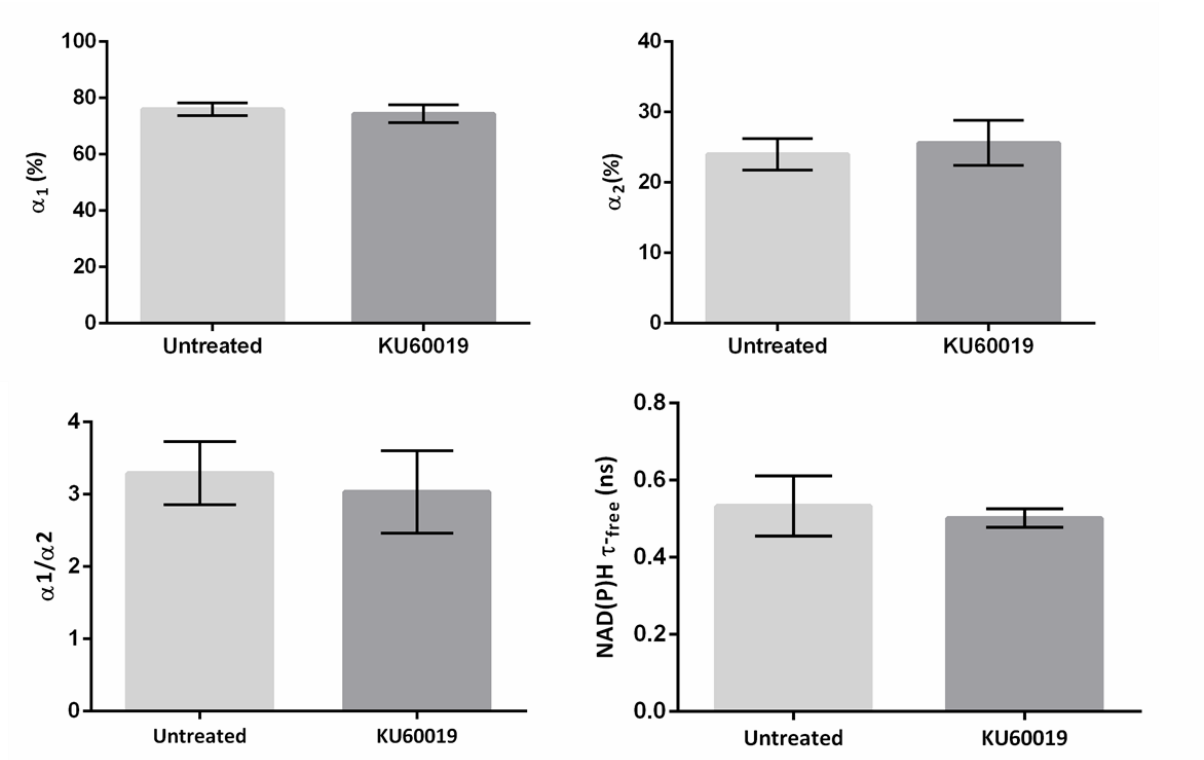

Figure 6.3 : The relative fractions of free and bound NAD(P)H in H9c2 cells (n=3). The relative fractions of free (α1) and bound (α2) NAD(P)H did not change significantly, nor did the ratio of free to bound NADPH between control (n=3) and KU-treated cell cultures (n=3). The autofluorescence lifetime of τ_{free} decreased, albeit not significantly (p=0.1634). Stastical differences were

determined with a Student's t-test (two-tailed) and error bars are presented as mean ± standard deviation.

A single experiment was performed in HEK293 cells with 0.03% DMSO (control) and compared to HEK293 cells treated with 3 µM KU60019 to determine if a similar trend is observed (Fig 6.4). A significant decrease was observed in the τ-$_{bound}$ NAD(P)H values for KU60019 treated HEK239 cells (2.663 ±0.1090 ns) compared to the control treated cells (2.990 ± 0.1122 ns; p= 0.0031) . These values are higher than was reported by Blacker et al. (2014) but could merely be a reflection of the small sample size number as well as the combined analysis of the cytosolic and mitochondrial compartments in this study. However, similarly to the H9c2 cells, a significant reduction was observed in τ-$_{bound}$ NAD(P)H lifetime mean values (ns). The relative fractions of τ-$_{bound}$ NAD(P)H and τ-$_{free}$ NAD(P)H measured as α1(%) and α2(%) did not differ (Fig 6.4), which is similar to the observations made in H9c2 cells (Fig 6.2 and Fig 6.3). Interestingly, the τ-$_{free}$ NAD(P)H lifetime decreases significantly (p=0.0474) in HEK293 cells but not in H9c2 cells, but this could again potentially be a sample size effect.

When using the equation described by Blacker et al. (2014) and discussed previously, with the biochemically quantified [NADH] and [NADPH] concentration values in HEK293 cells (Pollak et al. 2007), a significant decrease (p=0.0351) is observed in the [NADPH]/[NADH] ratio in KU60019 treated cells (0.7043 ± 0.1122) compared to DMSO-treated HEK293 cells (1.411 ± 0.5257) and suggest that the decrease observed in the τ-$_{bound}$ NAD(P)H fluorescence lifetime decay is driven by an increase in the [NADH] concentration (Fig 6.4).

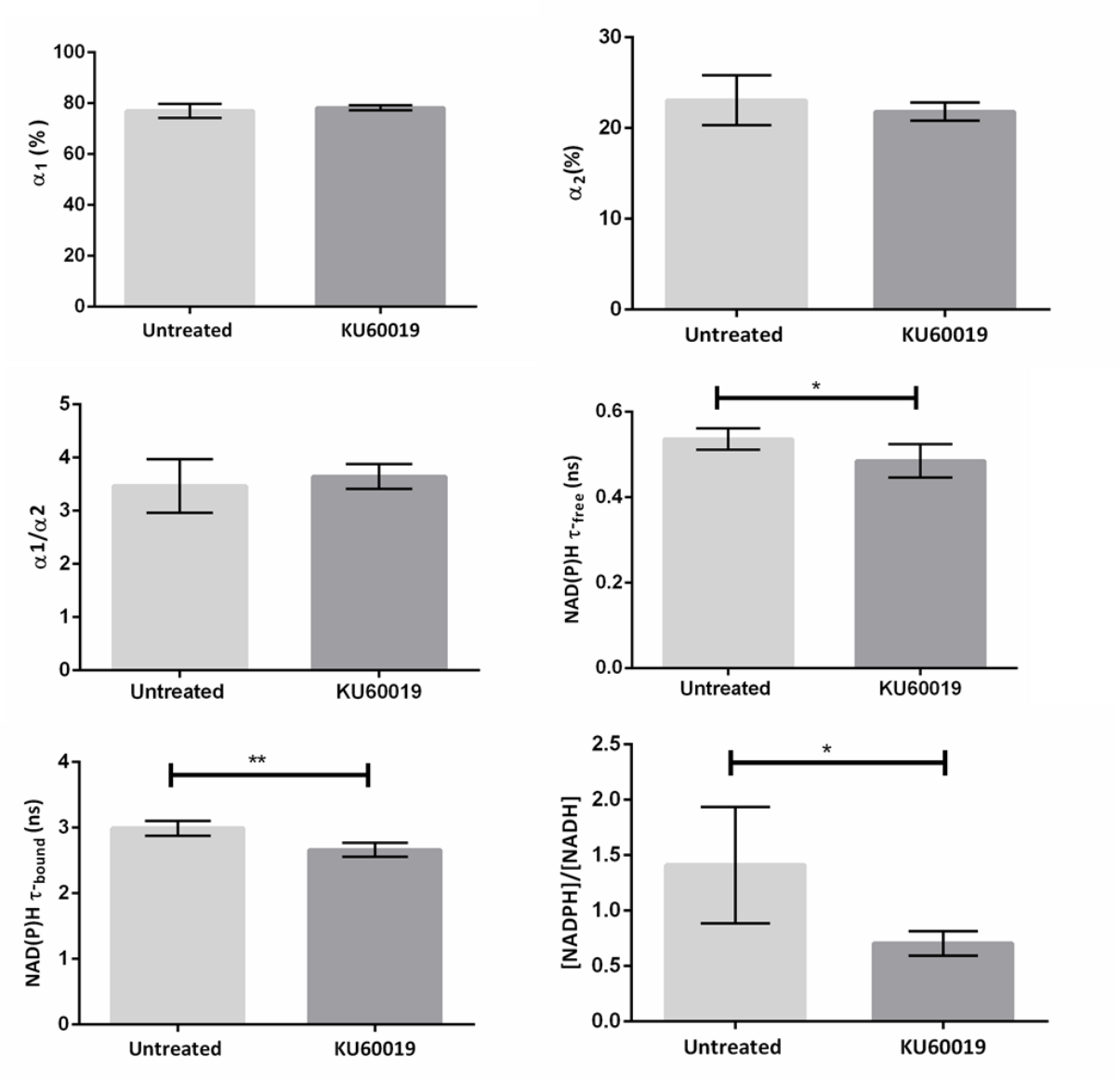

Figure 6.4: NAD(P)H fluorescence decay responses to KU60019 treatment in HEK293 cells. The relative fractions of free (α1) and bound (α2) NAD(P)H did not change significantly, nor did the ratio of free to bound NADPH between control (n=1) and KU-treated cell cultures (n=1). The autofluorescence lifetime of τ_{free} decreased significantly (p=0.0474), as well as did the NAD(P)H τ_{bound} lifetime (ns) (p=0.0031). When calculating the contribution of [NADPH]/[NADH] to the NAD(P)H τ_{bound} lifetime (ns), a significant decrease is observed in KU60019 HEK293 cells (p=0.0351), which suggests an increase in [NADH]. * p< 0.05; ** p < 0.005 versus Untreated with a two-tailed Student's t-test. Error bars are presented as mean ± standard deviation.

The previously observed decreased oxidative phosphorylation rate and decreased NADH oxidation in the presence of ATM inhibition, suggests that ATM plays a functional role in the ETC and oxidative phosphorylation. No significant changes were observed in either α_{bound} or τ_{free}, in line with previous reports that NAD(P)H τ2 can effectively and non-invasively quantify diversions of carbon away from the TCA cycle or the ETC (Sharick et al. 2018) (Fig 6.4). The observed decrease in cellular NAD(P)H in the presence of the ATM inhibitor,

KU60019, in this study agrees with the observation that cells expressing the C2291L-ATM mutant construct has a decreased flux of glucose through the PPP, consequently increasing glucose consumption and lactate generation through glycolysis and accordingly decreasing NADPH (Zhang et al. 2018). In light of these results, we suggest that the absence or inhibition of ATM does not only result in metabolic disturbances, but also mitochondrial dysfunction. This can be either through a decrease in NADPH because of an increase in NADH (as suggested in the HEK293 cells, Fig 6.4), which compromises the mitochondrial ROS scavenging systems or by shifting the cell metabolism towards glycolysis, and is often associated with pathological conditions in the heart.

In conclusion, this study showed that ATM is located within cardiac mitochondria under normoxic conditions. It contributes towards a better understanding of the potential role of ATM in mitochondrial function through ETC complex I, as well as its contribution towards the development of cardiovascular dysfunction by decreasing oxidative phosphorylation efficiency. The results presented here emphasize the need to further establish the role of ATM and to determine whether ATM directly phosphorylates mitochondrial proteins, is activated in response to mitochondrial damage (Shiloh & Ziv 2013) and can be imported in response to stress. Our results do not exclude any of these possibilities.

Chapter 7 : Conclusion

Mitochondrial dysfunction lies at the heart of the development of cardiomyopathy and T2D. Obesity and insulin resistance are associated with mitochondrial disturbances, and contribute towards the development of cardiac dysfunction. ATM has previously been associated with mitochondria, and the absence thereof results in decreased mitochondrial respiration, ATP synthesis and structural abnormalities. In the cytosol, ATM plays a role in insulin signalling, and is down-regulated in high fat conditions. Moreover, when ATM is absent, visceral fat accumulation increases under high-fat conditions.

This study therefore investigated the role of mitochondrial ATM in obesity and the effect thereof on the heart, by evaluating whether (i) ATM can be down-regulated under high-fat conditions in cell culture; (ii) where ATM is localised in the mitochondria and if it affects mitochondrial oxidative phosphorylation and the redox status using H9c2 cells; and (iii) determine whether ATM plays a role in mitochondrial oxidative phosphorylation and mitophagy in obesity using *ex vivo* perfused hearts from fiet-induced obese rats.

In view of the observation that ATM is down-regulated in high fat fed conditions and its role in insulin resistance and the Akt-pathway, this study set out to determine whether ATM can likewise be down-regulated in an undifferentiated H9c2 rat cardiomyoblast cell line in response to high levels of palmitic and oleic acid. The saturated fatty acid, palmitate, is commonly used to induce insulin resistance in cell culture, and additionally contributes towards apoptosis and toxicity. Interestingly, palmitate alone was not sufficient to significantly reduce total ATM, Akt or mTOR protein levels, however, when combined with insulin a significant reduction was noted in both these parameters. The combination of oleate and palmitate in the presence insulin (100 nM) increased ATM, Akt and mTOR protein levels. This would suggest, specifically with regards to these proteins, that insulin resistance induced with either insulin alone, compared to insulin and high free fatty acids, differ in their mechanism. The combination of oleate and palmitate was sufficient to decrease insulin stimulated-glucose uptake, but increased both total ATM and Akt expression as well as the phosphorylation of these proteins. However, none of the treatments had any significant effect on the phospho-protein/total protein ratio. Taken

together, this model provides an initial examination of ATM in a hyperlipidaemic insulin resistant H9c2 model that can be manipulated with the addition or combination of saturated and monounsaturated free fatty acids as well as insulin. This model has several shortcomings that are discussed in Section 7.3.

Mitochondrial dysfunction has been associated with obesity, and although ATM has been associated with mitochondria, its location and precise function was yet to be determined. The use of a digitonin and Lubrol-WX based disruption of the outer and inner mitochondrial membrane identified the location of ATM on the inner mitochondrial membrane of cardiac mitochondria from male Wistar rats under normoxic conditions. This finding was further confirmed with SR-SIM microscopy, which although limited in resolution (approximately 120 µm), revealed that ATM is evenly spread across the mitochondria prior to disruption with digitonin, whereafter it starts to form punctates that remain visible after 20 minutes of digitonin treatment, and is independent of the outer membrane. We concluded that this confirms ATM's association with the mitoplast. The protein's location on the inner membrane was however, also confirmed with western blotting and proteinase K digestion, and is, to the best of our knowledge, the first report of ATM localization on the cardiac inner mitochondrial membrane.

The association of the protein with the IMM suggests a potential role in oxidative phosphorylation. This was initally investigated with *ex vivo* perfusion of young control male Wistar rat hearts with and without KU60019. Compared to controls, and in line with literature, a reduction in ATP synthesis, as estimated by oxidative phosphorylation process, as well as significant uncoupling (ADP/O) were observed in a carbohydrate medium (GM) with KU60019 compared to DMSO (vehicle) alone. No differences were observed when the fatty acid (PCM) was used as substrate. These substrates respectively evaluate the glutamate-aspartate shuttle and β-oxidation in mitochondria. The downregulation of GM-mediated oxidative phosphorylation in response to KU60019 suggests that the inhibition of ATM either influences Complex I mediated oxidation structurally or limits its ability to oxidize substrates. Moreover, ATM inhibition has previously been reported to contribute to the down-regulation of Complex IV, and decreased levels of Complex I has been reported in the absence of ATM. Complex IV inhibition can decrease the redox centre of Complex I and III, as well. This study found that some proteins in the complexes were reduced when ATM

was inhibited, which would suggest a post-transcriptional effect. It would be of value to do a co-immunoprecipitation with the complexes in order to determine whether ATM physically associates with Complex I.

Lastly, if the inhibition of ATM has an inhibitory effect on Complex I, it would fail to explain the high mitochondrial oxidative stress that is observed in A-T in patients, and in the absence of ATM in cell culture and animal models. Complex I produces superoxide during substrate oxidation, which is released into the mitochondrial matrix. Most of the superoxide is dismutated to hydrogen peroxide that is neutralised by NADPH-derived redox system within the matrix which is dependent on thioredoxin and glutathione. If the hydrogen peroxide is not neutralised in the matrix it will be released by Complex III into the cytosol. ATM has been implicated in the regulation of pentose phosphate pathway in the cytosol, where it contributes to the production of NADPH and thioredoxin through the PPP. It is thus possible that the inhibition of ATM can disrupt Complex I oxidation as well as decrease the availability of thioredoxin in the mitochondrial matrix, which could contribute towards higher hydrogen peroxide levels. It would thus be of great value to monitor hydrogen peroxide production within each of the oxidative phosphorylation substrate buffers with KU60019 as well as inhibitors specific to each complex such as rotenone (Complex I inhibitor) and Antimycin C (Complex III inhibitor). This study evaluated NAD(P)H fluorescence in H9c2 cells treated with KU60019. NADH that is associated with Complex I significantly contributes to overall NADH fluorescence. Although NAD(P)H lifetime fluorescence decay cannot distinguish between NADH and NADPH fluorescence, we observed a significant decrease in NAD(P)H lifetime when cells are treated with KU60019. In line with literature, this suggests that NADPH is decreased whilst NADH is increased, and was confirmed in HEK293 cells. An increase in NADH could potentially be the result of decreased NADH oxidation and consequently decrease NAD^+ reduction, which would agree with a model where ATM inhibition interferes with Complex I substrate oxidation.

This study used mitochondria of ex vivo perfused hearts from a well-characterised obese male Wistar rat model to determine the effect of the ATM activators, insulin and chloroquine in the presence and absence of KU60019 on oxidative phosphorylation and mitophagy.

The inhibition of ATM resulted in a general decrease in State 3 oxygen consumption and ATP synthesis, and agrees with literature in this regard. However, it did not decrease uncoupling (ADP/O levels) or resting respiration (State 4). It is important to note that the ADP/O values will not change unless the ETC complexes are changed, and will not change in response to altered substrate oxidation. A reduction in the subcomplexes of the mitochondrial ETC was observed, which suggests that the inhibition of ATM can alter substrate oxidation possibly through altering the ETC complexes, and consequently reducing their efficiency. This effect was observed in mitochondria from both chow-fed and DIO rat hearts. However, a significant decrease was observed in the ADP/O ratio of DIO hearts perfused with a combination of KU60019 and insulin in both the GM and the PCM substrate. Interestingly, this improved State 3 recovery after 20 minute of anoxia. Although this suggests uncoupling, it was not supported with an increase in UCP3, which remained at basal levels. The combination of insulin and ATM inhibition also significantly decreased the RCR value of mitochondria from chow-fed hearts in a GM substrate but had no effect in a PCM substrate when compared to hearts perfused with insulin alone. All other effects noted in the oxidative phosphorylation process were brought about by the use of either a carbohydrate or a fatty acid substrate rather than diet-induced obesity. In conclusion, the inhibition of ATM only had an effect in the mitochondria of obese rat hearts in the presence of insulin, but suggests that mitochondrial efficiency and the substrate utilisation by Complex I in the presence of insulin can be significantly affected when ATM is inhibited.

Insulin overall improved all parameters of oxidative phosphorylation when a carbohydrate substrate was used. This agrees with literature that has shown improved oxidative phosphorylation in the presence of insulin, and was reflected by decreased fission (Drp1) which would suggest that fusion is increased. Moreover, no autophagy was detected, and PINK was decreased in mitochondria from both chow-fed and DIO hearts, whilst Parkin was increased. The loss of autophagy corresponds well with the activation of the Akt pathway that will, according to literature, result in upregulation of mTOR activity. Taken together, this might indicate that a consistently high presence of insulin could result in accumulation of defective mitochondria and increased oxidative stress in mitochondria from chow-fed hearts. This might lead to the recruitment of Parkin to depolarized mitochondria in an aim to re-establish homeostasis. In conclusion, it would thus indicate that ATM plays a role

downstream in insulin signalling within the Akt-mTOR pathway and its effects on mitochondrial oxidative phosphorylation.

The inhibition of ATM did have a significant effect on autophagy , more so r than mitophagy, and although increased Parkin accumulation was seen in mitochondria from perfused chow-fed rat hearts, this effect did not correlate with an increase in PINK. It can potentially suggest mitochondria might be targeted by a Parkin-dependent mitophagy pathway, but this result could not be duplicated when investigated using chloroquine. Taken together, these results would rather suggest that the inhibition of ATM results in decreased autophagy due to upregulation of the mTOR pathway activity in the cytosol, as was shown by the significant reduction in LC3-II protein accumulation, p62, as well as the loss of fission (Drp1) that were all independent of diet.

Chloroquine had no effect on oxidative phosphorylation, except for an increase in State 4 respiration. This did not however influence any of the other parameters, irrespective of diet. Regardless, it did result in a significant decrease in both PINK and Parkin as mitophagy markers, and increased LC3-II significantly in mitochondria from both chow-fed and DIO animals which are consistent with its role as a lysosomal inhibitor. The addition of KU60019 in combination with chloroquine, increased ATP synthesis, State 3 and State 4 respiration but did not influence ADP/O or RCR values. The underlying mechanism of this is unknown.

The combination of KU60019 and chloroquine did shed light on the inhibition of ATM. The inhibition of ATM decreased the lipidated LC3-II significantly both in the presence and absence of chloroquine. This suggests that the autophagosomal membrane failed to form, potentially due to an increase in mTORCI. Interestingly, mTOR has recently been implicated in PINK and Parkin mitophagy, and highlights the negative feedback role of ATM on mTORCI.

Taken together, this study showed that ATM is located on the inner mitochondrial membrane of cardiac mitochondria. The inhibition of ATM resulted in decreased carbohydrate stimulated oxidative phosphorylation in cardiac mitochondria, potentially through Complex I. This is supported by the observation that ATM inhibition decreased NADPH and increased NADH accumulation in H9c2 cells. The effect of ATM inhibition on oxidative phosphorylation was not influenced by obesogenic diet, except in mitochondria from insulin-perfused DIO hearts. The inhibition of ATM, as well the perfusion of chow-fed

rat hearts with insulin and insulin+ KU60019 had a significant effect on fission (DrpI). The decreased autophagy marker (LC3-II) seems to be associated with the cytosolic role of ATM which was highlighted by the significant decrease of LC3-II, and consequently the autophagosomal membrane formation even in the presence of chloroquine, rather than a mitochondrial role.

7.2 Future work:

The role of ATM as a potential regulator of ETC substrate utilisation and the effects of its inhibition on the redox status of the mitochondria is a very interesting result. Together with its potential role in Parkin-mediated mitophagy, the results justify further investigation into the mitochondrial role of ATM.

This would require further evaluation with different substrates, such as succinate, as well as an in-depth analysis of the underlying metabolomics within the ETC chain. Oxidative stress also needs to be evaluated, both within the mitochondrial matrix with regards to superoxide production as well as mitochondrial hydrogen peroxide production. This may initially be done in H9c2 cells. Oxidative stress can also influence mitophagy, and a more in depth analysis is required of both the autophagy as well as mitophagy markers other than PINK and Parkin. Mitophagy and autophagy markers including Beclin-1, Mfn1 and 2, Opa1, Rab and ULK1 will be further investigated based on the observation that dysfunctional mitophagy and autophagy, rather than oxidative phosphorylation might contribute to mitochondrial dysfunction in obesity. Moreover, the decrease observed in fission, would suggest a role for ATM in mitochondrial dynamics that will require further analysis with both mitochondrial fission (FIS1, Drp1) and fusion proteins(Mfn1, Mfn2, Opa1). ATM is potentially an attractive microscopy target with regards to mitochondrial dynamics as well as autophagy, based on well-established microscopy techniques such as SR-SIM to monitor the formation, development and recruitment of the autophagosomal membrane.

This project brought about an exciting collaboration with researchers at the Rutherford Appleton Laboratory (UK), who's research focus on mTOR. The project will aim to maintain the collaboration with RAL to extend the 2-P-FLIM results to include other known

mitochondrial ETC inhibitors, and monitor the change in the mitochondrial redox status in response to the free fatty acids evaluated in this study.

The H9c2 model is currently under further development within our laboratory, and will gain from cell viability assays as well as a better characterisation of the effect of palmitic acid alone compared to a combination of palmitate and oleate. Moreover, an evaluation of the model with cell culture media in which adipocytes have previously been differentiated might result in a more applicable evaluation of the effect of obesity on ATM protein expression.

7.3 Limitations:

The H9c2 cell culture model currently poses the greatest limitation in this study and several aspects should be improved. The model will have to be optimised further to address the role of ATM levels in response to obesity and insulin resistance. The first aspect is the lack of a cell viability assay. ATM is a known regulator of p53 which modulates apoptosis. Some of the protein level decreases that were observed, could well be due to cellular apoptosis in response to lipotoxicity, especially when compared to insulin alone, which is a known growth factor. Secondly, fatty acids tend to oxidise prior to their use in cell culture, which can influence their function. Moreover, conjugation with BSA tends to improve fatty acid solubility and uptake. It is therefore pertinent to test this model with BSA-conjugated fatty acids and determine both uptake and fatty acid oxidation of palmitate and oleate respectively, as well as combined. A cell viability test using reagents such as propidium iodide (live/dead cells) or an MTT (3-(4,5-dimethylthiazol-2-yl)-2,5-diphenyltetrazolium bromide)- assay that measure mitochondrial NAD(P)H-dependent cellular oxidoreductase enzymes will give an indication of apoptosis in treated H9c2 cells. Once these are established, the model should offer a more reliable assessment of the role of ATM in obesity.

With regards to the localisation of ATM, SR-SIM microscopy is limited in its size detection resolution, which is currently approximately 120 nm. In order to conclusively use SR-SIM as a method to confirm ATM localisation, it would require the use of a fourth marker that is specific to the inner mitochondrial membrane. Moreover, and a major shortcoming

regarding the use of western blotting for the determination of location, is the lack of a matrix marker in this study.

No other mitochondrial complex inhibitors were tested in this study, nor any other combinations of substrates such as succinate and malate, which would give a clearer indication which complex is influenced by ATM inhibition. The mitochondrial membrane potential can also impact ATP synthesis, and the effect of ATM inhibition on mitochondrial membrane potential was not investigated. The NAD(P)H values were only investigated in H9c2 cell culture, and no other controls such as rotenone that inhibits Complex 1 and is known to influence NAD(P)H lifetime decay, were included in the 2-P-FLIM study. The use of a colorimetric NAD/NADH kit would complement the 2-P-FLIM data obtained in this study. Colorometric and fluorescent detection of ATP production and ROS level detection, respectively would contribute significantly towards a better understanding of the role of ATM in oxidative phosphorylation.

Chapter 8 : References

Adamowicz, M., Vermezovic, J. & d'Adda di Fagagna, F., 2016. NOTCH1 Inhibits Activation of ATM by Impairing the Formation of an ATM-FOXO3a-KAT5/Tip60 Complex. *Cell Reports*, 16(8), pp.2068–2076.

Adamson, A.W. et al., 2002. ATM is activated in response to N-methyl-N'-nitro-N-nitrosoguanidine-induced DNA alkylation. *Journal of Biological Chemistry*, 277(41), pp.38222–38229.

Ahmed, M. & Rahman, N., 2006. ATM and breast cancer susceptibility. *Oncogene*, 25(43), pp.5906–5911.

Alexander, A. et al., 2010. ATM signals to TSC2 in the cytoplasm to regulate mTORC1 in response to ROS. *Proceedings of the National Academy of Sciences*, 107(9), pp.4153–4158.

Alexander, A. & Walker, C.L., 2011. Differential localization of ATM is correlated with activation of distinct downstream signaling pathways. *Cell Cycle*, 9(18), pp.3685–3686.

Allmann, D.W. et al., 1966. The Membrane Systems of the Mitochondrion I . The S Fraction of the Outer Membrane of Beef Heart Mitochondria. *Archives of Biochemistry and Biophysics*, 115(1), pp.153–164.

Alwan, A. et al., 2010. Monitoring and surveillance of chronic non-communicable diseases: Progress and capacity in high-burden countries. *The Lancet*, 376(9755), pp.1861–1868.

Ambrose, M. & Gatti, R.A., 2013. Pathogenesis of ataxia-telangiectasia: the next generation of ATM functions. *Blood*, 121(20), pp.4036–4045.

Ambrose, M., Goldstine, J. V. & Gatti, R.A., 2007. Intrinsic mitochondrial dysfunction in ATM-deficient lymphoblastoid cells. *Human Molecular Genetics*, 16(18), pp.2154–2164.

Anderson, E.J., Katunga, L.A. & Willis, M.S., 2012. Mitochondria as a source and target of lipid peroxidation products in healthy and diseased heart. *Clinical and Experimental Pharmacology and Physiology*, 39(2), pp.179–193.

Andres, A.M. et al., 2015. A time to reap, a time to sow: Mitophagy and biogenesis in cardiac

pathophysiology. *Journal of Molecular and Cellular Cardiology*, 78, pp.62–72.

Aon, M.A. et al., 2012. Glutathione / thioredoxin systems modulate mitochondrial H 2 O 2 emission : An experimental-computational study. *Journal of General Physiology*, 139(6), pp.479–491.

Armata, H.L. et al., 2010. Requirement of the ATM/p53 tumor suppressor pathway for glucose homeostasis. *Molecular and Cellular Biology*, 30(24), pp.5787–5794.

Armoni, M. et al., 2005. Free fatty acids repress the GLUT4 gene expression in cardiac muscle via novel response elements. *Journal of Biological Chemistry*, 280(41), pp.34786–34795.

Asamoah, K.A., Robb, D.A. & Furman, B.L., 1990. Chronic chloroquine treatment enhances insulin release in rats. *Diabetes Research and Clinical Practice*, 9(3), pp.273–278.

Bachmann, E., Allmann, D.W. & Green, D.E., 1966. The Membrane Systems of the Mitochondrion I . The S Fraction of the Outer Membrane of Beef Heart Mitochondria. *Archives of Biochemistry and Biophysics*, 115(1), pp.153–164.

Bakkenist, C.J. & Kastan, M.B., 2003. DNA damage activates ATM through intermolecular autophosphorylation and dimer dissociation. *Nature*, 421(6922), pp.499–506.

Bar, R.S. et al., 1978. Extreme Insulin Resistance in Ataxia Telangiectasia. *New England Journal of Medicine*, 298(21), pp.1164–1171.

Baretić, D. et al., 2017. Structures of closed and open conformations of dimeric human ATM. *Science Advances*, (5), p.e1700933.

Barlow, C. et al., 1996. Atm-deficient mice: A paradigm of ataxia telangiectasia. *Cell*, 86(1), pp.159–171.

Barlow, C. et al., 2000. ATM is a cytoplasmic protein in mouse brain required to prevent lysosomal accumulation. *Proceedings of the National Academy of Sciences*, 97(2), pp.871–876.

Bartolomé, A. et al., 2017. MTORC1 Regulates both General Autophagy and Mitophagy Induction after Oxidative Phosphorylation Uncoupling. *Molecular and Cellular Biology*,

37(23), pp.e00441-17.

Barzilai, A., Rotman, G. & Shiloh, Y., 2002. ATM deficiency and oxidative stress: A new dimension of defective response to DNA damage. *DNA Repair*, 1(1), pp.3–25.

Bedard, K. & Krause, K.-H., 2007. The NOX Family of ROS-Generating NADPH Oxidases: Physiology and Pathophysiology. *Physiological Reviews*, 87(1), pp.245–313.

Bencokova, Z. et al., 2009. ATM activation and signaling under hypoxic conditions. *Molecular and Cellular Biology*, 29(2), pp.526–537.

Bensimon, A., Aebersold, R. & Shiloh, Y., 2011. Beyond ATM: The protein kinase landscape of the DNA damage response. *FEBS Letters*, 585(11), pp.1625–1639.

Bertrand, L. et al., 2006. AMPK activation restores the stimulation of glucose uptake in an in vitro model of insulin-resistant cardiomyocytes via the activation of protein kinase B. *American journal of physiology. Heart and Circulatory Physiology*, 291(1), pp.H239-50.

Bertrand, L. et al., 2008. Insulin signalling in the heart. *Cardiovascular Research*, 79(2), pp.238–248.

Bessman, S.P., Mohan, C. & Zaidise, I., 1986. Intracellular site of insulin action: mitochondrial Krebs cycle. *Proceedings of the National Academy of Sciences*, 83(14), pp.5067–70.

Beutner, G. et al., 2001. Identification of a Ryanodine Receptor in Rat Heart Mitochondria. *Journal of Biological Chemistry*, 276(24), pp.21482–21488.

Beutner, G. et al., 2005. Type 1 ryanodine receptor in cardiac mitochondria: Transducer of excitation-metabolism coupling. *Biochimica et Biophysica Acta - Biomembranes*, 1717(1), pp.1–10.

Bevan, A.P. et al., 1997. Chloroquine extends the lifetime of the activated insulin receptor complex in endosomes. *Journal of Biological Chemistry*, 272(43), pp.26833–26840.

Bhatti, J.S., Bhatti, G.K. & Reddy, P.H., 2017. Mitochondrial dysfunction and oxidative stress in metabolic disorders — A step towards mitochondria based therapeutic strategies. *Biochimica et Biophysica Acta - Molecular Basis of Disease*, 1863(5), pp.1066–1077.

Bhatti, S. et al., 2011. ATM protein kinase: The linchpin of cellular defenses to stress. *Cellular and Molecular Life Sciences*, 68(18), pp.2977–3006.

Bird, D.K. et al., 2005. Metabolic mapping of MCF10A human breast cells via multiphoton fluorescence lifetime imaging of the coenzyme NADH. *Cancer Research*, 65(19), pp.8766–8773.

Blacker, T.S. et al., 2013. Activated barrier crossing dynamics in the non-radiative decay of NADH and NADPH. *Chemical Physics*, 422, pp.184–194.

Blacker, T.S. et al., 2014. Separating NADH and NADPH fluorescence in live cells and tissues using FLIM. *Nature Communications*, 5(May), pp.1–9.

Blacker, T.S. & Duchen, M.R., 2016. Investigating mitochondrial redox state using NADH and NADPH autofluorescence. *Free Radical Biology and Medicine*, 100, pp.53–65.

Boder, E. & Sedgwick, R.P., 1958. Ataxia-telangiectasia. *Pediatrics*, 21, pp.526–554.

Bonnard, C. et al., 2008. Mitochondrial dysfunction results from oxidative stress in the skeletal muscle of diet-induced insulin resistant mice. *Journal of Clinical Investigation*, 118(2), pp.789–800.

Botchway, S.W. et al., 2015. A series of flexible design adaptations to the Nikon E-C1 and E-C2 confocal microscope systems for UV, multiphoton and FLIM imaging. *Journal of Microscopy*, 258(1), pp.68–78.

Boudina, S. et al., 2009. Contribution of impaired myocardial insulin signaling to mitochondrial dysfunction and oxidative stress in the heart. *Circulation*, 119(9), pp.1272–83.

Boudina, S. et al., 2007. Mitochondrial Energetics in the Heart in Obesity-Related Diabetes: direct evidence for increased uncoupled respiration and activation of uncoupling proteins. *Diabetes*, 56, pp.2457–2466.

Boudina, S. & Abel, E.D., 2010. Diabetic cardiomyopathy, causes and effects. *Reviews in Endocrine and Metabolic Disorders*, 11(1), pp.31–39.

Bradford, M.M., 1976. A rapid and sensitive method for the quantitation of microgram

quantities of protein utilizing the principle of protein-dye binding. *Analytical Biochemistry*, 72(1–2), pp.248–254.

Brand, M.D. & Nicholls, D.G., 2011. Assessing mitochondrial dysfunction in cells. *The Biochemical Journal*, 435(2), pp.297–312.

Brennan, J.P. et al., 2006. Mitochondrial uncoupling, with low concentration FCCP, induces ROS-dependent cardioprotection independent of KATPchannel activation. *Cardiovascular Research*, 72(2), pp.313–321.

Bugger, H. et al., 2010. Proteomic remodelling of mitochondrial oxidative pathways in pressure overload-induced heart failure. *Cardiovascular Research*, 85(2), pp.376–384.

Bugger, H. & Abel, E.D., 2010. Mitochondria in the diabetic heart. *Cardiovascular Research*, 88(2), pp.229–240.

Bugger, H. & Abel, E.D., 2008. Molecular mechanisms for myocardial mitochondrial dysfunction in the metabolic syndrome. *Clinical Science*, 210(114), pp.195–210.

Burma, S. et al., 2001. ATM Phosphorylates Histone H2AX in Response to DNA Double-strand Breaks. *Journal of Biological Chemistry*, 276(45), pp.42462–42467.

Burnette, B. & Batra, P.P., 1985. A combination of methods for the preparation of highly intact mitoplasts from beef heart mitochondria. *Analytical Biochemistry*, 145(1), pp.80–86.

Buzin, C.H. et al., 2003. Comprehensive scanning of the ATM gene with DOVAM-S. *Human Mutation*, 21(2), pp.123–131.

Cadenas, S., 2018. Mitochondrial uncoupling, ROS generation and cardioprotection. *Biochimica et Biophysica Acta (BBA) - Bioenergetics*, 1859(9), pp.940–950.

Cai, L. et al., 2002. Hyperglycemia-induced apoptosis in mouse myocardium: mitochondrial cytochrome e-mediated caspase-3 activation pathway. *Diabetes*, 51, pp.1938–1948.

Cam, H. et al., 2010. mTORC1 Signaling under Hypoxic Conditions Is Controlled by ATM-Dependent Phosphorylation of HIF-1α. *Molecular Cell*, 40(4), pp.509–520.

Cardaci, S., Filomeni, G. & Ciriolo, M.R., 2012. Redox implications of AMPK-mediated signal transduction beyond energetic clues. *Journal of Cell Science*, 125(9), pp.2115–2125.

Ceriello, A. & Motz, E., 2004. Is Oxidative Stress the Pathogenic Mechanism Underlying Insulin Resistance, Diabetes, and Cardiovascular Disease? The Common Soil Hypothesis Revisited. *Arteriosclerosis, Thrombosis, and Vascular Biology*, 24(5), pp.816–823.

Chaanine, A.H. et al., 2015. High-dose chloroquine is metabolically cardiotoxic by inducing lysosomes and mitochondria dysfunction in a rat model of pressure overload hypertrophy. *Physiological Reports*, 3(7), pp.1–18.

Chakraborty, S. et al., 2016. Quantification of the Metabolic State in Cell-Model of Parkinson's Disease by Fluorescence Lifetime Imaging Microscopy. *Scientific Reports*, 6(1), p.19145.

Chan, T.L., Greenawalt, J.W. & Pedersen, P.L., 1970. Biochemical and ultrastructural properties of a mitochondrial inner membrane fraction deficient in outer membrane and matrix activities. *Journal of Cell Biology*, 45(2), pp.291–305.

Chance, B. et al., 1979. Oxidation-Reduction Ratio Studies of Mitochondria in Freeze-trapped Samples. *Journal of Biological Chemistry*, 254(11), pp.4764–4771.

Chen, B.P.C. et al., 2007. Ataxia telangiectasia mutated (ATM) is essential for DNA-PKcs phosphorylations at the Thr-2609 cluster upon DNA double strand break. *Journal of Biological Chemistry*, 282(9), pp.6582–6587.

Chen, G. & Lee, E.Y.H.P., 1996. The product of the ATM gene is a 370-kDa nuclear phosphoprotein. *Journal of Biological Chemistry*, 271(52), pp.33693–33697.

Chen, Q. et al., 2003. Production of reactive oxygen species by mitochondria: Central role of complex III. *Journal of Biological Chemistry*, 278(38), pp.36027–36031.

Chen, Q., Hoppel, C.L. & Lesnefsky, E.J., 2006. Blockade of electron transport before cardiac ischemia with the reversible inhibitor amobarbital protects rat heart mitochondria. *The Journal of Pharmacology and Experimental Therapeutics*, 316(1), pp.200–207.

Chen, Y. & Dorn II, G.W., 2013. PINK1- Phosphorylated Mitofusin 2 is a Parkin Receptor for

Culling Damaged Mitochondria. *Science*, 340(6131), pp.471–475.

Chen, Y., Liu, Y. & Dorn, G.W., 2011. Mitochondrial fusion is essential for organelle function and cardiac homeostasis. *Circulation Research*, 109(12), pp.1327–1331.

Cheng, Z., Tseng, Y. & White, M.F., 2017. Insulin signaling meets mitochondria in metabolism. *Trends in Endocrinology & Metabolism*, 21(10), pp.589–598.

Ching, J.K. et al., 2014. ATM impacts IGF-1 signaling in skeletal muscle . *Experimental Physiology*, 98(2), pp.526–535.

Choubey, V. et al., 2014. BECN1 is involved in the initiation of mitophagy: It facilitates PARK2 translocation to mitochondria. *Autophagy*, 10(6), pp.1105–1119.

Cole, M.A. et al., 2011. A high fat diet increases mitochondrial fatty acid oxidation and uncoupling to decrease efficiency in rat heart. *Basic Research in Cardiology*, 106, pp.447–457.

Connelly, P.J. et al., 2016. Recessive mutations in the cancer gene Ataxia Telangiectasia Mutated (ATM), at a locus previously associated with metformin response, cause dysglycaemia and insulin resistance. *Diabetic Medicine*, 33(3), pp.371–375.

Cosentino, C., Grieco, D. & Costanzo, V., 2011. ATM activates the pentose phosphate pathway promoting anti-oxidant defence and DNA repair. *The European Molecular Biology Organization (EMBO) Journal*, 30(3), pp.546–555.

Crane, F.L. et al., 1994. Coenzyme Q10, plasma membrane oxidase and growth control. *Molecular Aspects of Medicine*, 15, pp.s1–s11.

Cremona, C.A. & Behrens, A., 2014. ATM signalling and cancer. *Oncogene*, (33), pp.3351–3360.

D'Souza, A.D. et al., 2012. Reducing Mitochondrial ROS Improves Disease-related Pathology in a Mouse Model of Ataxia-telangiectasia. *Molecular Therapy*, 21(1), pp.42–48.

Dagda, R.K. et al., 2009. Loss of PINK1 function promotes mitophagy through effects on oxidative stress and mitochondrial fission. *Journal of Biological Chemistry*, 284(20), pp.13843–13855.

Daniel, J.A. et al., 2008. Multiple autophosphorylation sites are dispensable for murine ATM activation in vivo. *Journal of Cell Biology*, 183(5), pp.777–783.

Daniel, L.L. et al., 2016. Ataxia telangiectasia-mutated kinase deficiency exacerbates left ventricular dysfunction and remodeling late after myocardial infarction. *American Journal of Physiology - Heart and Circulatory Physiology*, 311(2), pp.445–452.

Deavall, D.G. et al., 2012. Drug-induced oxidative stress and toxicity. *Journal of Toxicology*, 2012, pp.1–13.

Dianov, G.L. & Hübscher, U., 2013. Mammalian base excision repair: The forgotten archangel. *Nucleic Acids Research*, 41(6), pp.3483–3490.

Diokmetzidou, A. et al., 2016. Desmin and αB-crystallin interplay in the maintenance of mitochondrial homeostasis and cardiomyocyte survival. *Journal of Cell Science*, 129(20), pp.3705–3720.

Ditch, S. & Paull, T.T., 2012. The ATM protein kinase and cellular redox signaling: Beyond the DNA damage response. *Trends in Biochemical Sciences*, 37(1), pp.15–22.

Doenst, T., Nguyen, T.D. & Abel, E.D., 2013. Cardiac metabolism in heart failure : implications beyond ATP production. *Circulation Research*, 113(6), pp.709–724.

Dong, B. et al., 2012. TLR4 regulates cardiac lipid accumulation and diabetic heart disease in the nonobese diabetic mouse model of type 1 diabetes. *American Journal of Physiology - Heart and Circulatory Physiology*, 303(6), pp.H732–H742.

Doran, E. & Halestrap, A.P., 2000. Cytochrome c release from isolated rat liver mitochondria can occur independently of outer-membrane rupture: possible role of contact sites. *The Biochemical Journal*, 348 Pt 2, pp.343–350.

Dorn, G.W. & Kitsis, R.N., 2015. The mitochondrial dynamism-mitophagy-cell death interactome: Multiple roles performed by members of a mitochondrial molecular ensemble. *Circulation Research*, 116(1), pp.167–182.

Dorn, G.W., Vega, R.B. & Kelly, D.P., 2015. Mitochondrial biogenesis and dynamics in the developing and diseased heart. *Genes and Development*, 29(19), pp.1981–1991.

Druzhyna, N.M., Wilson, G.L. & Ledoux, S.P., 2009. Mitochondrial DNA repair in aging and disease. *Mechanisms of Ageing and Development*, 129(7–8), pp.383–390.

Duchen, M.R., Surin, A. & Jacobson, J.B.T.-M. in E., 2003. [17] Imaging mitochondrial function in intact cells. In *Biophotonics, Part B*. Academic Press, pp. 353–389.

Eaton, J.S. et al., 2007. Ataxia-telangiectasia mutated kinase regulates ribonucleotide reductase and mitochondrial homeostasis. *Journal of Clinical Investigation*, 117(9), pp.2723–2734.

Egan, D.F. et al., 2011. Phosphorylation of ULK1 (hATG1) by AMP-Activated Protein Kinase Connects Energy Sensing to Mitophagy. *Science*, 331, pp.456–461.

Eisenberg, T. et al., 2009. Induction of autophagy by spermidine promotes longevity. *Nature Cell Biology*, 11(11), pp.1305–1314.

Emerling, B.M. et al., 2009. Hypoxic activation of AMPK is dependent on mitochondrial ROS but independent of an increase in AMP/ATP ratio. *Free Radical Biology and Medicine*, 46(10), pp.1386–1391.

Espach, Y., 2017. *An investigation into the importance of the ATM protein in the myocardial pathology associated with insulin resistance and type 2 diabetes*, PhD dissertation; Stellenbosch University; South Africa.

Espach, Y. et al., 2015. ATM protein kinase signaling, Type 2 Diabetes and cardiovascular disease. *Cardiovascular Drugs Therapy*, 29, pp.51–58.

Evans, T.D. et al., 2017. Target acquired: Selective autophagy in cardiometabolic disease. *Science Signaling*, 10(468), p.eaag2298.

Fandrey, J., Gorr, T.A. & Gassmann, M., 2006. Regulating cellular oxygen sensing by hydroxylation. *Cardiovascular Research*, 71(4), pp.642–651.

Fang, E.F. et al., 2016. NAD+Replenishment Improves Lifespan and Healthspan in Ataxia Telangiectasia Models via Mitophagy and DNA Repair. *Cell Metabolism*, 24(4), pp.566–581.

Fernandes, N. et al., 2005. DNA damage-induced association of ATM with its target proteins

requires a protein interaction domain in the N terminus of ATM. *Journal of Biological Chemistry*, 280(15), pp.15158–15164.

Finkel, T., 2011. Signal transduction by reactive oxygen species. *Journal of Cell Biology*, 194(1), pp.7–15.

Fischer, Y., Rose, H. & Kammermeier, H., 1991. Highly insulin-responsive isolated rat heart muscle cells yielded by a modified isolation method. *Life Sciences*, 49(23), pp.1679–1688.

Florez, J.C. et al., 2012. The C allele of ATM rs11212617 does not associate with metformin response in the diabetes prevention program. *Diabetes Care*, 35(9), pp.1864–1867.

Forrester, S.J. et al., 2018. Reactive Oxygen Species in Metabolic and Inflammatory Signaling. *Circulation Research*, 122(6), pp.877–902.

Fortini, P. et al., 2012. DNA damage response by single-strand breaks in terminally differentiated muscle cells and the control of muscle integrity. *Cell Death and Differentiation*, 19(11), pp.1741–1749.

Foster, C.R. et al., 2011. Ataxia telangiectasia mutated kinase plays a protective role in β-adrenergic receptor-stimulated cardiac myocyte apoptosis and myocardial remodeling. *Molecular and Cellular Biochemistry*, 353(1–2), pp.13–22.

Foster, C.R. et al., 2012. Lack of ataxia telangiectasia mutated kinase induces structural and functional changes in the heart: Role in β-adrenergic receptor-stimulated apoptosis. *Experimental Physiology*, 97(4), pp.506–515.

Frank, M. et al., 2012. Mitophagy is triggered by mild oxidative stress in a mitochondrial fission dependent manner. *Biochimica et Biophysica Acta - Molecular Cell Research*, 1823(12), pp.2297–2310.

Fu, T. et al., 2018. Mitophagy Directs Muscle-Adipose Crosstalk to Alleviate Dietary Obesity. *Cell Reports*, 23(5), pp.1357–1372.

Fu, X. et al., 2008. Etoposide Induces ATM-Dependent Mitochondrial Biogenesis through AMPK Activation. *PLoS ONE*, 3(4), p.e2009.

Fukushima, A. & Lopaschuk, G.D., 2016. Acetylation control of cardiac fatty acid β-oxidation and energy metabolism in obesity, diabetes, and heart failure. *Biochimica et Biophysica Acta - Molecular Basis of Disease*, 1862(12), pp.2211–2220.

Gafni, A. & Brand, L., 1976. Fluorescence decay studies of reduced nicotinamide adenine dinucleotide in solution and bound to liver alcohol dehydrogenase. *Biochemistry*, 15(15), pp.3165–3171.

Gao, D., Griffiths, H.R. & Bailey, C.J., 2009. Oleate protects against palmitate-induced insulin resistance in L6 myotubes. *British Journal of Nutrition*, 102(11), pp.1557–1563.

Gatti, R.A. et al., 1988. Localization of an ataxia-telangiectasia gene to chromosome 11q22-23. *Nature*, 336(6199), pp.577–580.

Gatti, R.A. et al., 2001. The pathogenesis of ataxia-telangiectasia: Learning from a Rosetta Stone. *Clinical Reviews in Allergy and Immunology*, 20(1), pp.87–108.

Gilda, J.E. & Gomes, A. V., 2013. Stain Free Total Protein Staining is a Superior Loading Control to β-Actin for Western Blots. *Analytical Biochemistry*, 440(2), pp.1–6.

Goglia, F. & Skulachev, V.P., 2003. A function for novel uncoupling proteins: antioxidant defense of mitochondrial matrix by translocating fatty acid peroxides from the inner to the outer membrane leaflet. *The Federation of American Societies for Experimental Biology Journal*, 17(12), pp.1585–1591.

Goodarzi, A.A., Jeggo, P. & Lobrich, M., 2010. The influence of heterochromatin on DNA double strand break repair: Getting the strong, silent type to relax. *DNA Repair*, 9(12), pp.1273–1282.

Greenawalt, J.W., 1974. The isolation of outer and inner mitochondrial membranes. *Methods in Enzymology*, 31, pp.310–323..

Guo, Z., Kozlov, S., Lavin, M.F., Person, M.D. & Paull, T.T., 2010. ATM activation by oxidative stress. *Science*, 330(6003), pp.517–521.

Guzy, R.D. et al., 2005. Mitochondrial complex III is required for hypoxia-induced ROS production and cellular oxygen sensing. *Cell Metabolism*, 1(6), pp.401–408.

Ha, H. & Pak, Y., 2005. Modulation of the caveolin-3 and Akt status in caveolae by insulin resistance in H9c2 cardiomyoblasts. *Experimental and Molecular Medicine*, 37(3), pp.169–178.

Hackenbrock, C.R., 1972. Energy-Linked Ultrastructural Transformations in Isolated Liver Mitochondria and Mitoplasts. *The Journal of Cell Biology*, 53(2), pp.450–465.

Halaby, M.-J., Kastein, B.K. & Yang, D.-Q., 2013. Chloroquine stimulates glucose uptake and glycogen synthase in muscle cells through activation of Akt. *Biochemical and Biophysical Research Communications*, 435(4), pp.708–713.

Halaby, M.J. et al., 2008. ATM protein kinase mediates full activation of Akt and regulates glucose transporter 4 translocation by insulin in muscle cells. *Cellular Signalling*, 20(8), pp.1555–1563.

Hall, J.C., Sordahl, L.A. & Stefko, P.L., 1960. The Effect of Insulin on Oxidative Phosphorylation in Normal and Diabetic Mitochondria. *Journal of Biochemistry*, 235(5), pp.1536–1539.

Han, M.S. et al., 2013. JNK Expression by Macrophages promotes obesity-induced insulin resistance and inflammation. *Science*, 339, pp.218–222.

Hartlerode, A.J. & Scully, R., 2009. Mechanisms of double-strand break repair in somatic mammalian cells. *Biochemical Journal*, 423(2), pp.157–168.

He, C. & Klionsky, D.J., 2009. Regulation Mechanisms and Signaling Pathways of Autophagy. *Annual Review of Genetics*, 43, pp.67–93.

Heintzmann, R. & Cremer, C.G., 1999. Laterally modulated excitation microscopy: improvement of resolution by using a diffraction grating. In *SPIE 3568, Optical Biopsies and Microscopic Techniques III*. pp. 185–196.

Hescheler, J. et al., 1991. Morphological, biochemical, and electrophysiological characterization of a clonal cell (H9c2) line from rat heart. *Circulation Research*, 69(6), pp.1476–1486.

Hoehn, K.L. et al., 2009. Insulin resistance is a cellular antioxidant defense mechanism.

Proceedings of the National Academy of Sciences, 106(42), pp.17787–92.

Holmström, K.M. & Finkel, T., 2014. Cellular mechanisms and physiological consequences of redox-dependent signalling. *Nature Reviews: Molecular Cell Biology*, 15(6), pp.411–421.

Hoppel, C.L. et al., 1998. The malonyl coA sensitive form of carnitine palmitoyltransferase is not localised exclusively in the outer membrane of rat liver mitochondria. *Journal of Biological Chemistry*, 273(36), pp.23495–23503.

Hopps, E. et al., 2010. A novel component of the metabolic syndrome: The oxidative stress. *Nutrition, Metabolism and Cardiovascular Diseases*, 20(1), pp.72–77.

Hovius, R. et al., 1990. Improved methods to isolate and subfractionate rat liver mitochondria. Lipid composition of the inner and outer membrane. *Biochimica et biophysica acta*, 1021(2), pp.217–226.

Hresko, R.C. & Mueckler, M., 2005. mTOR-RICTOR is the Ser473 kinase for Akt/protein kinase B in 3T3-L1 adipocytes. *Journal of Biological Chemistry*, 280(49), pp.40406–40416.

Hu, H. et al., 2010. ATM is down-regulated by N-Myc-regulated microRNA-421. *Proceedings of the National Academy of Sciences*, 107(4), pp.1506–1511.

Hu, M. et al., 2016. Metformin Protects H9C2 Cardiomyocytes from High-Glucose and Hypoxia/Reoxygenation Injury via Inhibition of Reactive Oxygen Species Generation and Inflammatory Responses: Role of AMPK and JNK. *Journal of Diabetes Research*, 2016(Article ID 2961954), pp.1–9.

Huang, S., Heikal, A.A. & Webb, W.W., 2002. Two-Photon Fluorescence Spectroscopy and Microscopy of NAD(P)H and Flavoprotein. *Biophysical Journal*, 82, pp.2811–2825.

Huisamen, B. et al., 2014. P649A possible role for the ATM protein in the myocardial pathology associated with obesity and insulin resistance. *Cardiovascular Research*, 103(suppl_1), p.S118.

Huisamen, B., 2003. Protein kinase B in the diabetic heart. *Molecular and Cellular Biochemistry*, 249(1), pp.31–38.

Huisamen, B., Donthi, R. V. & Lochner, A., 2001. Insulin in combination with Vanadate stimulates glucose transport in isolated cardiomyocytes from obese Zucker rats. *Cardiovascular Drugs and Therapy*, 15(5), pp.445–452.

Hunter, T., 1995. Protein kinases and phosphatases: the yin and yang of protein phosphorylation and signaling. *Cell*, 80(2), pp.225–236.

Huppertz, C. et al., 2001. Uncoupling Protein 3 (UCP3) Stimulates Glucose Uptake in Muscle Cells through a Phosphoinositide 3-Kinase-dependent Mechanism. *Journal of Biological Chemistry*, 276(16), pp.12520–12529.

Ikeda, Y. et al., 2009. Cardiac-specific deletion of LKB1 leads to hypertrophy and dysfunction. *Journal of Biological Chemistry*, 284(51), pp.35839–35849.

Imseng, S., Aylett, C.H. & Maier, T., 2018. Architecture and activation of phosphatidylinositol 3-kinase related kinases. *Current Opinion in Structural Biology*, 49, pp.177–189.

Itakura, E. et al., 2012. Structures containing Atg9A and the ULK1 complex independently target depolarized mitochondria at initial stages of Parkin-mediated mitophagy. *Journal of Cell Science*, 125(6), pp.1488–1499.

Jakobsen, M.U. et al., 2009. Major types of dietary fat and risk of coronary heart disease : a pooled analysis of 11 cohort studies 1 – 3. *The American Journal of Clinical Nutrition*, 89, pp.1425–1433.

Javadov, S. et al., 2011. Expression of mitochondrial fusion-fission proteins during post-infarction remodeling: The effect of NHE-1 inhibition. *Basic Research in Cardiology*, 106(1), pp.99–109.

Jawhari, S., Ratinaud, M.H. & Verdier, M., 2016. Glioblastoma, hypoxia and autophagy: A survival-prone “ménage-à-trois.” *Cell Death and Disease*, 7(10), pp.1–10.

Jeong, I. et al., 2010. Role of ataxia telangiectasia mutated in insulin signaling of muscle-derived cell lines and mouse soleus. *Acta Physiologica*, 198(4), pp.465–475.

Jeyakumar, S.M. et al., 2009. Fatty acid desaturation index correlates with body mass and adiposity indices of obesity in Wistar NIN obese mutant rat strains WNIN/Ob and

WNIN/GR-Ob. *Nutrition and Metabolism*, 6, pp.1–8.

Jheng, H.-F. et al., 2012. Mitochondrial Fission Contributes to Mitochondrial Dysfunction and Insulin Resistance in Skeletal Muscle. *Molecular and Cellular Biology*, 32(2), pp.309–319.

Jia, L. et al., 2017. Haplodeficiency of ataxia telangiectasia mutated accelerates heart failure after myocardial infarction. *Journal of the American Heart Association*, 6, p.e006349.

Jiang, X. et al., 2006. The FATC domains of PIKK proteins are functionally equivalent and participate in the Tip60-dependent activation of DNA-PKcs and ATM. *Journal of Biological Chemistry*, 281(23), pp.15741–15746.

Jiao, H. et al., 2015. Chaperone-like protein p32 regulates ULK1 stability and autophagy. *Cell Death and Differentiation*, 22(11), pp.1812–1823.

Kadenbach, B., 2003. Intrinsic and extrinsic uncoupling of oxidative phosphorylation. *Biochimica et Biophysica Acta - Bioenergetics*, 1604(2), pp.77–94.

Kahn, R. et al., 2005. The metabolic syndrome: time for a critical appraisal: joint statement from the American Diabetes Association and the European Association for the Study of Diabetes. *Diabetes Care*, 28(9), pp.2289–2304.

Kahn, S.E., Hull, R.L. & Utzschneider, K.M., 2006. Mechanisms linking obesity to insulin resistance and type 2 diabetes. *Nature*, 444(7121), pp.840–846.

Kamsler, A. et al., 2001. Increased Oxidative Stress in Ataxia Telangiectasia Evidenced by Alterations in Redox State of Brains from Atm-deficient Mice Increased Oxidative Stress in Ataxia Telangiectasia Evidenced by Alterations in Redox State of Brains from Atm-deficient Mice 1. *Cancer Research*, 61, pp.1849–1854.

Kanamori, H. et al., 2015. Autophagic adaptations in diabetic cardiomyopathy differ between type 1 and type 2 diabetes. *Autophagy*, 11(7), pp.1146–1160.

Kasahara, A. et al., 2013. Mitochondrial Fusion Directs Cardiomyocyte Differentiation via Calcineurin and Notch Signaling. *Science*, 342, pp.734–738.

Kastan, M.B. & Lim, D.S., 2000. The many substrates and functions of ATM. *Nature Reviews:*

Molecular Cell Biology, 1(3), pp.179–186.

Kato, H. et al., 2008. Identification of p32 as a novel substrate for ATM in heart. *Biochemical and Biophysical Research Communications*, 366(4), pp.885–891.

Khoronenkova, S. V. & Dianov, G.L., 2015. ATM prevents DSB formation by coordinating SSB repair and cell cycle progression. *Proceedings of the National Academy of Sciences*, 112(13), pp.3997–4002.

Kim, J. et al., 2016. AMPK activators: Mechanisms of action and physiological activities. *Experimental and Molecular Medicine*, 48(4), pp.e224-12.

Kim, J., Wei, Y. & Sowers, J.R., 2008. Role of Mitochondrial Dysfunction in Insulin Resistance. *Circulation Research*, 102, pp.401–414.

Kim, S. et al., 1999. Substrate Specificities and Identification of Putative Substrates of ATM Kinase Family Members. *Journal of Biological Chemistry*, 274(53), pp.37538–37543.

Kimes, B.W. & Brandt, B.L., 1976. Properties of a clonal muscle cell line from rat heart. *Experimental Cell Research*, 98(2), pp.367–381.

Kirichok, Y., Krapivinsky, G. & Clapham, D.E., 2004. The mitochondrial calcium uniporter is a highly selective ion channel. *Nature*, 427(6972), pp.360–4.

Kitada, T. et al., 1998. Mutations in the parkin gene cause autosomal recessive juvenile parkinsonism. *Nature*, 392, p.605.

Klionsky, D.J. et al., 2016. Guidelines for the use and interpretation of assays for monitoring autophagy (3rd edition). *Autophagy*, 12(1), pp.1–222.

Kobashigawa, L.C. et al., 2014. Metformin protects cardiomyocyte from doxorubicin induced cytotoxicity through an AMP-activated protein kinase dependent signaling pathway: An in Vitro study. *PLoS ONE*, 9(8), p.e104888.

Kobayashi, J. et al., 2015. Increased oxidative stress in AOA3 cells disturbs ATM-dependent DNA damage responses. *Mutation Research/Genetic Toxicology and Environmental Mutagenesis*, 782, pp.42–50.

Kobayashi, S. & Liang, Q., 2015. Autophagy and mitophagy in diabetic cardiomyopathy. *Biochimica et Biophysica Acta - Molecular Basis of Disease*, 1852(2), pp.252–261.

Kraft, C., Peter, M. & Hofmann, K., 2010. Selective autophagy: ubiquitin-mediated recognition and beyond. *Nature Cell Biology*, 12(9), pp.836–841.

Kroemer, G., Mariño, G. & Levine, B., 2010. Autophagy and the Integrated Stress Response. *Molecular Cell*, 40(2), pp.280–293.

Kruger, H.S. et al., 2005. Obesity in South Africa: Challenges for government and health professionals. *Public Health Nutrition*, 8(5), pp.491–500.

Kubli, D.A. et al., 2015. PINK1 is dispensable for mitochondrial recruitment of parkin and activation of mitophagy in cardiac myocytes. *PLoS ONE*, 10(6), p.e0130707.

Kubli, D.A. & Gustafsson, Å.B., 2012. Mitochondria and mitophagy: The yin and yang of cell death control. *Circulation Research*, 111(9), pp.1208–1221.

Kühlbrandt, W., 2015. Structure and function of mitochondrial membrane protein complexes. *BioMed Central Biology*, 13, pp.89–100.

Kurz, E.U., Douglas, P. & Lees-Miller, S.P., 2004. Doxorubicin activates ATM-dependent phosphorylation of multiple downstream targets in part through the generation of reactive oxygen species. *Journal of Biological Chemistry*, 279(51), pp.53272–53281.

Kuznetsov, A. V. et al., 2015. H9c2 and HL-1 cells demonstrate distinct features of energy metabolism, mitochondrial function and sensitivity to hypoxia-reoxygenation. *Biochimica et Biophysica Acta - Molecular Cell Research*, 1853(2), pp.276–284.

Kwon, B., Lee, H.K. & Querfurth, H.W., 2014. Oleate prevents palmitate-induced mitochondrial dysfunction, insulin resistance and inflammatory signaling in neuronal cells. *Biochimica et Biophysica Acta - Molecular Cell Research*, 1843(7), pp.1402–1413.

Kwon, B. & Querfurth, H.W., 2015. Palmitate activates mTOR/p70S6K through AMPK inhibition and hypophosphorylation of raptor in skeletal muscle cells: Reversal by oleate is similar to metformin. *Biochimie*, 118, pp.141–150.

Lakowicz, J.R. et al., 1992. Fluorescence lifetime imaging of free and protein-bound NADH.

Proceedings of the National Academy of Sciences, 89, pp.1271–1275.

Lau, W.C.Y. et al., 2016. Structure of the human dimeric ATM kinase. *Cell Cycle*, 15(8), pp.1117–1124.

Lavin, M.F., 2008. Ataxia-telangiectasia: from a rare disorder to a paradigm for cell signalling and cancer. *Nature reviews: Molecular Cell Biology*, 9(10), pp.759–769.

Lee, H.J. et al., 2015. Tyrosine 370 phosphorylation of ATM positively regulates DNA damage response. *Cell Research*, 25(2), pp.225–236.

Lee, J.-H. et al., 2018. ATM directs DNA damage responses and proteostasis via genetically separable pathways. *Science Signaling*, 11(512), p.eaan5598.

Lee, J.-H. & Paull, T.T., 2004. Direct activation of the ATM protein kinase by the Mre11/Rad50/Nbs1 complex. *Science*, 304(5667), pp.93–96.

Lee, J.H. et al., 2013. Ataxia Telangiectasia-Mutated (ATM) kinase activity is regulated by ATP-driven conformational changes in the Mre11/Rad50/Nbs1 (MRN) complex. *Journal of Biological Chemistry*, 288(18), pp.12840–12851.

Lee, Y. et al., 2011. Mitochondrial autophagy by Bnip3 involves Drp1-mediated mitochondrial fission and recruitment of Parkin in cardiac myocytes. *American Journal of Physiology - Heart and Circulatory Physiology*, 301(5), pp.H1924–H1931.

Van Leeuwen, N. et al., 2012. A gene variant near ATM is significantly associated with metformin treatment response In type 2 diabetes: A replication and meta-analysis of five cohorts. *Diabetologia*, 55(7), pp.1971–1977.

Leopoldo, A.S. et al., 2016. Classification of different degrees of adiposity in sedentary rats. *Brazilian Journal of Medical and Biological Research*, 49(4), pp.1–9.

Lesnefsky, E.J. et al., 2004. Blockade of electron transport during ischemia protects cardiac mitochondria. *Journal of Biological Chemistry*, 279(46), pp.47961–47967.

Lesnefsky, E.J. et al., 2001. Mitochondrial Dysfunction in Cardiac Disease : Ischemia – Reperfusion , Aging , and Heart Failure. *Journal of Molecular and Cellular Cardiology*, 33, pp.1065–1089.

Li, R. et al., 2017. ATM signals to AMPK to promote autophagy and positively regulate DNA damage in response to cadmium-induced ROS in mouse spermatocytes. *Environmental Pollution*, 231, pp.1560–1568.

Li, X. et al., 2009. Activation of the AMPK-FOXO3 Pathway Reduces Fatty Acid – Induced Increase in Intracellular Reactive Oxygen Species by Upregulating Thioredoxin. *Diabetes*, 58, pp.2246–2257.

Liang, Q. & Kobayashi, S., 2016. Mitochondrial quality control in the diabetic heart. *Journal of Molecular and Cellular Cardiology*, 95, pp.57–69.

Liu, T. et al., 2015. High-fat diet alters serum fatty acid profiles in obesity prone rats : implications for in-vitro studies. *Lipids*, 50(10), pp.997–1008.

Llorca, O. et al., 2003. Electron microscopy and 3D reconstructions reveal that human ATM kinase uses an arm-like domain to clamp around double-stranded DNA. *Oncogene*, 22(25), pp.3867–3874.

Lopaschuk, G.D. et al., 2010. Myocardial fatty acid metabolism in health and disease. *Physiological Reviews.*, 90, pp.207–258.

Lowry, O.H. et al., 1951. Protein measurement with the Folin henol reagent. *Journal of Biological Chemistry*, 193(1), pp.265–275.

Martin, O.J. et al., 2014. A Role for PGC-1 Coactivators in the Control of Mitochondrial Dynamics during Postnatal Cardiac Growth. *Circulation Research*, 114(4), pp.626–636.

Matsuoka, S. et al., 2007. ATM and ATR substrate analysis reveals extensive protein networks responsive to DNA damage. *Science*, 316(5828), pp.1160–1166.

Mayevsky, A. & Barbiro-Michaely, E., 2009. Use of NADH fluorescence to determine mitochondrial function in vivo. *The International Journal of Biochemistry & Cell Biology*, 41(10), pp.1977–1988.

Mayosi, B.M. et al., 2009. The burden of non-communicable diseases in South Africa. *The Lancet*, 374(9693), pp.934–947.

Melser, S., Lavie, J. & Bénard, G., 2015. Mitochondrial degradation and energy metabolism.

Biochimica et Biophysica Acta - Molecular Cell Research, 1853(10), pp.2812–2821.

Menard, C. et al., 1999. Modulation of L-type calcium channel expression during retinoic acid- induced differentiation of H9C2 cardiac cells. *Journal of Biological Chemistry*, 274, pp.29063–29070.

Mercer, J.R. et al., 2010. DNA damage links mitochondrial dysfunction to atherosclerosis and the metabolic syndrome. *Circulation Research*, 107(8), pp.1021–1031.

Mercer, J.R. et al., 2012. The mitochondria-targeted antioxidant MitoQ decreases features of the metabolic syndrome in ATM +/-/ApoE -/- mice. *Free Radical Biology and Medicine*, 52(5), pp.841–849.

Micklesfield, L.K. et al., 2013. Socio-cultural, environmental and behavioural determinants of obesity in black South African women. *Cardiovascular Journal of Africa*, 24(9–10), pp.369–75.

Mongiardi, M.P. et al., 2011. Oxygen sensing is impaired in ATM-defective cells. *Cell Cycle*, 10(24), pp.4311–4320.

Morita, A. et al., 2014. Mitochondria are required for ATM activation by extranuclear oxidative stress in cultured human hepatoblastoma cell line Hep G2 cells. *Biochemical and Biophysical Research Communications*, 443(4), pp.1286–1290.

Morrish, F. et al., 2006. Thyroid hormone receptor isoforms localize to cardiac mitochondrial matrix with potential for binding to receptor elements on mtDNA. *Mitochondrion*, 6(3), pp.143–148.

Moyzis, A.G., Sadoshima, J. & Gustafsson, Å.B., 2015. Mending a broken heart: the role of mitophagy in cardioprotection. *American Journal of Physiology. Heart and Circulatory Physiology*, 308(3), pp.H183-92.

Nabben, M. et al., 2011. Significance of uncoupling protein 3 in mitochondrial function upon mid- and long-term dietary high-fat exposure. *Federation of American Societies for Experimental Biology Letters*, 585(24), pp.4010–4017.

Narendra, D.P. et al., 2010. p62/SQSTM1 is required for Parkin-induced mitochondrial

clustering but not mitophagy; VDAC1 is dispensable for both. *Autophagy*, 6(8), pp.1090–1106.

Nazio, F. & Cecconi, F., 2017. Autophagy up and down by outsmarting the incredible ULK. *Autophagy*, 13(5), pp.967–968.

Nguyen, T.N., Padman, B.S. & Lazarou, M., 2016. Deciphering the Molecular Signals of PINK1/Parkin Mitophagy. *Trends in Cell Biology*, 26(10), pp.733–744.

Nickel, A.G. et al., 2015. Reversal of mitochondrial transhydrogenase causes oxidative stress in heart failure. *Cell Metabolism*, 22(3), pp.472–484.

Van Nieuwenhoven, F. a et al., 1998. Stable transfection of fatty acid translocase (CD36) in a rat heart muscle cell line (H9c2). *Journal of Lipid Research*, 39(10), pp.2039–47.

Nishida, K. et al., 2009. The role of autophagy in the heart. *Cell Death and Differentiation*, 16, pp.31–38.

Nobuhara, M. et al., 2013. Mitochondrial dysfunction caused by saturated fatty acid loading induces myocardial insulin-resistance in differentiated H9c2 myocytes: A novel ex vivo myocardial insulin-resistance model. *Experimental Cell Research*, 319(7), pp.955–966.

O'Neill, H.M., 2013. AMPK and exercise: Glucose uptake and insulin sensitivity. *Diabetes and Metabolism Journal*, 37(1), pp.1–21.

Ohlendieck, K. et al., 1986. Enrichment and biochemical characterization of boundary membrane contact sites from rat-liver mitochondria. *Biochimica et Biophysica Acta*, 860, pp.672–689.

Opie, L.H., 2004. *Heart physiology : from cell to circulation* 4th ed., Philadelphia: Lippincott Williams & Wilkins.

Ousset, M. et al., 2010. Loss of ATM positively regulates the expression of hypoxia inducible factor 1 (HIF-1) through oxidative stress: Role in the physiopathology of the disease. *Cell Cycle*, 9(14), pp.2814–2822.

Ouwens, D.M. et al., 2007. Cardiac contractile dysfunction in insulin-resistant rats fed a high-fat diet is associated with elevated CD36-mediated fatty acid uptake and esterification.

Diabetologia, 50(9), pp.1938–1948.

Owen, M.R., Doran, E. & Halestrap, A.P., 2000. Evidence that metformin exerts its anti-diabetic effects through inhibition of complex 1 of the mitochondrial respiratory chain. *The Biochemical Journal*, 348 Pt 3, pp.607–614.

Palomer, X. et al., 2018. Palmitic and Oleic Acid: The Yin and Yang of Fatty Acids in Type 2 Diabetes Mellitus. *Trends in Endocrinology and Metabolism*, 29(3), pp.178–190.

Papanicolaou, K.N. et al., 2011. Mitofusin-2 maintains mitochondrial structure and contributes to stress-induced permeability transition in cardiac myocytes. *Molecular and Cellular Biology*, 31(6), pp.1309–1328.

Parra, V. et al., 2014. Insulin stimulates mitochondrial fusion and function in cardiomyocytes via the Akt-mTOR-NFkB-Opa-1 signaling pathway. *Diabetes*, 63(1), pp.75–88.

Patel, A.Y. et al., 2011. Ataxia telangiectasia mutated influences cytochrome c oxidase activity. *Biochemical and Biophysical Research Communications*, 405(4), pp.599–603.

Patel, R.P. et al., 1999. Biological aspects of reactive nitrogen species. *Biochimica et Biophysica Acta - Bioenergetics*, 1411(2–3), pp.385–400.

Patten, V. et al., 2017. Cardiomyocyte differentiation: Experience and observations from 2 laboratories. *South African Heart Journal*, 14(2), pp.96–107.

Paull, T.T., 2015. Mechanisms of ATM Activation. *Annual Review of Biochemistry*, 84(1), pp.711–738.

Pawlak, D.B., Kushner, J.A. & Ludwig, D.S., 2004. Effects of dietary glycaemic index on adiposity, glucose homeostasis and plasma lipids in animals. *Lancet*, 364, pp.778–785.

Pellegrini, M. et al., 2006. Autophosphorylation at serine 1987 is dispensable for murine Atm activation in vivo. *Nature*, 443, pp.222–225.

Perdomo, L. et al., 2015. Protective role of oleic acid against cardiovascular insulin resistance and in the early and late cellular atherosclerotic process. *Cardiovascular Diabetology*, 14(75–87).

Pickup, J.D. & Pugh, R.J., 1960. FAMILIAL ATAXIA-TELANGIECTASIA. *Archives of Disease in Childhood*, 36(187), pp.344–346.

Pilz, S. et al., 2006. Free Fatty Acids Are Independently Associated with All-Cause and Cardiovascular Mortality in Subjects with Coronary Artery Disease. *The Journal of Clinical Endocrinology & Metabolism*, 91(7), pp.2542–2547.

Podrez, E.A. et al., 1999. Myeloperoxidase-generated reactive nitrogen species convert LDL into an atherogenic form in vitro. *Journal of Clinical Investigation*, 103(11), pp.1547–1560.

Pollak, N., Niere, M. & Ziegler, M., 2007. NAD kinase levels control the NADPH concentration in human cells. *Journal of Biological Chemistry*, 282(46), pp.33562–33571.

Powrie, J.K. et al., 1993. Effects of chloroquine on the dyslipidemia of non-insulin-dependent diabetes mellitus. *Metabolism*, 42(4), pp.415–419.

Powrie, J.K. et al., 1991. Mode of action of chloroquine in patients with non-insulin-dependent diabetes mellitus. *American Journal of Physiology-Endocrinology and Metabolism*, 260(6), pp.E897–E904.

Qatanani, M. & Lazar, M.A., 2007. Mechanisms of obesity-associated insulin resistance: Many choices on the menu. *Genes and Development*, 21(12), pp.1443–1455.

Qi, Y. et al., 2016. ATM mediates spermidine-induced mitophagy via PINK1 and Parkin regulation in human fibroblasts. *Scientific Reports*, 6, p.24700.

Qian, W. et al., 2012. Mitochondrial hyperfusion induced by loss of the fission protein Drp1 causes ATM-dependent G2/M arrest and aneuploidy through DNA replication stress. *Journal of Cell Science*, 125(23), pp.5745–5757.

Razani, B., Feng, C. & Semenkovich, C.F., 2010. P53 Is Required for Chloroquine-Induced Atheroprotection But Not Insulin Sensitization. *The Journal of Lipid Research*, 51(7), pp.1738–1746.

Redmann, M. et al., 2017. Inhibition of autophagy with bafilomycin and chloroquine decreases mitochondrial quality and bioenergetic function in primary neurons. *Redox*

Biology, 11, pp.73–81.

Ren, J. et al., 2010. Mitochondrial biogenesis in the metabolic syndrome and cardiovascular disease. *Journal of Molecular Medicine*, 88, pp.993–1001.

Ren, Y. et al., 2017. Adiponectin modulates oxidative stress-induced mitophagy and protects C2C12 myoblasts against apoptosis. *Scientific Reports*, 7, p.3209.

Rikka, S. et al., 2011. Bnip3 impairs mitochondrial bioenergetics and stimulates mitochondrial turnover. *Cell Death and Differentiation*, 18(4), pp.721–731.

Ritov, V.B. et al., 2005. Deficiency of subsarcolemmal mitochondria in obesity and type 2 diabetes. *Diabetes*, 54(1), pp.8–14.

Rivera-Calzada, A. et al., 2015. Structure and Assembly of the PI3K-like Protein Kinases (PIKKs) Revealed by Electron Microscopy. *American Institute of Mathematical Sciences Biophysics*, 2(2), pp.36–57.

Rivero-Gutiérrez, B. et al., 2014. Stain-free detection as loading control alternative to Ponceau and housekeeping protein immunodetection in Western blotting. *Analytical Biochemistry*, 467, pp.1–3.

Roberts, C.K. & Sindhu, K.K., 2009. Oxidative stress and metabolic syndrome. *Life Sciences*, 84(21–22), pp.705–712.

Roberts Stein, L. & Shin-ichiro, I., 2012. The dynamic regulation of NAD metabolism in mitochondria. *Trends in Endocrinology & Metabolism*, 23(9), pp.420–428.

Rodriguez-Sinovas, A. et al., 2006. Translocation of connexin 43 to the inner mitochondrial membrane of cardiomyocytes through the heat shock protein 90-dependent TOM pathway and its importance for cardioprotection. *Circulation Research*, 99(1), pp.93–101.

Rosca, M.G. et al., 2008. Cardiac mitochondria in heart failure: Decrease in respirasomes and oxidative phosphorylation. *Cardiovascular Research*, 80(1), pp.30–39.

Rosca, M.G. et al., 2012. Oxidation of fatty acids is the source of increased mitochondrial reactive oxygen species production in kidney cortical tubules in early diabetes.

Diabetes, 61(8), pp.2074–2083.

Rosca, M.G. & Hoppel, C.L., 2010. Mitochondria in heart failure. *Cardiovascular Research*, 88(1), pp.40–50.

Rösen, P. & Wiernsperger, N.F., 2006. Metformin delays the manifestation of diabetes and vascular dysfunction in Goto-Kakizaki rats by reduction of mitochondrial oxidative stress. *Diabetes/Metabolism Research and Reviews*, 22(4), pp.323–330.

Rotman, G. & Shiloh, Y., 1998. ATM: From gene to function. *Human Molecular Genetics*, 7(10), pp.1555–1563.

Ryu, S.-Y. et al., 2011. Single channel characterization of the mitochondrial ryanodine receptor in heart mitoplasts. *The Journal of Biological Chemistry*, 286(24), pp.21324–21329.

Salie, R., Huisamen, B. & Lochner, A., 2014. High carbohydrate and high fat diets protect the heart against ischaemia / reperfusion injury. *Cardiovascular Diabetology*, 13, pp.109–121.

Sapkota, G.P. et al., 2002. (ATM) -mediated phosphorylation of LKB1 / STK11 at Thr-366. *Biochemical Journal*, 516, pp.507–516.

Sarbassov, D.D. et al., 2005. Phosphorylation and Regulation of Akt / PKB by the Rictor-mTOR Complex. *Science*, 307, pp.1098–1101.

Sardão, V.A. et al., 2009. Morphological alterations induced by doxorubicin on H9c2 myoblasts: Nuclear, mitochondrial, and cytoskeletal targets. *Cell Biology and Toxicology*, 25(3), pp.227–243.

Sarkaria, J.N. et al., 1999. Inhibition of ATM and ATR kinase activities by the radiosensitizing agent, caffeine. *Cancer Research*, 59(17), pp.4375–4382.

Savitsky, K., Bar-Shira, A., et al., 1995a. A single ataxia telangiectasia gene with a product similar to PI-3 kinase. *Science*, 268(5218), pp.1749–1753.

Savitsky, K., Sfez, S., et al., 1995b. The complete sequence of the coding region of the ATM gene reveals similarity to cell cycle regulators in different species. *Human Molecular*

Genetics, 4(11), pp.2025–2032.

Sazanov, L.A., 2015. A giant molecular proton pump: Structure and mechanism of respiratory complex I. *Nature Reviews: Molecular Cell Biology*, 16(6), pp.375–388.

Scheffler, I.E., 2001. A century of mitochondrial research: Achievements and perspectives. *Mitochondrion*, 1(1), pp.3–31.

Schnaitman, C., Erwin, V.G. & Greenawalt, J.W., 1967. The submitochondrial localization of monoamine oxidase: an enzymatic marker for the outer membrane of rat liver mitochondria. *The Journal of Cell Biology*, 32, pp.719–735.

Schnaitman, C. & Greenawalt, J.W., 1968. Enzymatic properties of the inner and outer membranes of rat liver mitochondria. *The Journal of Cell Biology*, 38(1), pp.158–175.

Schneider, J.G. et al., 2006. ATM-dependent suppression of stress signaling reduces vascular disease in metabolic syndrome. *Cell Metabolism*, 4(5), pp.377–389.

Schon, E.A. & Manfredi, G., 2003. Neuronal degeneration and mitochondrial dysfunction. *Journal of Clinical Investigation*, 111(3), pp.303–312.

Schubert, R., Reichenbach, J. & Zielen, S., 2005. Growth factor deficiency in patients with ataxia telangiectasia. *Clinical and Experimental Immunology*, 140(3), pp.517–519.

Semlitsch, M. et al., 2011. ATM protects against oxidative stress induced by oxidized low-density lipoprotein. *DNA Repair*, 10(8), pp.848–860.

Serpillon, S. et al., 2009. Superoxide production by NAD(P)H oxidase and mitochondria is increased in genetically obese and hyperglycemic rat heart and aorta before the development of cardiac dysfunction. The role of glucose-6-phosphate dehydrogenase-derived NADPH. *American Journal of Physiology - Heart and Circulatory Physiology*, 297(1), pp.H153–H162.

Shackelford, R.E. et al., 2001. The Ataxia telangiectasia Gene Product Is Required for Oxidative Stress-induced G1 and G2 Checkpoint Function in Human Fibroblasts. *Journal of Biological Chemistry*, 276(24), pp.21951–21959.

Shadel, G.S., 2008. Expression and maintenance of mitochondrial DNA: new insights into

human disease pathology. *The American Journal of Pathology*, 172(6), pp.1445–1456.

Shadel, G.S. & Horvath, T.L., 2015. Mitochondrial ROS Signaling in Organismal Homeostasis. *Cell*, 163(3), pp.560–569.

Shao, D. & Tian, R., 2016. Glucose Transporters in Cardiac Metabolism and Hypertrophy. *Comprehensive Physiology*, 6(1), pp.331–351.

Sharick, J.T. et al., 2018. Protein-bound NAD(P)H Lifetime is Sensitive to Multiple Fates of Glucose Carbon. *Scientific Reports*, 8(1), pp.1–13.

Sharma, N.K. et al., 2014. Intrinsic mitochondrial DNA repair defects in ataxia telangiectasia. *DNA Repair*, 13(1), pp.22–31.

Shaw, R.J. et al., 2004. The tumor suppressor LKB1 kinase directly activates AMP-activated kinase and regulates apoptosis in response to energy stress. *Proceedings of the National Academy of Sciences*, 101(10), pp.3329–3335.

Shen, C. & Houghton, P.J., 2013. The mTOR pathway negatively controls ATM by up-regulating miRNAs. *Proceedings of the National Academy of Sciences*, 110(29), pp.11869–74.

Shiloh, Y., 2001. ATM and ATR: Networking cellular responses to DNA damage. *Current Opinion in Genetics and Development*, 11(1), pp.71–77.

Shiloh, Y., 2003. ATM and related protein kinases: safeguarding genome integrity. *Nature reviews: Cancer*, 3(3), pp.155–168.

Shiloh, Y., 2006. The ATM-mediated DNA-damage response: taking shape. *Trends in Biochemical Sciences*, 31(7), pp.402–410.

Shiloh, Y. & Ziv, Y., 2012. The ATM protein: The importance of being active. *Journal of Cell Biology*, 198(3), pp.273–275.

Shiloh, Y. & Ziv, Y., 2013. The ATM protein kinase: regulating the cellular response to genotoxic stress, and more. *Nature Reviews: Molecular Cell Biology*, 14(4), pp.197–210.

Shintani, T. & Klionsky, D.J., 2004. Autophagy in Health and Disease: A Double-Edged Sword.

Science, 306(5698), pp.990–995.

Sileikyte, J. et al., 2011. Regulation of the inner membrane mitochondrial permeability transition by the outer membrane translocator protein (peripheral benzodiazepine receptor). *Journal of Biological Chemistry*, 286(2), pp.1046–1053.

Skala, M.C. et al., 2007a. In vivo Multiphoton Fluorescence Lifetime Imaging of Protein-bound and Free NADH in Normal and Pre-cancerous Epithelia. *Journal of Biomedical Optics*, 12(2), p.024014.

Skala, M.C. et al., 2007b. In vivo multiphoton microscopy of NADH and FAD redox states, fluorescence lifetimes, and cellular morphology in precancerous epithelia. *Proceedings of the National Academy of Sciences*, 104(49), pp.19494–19499.

So, S., Davis, A.J. & Chen, D.J., 2009. Autophosphorylation at serine 1981 stabilizes ATM at DNA damage sites. *Journal of Cell Biology*, 187(7), pp.977–990.

Söhnel, A.-C. et al., 2016. Probing of protein localization and shuttling in mitochondrial microcompartments by FLIM with sub-diffraction resolution. *Biochimica et Biophysica Acta (BBA) - Bioenergetics*, 1857(8), pp.1290–1299.

Solinas, G. & Becattini, B., 2017. JNK at the crossroad of obesity, insulin resistance, and cell stress response. *Molecular Metabolism*, 6(2), pp.174–184.

Sordahl, L.A. et al., 1972. The Mitochondrion. *Methods in Pharmacology*, 67, pp.417–440.

Soutar, M.P.M. et al., 2018. AKT signalling selectively regulates PINK1 mitophagy in SHSY5Y cells and human iPSC-derived neurons. *Scientific Reports*, 8, p.8855.

Sparks, L.M. et al., 2005. A High-Fat Diet Coordinately Downregulates Genes Required for Mitochondrial Oxidative Phosphorylation in Skeletal Muscle. *Diabetes*, 54, pp.1926–1933.

Srisakuldee, W. et al., 2014. The FGF-2-triggered protection of cardiac subsarcolemmal mitochondria from calcium overload is mitochondrial connexin 43-dependent. *Cardiovascular Research*, 103(1), pp.72–80.

Srivastava, S., 2016. Emerging therapeutic roles for NAD+ metabolism in mitochondrial and

age-related disorders. *Clinical and Translational Medicine*, 5(1), p.25.

Stagni, V., Cirotti, C. & Barilà, D., 2018. Ataxia-Telangiectasia Mutated Kinase in the Control of Oxidative Stress, Mitochondria, and Autophagy in Cancer: A Maestro With a Large Orchestra. *Frontiers in Oncology*, 8, pp.73–79.

Stagni, V., Santini, S. & Barilà, D., 2013. *Genetic disorders; Chapter 7: Molecular Bases of Ataxia Telangiectasia : One Kinase Multiple Functions*. IntechOpen (ed.Maria Puiu)

Stanley, W.C., Recchia, F.A. & Lopaschuk, G., 2005. The role of fatty acid oxidation in cardiac ischemia and reperfusion. *Physiological Reviews*, 85, pp.1093–1129.

Stern, N. et al., 2002. Accumulation of DNA damage and reduced levels of nicotine adenine dinucleotide in the brains of Atm-deficient mice. *Journal of Biological Chemistry*, 277(1), pp.602–608.

Stewart-Ornstein, J. & Lahav, G., 2017. P53 dynamics in response to DNA damage vary across cell lines and are shaped by efficiency of DNA repair and activity of the kinase ATM. *Science Signaling*, 1, p.eaah6671.

Storozhuk, Y. et al., 2013. Metformin inhibits growth and enhances radiation response of non-small cell lung cancer (NSCLC) through ATM and AMPK. *British Journal of Cancer*, 108, pp.2021–32.

Stubbs, C.D. et al., 2005. The use of time-resolved fluorescence imaging in the study of protein kinase C localisation in cells. *BioMed Central Cell Biology*, 6, pp.22–35.

Stuck, B.J. et al., 2008. Metabolic switch and hypertrophy of cardiomyocytes following treatment with angiotensin II are prevented by AMP-activated protein kinase. *Journal of Biological Chemistry*, 283(47), pp.32562–32569.

Stump, C.S. et al., 2003. Effect of insulin on human skeletal muscle mitochondrial ATP production , protein synthesis , and mRNA transcripts. *Proceedings of the National Academy of Sciences*, 100(13), pp.7996–8001.

Su, Y. & Swift, M., 2000. Mortality Rates among Carriers of Ataxia-Telangiectasia Mutant Alleles. *Annals of Internal Medicine*, 133(10), pp.770–778.

Sullivan, K.D., Palaniappan, V. V & Espinosa, J.M., 2015. ATM regulates cell fate choice upon p53 activation by modulating mitochondrial turnover and ROS levels. *Cell Cycle*, 14(1), pp.56–63.

Sun, Y. et al., 2007. DNA Damage-Induced Acetylation of Lysine 3016 of ATM Activates ATM Kinase Activity. *Molecular and Cellular Biology*, 27(24), pp.8502–8509.

Sun, Y. et al., 2009. Histone H3 methylation links DNA damage detection to activation of the tumour suppressor Tip60. *Nature Cell Biology*, 11(11), pp.1376–1382.

Suzuki, A. et al., 2004. IGF-1 phosphorylates AMPK-α subunit in ATM-dependent and LKB1-independent manner. *Biochemical and Biophysical Research Communications*, 324(3), pp.986–992.

Syllaba, L. & Henner, K., 1926. Contribution a l'independance de l'athetose double idiopathique et congenitale. *Revue Neurologique (Paris)*, 1, pp.541–62.

Takagi, M. et al., 2015. ATM Regulates Adipocyte Differentiation and Contributes to Glucose Homeostasis. *Cell Reports*, 10(6), pp.957–967.

Taylor, A.M.R. et al., 2015. Ataxia telangiectasia: More variation at clinical and cellular levels. *Clinical Genetics*, 87(3), pp.199–208.

Thomas, R.L., Kubli, D.A. & Gustafsson, Å.B., 2011. Bnip3-mediated defects in oxidative phosphorylation promote mitophagy. *Autophagy*, 7(7), pp.775–777.

Tian, W. et al., 2015. Phosphorylation of ULK1 by AMPK regulates translocation of ULK1 to mitochondria and mitophagy. *Federation of European Biochemical Societies* (*FEBS) Letters*, 589(15), pp.1847–1854.

Tomimatsu, N. et al., 2007. Ku70/80 modulates ATM and ATR signaling pathways in response to DNA double strand breaks. *Journal of Biological Chemistry*, 282(14), pp.10138–10145.

Tong, M. & Sadoshima, J., 2016. Mitochondrial autophagy in cardiomyopathy. *Current Opinion in Genetics and Development*, 38, pp.8–15.

Tripathi, D.N. et al., 2016. A new role for ATM in selective autophagy of peroxisomes

(pexophagy). *Autophagy*, 12(4), pp.711–712.

Tripathi, D.N. et al., 2013. Reactive nitrogen species regulate autophagy through ATM-AMPK-TSC2-mediated suppression of mTORC1. *Proceedings of the National Academy of Sciences*, 110(32), pp.E2950-7.

Tsai, W.-B. et al., 2008. Functional interaction between FOXO3a and ATM regulates DNA damage response. *Nat Cell Biol*, 10(4), pp.460–467.

Tsuruta, F., Masuyama, N. & Gotoh, Y., 2002. The phosphatidylinositol 3-kinase (PI3K)-Akt pathway suppresses Bax translocation to mitochondria. *Journal of Biological Chemistry*, 277(16), pp.14040–14047.

Tzagoloff, A., 1982. *Mitochondria*, Plenum Press (Springer Science and Business press), New York and London.

Ubhayasekera, S.J.K.A. et al., 2013. Free fatty acid determination in plasma by GC-MS after conversion to Weinreb amides. *Analytical and Bioanalytical Chemistry*, 405(6), pp.1929–1935.

Ussher, J. et al., 2009. Role of the atypical protein kinase Cζ in regulation of 5'-AMP-activated protein kinase in cardiac and skeletal muscle. *American Journal of Physiology-Endocrinology and Metabolism*, 297(2), pp.E349–E357.

Uziel, T. et al., 1996. Genomic Organization of the ATM Gene. *Genomics*, 33(0201), pp.317–320.

Valente, E.M. et al., 2004. Hereditary Early-Onset Parkinsons Disease Caused by Mutations in PINK1. *Science*, 304(5674), pp.1158–1160.

Valentin-Vega, Y.A. et al., 2012. Mitochondrial dysfunction in ataxia-telangiectasia. *Blood*, 119(6), pp.1490–1500.

Vásquez-Trincado, C. et al., 2016. Mitochondrial dynamics, mitophagy and cardiovascular disease. *Journal of Physiology*, 594(3), pp.509–525.

Venter, H. et al., 1991. Myocardial Membrane Cholesterol: Effects of Ischaemia. *Journal of Molecular and Cellular Cardiology*, 23, pp.1271–1286.

Vidal-Puig, A.J. et al., 2000. Energy Metabolism in Uncoupling Protein 3 Gene Knockout Mice. *Journal of Biological Chemistry*, 275(21), pp.16258–16266.

Viniegra, J.G. et al., 2004. Full activation of PKB?Akt in response to insulin or ionizing radiation is mediated through ATM. *Journal of Biological Chemistry*, 280, pp.4029–4036.

Viniegra, J.G. et al., 2005. Full activation of PKB/Akt in response to insulin or ionizing radiation is mediated through ATM. *Journal of Biological Chemistry*, 280(6), pp.4029–4036.

Vishwasrao, H.D. et al., 2005. Conformational dependence of intracellular NADH on metabolic state revealed by associated fluorescence anisotropy. *Journal of Biological Chemistry*, 280(26), pp.25119–25126.

Vorster, H.H., 2002. The emergence of cardiovascular disease during urbanisation of Africans. *Public Health Nutrition*, 5(1A), pp.239–243.

Wakita, M., Nishimura, G. & Tamura, M., 1995. Some characteristics of the fluorescence lifetime of reduced pyridine nucleotides in isolated mitochondria, isolated hepatocytes, and perfused rat liver In Situ. *Journal of Biochemistry*, 118(6), pp.1151–1160.

Wang, Y. et al., 2017. Saturated palmitic acid induces myocardial inflammatory injuries through direct binding to TLR4 accessory protein MD2. *Nature Communications*, 8, pp.1–13.

Watkins, S.J., Borthwick, G.M. & Arthur, H.M., 2011. The H9C2 cell line and primary neonatal cardiomyocyte cells show similar hypertrophic responses in vitro. *In Vitro Cellular Developmental Biology-Animal*, 47, pp.125–131.

Watt, M.J. et al., 2006. Fatty acids stimulate AMP-activated protein kinase and enhance fatty acid oxidation in L6 myotubes. *Journal of Physiology*, 574(1), pp.139–147.

Watters, D. et al., 1999. Localization of a portion of extranuclear ATM to peroxisomes. *Journal of Biological Chemistry*, 274(48), pp.34277–34282.

Watters, D.J., 2003. Oxidative stress in ataxia telangiectasia. *Redox Report*, 8(1), pp.23–29.

Wei, C.D. et al., 2013. Palmitate induces H9c2 cell apoptosis by increasing reactive oxygen species generation and activation of the ERK1/2 signaling pathway. *Molecular Medicine Reports*, 7(3), pp.855–861.

Wei, H., Liu, L. & Chen, Q., 2015. Selective removal of mitochondria via mitophagy: Distinct pathways for different mitochondrial stresses. *Biochimica et Biophysica Acta - Molecular Cell Research*, 1853(10), pp.2784–2790.

Westermeier, F., Navarro-Marquez, M., López-Crisosto, C., et al., 2015. Defective insulin signaling and mitochondrial dynamics in diabetic cardiomyopathy. *Biochimica et Biophysica Acta (BBA) - Molecular Cell Research*, 1853(5), pp.1113–1118.

Weyemi, U. et al., 2015. NADPH oxidase 4 is a critical mediator in Ataxia telangiectasia disease. *Proceedings of the National Academy of Sciences*, 112(7), pp.2121–2126.

Williams, G.S.B., Boyman, L. & Lederer, W.J., 2015. Mitochondrial calcium and the regulation of metabolism in the heart. *Journal of Molecular and Cellular Cardiology*, 78, pp.35–45.

Witek, P. et al., 2016. The effect of a number of H9C2 rat cardiomyocytes passage on repeatability of cytotoxicity study results. *Cytotechnology*, 68(6), pp.2407–2415.

Wu, W. et al., 2014. ULK1 translocates to mitochondria and phosphorylates FUNDC1 to regulate mitophagy. *European Molecular Biology Organization Reports*, 15(5), pp.566–575.

Xiao, B. et al., 2017. Reactive oxygen species trigger Parkin/PINK1 pathway–dependent mitophagy by inducing mitochondrial recruitment of Parkin. *Journal of Biological Chemistry*, 292(40), pp.16697–16708.

Yadav, R.B. et al., 2013. mTOR direct interactions with Rheb-GTPase and raptor: sub-cellular localization using fluorescence lifetime imaging. *BioMed Central Cell Biology*, 14(1), p.3.

Yamano, K., Matsuda, N. & Tanaka, K., 2016. The ubiquitin signal and autophagy: an orchestrated dance leading to mitochondrial degradation. *European Molecular Biology Organization Reports*, 17(3), pp.300–316.

Yang, D.-Q. & Kastan, M.B., 2000. Participation of ATM in insulin signalling through

phosphorylation of eIF-4E-binding protein 1. *Nature Cellular Bioliogy*, 2(12), pp.893–898.

Yang, J.-Y. et al., 2009. Insulin stimulates Akt translocation to mitochondria: Implications on dysregulation of mitochondrial oxidative phosphorylation in diabetic myocardium. *Journal of Molecular and Cellular Cardiology*, 46(6), pp.1–20.

Yang, J. & Holman, G.D., 2006. Long-term metformin treatment stimulates cardiomyocyte glucose transport through an AMP-activated protein kinase-dependent reduction in GLUT4 endocytosis. *Endocrinology*, 147(6), pp.2728–36.

Yee, S.W., Chen, L. & Giacomini, K.M., 2012. The role of ATM in response to metformin treatment and activation of AMPK. *Nature Genetics*, 44(4), pp.359–360.

Yu, Q. & Heikal, A.A., 2009. Two-photon autofluorescence dynamics imaging reveals sensitivity of intracellular NADH concentration and conformation to cell physiology at the single-cell level. *Journal of Photochemistry and Photobiology B: Biology*, 95(1), pp.46–57.

Yusuf, S. et al., 2001. Clinical Cardiology : New Frontiers Global Burden of Cardiovascular Diseases. *American Heart Association Journal*, 104, pp.2746–2753.

Zakikhani, M. et al., 2012. Alterations in Cellular Energy Metabolism Associated with the Antiproliferative Effects of the ATM Inhibitor KU-55933 and with Metformin. *PLoS ONE*, 7(11), p.e49513.

Zhan, H. et al., 2016. Ataxia telangiectasia mutated in cardiac fibroblasts regulates doxorubicin-induced cardiotoxicity. *Cardiovascular Research*, 110(1), pp.85–95.

Zhang, J. et al., 2013. A TSC signaling node at the peroxisome regulates mTORC1 and autophagy in response to ROS. *Nature Cell Biology*, 15(10), pp.1186–1196.

Zhang, J. et al., 2015. ATM functions at the peroxisome to induce pexophagy in response to ROS. *Nature Cell Biology*, 17(10), pp.1259–1269.

Zhang, J. et al., 2015. Supp info: ATM functions at the peroxisome to induce pexophagy in response to ROS. *Nature Cell Biology*, 13267, pp.1–18.

Zhang, J. & Ney, P.A., 2009. Role of BNIP3 and NIX in cell death, autophagy, and mitophagy. *Cell Death and Differentiation*, 16(7), pp.939–946.

Zhang, Y. et al., 2018. Mitochondrial redox sensing by the kinase ATM maintains cellular antioxidant capacity. *Science Signaling*, 11, p.eaaq0702.

Zhou, G. et al., 2001. Role of AMP-activated protein kinase in mechanism of metformin action. *The Journal of clinical investigation*, 108(8), pp.1167–74.

Zhou, K. et al., 2011. Common variants near ATM are associated with glycemic response to metformin in type 2 diabetes. *Nature genetics*, 43(2), pp.117–120.

Zhou, Q. et al., 2016. Chloroquine increases glucose uptake via enhancing GLUT4 translocation and fusion with the plasma membrane in L6 cells. *Cellular Physiology and Biochemistry*, 38(5), pp.2030–2040.

Zhou, Y. et al., 2017. Regulation of the DNA Damage Response by DNA-PKcs Inhibitory Phosphorylation of ATM. *Molecular Cell*, 65(1), pp.91–104.

Addendum A: Chapter 4 additional information

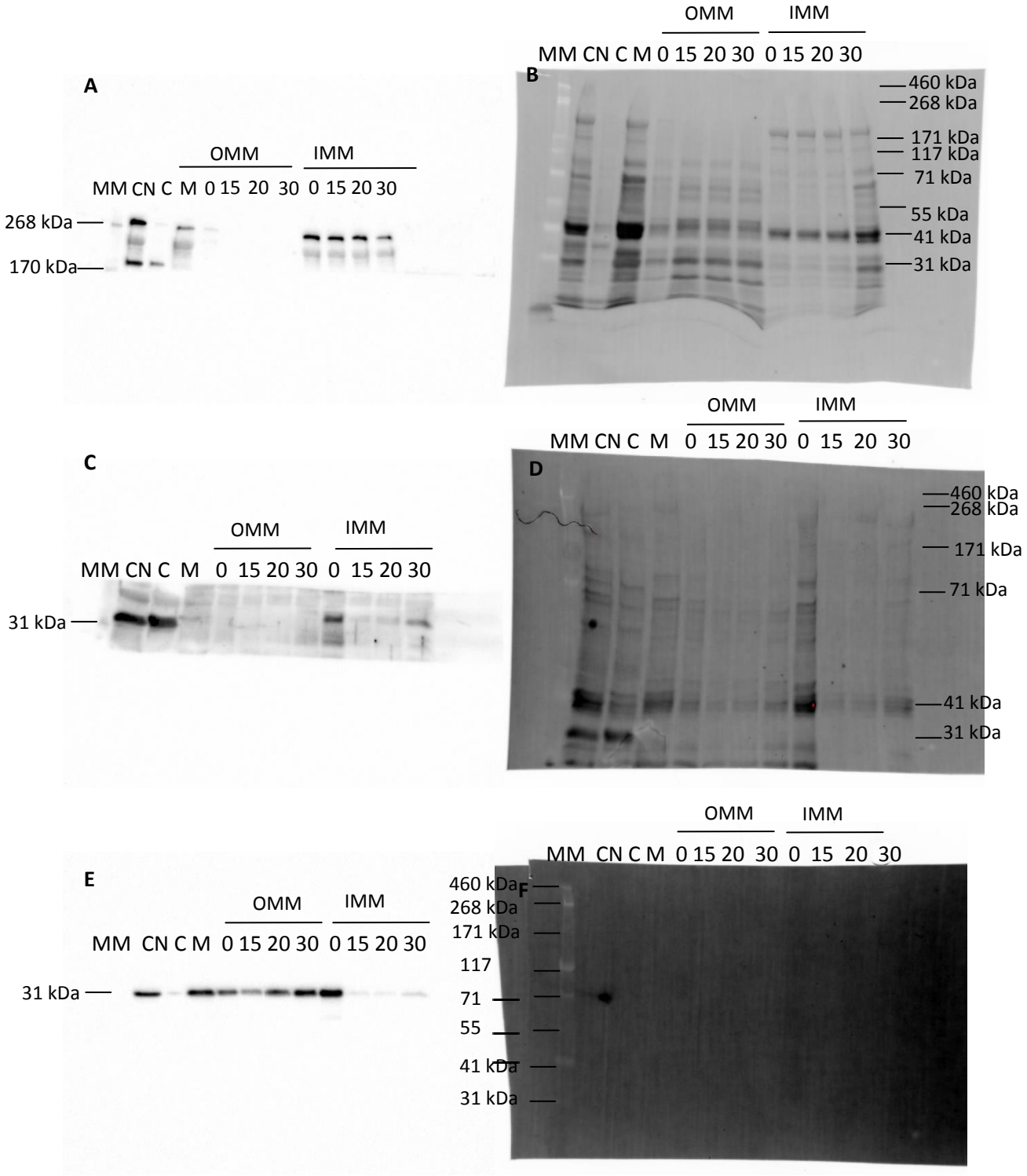

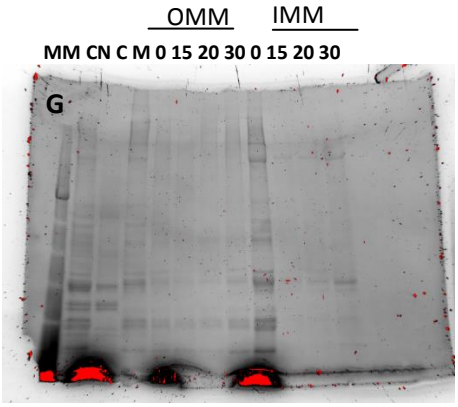

Figure A1: Uncropped ATM (Fig A1.a) and its total protein membrane (Fig A2.b) prior to being cut below the 170 kDa mark (1st lane, left; HiMark™ Pre-stained Protein Standard, Invitrogen, ThermoFischer) and probed overnight with anti-rabbit monoclonal ATM antibody(Cell Signalling Technologies, D2E2). Fig A1.c: **Uncropped ANT** 1/2/3/4 (left) and its total protein membrane (Fig A1.d) prior to being cut above the 41 kDa mark (1st lane, left; HiMark™ Pre-stained Protein Standard, Invitrogen, ThermoFischer) and probed overnight with anti-rabbit polyclonal ANT1/2/3/4 antibody (H-188, sc-11433, Santa Cruz Biotechnoglogy). **Figure A1.e: Uncropped VDAC** and its total protein membrane (Fig A1.f) prior to being cut at the 41 kDa mark(1st lane, left; HiMark™ Pre-stained Protein Standard, Invitrogen, ThermoFischer) and probed overnight with anti-rabbit monoclonal VDAC (Cell Signalling technologies, D73D12). Due to the dark transfer the original 4–15% Mini-PROTEAN® TGX™ Precast Protein Gel (BioRad, #4561086) image is included (bottom). All the membranes were loaded as follows: HiMark™ Pre-stained Protein Standard, Invitrogen, ThermoFischer, Nucleus and cell membrane fraction(CN), cytosolic fraction(C), M/S isolated mitochondrial fraction(M), OMM fraction at 0 min, 15 min, 20 min and 30 min 1.2% digitonin permeabilisation, IMM(mitoplast consisting of inner mitochondrial membrane and matrix) fraction at 0 min, 15 min, 20 min and 30 min 1.2% digitonin treatment.

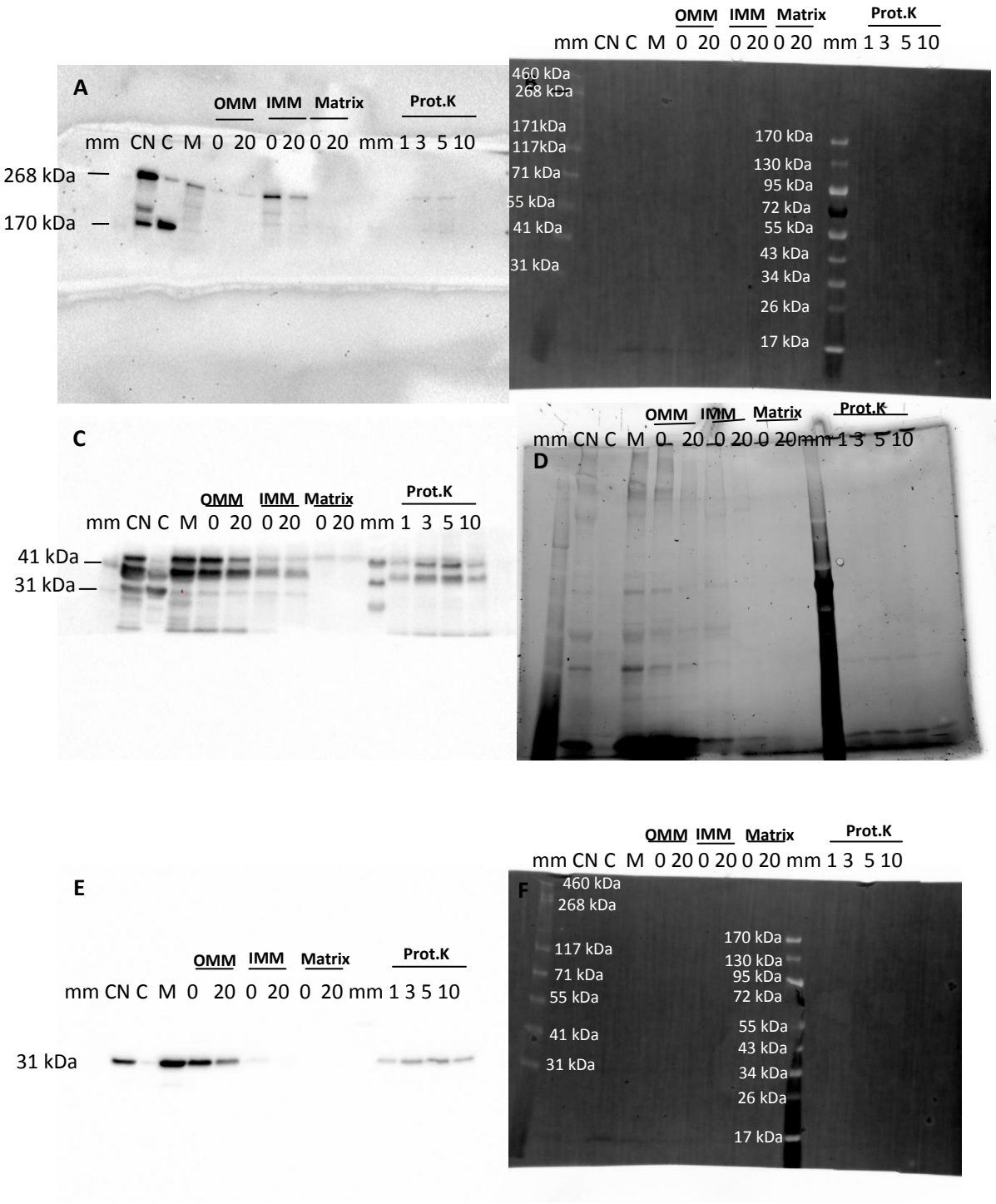

Figure A2: Mitochondrial and mitoplast subfractionation and Proteinase K digestion: Isolated mitochondria was fractionated into outer mitochondrial (OMM) membrane and mitoplast fractions with 1.2% digitonin and the latter was further separated into inner mitochondrial membrane (IMM) and matrix fractions. The fractions and probed for ATM (Fig 3.a), ANT (Fig A2.c, same membrane as ATM, Fig A2b) and VDAC (Fig A2.e). The total protein membranes are shown respectively in Fig A2b (on which both ATM and ANT was probed), and Fig. A2.f. Figure A2d shows the corresponding 4–15% Mini-PROTEAN® TGX™ Precast Protein Gel (BioRad, #4561086) for Fig A2.b, which was loaded as follows: MM: HiMark™ Pre-stained Protein Standard, Invitrogen, ThermoFischer, Nucleus

and cell membrane fraction(CN), cytosolic fraction(C), M/S isolated mitochondrial fraction(M), OMM fraction at 0 min and 20 min 1.2% digitonin permeabilisation, IMM at 0 and 20 min 1.2% digitonin treatment, and the matrix fraction at 0 and 20 min 1.2% digitonin treatment; mm (PageRuler™ Prestained Protein Ladder, 10 to 180 kDa, Thermo Fischer Scientific), 1 min, 3 min, 5 min and 10 min M/S isolated mitochondrial Proteinase K digest fractions. The gels were loaded with the same lysates, electrophoresed in the same chamber and transferred in the same chamber. Due to incomplete transfer in the 41 kDa size region (Fig A2f), it is not possible to exclude the presence of VDAC in the matrix fractions.

Addendum B: Publications

Title: Ataxia-Telangiectasia Mutated is located in cardiac mitochondria and impacts oxidative phosphorylation **(Submitted to *Scientific Reports*, under review)**

Authors:

Marguerite Blignaut[1], Ben Loos[2], Stanley W. Botchway[4,5], Anthony W. Parker[4,6], Barbara Huisamen[1,3]

Departments where work was performed:

Department of Biomedical Sciences, Division Medical Physiology, Faculty of Medicine and Health Sciences, Tygerberg Campus, South Africa

Department of Physiological Sciences, Faculty of Sciences, Stellenbosch University, South Africa

Rutherford Appleton Laboratory, Science and Technology Facility Council, Oxfordshire, UK

Authors affiliations:

[1]Division of Medical Physiology, Department of Biomedical Sciences, Faculty of Medicine and Health Sciences, Stellenbosch University, Tygerberg, 7505.

[2] Department of Physiological Sciences, Faculty of Sciences, Stellenbosch University, South Africa

[3] Biomedical, Research and Innovation Platform, South African Medical Research Council, Tygerberg, 7505.

[4] Central Laser Facility, Research Complex at Harwell, STFC Rutherford Appleton Laboratory, Harwell Campus, Didcot, OX11 0QX, UK

[5] Oxford Brookes University, Department of Biological and Medical Sciences, Oxford, OX3 0BP, UK

[6] Department of Physics, Faculty of Science, Stellenbosch University, Private Bag X1, Matieland, South Africa, 7602.

Corresponding author:

Marguerite Blignaut

PO Box 19063, Division of Medical Physiology, Department of Biomedical Sciences, Faculty of Medicine and Health Sciences, Tygerberg, South Africa, 7505.

Email: 13813412@sun.ac.za

Telephone: +27832399256

Fax: +27219389476

Abstract:

The absence of Ataxia-Telangiectasia mutated protein kinase (ATM) is associated with neurological, metabolic and cardiovascular defects. The protein has been associated with mitochondria and its absence results in mitochondrial dysfunction. Furthermore, it can be activated in the cytosol by mitochondrial oxidative stress and mediates a cellular anti-oxidant response through the pentose phosphate pathway (PPP). However, the precise location and function of ATM within mitochondria and its role in oxidative phosphorylation is still unknown. We show that ATM is found endogenously within cardiac myocyte mitochondria under normoxic conditions and is consistently associated with the inner mitochondrial membrane. Acute *ex vivo* inhibition of ATM protein kinase significantly decreased mitochondrial electron transfer chain Complex I-mediated oxidative phosphorylation rate but did not decrease coupling efficiency or oxygen consumption rate during β-oxidation. Chemical inhibition of ATM in rat cardiomyoblast cells (H9c2) significantly decreased the excited-state autofluorescence lifetime of enzyme-bound reduced NADH and its phosphorylated form, NADPH (NAD(P)H; 2.77 ± 0.26 ns compared to 2.57 ±0.14 ns in KU60019-treated cells). This suggests an interaction between mitochondrial ATM and the electron transfer chain in the mitochondria, and hence may have an important role in oxidative phosphorylation in terminally differentiated cells such as cardiomyocytes.

Author contributions statement:

MB wrote the main manuscript text and prepared Fig 1, 3, 4 and 5. BL prepared Fig 2 and performed all SR-SIM experiments. MB worked under the supervision of SWB and AWP at RAL, and BH at SU. All authors reviewed the manuscript

Title page:

Authors: Marguerite Blignaut[1], Yolandi Espach[1], Mignon van Vuuren[1], Karthik Dhanabalan[1], Barbara Huisamen[1,2]

Title: Revisiting the cardiotoxic effect of chloroquine **(accepted with revisions by *Cardiovascular Drugs and Therapy*, resubmitted)**

Affiliations:

1. Division of Medical Physiology, Department of Biomedical Sciences, Faculty of Medicine and Health Sciences, Stellenbosch University, Tygerberg, South Africa.
2. South African Medical Research Council, Biomedical Research and Innovation Platform, Tygerberg, South Africa.

Corresponding author: bh3@sun.ac.za; +27 21 938 9688

ORCID ID's:

M Blignaut: 0000-0001-7645-9780

Y Espach: 0000-0003-0404-1267

M van Vuuren: 0000-0002-1130-171X

K Dhanabalan: 0000-0002-6619-6363

B Huisamen: 0000-0001-7074-0360

Acknowledgements: We acknowledge funding from the South African National Research Foundation

Abstract:

Purpose: Cardiotoxicity is a well-known side effect of Chloroquine. Several studies have proposed chloroquine as a potential anti-diabetic treatment but did not address this problem. The current study investigated the effect of *ex vivo* chloroquine treatment on 1) heart function and glucose uptake, 2) mitochondrial function and 3) *in vivo* treatment on heart function.

Methods: Control or obese male Wistar rats were used throughout. Dose responses of increasing chloroquine concentrations versus vehicle on cardiac function were measured using isolated, Langendorff perfused hearts while glucose uptake and cell viability were determined in ventricular cardiomyocytes. Mitochondrial function was assessed with a

Clark-type oxygraph (Hansatech) after *ex vivo* perfusion with 30 µM chloroquine vs vehicle. Animals were treated orally with 5 mg/kg/day chloroquine for 6 weeks.

Results: Acute chloroquine treatment of 10 µM was sufficient to significantly decrease heart function as determined by RPP ($p<0.05$) while 30 µM significantly reduced heart rate ($p<0.05$). Chloroquine became toxic to isolated cardiomyocytes at high concentrations (100 µM), and could not induce cardiomyocyte glucose uptake. *Ex vivo* treatment had no effect on mitochondrial function in DIO animals, but increased oxygen consumption in age-matched control animals. Chronic low-dose *in vivo* chloroquine treatment significantly decreased aortic output and total work in hearts ($p<0.005$).

Conclusion: Low and intermediate chloroquine doses administered either chronically or acutely is sufficient to result in myocardial dysfunction.

Keywords: Chloroquine, cardiotoxicity, mitochondrial dysfunction, insulin resistance, diabetes

Author contributions statement:

MB wrote the main manuscript text and prepared Fig 3 and generated the related data. YE prepared Fig 1, 2 and 5 and generated the related data with the exception of Fig 5 where KD generated the data. MvV prepared Fig 4 and generated the related data. MB, YE, MvV and KD worked under the supervision of BH at SU. All authors reviewed the manuscript

Addendum C : Insulin resistance in diet induced obese rats (DIO):

The chow-fed age-matched rats and diet induced obese (DIO) rats used during this study were part of a much larger cohort of Wistar rats fed either rat chow or the DIO diet (Chapter 5, Table 5.1). A representative group of the larger cohort was subjected to an oral glucose intolerance test and a Homeostatic model assessment (HOMA) to determine insulin resistance (IR) from basal (fasting) glucose by Mr Sybrand Smith as part of his PhD study. The results are presented in Fig. C1 and Fig C2.

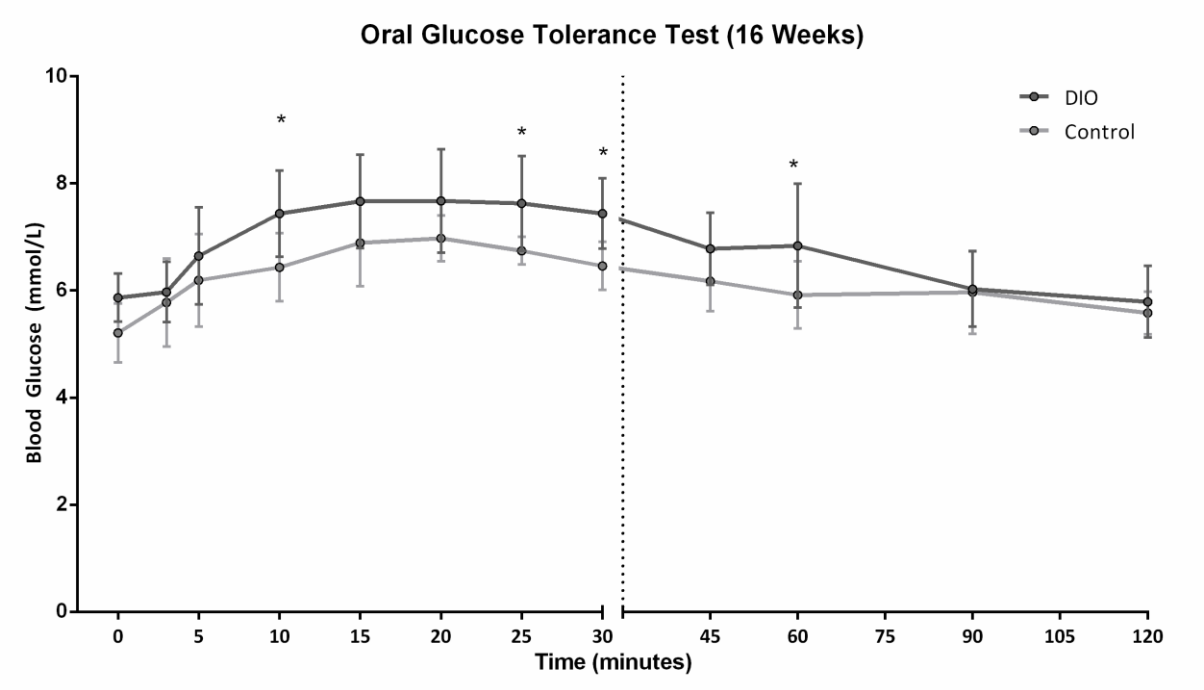

Figure C1: Oral glucose intolerance test of male Wistar rats at 16 weeks of age, after being fed a diet inducing obesity (DIO) diet for 6 weeks compared to chow-fed age-matched controls. 2-Way ANOVA, Bonferroni post-hoc test, *p<0.05

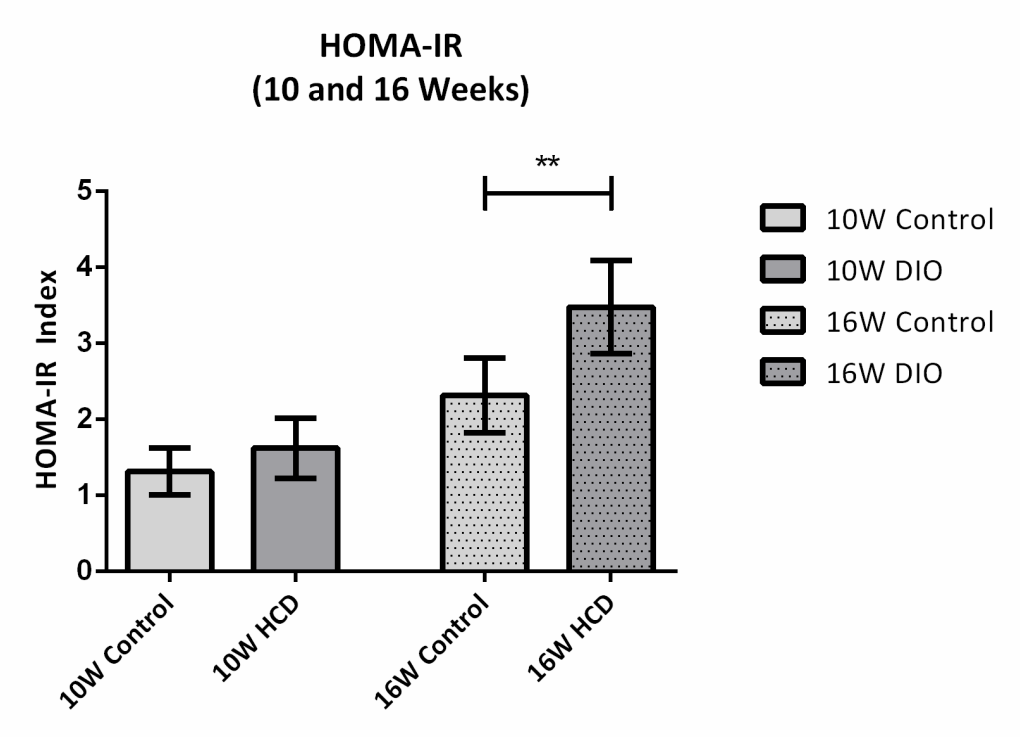

Figure C2: HOMA-IR of male Wistar rats at the age of 10 weeks prior to being fed a DIO-diet for 6 weeks, and HOMA-IR after being fed DIO (shown as HCD on x-axis) for 6 weeks compared to their age-matched controls .

Addendum D: Mitochondrial respiration of hearts perfused with a combination of KU60019 and chloroquine compared to KU60019 alone

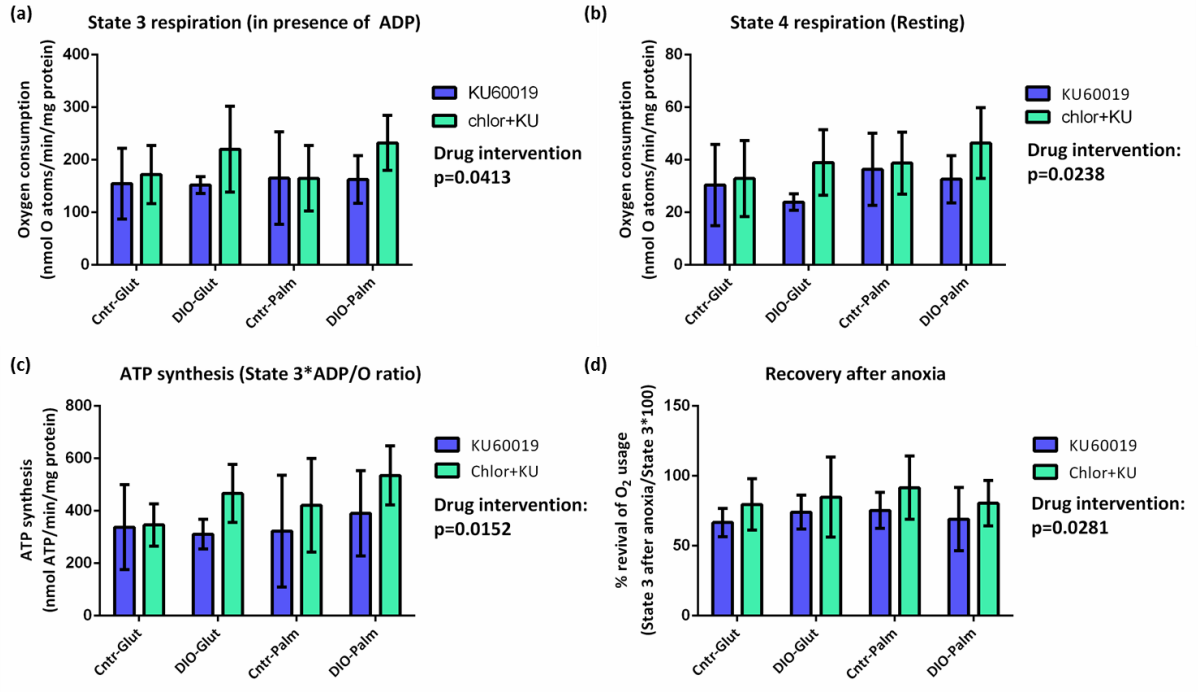

Figure D1: Mitochondria from DIO hearts perfused with a combination of chloroquine and KU60019 compared to KU60019 alone, had an effect on State 3 and 4 respiration as well as ATP synthesis and recovery after anoxia ($p<0.05$ taken as significant, 2-Way ANOVA, Bonferonni post-hoc test).